7. SENSITIVITY TO EMISSION CHANGES

7.1 SENSITIVITY TO EMISSION CHANGES UNDER SUMMER CONDITIONS

A large number of sensitivity simulations were conducted in developing the UAM-AERO model, since predicted sensitivity to emission changes is the main use of models of this type. A series of sensitivity simulations were performed to investigate the predicted response of the UAM-AERO model to basinwide changes in emission strengths under summer conditions. The emission scenarios included 50 percent reductions in the basinwide emissions of NO_x, VOC, NO_x and VOC, NH_3, SO_2, and PM. In addition, the results with unadjusted PM emissions, labeled 100 percent PM emissions increase, are included to illustrate the effects of the PM emissions adjustment. Only the emission inputs were altered in the simulations; the boundary conditions and initial conditions were identical to those used for the baseline simulations.

The results for the sensitivity simulations are summarized in **Tables 7-1 and 7-2**. Table 7-1 shows the effects of NO_x, VOC, and NO_x and VOC emission reductions on 1-hr ozone, NO_2, and NO concentrations on June 24 and 25. These species are unaffected by changes in NH_3, SO_2, and PM emissions. Table 7-2 shows the effects of the emission changes on 24-hr average concentrations of nitrate, ammonium, sulfate, organic material, PM mass, nitric acid, and ammonia. Both tables include the maximum concentration in the domain, the concentration at the monitoring station with the highest observation of the species, and the average concentrations at the monitoring stations. In most cases, the effects of the emission changes were similar on June 24 and 25, so Table 7-2 includes the average results for these two days.

7.1.1 Effects of Emission Changes on Ozone, NO_2, and NO Concentrations

The VOC emission reduction case shows the largest effect on ozone concentrations. The 1-hr ozone maxima at the stations with the highest observed value is predicted to decrease by 41 and 42 percent on June 24 and 25 in response to a 50 percent VOC reduction. The maximum ozone concentration in the domain is estimated to decrease by 33 to 35 percent (451 to 272 ppb on June 24 and 353 to 230 ppb on June 25) with the VOC reduction. The average ozone at the monitoring stations is also estimated to drop by 20 percent under the VOC reduction scenario.

The results are quite different for the 50 percent NO_x emission reduction. The ozone concentrations in the summer simulation are predicted to increase on average in response to the NO_x emission reduction. The 1-hr maximum concentration in the domain is predicted to increase by 11 percent on June 24 and decrease by 15 on June 25 with the 50 percent NO_x reduction. The maximum ozone at the highest monitoring stations is predicted to increase by 20 percent on June 24 and decrease by 7 percent on June 25.

The effects of a combined 50 percent reduction in NO_x and VOC emissions is in between those for separate NO_x and VOC emission reductions. The domainwide peak ozone is predicted to decrease by 17 to 26 percent with the combined NO_x and VOC reductions (451 to 338 ppb on June 24 and 353 to 261 ppb on June 25). Ozone concentrations at the monitoring stations with the highest observed ozone are estimated to decline by 4 to 18 percent under this scenario. The average ozone is almost unaffected by the 50 percent NO_x and VOC reduction.

The effects of the NO_x and VOC emission changes on NO_2 and NO are more linear than their effects on ozone. The average NO_2 concentrations are predicted to decrease by 54 to 56 percent with the 50 percent NO_x reduction, and 51 to 53 percent with the NO_x and VOC emission reduction. The average NO concentrations are predicted to decrease by 72 and 65 percent with the 50 percent NO_x reduction and the 50 percent NO_x and VOC emission reduction, respectively. The reduction in VOC emissions is predicted to increase the average NO concentrations and to slightly reduce the average NO_2 concentrations. The peak 1-hr NO_2 concentrations in the domain are estimated to decline by 6 to 8 percent in response to the 50 percent VOC reduction and 32 to 34 percent in response to the 50 percent NO_x reduction.

7.1.2 Effects of Emission Changes on PM Nitrate Concentrations

The results for the summer simulations predict basinwide reductions in NO_x emissions, NO_x and VOC emissions, and ammonia emissions will reduce ambient $PM_{2.5}$ and PM_{10} nitrate significantly. At Riverside, the SCAQS station with the highest nitrate, a 50 percent reduction in NO_x emissions is predicted to reduce $PM_{2.5}$ and PM_{10} nitrate by 46 and 42 percent, respectively. This result shows a fairly linear response for nitrate to NO_x emission changes. A 50 percent reduction in NO_x and VOC emissions shows a slightly smaller reduction in PM nitrate at Riverside. A 50 reduction in ammonia emissions is predicted to decrease ambient PM_{10} nitrate by only 16 percent at Riverside. These results suggest PM nitrate is NO_x-limited, rather than NH_3-limited, at Riverside. It is consistent with the ambient data for Riverside, which show low nitric acid levels and high ammonia levels.

The effects of emission reductions on the average PM nitrate at other SCAQS stations is different than that for Riverside. The simulations indicate the 50 percent NO_x emission reduction reduces the average $PM_{2.5}$ and PM_{10} nitrate by 20 and 18 percent at SCAQS stations. The 50 percent NO_x and VOC emission reduction reduces the average $PM_{2.5}$ and PM_{10} nitrate by 22 and 20 percent. However, the 50 percent ammonia emission reduction reduces the average $PM_{2.5}$ and PM_{10} nitrate by 41 and 37 percent. These results suggest PM nitrate levels at SCAQS stations are more ammonia-limited than NO_x-limited on average. Recall, only one of the eight SCAQS stations, Riverside, is directly downwind of the major ammonia emission sources in the inland area, so it is not surprising that the model predicts a higher sensitivity to ammonia emissions than NO_x emissions on average at these stations.

The predicted changes in the maximum PM nitrate concentration anywhere in the domain are similar for NO_x, NO_x and VOC, and NH_3 emission reductions. $PM_{2.5}$ nitrate is predicted to decrease by 30, 30, and 35 percent for 50 percent NO_x, NO_x and VOC, and NH_3

emission reductions. PM_{10} nitrate is predicted to decrease by 32, 32, and 34 percent for 50 percent NO_x, NO_x and VOC, and NH_3 emission reductions. Thus, the peak nitrate in the domain is comparably limited by ammonia and NO_x emissions. Also note, the results are the same with the 50 percent NO_x reduction and the 50 percent NO_x and VOC emission reductions, indicating little VOC influence on the peak nitrate when NO_x is reduced.

The effects of other emission scenarios on PM nitrate are generally small. A 50 percent VOC emission reduction alone is predicted to reduce the domainwide maximum $PM_{2.5}$ and PM_{10} nitrate concentrations by 13 and 9 percent. This effect occurs because nitric acid is produced more slowly with lower VOC emissions. The predicted effect of VOC emission reductions alone is smaller at the peak SCAQS station and on average at the SCAQS stations (6 to 8 percent PM nitrate reduction). A 50 percent reduction in SO_2 emissions does not affect the maximum PM nitrate in the domain or at the SCAQS station with the highest nitrate, however, it is predicted to increase the average PM nitrate at the SCAQS stations by 7 to 8 percent. The reason for this response is the competition for ammonia at most SCAQS stations. Under ammonia-limited conditions, lowering the sulfate levels frees up ammonium and allows for increased levels of ammonium nitrate aerosol formation. Lastly, the 50 percent decrease and 100 percent increase in PM emissions have a negligible effect on PM nitrate. The changes in PM emissions on nitrate are directional as expected; decreasing PM emissions, which are mostly coarse, slightly reduces the surface area of coarse particles so more of the nitric acid condenses on small ($PM_{2.5}$) particles.

7.1.3 Effects of Emission Changes on PM Ammonium Concentrations

The predicted effects of changes in the basinwide NO_x emissions, NO_x and VOC emissions, and ammonia emissions on ammonium are significant and nonlinear. At Riverside, separate 50 percent reductions in NO_x and NH_3 emissions are predicted to reduce PM_{10} ammonium by 33 and 14 percent, respectively. However, at the SCAQS stations (taken as a group), 50 percent reductions in NO_x and NH_3 emissions are predicted to reduce the average PM_{10} ammonium by 11 and 32 percent, respectively. These results are consistent with ammonium nitrate production being NO_x-limited at Riverside and ammonia-limited at the majority of SCAQS stations. The peak PM_{10} ammonium in the domain is predicted to be reduced by 22 and 32 percent with 50 percent reductions in NO_x and NH_3 emissions, respectively. The results for reduction of both NO_x and VOC emissions on PM ammonium are similar to those for NO_x emission reduction alone.

Changes in SO_2 emissions are predicted to have a minor effect on ammonium. PM_{10} ammonium is predicted to decrease by 3 to 6 percent in response to a 50 percent SO_2 emission reduction. These results are consistent with the fact that most of the ammonium in the SoCAB aerosol is associated with nitrate rather than sulfate; however, the model's response may underestimate the real world response because the model underestimates the observed sulfate in the baseline simulation.

7.1.4 Effects of Emission Changes on Organic PM Concentrations

The predicted effects of emission changes on organic PM are greatest for the primary PM emission reduction case. The 50 percent PM emission reduction is predicted to reduce $PM_{2.5}$ OM by 31 percent at the SCAQS station with highest observed $PM_{2.5}$ OM and by 27 percent on average at the SCAQS stations. The peak $PM_{2.5}$ OM in the domain is predicted to decrease by only 10 percent in response to the same PM emission reduction. The PM_{10} OM concentrations are predicted to decrease by 35 and 32 percent at the highest and average SCAQS stations. The peak PM_{10} OM in the domain is predicted to decrease by 17 percent in response to the 50 percent PM emission reduction.

Reduction in VOC emissions also reduces organic PM concentrations by modest amounts. The 50 percent VOC emission reduction is predicted to lower $PM_{2.5}$ OM levels by 10 percent at the SCAQS station with the highest observed $PM_{2.5}$ OM and by 8 percent on average at the SCAQS stations. The effects of VOC emission reduction on the PM_{10} OM is smaller than $PM_{2.5}$ OM because most of the secondary OM is contained in the $PM_{2.5}$ aerosol. These results are consistent with our observation that the model predicted OM is mostly primary OM, rather than secondary OM.

Concurrent reductions in NO_x and VOC emissions are predicted to be slightly less effective than reducing VOC emissions alone on $PM_{2.5}$ organic material. The model predicts a 4 percent reduction in $PM_{2.5}$ OM at the SCAQS stations for the combined 50 percent NO_x and VOC emission reduction. A reduction of NO_x emissions alone is predicted to slightly increase OM (up to 6 percent at the highest station). The reason reduction in NO_x emissions enhances OM is that VOCs are oxidized more rapidly at higher VOC/NO_x ratios.

7.1.5 Effects of Emission Changes on PM Mass Concentrations

The model predicts reduction in ammonia emissions and primary PM emissions have the largest effects on ambient $PM_{2.5}$ and PM_{10}, respectively. On average at the SCAQS stations, a 50 percent ammonia emission reduction is predicted to reduce $PM_{2.5}$ and PM_{10} mass by 21 and 13 percent. At Riverside, which had the highest observed PM mass, a 50 percent ammonia emission reduction is predicted to decrease the $PM_{2.5}$ and PM_{10} mass by 17 and 6 percent. A 50 percent reduction in primary PM emissions is predicted to reduce $PM_{2.5}$ and PM_{10} mass by 15 and 24 percent at the highest station, respectively.

The next most effective emission reductions are for NO_x and NO_x and VOC. At Riverside, $PM_{2.5}$ and PM_{10} mass is estimated to decrease by 12 and 14 percent in response to a 50 percent NO_x emission reduction. A combined 50 percent reduction of NO_x and VOC emissions is estimated to reduce the $PM_{2.5}$ and PM_{10} at Riverside by 13 percent.

VOC and SO_2 emission reductions are predicted to have smaller effects on ambient PM mass. The 50 percent VOC emission reduction is estimated to reduce $PM_{2.5}$ mass by 6 percent at Riverside and 4 percent on average at the SCAQS stations. The VOC emission reduction is estimated to reduce PM_{10} mass by 3 percent at Riverside and 2 percent on average at the

SCAQS stations. Also, because SO_2 emissions are relatively low in the SoCAB (compared to areas outside of California), the predicted effects of further reduction of SO_2 emissions by 50 percent is small (2-3 percent) on $PM_{2.5}$ and PM_{10} mass. Note the effects of SO_2 emission changes may be underestimated in these simulations because the model underpredicted the observed sulfate levels. However, even if the correct response is double the predicted response, the effects of SO_2 emission reductions are still likely to be small compared to the effects of PM, NH_3, and NO_x emission reductions.

The results for the 100 percent increase in PM emissions indicate $PM_{2.5}$ and PM_{10} mass levels at the highest station would increase by 30 and 47 percent, respectively. The PM levels predicted with doubled PM emissions significantly exceed the observations.

7.1.6 Effects of Emission Changes on Nitric Acid Concentrations

The reduction in NH_3 and NO_x emissions are predicted to have the largest effect on ambient nitric acid concentrations at the SCAQS stations. Lowering of the NH_3 emissions is estimated to increase the nitric acid concentrations by 57 percent at the SCAQs stations. This result is not unexpected because reductions in ammonia at locations where ammonium nitrate formation is ammonia-limited shift nitrate from the aerosol to the gas-phase. Reducing NO_x emissions by 50 percent is estimated to decrease ambient nitric acid levels by 36 percent at the SCAQS stations. This reduction is less than linear because reducing NO_x emissions also increases the VOC/NO_x ratio which enhances the relative NO_x oxidation rates.

Concurrent reductions of VOC and NO_x emissions is estimated to lower nitric acid levels more than reducing NO_x or VOC emissions alone. On average at the SCAQS stations, lowering VOC and NO_x emissions by 50 percent is estimated to reduce nitric acid by 41 percent, whereas lowering VOC and NO_x emissions separately by 50 percent is estimated to reduce nitric acid by 17 and 36 percent, respectively.

Reducing SO_2 emissions is also estimated to reduce nitric acid levels. On average for the SCAQS stations, a 50 percent SO_2 emission reduction is estimated to reduce nitric acid concentrations by 13 percent. In areas where ammonium nitrate formation is ammonia-limited, reducing SO_2 emissions reduces ammonium sulfate levels which, in turn, frees up ammonia that can then react with nitric acid to form more ammonium nitrate aerosol. The competition for ammonia links the effects of NO_x and SO_2 emission controls on nitric acid and PM.

7.1.7 Effects of Emission Changes on Ammonia Concentrations

Reductions in ammonia emissions are predicted to have more than a proportionate affect on ammonia concentrations. A 50 percent reduction in ammonia emissions is predicted to reduce ambient ammonia by 66 percent at SCAQS stations on average. The reason for this nonlinear effect is the competition for ammonia to make ammonium nitrate.

Lowering NO_x emissions and NO_x and VOC emissions is predicted to increase ambient ammonia levels by modest amounts (15 to 17 percent). With lower NO_x emissions, there is less nitric acid available to scavenge ammonia so more ammonia remains in the gas phase.

7.1.8 Effects of Emission Changes on Sulfate Concentrations

Reductions in SO_2 and PM emissions are predicted to affect the sulfate levels in the summer simulation. Reductions in NO_x, VOC, and NH_3 emissions are not predicted to influence the sulfate levels. The 50 percent SO_2 emission reduction is predicted to reduce $PM_{2.5}$ sulfate by 32 percent on average and reduce PM_{10} sulfate by 26 to 31 percent. The reductions in ambient concentration are less than one-to-one because of the effects of background sulfate levels and primary sulfate emissions. The emissions inventory includes a small amount of primary sulfate emissions and the results for the case with 50 percent PM emission reduction show 4 to 6 percent lower PM_{10} sulfate levels. The results for the case with 100 percent increase in PM emissions show 9 to 12 percent higher PM_{10} sulfate levels.

7.1.9 Effects of Emission Changes on Deposition Rates

The estimated effects of the regionwide changes in emissions on pollutant deposition rates is shown in **Table 7-3**. The results show ozone deposition is predicted to decline with a 50 percent VOC emission reduction and with a 50 NO_x and VOC emission reduction; however, ozone deposition is predicted to increase with a 50 percent NO_x emission reduction. Deposition of nitric acid is estimated to decrease by 9, 44, and 47 percent in response to 50 percent reductions in VOC, NO_x and VOC, and NO_x emissions, respectively. Deposition of NO_2 is predicted to decline by 56 and 65 percent in response to 50 percent reductions in NO_x and VOC, and NO_x emissions, respectively; however, NO_2 deposition is estimated to increase with VOC emission reduction alone. The changes in ozone, nitric acid, and NO_2 deposition are consistent with the current understanding of the changes in ambient concentrations.

Ammonia deposition is predicted to decrease by 53 percent in response to a 50 percent reduction in ammonia emissions. Ammonia deposition is estimated to increase by 26 and 30 percent in response to a 50 percent reduction in NO_x and VOC, and NO_x emissions, respectively. SO_2 deposition is estimated to decrease linearly with SO_2 emission reductions. Formic and acetic acid deposition rates are estimated to decrease with both VOC and NO_x, and VOC emission reductions.

The deposition rate of PM_{10} nitrate is predicted to decrease with reductions in NO_x, NO_x and VOC, NH_3, and PM emissions, and to increase with reduction in SO_2 emissions. PM_{10} ammonium deposition is estimated to decrease with reductions in NO_x, NO_x and VOC, NH_3, and SO_2 emissions. Sulfate deposition is responsive to reductions in SO_2 emissions and PM emissions. Deposition of primary EC and crustal PM_{10} is predicted to decrease by 39 and 44 percent in response to a 50 percent PM emission reduction. Deposition of organic material (primary+secondary) is estimated to decline by 31 percent in response to a 50 percent PM

emission reduction. These estimated changes in deposition with emission changes are consistent with the estimated changes in ambient concentrations.

7.2 SENSITIVITY TO EMISSION CHANGES UNDER FALL CONDITIONS

A subset of emission sensitivity simulations were run for the fall episode. The purpose of the analysis was to investigate the response of the modeling system under conditions with higher aerosol loadings and less photochemistry than in the summer. The results should be interpreted cautiously because the model performance for the fall episode was poorer than expected, especially on December 11. Simulations were run to examine the model's response to 50 percent reductions in the regionwide emissions of NO_x, VOC, NO_x and VOC, and SO_2. In addition, a simulation with a 100 percent increase in PM emissions is included, which includes the results with the original PM emissions (i.e., before the 50 percent reduction of the PM emissions included in the baseline and all other runs).

The results for the sensitivity simulations are summarized in **Tables 7-4 and 7-5**. Table 7-4 shows the effects of NO_x, VOC, and NO_x and VOC emission reductions on 1-hr ozone, NO_2, and NO concentrations on December 10 and 11. These species are unaffected by changes in SO_2 and PM emissions. Table 7-5 shows the effects of the emission changes on 24-hr average concentrations of nitrate, ammonium, sulfate, organic material, PM mass, nitric acid, and ammonia. Both tables include the maximum concentration in the domain, the concentration at the monitoring station with the highest observation of the species, and the average concentrations at the monitoring stations. In most cases, the effects of the emission changes were similar on December 10 and 11, so Table 7-5 includes the average results for these two days.

7.2.1 Effects of Emission Changes on Ozone, NO_2, and NO Concentrations

The baseline ozone predictions were not particularly high for the December episode, however, the model's ozone response was quite sensitive to emission changes. The 50 percent VOC emission reduction case shows decreases in predicted ozone levels that are similar on a percentage basis to those predicted for the summer episode. The results for NO_x emission reductions show large percentage increases in ozone concentrations (58 to 79 percent or +30 ppb at the highest station). Modest ozone increases were also predicted for the combined NO_x and VOC emission reduction. These results suggest ozone levels in the fall are quite sensitive to NO_x emission levels and the VOC-to-NO_x ratio of the emissions.

The effects of the NO_x and VOC emission changes on NO_2 and NO are also significant. The average NO_2 concentrations are predicted to decrease by 25 to 22 percent with the 50 percent NO_x reduction, and 33 percent with the NO_x and VOC emission reduction. The average NO concentrations are predicted to decrease by 75 and 63 percent with the 50 percent NO_x reduction and the 50 percent NO_x and VOC emission reduction, respectively. The reduction in VOC emissions is predicted to increase the average NO concentrations and to

reduce the average NO_2 concentrations by 14 to 17 percent. The peak 1-hr NO_2 concentrations in the domain are estimated to decline by 5 to 13 percent in response to the 50 percent VOC reduction and 25 to 38 percent in response to the 50 percent NO_x reduction. These responses are plausible for fall conditions where the photochemistry appears to operate in a low to moderate VOC-to-NO_x regime that is quite sensitive to NO_x and VOC emission changes.

7.2.2 Effects of Emission Changes on PM Nitrate Concentrations

The PM nitrate levels are estimated to increase with decreased NO_x emissions in the fall. $PM_{2.5}$ nitrate is estimated to increase by 9 percent on average and 20 percent at the highest SCAQS station. The maximum $PM_{2.5}$ nitrate in the domain is predicted to increase by 42 percent with the 50 percent NO_x emission reduction. This response is due to the chemical system operating in higher VOC-to-NO_x regime where nitric acid production is much more efficient and where there is ample ammonia to make ammonium nitrate. With a 50 percent VOC emission reduction, $PM_{2.5}$ nitrate is 27 percent lower on average and 28 percent lower at the highest SCAQS station. The peak $PM_{2.5}$ nitrate anywhere in the domain is predicted to be 42 percent lower with the reduced VOC emissions. The results for the 50 percent NO_x and VOC reduction show 29 percent lower $PM_{2.5}$ nitrate on average and a 20 percent lower domainwide peak $PM_{2.5}$ nitrate. The PM_{10} predictions are slightly less sensitive than the $PM_{2.5}$ predictions to emission changes. The high PM nitrate sensitivity to VOC and NO_x changes is similar to that predicted for ozone and NO_2, and is primarily due to the sensitivity of the gas-phase chemistry under fall conditions. In addition, as was predicted for the summer case, the SO_2 emission reduction is estimated to increase the PM nitrate by 3 to 8 percent. With lower SO_2, there is less sulfate, and therefore, more ammonia available to form ammonium nitrate.

7.2.3 Effects of Emission Changes on PM Ammonium Concentrations

Reduction in VOC and VOC and NO_x emissions are estimated to be relatively effective in reducing PM ammonium concentrations. The 50 percent VOC reduction and VOC and NO_x reduction are estimated to reduce the average PM ammonium concentrations by 22 and 23 percent, respectively. The NO_x emission reduction is estimated to increase PM ammonium because of the enhance nitric acid production under this scenario.

7.2.4 Effects of Emission Changes on Sulfate Concentrations

The sulfate concentrations are fairly low in the fall simulation and a significant part of the modeled sulfate is provided by boundary conditions, rather than from conversion of SO_2. The only emission changes that significantly affect the sulfate levels predicted for the fall are SO_2 emissions. The maximum $PM_{2.5}$ sulfate levels are predicted to decrease by 26 percent when SO_2 emissions are reduced 50 percent. The reductions are smaller on average at the SCAQS stations.

7.2.5 Effects of Emission Changes on Nitric Acid Concentrations

The nitric acid concentrations are predicted to decline by 21 percent on average in response to both a 50 percent VOC reduction and a 50 percent VOC and NO_x reduction. Nitric acid is estimated to increase by 4 percent, on average, in response to a 50 percent reduction in NO_x emissions. These results are consistent with those for PM nitrate described above. The peak nitric acid concentration in the domain responds in a different manner. The NO_x emission reduction decreases the peak nitric acid by 72 percent. Clearly, the peak nitric acid is controlled by the availability of NO_x.

7.2.6 Effects of Emission Changes on Organic PM Concentrations

The ambient concentrations of organic particulate matter are predicted to decrease by 5 to 9 percent with either a 50 percent VOC emission reduction or a 50 percent VOC and NO_x emission reduction. However, with the 50 percent NO_x emission reduction, the model predicts 5 to 9 percent higher $PM_{2.5}$ OM levels. The reason for this response to NO_x reductions is the enhancement of VOC oxidation under conditions with higher VOC-to-NO_x ratios. Changing SO_2 emissions did not significantly affect predicted OM levels.

7.2.7 Effects of Emission Changes on PM Mass Concentrations

Changes in the gaseous emissions have only a minor effect on PM mass in the fall simulation because the mass is mostly determined by the primary emissions. The $PM_{2.5}$ mass at the highest stations is predicted to increase by 6 percent with the 50 percent NO_x reduction and decrease 7 percent with 50 percent VOC and VOC and NO_x reductions, respectively. The PM_{10} mass at the highest stations is estimated to increase by 3 percent with the 50 percent NO_x reduction and decrease 4 percent with 50 percent VOC and VOC and NO_x reductions, respectively. Whereas, a 100 percent increase in primary PM emissions increases the predicted $PM_{2.5}$ and PM_{10} concentrations by 71 and 82 percent at the highest stations. These sensitivities are not realistic because the winter emissions inventory drastically overestimates primary emissions, which makes the effects of changes in gaseous emissions on secondary PM appear unrealistically small.

7.2.8 Effects of Emission Changes on Deposition

The predicted effects of the emission changes on regional deposition rates are summarized in **Table 7-6**. The effects on deposition are often similar to the effects on the average concentrations at the SCAQS stations.

The deposition of most gases is predicted to increase in the simulation with 50 percent NO_x emission reduction. For example, ozone, formic acid, acetic acid, hydrogen peroxide, and PAN deposition are predicted to increase substantially because the photochemistry is more

efficient in the higher VOC-to-NO_x regime. However, nitric acid and NO_2 deposition are estimated to decrease by 22 and 39 percent with the 50 percent NO_x emission reduction. PM nitrate and sulfate deposition are increased slightly under this scenario.

The 50 percent VOC emission reduction is estimated to reduce ozone, NO_2, nitric acid, formic acid, and acetic acid deposition by 10 to 19 percent. Large reductions in deposition are estimates for PAN and aldehydes. PM nitrate deposition is estimated to decrease by 5 percent with 50 percent lower VOC emissions.

The deposition of all species except ozone and hydrogen peroxide is lower for the scenario with reduced VOC and NO_x emissions. NO_2, nitric acid, formic acid, acetic acid, and PAN deposition are estimated to decrease by 40, 29, 18, 18, and 5 percent in this case. PM nitrate and ammonium are also predicted to decline by 6 and 14 percent.

Reduction in SO_2 emissions is estimated to reduce SO_2 deposition by 48 percent and reduce sulfate deposition by only 2 percent in the fall. PM nitrate deposition is estimated to increase, while nitric acid deposition is estimated to decrease.

Lastly, the results for the 100 percent increase in primary PM emissions suggests deposition of all components of PM would increase. Deposition of OM, EC, and crustal material is estimated to increase by 76, 87, and 93 percent. PM nitrate and ammonium deposition is estimated to increase by 13 and 7 percent, and sulfate deposition is estimated to increase by 33 percent. The increased deposition of secondary aerosol occurs because more of the secondary material condenses on larger particles and, therefore, deposits more rapidly with higher primary emissions (which are mostly coarse mode particles). However, the large increase in sulfate deposition is partially due to enhanced primary sulfate emissions under this scenario.

Table 7-1. Predicted response in 1-hr ozone, NO_2, and NO concentrations to regionwide emission changes for the June 24-25, 1987 episode.

Case	Day	Maximum Concentration in Domain	Percent Change	Concentration at Highest Station	Percent Change	Average Concentration at Stations	Percent Change
Ozone (ppb)							
Baseline	175	404.8	0	152.2	0	90.6	0
Baseline	176	353.5	0	199.1	0	85.5	0
50% NO_x Reduction	175	451.2	11	183.1	20	103.7	14
50% NO_x Reduction	176	300.5	-15	185	-7	103.8	21
50% VOC Reduction	175	272	-33	88.9	-42	72.2	-20
50% VOC Reduction	176	230.1	-35	118.2	-41	66.3	-22
50% NO_x and VOC	175	337.8	-17	146.6	-4	89.4	-1
50% NO_x and VOC	176	261.2	-26	164.1	-18	86.3	1
NO_2 (ppb)							
Baseline	175	230.3	0	92.5	0	35.1	0
Baseline	176	279.9	0	99.4	0	42.9	0
50% NO_x Reduction	175	156.7	-32	49	-47	15.4	-56
50% NO_x Reduction	176	185.6	-34	38.4	-61	19.6	-54
50% VOC Reduction	175	217.6	-6	87.4	-5	34.9	-1
50% VOC Reduction	176	257	-8	76.9	-23	42	-2
50% NO_x and VOC	175	153.3	-33	49.5	-46	16.6	-53
50% NO_x and VOC	176	178.5	-36	48.3	-51	21	-51

Table 7-1. Predicted response in 1-hr ozone, NO_2, and NO concentrations to regionwide emission changes for the June 24-25, 1987 episode.

Case	Day	Maximum Concentration in Domain	Percent Change	Concentration at Highest Station	Percent Change	Average Concentration at Stations	Percent Change
NO (ppb)							
Baseline	175	633.9	0	16.5	0	15.2	0
Baseline	176	867.9	0	19.3	0	19.6	0
50% NO_x Reduction	175	276.7	-56	5	-70	4.2	-72
50% NO_x Reduction	176	385.9	-56	3.6	-81	5.4	-72
50% VOC Reduction	175	648.1	2	19.3	17	17.6	16
50% VOC Reduction	176	896.1	3	23.8	23	22	12
50% NO_x and VOC	175	280.2	-56	6.1	-63	5.3	-65
50% NO_x and VOC	176	393.9	-55	4.3	-78	6.6	-66

Table 7-2. Predicted response in 24-hr average aerosol, nitric acid, and ammonia concentrations to region-wide emission changes for the June 24-25, 1987 episode.

Case	Maximum Concentration in Domain	Percent Change	Concentration at Highest Station	Percent Change	Average Concentration at Stations	Percent Change
$PM_{2.5}$ NO_3						
Baseline	48.1	0	26.8	0	16.8	0
50% NO_x Reduction	33.5	-30	14.4	-46	13.4	-20
50% VOC Reduction	42	-13	25.1	-7	15.5	-8
50% NO_x and VOC	33.7	-30	15.9	-41	13	-22
50% NH_3 Reduction	31.1	-35	22.4	-17	9.9	-41
50% SO_2 Reduction	48.2	0	26.9	0	18	7
50% PM Reduction	48.2	0	27.5	3	17.4	3
100% PM Increase	47.7	-1	26.6	-1	16.4	-2
PM_{10} NO_3						
Baseline	59	0	32.5	0	20.8	0
50% NO_x Reduction	40.1	-32	18.9	-42	17	-18
50% VOC Reduction	54	-9	30.7	-6	19.6	-6
50% NO_x and VOC	40.1	-32	20.3	-37	16.7	-20
50% NH_3 Reduction	38.8	-34	27.3	-16	13.1	-37
50% SO_2 Reduction	59.8	1	32.8	1	22.5	8
50% PM Reduction	59.1	0	32.5	0	20.4	-2
100% PM Increase	58.8	0.	32.5	0.	20.7	0.

Table 7-2. Predicted response in 24-hr average aerosol, nitric acid, and ammonia concentrations to region-wide emission changes for the June 24-25, 1987 episode.

Case	Maximum Concentration in Domain	Percent Change	Concentration at Highest Station	Percent Change	Average Concentration at Stations	Percent Change
$PM_{2.5}$ NH_4						
Baseline	15.9	0	10	0	7.7	0
50% NO_x Reduction	13.1	-18	6.4	-36	6.9	-11
50% VOC Reduction	13.9	-13	9.5	-5	7.3	-5
50% NO_x and VOC	12.4	-22	6.9	-31	6.8	-12
50% NH_3 Reduction	10.7	-32	8.6	-14	5.1	-34
50% SO_2 Reduction	15.4	-3	9.3	-7	7.3	-5
50% PM Reduction	15.7	-1	10.1	1	7.8	1
100% PM Increase	16	1	10.1	1	7.8	1
PM_{10} NH_4						
Baseline	19.7	0	12	0	9	0
50% NO_x Reduction	15.3	-22	8.1	-33	8	-11
50% VOC Reduction	18	-9	11.5	-4	8.7	-4
50% NO_x and VOC	15	-24	8.5	-29	7.9	-12
50% NH_3 Reduction	13.5	-32	10.4	-14	6.2	-32
50% SO_2 Reduction	19.2	-3	11.2	-6	8.5	-5
50% PM Reduction	19.7	0	12	0	9.1	1
100% PM Increase	19.9	1	12.2	2	9.2	2

Table 7-2. Predicted response in 24-hr average aerosol, nitric acid, and ammonia concentrations to region-wide emission changes for the June 24-25, 1987 episode.

Case	Maximum Concentration in Domain	Percent Change	Concentration at Highest Station	Percent Change	Average Concentration at Stations	Percent Change
$PM_{2.5}$ OM						
Baseline	19.1	0	8.7	0	6.4	0
50% NO_x Reduction	19.6	3	9.2	6	6.7	4
50% VOC Reduction	17.4	-9	7.8	-10	5.9	-8
50% NO_x and VOC	17.8	-7	8.1	-6	6.1	-6
50% NH_3 Reduction	18.9	-1	8.4	-3	6.3	-2
50% SO_2 Reduction	19.1	0	8.7	0	6.5	0
50% PM Reduction	17.2	-10	6	-31	4.7	-27
100% PM Increase	29	52	13.9	60	10.1	56
PM_{10} OM						
Baseline	27.7	0	17.1	0	12.9	0
50% NO_x Reduction	28.6	3	17.2	1	13.2	2
50% VOC Reduction	25.7	-7	16.5	-4	12.5	-4
50% NO_x and VOC	26.4	-5	16.6	-3	12.6	-2
50% NH_3 Reduction	27.6	0	17	0	12.9	0
50% SO_2 Reduction	27.7	0	17.1	0	12.9	0
50% PM Reduction	23	-17	11.1	-35	8.8	-32
100% PM Increase	46.3	67	28.9	69	21.3	65

Table 7-2. Predicted response in 24-hr average aerosol, nitric acid, and ammonia concentrations to region-wide emission changes for the June 24-25, 1987 episode.

Case	Maximum Concentration in Domain	Percent Change	Concentration at Highest Station	Percent Change	Average Concentration at Stations	Percent Change
$PM_{2.5}$ Mass						
Baseline	100.8	0	68	0	53.1	0
50% NO_x Reduction	93.8	-7	60	-12	50.1	-6
50% VOC Reduction	91.7	-9	63.9	-6	50.8	-4
50% NO_x and VOC	91.7	-9	58.8	-13	48.7	-8
50% NH_3 Reduction	77.4	-23	56.4	-17	42.2	-21
50% SO_2 Reduction	100.2	-1	66.7	-2	51.6	-3
50% PM Reduction	85.9	-15	57.8	-15	45.7	-14
100% PM Increase	130.1	29	88.4	30	68.3	29
PM_{10} Mass						
Baseline	159.8	0	120.7	0	89.8	0
50% NO_x Reduction	151.6	-5	103.3	-14	85.9	-4
50% VOC Reduction	149.8	-6	117.7	-3	87.7	-2
50% NO_x and VOC	148.5	-7	104.7	-13	84.7	-6
50% NH_3 Reduction	131.3	-18	113.5	-6	78.4	-13
50% SO_2 Reduction	159.6	0	117.9	-2	87.9	-2
50% PM Reduction	123.5	-23	91.3	-24	68.8	-23
100% PM Increase	233.2	46	177.8	47	129.4	44

Table 7-2. Predicted response in 24-hr average aerosol, nitric acid, and ammonia concentrations to region-wide emission changes for the June 24-25, 1987 episode.

Case	Maximum Concentration in Domain	Percent Change	Concentration at Highest Station	Percent Change	Average Concentration at Stations	Percent Change
$PM_{2.5}$ SO_4						
Baseline	32.7	0	7.4	0	8.1	0
50% NO_x Reduction	32.2	-1	7.4	0	8.2	2
50% VOC Reduction	32.4	-1	7.4	0	8.0	-1
50% NO_x and VOC	32.2	-1	7.4	0	8.1	1
50% NH_3 Reduction	33.4	2	7.2	-3	8.0	-1
50% SO_2 Reduction	22.3	-32	5.0	-32	5.5	-32
50% PM Reduction	30.5	-7	7.2	-3	8.0	-1
100% PM Increase	36.4	11	8.0	9	8.7	8
PM_{10} SO_4						
Baseline	39.3	0	8.7	0	10.8	0
50% NO_x Reduction	39.3	0	8.7	0	11.0	2
50% VOC Reduction	39.2	0	8.7	0	10.8	-1
50% NO_x and VOC	39.3	0	8.7	0	10.9	1
50% NH_3 Reduction	39.3	0	8.7	0	10.8	0
50% SO_2 Reduction	27.2	-31	6.4	-26	7.7	-29
50% PM Reduction	37.3	-5	8.2	-6	10.4	-4
100% PM Increase	43.3	10	9.8	12	11.8	9

Table 7-2. Predicted response in 24-hr average aerosol, nitric acid, and ammonia concentrations to region-wide emission changes for the June 24-25, 1987 episode.

Case	Maximum Concentration in Domain	Percent Change	Concentration at Highest Station	Percent Change	Average Concentration at Stations	Percent Change
HNO_3 (ppb)						
Baseline	34.3	0	4.6	0	3.8	0
50% NO_x Reduction	15.2	-56	3.6	-21	2.4	-36
50% VOC Reduction	27.2	-21	3.2	-30	3.1	-17
50% NO_x and VOC	16.7	-51	2.9	-36	2.2	-41
50% NH_3 Reduction	37.7	10	7.4	62	5.9	57
50% SO_2 Reduction	33.8	-2	4.3	-5	3.3	-13
50% PM Reduction	34.3	0	4.7	4	4	6
100% PM Increase	34.4	0	4.5	-1	3.8	0
NH_3 (ppb)						
Baseline	68.2	0	31.3	0	18	0
50% NO_x Reduction	73.1	7	36.5	17	20.9	17
50% VOC Reduction	68.1	0	32	2	18.8	5
50% NO_x and VOC	72.4	6	35.9	15	20.9	16
50% NH_3 Reduction	29.9	-56	11	-65	6.2	-66
50% SO_2 Reduction	68.6	1	32.3	3	18.8	5
50% PM Reduction	68.2	0	31.2	0	17.9	0
100% PM Increase	68.1	0	31	-1	17.7	-1

[a] Nitric acid at Burbank on June 24.

Table 7-3. Estimated effects of emissions changes on regional deposition rates for the June 24-25, 1987 episode.

Species	Baseline (moles/ hectare-day)	Percentage Change in Regional Deposition Rate						
		50% NO_x Reduction	50% VOC Reduction	NO_x & VOC Reduction	50% NH_3 Reduction	50% SO_2 Reduction	50% PM Reduction	100% PM Increase
O_3	2.86	7	-17	-4	0	0	0	0
NO_2	0.226	-65	16	-56	0	0	0	0
HNO_3	0.611	-47	-9	-44	28	-5	3	0
NH_3	0.146	30	2	26	-53	4	-3	-1
H_2O_2	0.25	14	-8	2	0	3	0	0
HCHO	0.197	2	-25	-22	0	0	0	0
CCHO	0.0513	4	-29	-28	0	0	0	0
RCHO	0.0169	3	-35	-34	0	0	0	0
PAN	0.0483	3	-41	-28	0	0	0	0
PPN	0.018	3	-41	-28	0	1	0	0
SO_2	0.0591	-1	0	-1	0	-53	0	0
FACD	0.0322	15	-38	-31	0	0	0	0
AACD	0.0215	6	-29	-26	0	0	0	0
HCL	0.0803	-2	0	-2	8	-3	-35	12
HONO	0.00191	-53	8	-48	0	0	0	0
XOOH	0.0464	39	-21	1	0	0	0	0
RNO_3	0.0257	5	-37	-31	0	0	0	0

Table 7-3. Estimated effects of emissions changes on regional deposition rates for the June 24-25, 1987 episode.

Species	Baseline (moles/ hectare-day)	Percentage Change in Regional Deposition Rate						
		50% NO_x Reduction	50% VOC Reduction	NO_x & VOC Reduction	50% NH_3 Reduction	50% SO_2 Reduction	50% PM Reduction	100% PM Increase
PM_{10} NO_3	6.07	-15	0	-13	-28	9	-19	3
PM_{10} NH_4	1.82	-12	1	-10	-28	-4	2	2
PM_{10} SO_4	3.66	3	1	4	3	-17	-8	10
PM_{10} EC	0.552	2	2	3	3	1	-39	78
PM_{10} OM	7.36	2	-1	0	2	1	-31	62
PM_{10} Crustal	19.1	1	1	1	2	0	-44	90
PM_{10} NA	1.83	1	0	1	1	2	-41	13
PM_{10} CL	0.236	11	0	11	-15	10	-82	25
PM_{10} H_2O	27.4	-3	0	-3	-6	-2	-25	6

Table 7-4. Predicted response in 1-hr ozone, NO_2, and NO concentrations to region-wide emission changes for the December 10-11, 1987 episode.

Run	Day	Maximum Concentration in Domain	Percent Change	Concentration at Highest Station	Percent Change	Average Concentration at Stations	Percent Change
Ozone(ppb)							
Baseline	344	90	0	40.8	0	34.7	0
Baseline	345	122	0	39.7	0	30.4	0
50% NO_x Reduction	344	185	106	73	79	75.8	118
50% NO_x Reduction	345	280	129	62.8	58	72.1	137
50% VOC Reduction	344	90	0	33	-19	21.9	-37
50% VOC Reduction	345	80	-35	34.1	-14	19.2	-37
50% NO_x and VOC	344	104	16	51.5	26	45.3	31
50% NO_x and VOC	345	108	-12	49.8	26	42.5	40
NO_2(ppb)							
Baseline	344	272	0	166.7	0	68.6	0
Baseline	345	320	0	114.5	0	65.8	0
50% NO_x Reduction	344	203	-25	149.7	-10	51.7	-25
50% NO_x Reduction	345	200	-38	116.4	2	51.3	-22
50% VOC Reduction	344	236	-13	123.9	-26	57.1	-17
50% VOC Reduction	345	303	-5	96.4	-16	56.3	-14
50% NO_x and VOC	344	152	-44	108	-35	46	-33
50% NO_x and VOC	345	186	-42	83.7	-27	44.3	-33

Table 7-4. Predicted response in 1-hr ozone, NO_2, and NO concentrations to region-wide emission changes for the December 10-11, 1987 episode.

Run	Day	Maximum Concentration in Domain	Percent Change	Concentration at Highest Station	Percent Change	Average Concentration at Stations	Percent Change
NO (ppb)							
Baseline	344	1015	0	340.9	0	105	0
Baseline	345	1496	0	490.5	0	130	0
50% NO_x Reduction	344	413	-59	114	-67	26.6	-75
50% NO_x Reduction	345	706	-53	169.6	-65	35.3	-73
50% VOC Reduction	344	1049	3	361.7	6	120	14
50% VOC Reduction	345	1515	1	507	3	144	11
50% NO_x and VOC	344	473	-53	142	-58	39.3	-63
50% NO_x and VOC	345	744	-50	214.2	-56	50.4	-61

Table 7-5. Predicted response in 24-hr average aerosol, nitric acid, and ammonia concentrations to region-wide emission changes for the December 10-11, 1987 episode.

Case	Maximum Concentration in Domain	Percent Change	Concentration at Highest Station	Percent Change	Average Concentration at Stations	Percent Change
$PM_{2.5}$ NO_3						
Baseline	61.4	0	20.3	0	18.7	0
50% NO_x Reduction	87	42	24.5	20	20.5	9
50% VOC Reduction	35.6	-42	14.7	-28	13.6	-27
50% NO_x and VOC	49	-20	14.5	-29	13.3	-29
50% SO_2 Reduction	66.1	8	21.2	4	19.3	3
100% PM Increase	62.3	1	20.3	0	18.6	-1
PM_{10} NO_3						
Baseline	81.6	0	24.8	0	22.8	0
50% NO_x Reduction	111.7	37	28.9	17	24.8	9
50% VOC Reduction	50.2	-38	18.2	-27	17.2	-25
50% NO_x and VOC	66.6	-18	17.8	-28	16.6	-27
50% SO_2 Reduction	86.9	6	25.8	4	23.6	4
100% PM Increase	84	3	24.8	0	22.8	0

Table 7-5. Predicted response in 24-hr average aerosol, nitric acid, and ammonia concentrations to region-wide emission changes for the December 10-11, 1987 episode.

Case	Maximum Concentration in Domain	Percent Change	Concentration at Highest Station	Percent Change	Average Concentration at Stations	Percent Change
$PM_{2.5}$ NH_4						
Baseline	18.9	0	8.8	0	6.4	0
50% NO_x Reduction	27.4	45	9.3	6	7	8
50% VOC Reduction	13.6	-28	6.8	-23	5	-22
50% NO_x and VOC	15.4	-18	6.5	-27	5	-23
50% SO_2 Reduction	19.8	5	8.9	1	6.5	1
100% PM Increase	20.9	11	9.6	9	7	10
PM_{10} NH_4						
Baseline	25.9	0	9.1	0	7.8	0
50% NO_x Reduction	35.5	37	10.3	14	8.4	9
50% VOC Reduction	16.3	-37	7.1	-21	6.2	-20
50% NO_x and VOC	21.1	-18	7	-23	6.1	-21
50% SO_2 Reduction	26.7	3	9.3	2	7.9	1
100% PM Increase	27.9	8	10.4	15	8.7	12

Table 7-5. Predicted response in 24-hr average aerosol, nitric acid, and ammonia concentrations to region-wide emission changes for the December 10-11, 1987 episode.

Case	Maximum Concentration in Domain	Percent Change	Concentration at Highest Station	Percent Change	Average Concentration at Stations	Percent Change
$PM_{2.5}$ SO_4						
Baseline	26	0	3.9	0	2.9	0
50% NO_x Reduction	26	0	3.9	2	3	1
50% VOC Reduction	25.4	-2	3.7	-3	2.8	-4
50% NO_x and VOC	25.6	-2	3.8	-2	2.9	-2
50% SO_2 Reduction	19.1	-26	3.3	-16	2.6	-12
100% PM Increase	36.8	42	5.8	50	4.6	55
PM_{10} SO_4						
Baseline	29.3	0	5.7	0	4.9	0
50% NO_x Reduction	29.3	0	5.9	2	4.9	1
50% VOC Reduction	28.6	-2	5.7	-1	4.7	-2
50% NO_x and VOC	28.8	-1	5.7	0	4.8	-1
50% SO_2 Reduction	22.1	-24	5.2	-10	4.5	-8
100% PM Increase	42.4	45	8.9	55	7.6	57

Table 7-5. Predicted response in 24-hr average aerosol, nitric acid, and ammonia concentrations to region-wide emission changes for the December 10-11, 1987 episode.

Case	Maximum Concentration in Domain	Percent Change	Concentration at Highest Station	Percent Change	Average Concentration at Stations	Percent Change
$PM_{2.5}$ Mass						
Baseline	190	0	116	0	86	0
50% NO_x Reduction	223	18	123	6	89	4
50% VOC Reduction	166	-13	107	-7	79	-8
50% NO_x and VOC	167	-12	107	-7	79	-8
50% SO_2 Reduction	190	0	116	1	86	0
100% PM Increase	308	63	197	71	141	65
PM_{10} Mass						
Baseline	388	0	242	0	186	0
50% NO_x Reduction	440	13	250	3	192	3
50% VOC Reduction	353	-9	232	-4	179	-4
50% NO_x and VOC	374	-4	233	-4	179	-4
50% SO_2 Reduction	401	3	243	0	188	1
100% PM Increase	700	81	440	82	333	79

Table 7-5. Predicted response in 24-hr average aerosol, nitric acid, and ammonia concentrations to region-wide emission changes for the December 10-11, 1987 episode.

Case	Maximum Concentration in Domain	Percent Change	Concentration at Highest Station	Percent Change	Average Concentration at Stations	Percent Change
HNO_3(ppb)						
Baseline	14.3	0	0.9	0	0.9	0
50% NO_x Reduction	4	-72	0.9	4	0.9	4
50% VOC Reduction	4.3	-70	0.7	-21	0.7	-21
50% NO_x and VOC	2.3	-84	0.7	-21	0.7	-21
50% SO_2 Reduction	10.7	-25	0.9	1	0.9	1
100% PM Increase	10.2	-28	0.9	5	0.9	5
NH_3(ppb)						
Baseline	363	0	38	0	32.5	0
50% NO_x Reduction	363	0	38.7	2	32	-1
50% VOC Reduction	369	2	38.8	2	34.4	6
50% NO_x and VOC	367	1	39.3	4	34.6	7
50% SO_2 Reduction	366	1	38	0	32.3	0
100% PM Increase	364	0	37.7	-1	31.3	-4

Table 7-5. Predicted response in 24-hr average aerosol, nitric acid, and ammonia concentrations to region-wide emission changes for the December 10-11, 1987 episode.

Case	Maximum Concentration in Domain	Percent Change	Concentration at Highest Station	Percent Change	Average Concentration at Stations	Percent Change
$PM_{2.5}$ OM						
Baseline	37.5	0	23.7	0	18	0
50% NO_x Reduction	40.7	9	24.8	5	18.8	5
50% VOC Reduction	34.3	-9	22.6	-5	17.1	-5
50% NO_x and VOC	35.6	-5	22.9	-3	17.4	-3
50% SO_2 Reduction	37.9	1	23.6	0	18	0
100% PM Increase	70.6	88	43.9	85	33.2	85
PM_{10} OM						
Baseline	75.7	0	46.9	0	38.3	0
50% NO_x Reduction	81.5	8	48.1	3	39.4	3
50% VOC Reduction	74	-2	45.8	-2	37.5	-2
50% NO_x and VOC	75.9	0	46.2	-2	37.9	-1
50% SO_2 Reduction	78.2	3	46.8	0	38.4	0
100% PM Increase	149	97	88.6	89	72.2	89

Table 7-5. Predicted response in 24-hr average aerosol, nitric acid, and ammonia concentrations to region-wide emission changes for the December 10-11, 1987 episode.

Case	Maximum Concentration in Domain	Percent Change	Concentration at Highest Station	Percent Change	Average Concentration at Stations	Percent Change
$PM_{2.5}$ EC						
Baseline	12	0	5.4	0	4	0
50% NO_x Reduction	12	0	5.4	1	4	1
50% VOC Reduction	11.9	-1	5.4	0	4	0
50% NO_x and VOC	12	0	5.4	0	4	0
50% SO_2 Reduction	12	0	5.4	0	4	0
100% PM Increase	23.9	99	10.6	97	7.8	96
PM_{10} EC						
Baseline	14.8	0	7.2	0	5.9	0
50% NO_x Reduction	14.8	0	7.3	1	5.9	1
50% VOC Reduction	14.7	-1	7.2	0	5.9	0
50% NO_x and VOC	14.8	0	7.2	0	5.9	1
50% SO_2 Reduction	14.8	0	7.2	0	5.9	0
100% PM Increase	29.3	98	14.2	96	11.5	96

Table 7-6. Estimated effects of emission changes on regional deposition rates for the December 10-11, 1987 episode.

Species	Baseline (moles/hectare-day)	Percentage Change in Regional Deposition Rate				
		50% NO_x Reduction	50% VOC Reduction	NO_x & VOC Reduction	50% SO_2 Reduction	100% PM Increase
O_3	0.777	33	-12	11	0	0
NO_2	0.205	-39	-10	-40	-1	0
HNO_3	0.155	-22	-19	-29	-4	-3
NH_3	0.268	2	8	9	1	-1
H_2O_2	0.007	70	-14	21	2	-0
HCHO	0.086	15	-30	-23	0	0
CCHO	0.033	6	-24	-22	0	0
RCHO	0.011	10	-31	-26	0	0
PAN	0.012	63	-34	-5	0	0
PPN	0.003	76	-36	-3	0	0
SO_2	0.104	3	3	0	-48	3
FACD	0.012	47	-33	-18	-1	0
AACD	0.010	25	-27	-18	-1	0
HCL	0.027	0	0	0	0	0
HONO	0.006	-51	-4	-50	0	0
XOOH	0.002	107	-20	25	2	0
RNO_3	0.009	35	-39	-23	0	0

Table 7-6. Estimated effects of emission changes on regional deposition rates for the December 10-11, 1987 episode.

Species	Baseline (grams/hectare-day)	Percentage Change in Regional Deposition Rate				
		50% NO_x Reduction	50% VOC Reduction	NO_x & VOC Reduction	50% SO_2 Reduction	100% PM Increase
PM_{10} NO_3	4.58	5	-5	-6	17	13
PM_{10} NH_4	1.21	-2	-2	-14	1	7
PM_{10} SO_4	0.94	3	2	2	-2	33
PM_{10} EC	0.55	0	0	0	0	87
PM_{10} OM	6.0	2	1	1	0	76
PM_{10} Crustal	18.3	0	0	0	0	93

Conclusions

This report is a description of a three-dimensional, urban acid deposition model and its application to the South Coast Air Basin of California. With an impending PM2.5 air quality standard, such a model will be a necessary component to evaluate the effect of emission control strategies on both gaseous and particulate concentration levels in an urban area. The model can be viewed as an extension of the photochemical air quality model into the particulate domain. The present model is based on a rigorous formulation of aerosol chemistry and physics, including both size and composition resolution. Computationally the aerosol model is as intensive as the gas-phase photochemical model on which it sits and computational efficiency issues will be important in its application. The current model includes only an empirical treatment of fogs and their effect on gas and aerosol evolution. This aspect could be made more rigorous in future work.

The full model has been delivered to the Air Resources Board for its use. It is anticipated that this model will be used in the future to evaluate trade-offs in gas and particle emissions control measures in conjunction with impending PM air quality standards.

Chapter 1 References

Pandis, S.N., Seinfeld, J.H., and Pilinis, C. (1992). Heterogeneous sulfate production in an urban fog, *Atmos. Environ., 26A*, 2509-2522.

Pandis, S. N., Wexler, A. S., Seinfeld, J. H. (1993) Secondary organic aerosol formation and transport - II. Predicting the ambient secondary organic aerosol size distribution. *Atmos. Environ. 27A*:2403-2416.

Pilinis, C., Seinfeld, J. H. (1988) Development and evaluation of an Eulerian photochemical gas-aerosol model. *Atmos. Environ., 22*:1985-2001.

Seinfeld, J. H. (1986). Atmospheric Chemistry and Physics of Air Pollution, John Wiley, New York, NY.

U.S. Environmental Protection Agency (1994) Ozone criteria document. Research Triangle Park, NC (in press).

Wexler, A. S., Lurmann, F. W., Seinfeld, J. H. (1994) Modeling urban and regional aerosols-1. Model development. *Atmos. Environ.*

Chapter 2 References

Allen A.G., Harrison, R.M., and Erisman, J. (1989) Field measurements of the dissociation of ammonium nitrate and ammonium chloride aerosols, *Atmos. Environ., 23*:1591-1599.

Bassett, M. and Seinfeld, J.H. (1983) Atmospheric equilibrium model of sulfate and nitrate aerosols, *Atmos. Environ., 17*:2237-2252.

Bassett, M. and Seinfeld, J.H. (1984) Atmospheric equilibrium model of sulfate and nitrate aerosols - II. Particle size analysis, *Atmos. Environ., 18*:1163-1170.

Cadle, S.H., Countess, R.J., Kelly, N.A. (1982) *Atmos. Environ., 16*:2501.

Covert, D. S. and Heintzenberg, J. (1984) Measurement of the degree of internal/external mixing of hygroscopic compounds and soot in atmospheric aerosols, *Sci. Total Environ., 36*:347-352.

Doyle, G.J., Tuazon, E.C., Graham, R.A., Mischke, T.M., Winer, A.M., Pitts, J.N. (1979) Simultaneous concentrations of ammonia and nitric acid in a polluted atmosphere and their equilibrium relationship to particulate ammonium nitrate, *Environ. Sci. Technol., 13*:1416-1419.

Eldering, A., Solomon, P.A., Salmon, L. G., Fall, T., and Cass, G.R. (1991) Hydrochloric acid: A regional perspective on concentrations and formation in the atmosphere of Southern California, *Atmos. Environ., 25A*:2091-2102.

Gelbard, F., Tambour, Y. and Seinfeld, J.H. (1980) Sectional representation for simulating aerosol dynamics, *J. Colloid Interface Sci., 76*:541-556.

Gray, H. A., Cass, G. R., Huntzicker, J. J., Heyerdahl, E. K., Rau, J. A. (1986) Characteristics of atmospheric organic and elemental carbon particle concentrations in Los Angeles. *Envir. Sci. Technol., 20*:580-589.

Grosjean, D. (1977) Aerosols Chapter 3, in *Ozone and Other Photochemical Oxidants*, National Academy of Sciences, Washington, D.C., 45-125.

Grosjean, D. (1982) The stability of particulate nitrate in the Los Angeles atmosphere, *Sci. Total Environ., 25*, 263-275.

Grosjean, D. and Seinfeld, J.H. (1989) Parametrization of the formation potential of secondary organic aerosols, *Atmos. Environ., 23*:1733-1747.

Hildemann, L.M., Russell, A.G., and Cass, G.R. (1984) Ammonia and nitric acid concentrations in equilibrium with atmospheric aerosols: Experiment vs. theory, *Atmos. Environ., 18*:1737-1750.

Larson, S. M., Cass, G. R. (1989) Characteristics of summer midday low-visibility events in the Los Angeles area. *Envir. Sci. Technol., 23*:281-289.

McMurry, P.H. and Stolzenburg, M.R. (1989) On the sensitivity of particle size to relative humidity for Los Angeles aerosols, *Atmos. Environ., 21*:2453-2466.

McMurry, P.H. and Zhang, X.Q. (1989) Size distributions of ambient organic and elemental carbon, *Aerosol Sci. and Technol., 10*:430-437.

Meng, Z. and Seinfeld, J.H. (1996) "Time Scales to Achieve Atmospheric Gas-Aerosol Equilibrium for Volatile Species," *Atmos. Environ., 30*:2889-2900.

Pandis S. N., Seinfeld, J.H., and Pilinis, C. (1992) Heterogeneous sulfate production in an urban fog, *Atmos. Environ., 26A*:2509-2522.

Pandis, S.N., Harley, R.A., Cass, G.R., and Seinfeld, J.H. (1992a) Secondary organic aerosol formation and transport, *Atmos. Environ., 26A*:2269-2282.

Pandis, S.N., Wexler, A.S., and Seinfeld, J.H. (1993) Secondary organic aerosol formation and transport - II. Predicting the ambient secondary organic aerosol size distribution, *Atmos. Environ., 27A*:2403-2416.

Pankow, J.F. (1987) Review and comparative analysis of the theories on partitioning between the gas and aerosol particulate phases in the atmosphere, *Atmos. Environ., 21*:2275-2283.

Pilinis, C. (1990) Derivation and numerical solution of the species mass distribution equations for multicomponent particulate systems, *Atmos. Environ., 24A*:1923-1928.

Pilinis, C. and Seinfeld, J.H. (1988) Development and evaluation of an Eulerian photochemical gas-aerosol model, *Atmos. Environ., 22*:1985-2001.

Pilinis, C., Seinfeld, J. H. (1987) Continued development of a general equilibrium model for inorganic multicomponent atmospheric aerosols. *Atmos. Environ., 21*:2453-2466.

Pilinis, C., Seinfeld, J.H., Grosjean, D. (1989) Water content of atmospheric aerosols. *Atmos. Environ., 23:*1601-1606.

Russell, A.G. and Cass, G.R. (1986) Verification of a mathematical model for aerosol nitrate and nitric acid formation and its use for control measure evaluation, *Atmos. Environ., 20*:2011-2025.

Russell, A.G., McCue, K.F., and Cass, G.R. (1988) Mathematical modeling of the formation of nitrogen containing air pollutants I. Evaluation of an Eulerian photochemical model, *Environ. Sci. Technol., 22:263-271.*

Russell, A.G., McRae, G.J., Cass, G.R. (1983) Mathematical modeling of the formation and transport of ammonium nitrate aerosol, *Atmos. Environ., 17*:949-964.

Saxena, P., Hudischewskyj, A.B., Seigneur, C., Seinfeld, J.H. (1986) A comparative study of equilibrium approaches to the chemical characterization of secondary aerosols, *Atmos. Environ., 20*:1471-1483.

Saxena, P., Seigneur, C., Peterson, T.W. (1983) Modeling of multiphase atmospheric aerosols, *Atmos. Environ., 17*:1315-1329.

Seigneur, C., Hudischewskyj, A.B., Seinfeld, J.H., Whitby, K.T., Whitby, E.R., Brock, J.R., and Barnes, H.M. (1986) Simulation of aerosol dynamics: A comparative review of mathematical models, *Aeros. Sci. Tech., 5*:205-222.

Seinfeld, J. H. (1986) *Atmospheric Physics and Chemistry of Air Pollution*, John Wiley & Sons, New York.

Seinfeld, J.H. (1989) Urban air pollution: State of science, *Science, 243*:745-752.

Stelson, A. W., Seinfeld, J. H. (1982a) Relative humidity and temperature dependence of the ammonium nitrate dissociation constant. *Atmos. Environ., 16*:983-992.

Stelson, A. W., Seinfeld, J. H. (1982b) Relative humidity and pH-dependence of the vapor pressure of ammonium nitrate-nitric acid solutions at 25°C. *Atmos. Environ., 16*:993-1000.

Stelson, A.W., Friedlander, S.K., and Seinfeld, J.H. (1979) A note on the equilibrium relationship between ammonia and nitric acid and particulate ammonium nitrate, *Atmos. Environ., 13*:369-371.

Tanner, R. L. (1982) An ambient experimental study of phase equilibrium in the atmosphere, *Atmos. Environ., 16*:2935-2942.

Turpin, B.J. and Huntzicker, J.J. (1991) Secondary formation of organic aerosol in the Los Angeles Basin: A descriptive analysis of organic and elemental carbon concentrations, *Atmos. Environ., 25A*:207-215.

Watson, J. G., Chow, J. C., Lurmann, F. W., Musarra, S. P. (1994b) Ammonium nitrate, nitric acid, and ammonia equilibrium in wintertime Phoenix, Arizona, *J. Air Waste Management Assoc., 44*:405-412.

Wexler, A. S., Lurmann, F. W., Seinfeld, J. H. (1994) Modeling urban and regional aerosols-1. Model development. *Atmos. Environ.*

Wexler, A. S., Seinfeld, J. H. (1990) The distribution of ammonium salts among a size and composition dispersed aerosol. *Atmos. Environ., 24A*:1231-1246.

Wexler, A.S. and Seinfeld, J.H. (1992) Analysis of aerosol ammonium nitrate: Departures from equilibrium during SCAQS, *Atmos. Environ., 26A*:579-591.

Chapter 3 References

Boyce, S. D., Hoffmann, M. R. (1984) Kinetics and mechanism of the formation of hydroxymethanesulfonic acid at low pH. *J. Phys. Chem., 88*:4740-4746.

Clarke, A. G., Radojevic, M. (1987) Oxidation of SO_2 in rainwater and its role in acid rain chemistry. *Atmos. Environ., 21*:1115-1123.

Daum, P. H., Kelly, T. J., Schwartz, S. E., Newman, L. (1984) Measurements of the chemical composition of stratiform clouds. Atmos. Environ., 18:2671-2684.

Facchini, M.C., Fuzzi, S., Lind, J.A. (1992) Phase-partitioning and chemical reactions of low-molecular-weight organic compounds in fog. *Tellus, 44B*:533-544.

Hoffmann, M.R. and Jacob, D.J. (1984) Kinetics and mechanisms of the catalytic oxydation of dissolved sulfur dioxide in aqueous solution: An application to nighttime fog water chemistry, in *SO_2, NO, and NO_2 Oxidation Mechanisms: Atmospheric Considerations*, edited by J.G. Calvert, Butterworth, Stoneham, MA, 63-100.

Hoffmann, M. R., Boyce, S. D. (1983) Catalytic autooxidation of aqueous sulfur dioxide in relationship to atmospheric systems. *Adv. Environ. Sci. Technol., 12*:148-189.

Hoffmann, M. R., Calvert, J. G. (1985) Chemical transformation modules for eulerian acid deposition models, vol. 2, The aqueous-phase chemistry, EPA/600/3-85/017, U.S. Environ. Prot. Agency, Research Triangle Park, N. C.

Jacob, D. J. (1986) Chemistry of OH in remote clouds and its role in the production of formic acid and peroxymonosulfate. *J. Geophys. Res., 91*:9807-9826.

Lee, Y. N., Schwartz, S. E. (1983) Kinetics of oxidation of aqueous sulfur(IV) by nitrogen dioxide, in Precipitation Scavenging, Dry Deposition and Resuspension, vol. 1, edited by H. R. Pruppacher, R. G. Semonin, and W. G. N. Slinn, Elsevier, New York.

Lelieveld, J., Crutzen, P.J. (1990) Influences of cloud photochemical processes on tropospheric ozone. *Nature* (London), *343*:227-233.

Lelieveld, J., Crutzen, P.J. (1991) The role of clouds in tropospheric photochemisty. *J. Atmos. Chem., 12*:229-267.

Lelieveld, J., Heintzenberg, J. (1992) Sulfate cooling effect on climate through in-cloud oxidation of anthropogenic SO_2. *Science, 258*:117-120.

Martin, L. R. (1984) Kinetic studies of sulfite oxidation in aqueous solution, in SO_2, NO, and NO_2 Oxidation Mechanisms: Atmospheric Considerations, edited by J. G. Calvert, pp. 63-100, Butterworth, Stoneham, MA.

Martin, L. R., Hill, M. W. (1987a) The iron catalyzed oxidation of sulfur: Reconciliation of the literature rates. *Atmos. Environ., 6:*1487-1490.

Martin, L. R., Hill, M. W. (1987b) The effect of ionic strength on the manganese catalyzed oxidation of sulfur(IV). *Atmos. Environ., 21*:2267-2270.

Munger, J. W., Jacob, D. J. Hoffmann, M. R. (1984) The occurrence of bisulfite-aldehyde addition products in fog- and cloudwater. *J. Atmos. Chem., 1*: 335.

Munger, J.W., Tiller, C., Hoffmann, M.R. (1986) Identification and quantification of hydroxymethanesulfonic acid in atmospheric water droplets. *Science, 231*:247-249.

Olson, T.M., Hoffmann, M.R. (1989) Hydroxyalkylsulfonate formation: Its role as a S(IV) reservoir in atmospheric water droplets. *Atmos. Environ., 23*:985-997.

Pandis, S. N., Seinfeld, J. H. (1989a) Sensitivity analysis of a chemical mechanism for aqueous-phase atmospheric chemistry. *J. Geophys. Res., 94*:1105-1126.

Pandis, S. N., Seinfeld, J. H. (1989a) Sensitivity analysis of a chemical mechanism for aqueous-phase atmospheric chemistry. *J. Geophys. Res., 94*:1105-1126.

Pandis, S. N., Seinfeld, J. H. (1989a) Sensitivity analysis of a chemical mechanism for aqueous-phase atmospheric chemistry. *J. Geophys. Res., 94*:1105-1126.

Pandis, S. N., Seinfeld, J. H. (1989b) Mathematical modeling of acid deposition due to radiation fog. *J. Geophys. Res., 94*:12911-12923.

Pandis, S. N., Seinfeld, J. H. (1989b) Mathematical modeling of acid deposition due to radiation fog. *J. Geophys. Res., 94*:12911-12923.

Penkett, S. A. (1972). Oxidation of SO_2 and the other atmospheric gases by ozone in aqueous solution. *Nature, 240*:105-106.

Seinfeld, J. H. (1986). Atmospheric Chemistry and Physics of Air Pollution, John Wiley, New York, NY.

Warneck, P. (1991) Chemical reactions in clouds. *Fres. J. Anal. Chem., 340*:585-590.

Warneck, P. (1992) Chemistry and photochemistry in atmospheric water drops. *Ber. Bunsen-Ges. Phys. Chem., 96*:454-460.

Chapter 4 References

Bromley L.A. (1973) *AIChE J.* **19**, 313-320.

Calvert J.G. and Stockwell W.R. (1983) *Environ. Sci. Technol.* **17**, 428-443.

Carter W.P.L. (1990) A detailed mechanism for the gas-phase atmospheric reactions of organic compounds. *Atmos. Environ.* **24A**, 481-518.

Carter W.P.L. and Lurmann F.W. (1991) Evaluation of a detailed gas phase atmospheric reaction mechanism using environmental chamber data. *Atmos. Environ.* **25A**, 2771-2806.

Chock D.P., Winkler S.L., and Sun P. (1994) A comparison of stiff chemistry solvers for air quality modeling. Paper presented at the *Air & Waste Management Association 87th Annual Meeting, Cincinnati, OH, June 19-24.*

Gelbard F. (1990) Modeling multicomponent aerosol particle growth by vapor condensation. *Aerosol Sci. Technol.* **12**, 399-412.

Gelbard F., Tambour Y., and Seinfeld J.H. (1980) Sectional representation for simulating aerosol dynamics. *J. Colloid Interface Sci.* **76**, 541-556.

Gery M.W., Whitten G.Z., and Killus J.P. (1988) Development and testing of the CBM-IV for urban and regional modeling. Report prepared by Systems Applications Inc., San Rafael, CA, EPA Contract No. 68-02-4136.

Gray H.A., Ligocki M.P., Moore G.E., Emery C.A., Kessler R.C., Cohen J.P., Chang C.C., Balestrini S.I., Douglas S.G., Schulhof R.R., Killus J.P., and Burton C.S. (1991) Deterministic modeling in the Navajo generating station visibility study. Volume II: appendices A-E. Report prepared for Salt River Project, Phoenix, AZ By Systems Applications International, San Rafael, CA, Report No. SYSAPP-91/045b, April.

Grosjean D. and Seinfeld J.H. (1989) Parameterization of the formation potential of secondary organic aerosols. *Atmos. Environ.* **23**, 1733-1747.

Hicks B.B., Baldocchi D.D., Meyers T.P., Hosker R.P., and Matt D.R. (1987) A preliminary multiple resistance routine for deriving dry deposition velocities from measured quantities. *Water, Air, Soil Poll.* **36**, 311-330.

Hildemann L.M., Russell A.M., and Cass G.R. (1984) Ammonia and nitric acid concentrations in equilibrium with atmospheric aerosols: experiment vs. theory. *Atmos. Environ.* **18**, 1737-1750.

Jacob D.J., Waldman J.M., Munger J.W., and Hoffmann M.R. (1984) A field investigation of physical and chemical mechanisms affecting pollutant concentrations in fog droplets. *Tellus* **36B**, 272-285.

Jacob D.J., Munger J.W., Waldman J.M., and Hoffmann M.R. (1986a) The H_2SO_4-HNO_3 NH_3 system at high humidities and in fogs. 1. Spatial and temporal patterns in the San Joaquin Valley of California. *J. Geophys. Res.* **91**, 1073-1088.

Jacob D.J., Munger J.W., Waldman J.M., and Hoffmann M.R. (1986b) The H_2SO_4-HNO_3 NH_3 system at high humidities and in fogs. 2. Comparison of field data with thermodynamic calculations. *J. Geophys. Res.* **91**, 1089-1096.

Jacob D.J., Shair F.H., Waldman J.M., Munger J.W., and Hoffmann M.R. (1987) Transport and oxidation of SO2 in a stagnant foggy valley. *Atmos. Environ.* **21**, 1305-1314.

Kim Y.P. and Seinfeld J.H. (1990) Simulation of multicomponent aerosol condensation by the moving sectional method. *J. Colloid Interface Sci.* **135**, 185-199.

Kim Y.P., Seinfeld J.H., and Saxena P. (1993a) Atmospheric gas - aerosol equilibrium I. Thermodynamic model. *Aerosol Sci. Technol.* **19**, 157-181.

Kim Y.P., Seinfeld J.H., and Saxena P. (1993b) Atmospheric gas - aerosol equilibrium II. Analysis of common approximations and activity coefficient calculation methods. *Aerosol Sci. Technol.* **19**, 182-198.

Kumar N., Lurmann F.W., and Carter W.P.L. (1995) Development of the flexible chemical mechanism version of the urban airshed model. Final report prepared for the California Air Resources Board, Sacramento, CA by Sonoma Technology, Inc., Santa Rosa, CA, STI-94470-1508-FR, August.

Kusik C.L. and Meissner H.P. (1978) *AIChE Symp. Ser.* **173**, 14-20.

Massman W.J. (1993) Partitioning ozone fluxes to sparse grass and soil and the inferred resistances to dry deposition. *Atmos. Environ.* **27A**, 167-174.

Munger J.W., Jacob D.J., Waldman J.M., and Hoffmann M.R. (1983) Fogwater chemistry in an urban atmosphere. *J. Geophys. Res.* **88**, 5109-5121.

Pandis S.N. (1996) Personal communication.

Pandis S.N. and Seinfeld J.H. (1989) Development of a state-of-the-art acid deposition model for the South Coast Air Basin of California. Report prepared for California Air Resources Board, Sacramento, CA, Contract No. A732-043.

Pandis S.N., Harley R.A., Cass G.R., and Seinfeld J.H. (1992a) Secondary organic aerosol formation and transport. *Atmos. Environ.* **26A**, 2269-2282.

Pandis S.N., Seinfeld J.H., and Pilinis C. (1992b) Heterogeneous sulfate production in an urban fog. *Atmos. Environ.* **26A**, 2509-2522.

Pandis S.N., Wexler A.S., and Seinfeld J.H. (1993) Secondary organic aerosol formation and transport - II. Predicting the ambient secondary organic aerosol size distribution. *Atmos. Environ.* **27A**, 2403-2416.

Peters J.M., Avol E., Cass G., Colome S., Gong H., Hering S., Linn W., London S., Lurmann F., Navidi W., Roberts P., Thomas D., and Reiss R. (1995) Epidemiologic investigation to identify chronic health effects of ambient air pollutants in Southern California: Phase II final report. Report prepared for the California Air Resources Board, Sacramento, CA by the University of Southern California School of Medicine Department of Preventive Medicine, Los Angeles, CA, Contract No. A033-186, May.

Pilinis C. and Seinfeld J.H. (1987) Continued development of a general equilibrium model for inorganic multicomponent atmospheric aerosols. *Atmos. Environ.* **21**, 2453-2466.

Pilinis C. and Seinfeld J.H. (1988) Development and evaluation of an Eulerian photochemical gas-aerosol model. *Atmos. Environ.* **22**, 1985-2001.

Pitzer K.S. (1979) In *Activity Coefficients in Electrolyte Solutions*, Vol. 1, Ptykowicz R.M., ed., CRC Press, Boca Raton, FL, p. 157.

Richards L.W., Musarra S., Lurmann F.W., and Kumar N. (1996) The STI atmospheric light-extinction model. Final report prepared for South Coast Air Quality Management District, Diamond Bar, CA by Sonoma Technology, Inc., Santa Rosa, CA, STI-91070-1564-FR, February.

Russell A., Winner D.A., Harley R.A., McCue K.F., and Cass G.R. (1993) Mathematical modeling and control of the dry deposition flux of nitrogen-containing air pollutants. *Environ. Sci. Technol.* **27**, 2772-2782.

SAI (1990a) User's guide for the urban airshed model. Volume I. Prepared by Systems Applications International, San Rafael, CA, Report No. SYSAPP-90/018a.

SAI (1990b) User's guide for the urban airshed model. Volume II: preprocessors and postprocessors for the UAM modeling system. Prepared by Systems Applications International, San Rafael, CA, Report No. SYSAPP-90/018b.

SAI (1990c) User's guide for the urban airshed model. Volume III: the diagnostic wind model. Prepared by Systems Applications International, San Rafael, CA, Report No. SYSAPP-90/018c.

SAI (1990d) User's guide for the urban airshed model. Volume IV: the emissions preprocessor system. Prepared by Systems Applications International, San Rafael, CA, Report No. SYSAPP-90/018d.

SAI (1990e) User's guide for the urban airshed model. Volume V: description and operation of the ROM-UAM interface program system. Prepared by Systems Applications International, San Rafael, CA, Report No. SYSAPP-90/018e.

Saxena P., Hildemann L.M., McMurry P.H., and Seinfeld J.H. (1995) Organics alter hygroscopic behaviour of atmospheric particles. *J. Geophys. Res.* **100**, 18755-18770.

Scire J.S., Strimaitis D.G., and Yamartino R.J. (1990) Model formulation and user's guide for the CALPUFF dispersion model. Report prepared for the California Air Resources Board, Sacramento, CA by Sigma Research Corporation, Concord, MA, Report No. A025-2, November.

Sehmel G.A. (1980) Particle and gas deposition, a review. *Atmos. Environ.* **14**, 983-1011.

Seigneur C., Hudischewskyi A.B., Seinfeld J.H., Whitby K.T., Whitby E.R., Brock J.R., and Barnes H.M. (1986) Simulation of aerosol dynamics: a comparative review of mathematical models. *Aerosol Sci. Technol.* **5**, 205-222.

Sheih C.M., Wesely M.L., and Walcek C.J. (1986) A dry deposition module for regional acid deposition. Report prepared for U.S. Environmental Protection Agency, Research Triangle Park, NC by Argonne National Laboratory, Argonne, IL and National Center for Atmospheric Research, Boulder, CO.

Slinn S.A. and Slinn W.G.N. (1980) Predictions for paticle deposition on natural waters. *Atmos. Environ.* **24**, 1013-1016.

Slinn W.G.N., Hasse L., Hicks B.B., Hogan A.W., Lai D., Liss P.S., Munnich K.O., Sehmel G.A., and Vittori O. (1978) Some aspects of the transfer of atmospheric trace constituents past the air-sea interface. *Atmos. Environ.* **12**, 2055-2087.

Solomon P.A., Fall T., Larson S.M., Lin P., Vasquez F., and Cass G.R. (1988) Acquisition of acid and aerosol concentration data for use in dry deposition studies in the South Coast Air Basin. Vol. I. Report prepared for the California Air Resources Board, Sacramento, CA by California Institute of Technology, Environmental Quality Lab Report No. 25, Contract No. A4-144-32.

Stelson A.W., Friedlander S.K., and Seinfeld J.H. (1979) A note on the equilibrium relationship between ammonia and nitric acid and particulate ammonium nitrate. *Atmos. Environ.* **13**, 369-371.

Stokes R.H. and Robinson R.A. (1966) *J. Phys. Chem.* **70**, 2126-2130.

Sun P., Chock D.P., and Winkler S.L. (1994) An implicit-explicit hybrid solver for a system of stiff kinetic equations. Paper presented at the *Air & Waste Management Association 87th Annual Meeting, Cincinnati, OH, June 19-24.*

Voldner E.C., Barrie L.A., and Sirois A. (1986) A literature review of dry deposition of oxides of sulphur and nitrogen with emphasis on long-range transport modeling in North America. *Atmos. Environ.* **20**, 2101-2123.

Waldman J.M. (1986) Depositional aspects of pollutant behavior in fog. Ph.D. Thesis, California Institute of Technology, Pasadena.

Watson J.G., Chow J.C., Lurmann F.W., and Musarra S.P. (1994a) Ammonium nitrate, nitric acid, and ammonia equilibrium in wintertime Phoenix, Arizona. *J. Air & Waste Manag. Assoc.* **44**, 405-412.

Watson J.G., Chow J.C., Lu Z., Fujita E.M., Lowenthal D.H., Lawson D.R., and Ashbaugh L.L. (1994b) Chemical mass balance source apportionment of PM_{10} during the Southern California Air Quality Study. *Aerosol Sci. Technol.* **21**, 1-36.

Wesely M. (1989) Parameterization of surface resistances to gaseous dry deposition in regional-scale numerical models. *Atmos. Environ.* **23**, 1293-1304.

Wexler A.S. and Seinfeld J.H. (1990) The distribution of ammonium salts among a size and composition dispersed aerosol. *Atmos. Environ.* **24A**, 1231-1246.

Wexler A.S. and Seinfeld J.H. (1992) Analysis of aerosol ammonium nitrate: departures from equilibrium during SCAQS. *Atmos. Environ.* **26A**, 579-591.

Wexler A.S., Lurmann F.W., and Seinfeld J.H. (1994) Modeling urban and regional aerosols: I. model development. *Atmos. Environ.* **28**, 531-546.

Zhang X (1990) Personal communication.

Chapter 5 References

Dickson R.J., Cass G.R., Markovich L.J., Oliver W.R., Wright D.A., Cioni C.A., Berard L.A., Wilkinson J.G., and Riswold J.R. (1991) Development of the ammonia emission inventory for the Southern California Air Quality Study. Draft final report prepared for Electric Power Research Institute, Palo Alto, CA by Radian Corporation, Sacramento, CA, Research Project 2333-4, September.

Fujita E.M., Croes B.E., Bennett C.L., Lawson D.R., Lurmann F.W., and Main H.H. (1992) Comparison of emission inventory and ambient concentration ratios of CO, NMOG, and NO_x in California's South Coast Air Basin. *J. Air & Waste Manag. Assoc.* **42**, 264-276.

Hidy G.M. (1984) *Aerosols - an Industrial and Environmental Science.* Academic Press, Inc., Orlando, FL.

Ingalls M.N., Smith L.R., and Kirksey R.E. (1989) Measurement of on-road vehicle emission factors in the California South Coast Air Basin. Volume 1, regulated emissions. Report prepared for the Coordinating Research Council, Atlanta, GA by the Southwest Research Institute, Atlanta, GA, No. SwRI-1604.

Lurmann F.W. and Main H.H. (1992) Analysis of the ambient VOC data collected in the Southern California Air Quality Study. Final report prepared for California Air Resources Board, Sacramento, CA by Sonoma Technology, Inc., Santa Rosa, CA, STI-99120-1161-FR, Contract No. A823-130, February.

Roberts P.T., Main H.H., and Lurmann F. (1991) Evaluation of VOC, NO_x, and ozone boundary conditions for the California South Coast Air Basin. Paper presented at the *Air & Waste Management Association International Speciality Conference, November*, STI-1172. In *Transactions No. 20: Tropospheric Ozone and the Environment II Effects, Modeling and Control,* A&WMA, Pittsburgh, PA.

SCAQMD (1994) Technical report V-A ozone modeling protocol. Final report prepared by South Coast Air Quality Management District, Diamond Bar, CA, September.

SCAQMD (1996) Personal communication between South Coast Air Quality Management District staff and Lurmann F.W. on PTEP projects.

Solomon P.A., Fall T., Larson S.M., Lin P., Vasquez F., and Cass G.R. (1988a) Acquisition of acid and aerosol concentration data for use in dry deposition studies in the South Coast Air Basin. Vol. I. Report prepared for the California Air Resources Board, Sacramento, CA by California Institute of Technology, Environmental Quality Lab Report No. 25, Contract No. A4-144-32.

Chapter 6 References

Lurmann F.W. and Main H.H. (1992) Analysis of the ambient VOC data collected in the Southern California Air Quality Study. Final report prepared for California Air Resources Board, Sacramento, CA by Sonoma Technology, Inc., Santa Rosa, CA, STI-99120-1161-FR, Contract No. A823-130, February.

Roberts P.T., Main H.H., and Lurmann F. (1991) Evaluation of VOC, NO_x, and ozone boundary conditions for the California South Coast Air Basin. Paper presented at the *Air & Waste Management Association International Specialty Conference, November*, STI-1172. In *Transactions No. 20: Tropospheric Ozone and the Environment II Effects, Modeling and Control,* A&WMA, Pittsburgh, PA.

SCAQMD (1991a) Meteorological and air quality assessment of the representativeness of the 1987 SCAQS intensive days. Air quality management plan, technical report V-A. Prepared by South Coast Air Quality Management District, El Monte, CA.

SCAQMD (1991b) Episodic PM10 model development and application for the South Coast Air Basin. Air quality management plan, technical report V-E. Prepared by South Coast Air Quality Management District, El Monte, CA.

SCAQMD (1996) Personal communication between South Coast Air Quality Management District staff and Lurmann F.W. on PTEP projects.

Solomon P.A., Fall T., Larson S.M., Lin P., Vasquez F., and Cass G.R. (1988) Acquisition of acid and aerosol concentration data for use in dry deposition studies in the South Coast Air Basin. Vol. I. Report prepared for the California Air Resources Board, Sacramento, CA by California Institute of Technology, Environmental Quality Lab Report No. 25, Contract No. A4-144-32.

Appendix A

Station Plots for the June 23-25, 1987 Episode

Figure A-1. Predicted (line) and observed (dots) 24-hr average $PM_{2.5}$ nitrate concentrations for June 23-25, 1987.

Figure A-2. Predicted (line) and observed (dots) 24-hr average PM_{10} nitrate concentrations for June 23-25, 1987.

Figure A-3. Predicted (line) and observed (dots) 24-hr average $PM_{2.5}$ ammonium concentrations for June 23-25, 1987.

Figure A-4. Predicted (line) and observed (dots) 24-hr average PM_{10} ammonium concentrations for June 23-25, 1987.

Figure A-5. Predicted (line) and observed (dots) 24-hr average $PM_{2.5}$ sulfate concentrations for June 23-25, 1987.

Figure A-6. Predicted (line) and observed (dots) 24-hr average PM_{10} sulfate concentrations for June 23-25, 1987.

Figure A-7. Predicted (line) and observed (dots) 24-hr average $PM_{2.5}$ mass concentrations for June 23-25, 1987.

Figure A-8. Predicted (line) and observed (dots) 24-hr average PM_{10} mass concentrations for June 23-25, 1987.

Figure A-9. Predicted (line) and observed (dots) 24-hr average $PM_{2.5}$ organic material concentrations for June 23-25, 1987.

Figure A-10. Predicted (line) and observed (dots) 24-hr average PM_{10} organic material concentrations for June 23-25, 1987.

Figure A-11. Predicted (line) and observed (dots) 24-hr average $PM_{2.5}$ elemental carbon concentrations for June 23-25, 1987.

Figure A-12. Predicted (line) and observed (dots) 24-hr average PM_{10} elemental carbon concentrations for June 23-25, 1987.

Figure A-13. Predicted (line) and observed (dots) 24-hr average PM_{10} sodium concentrations for June 23-25, 1987.

Figure A-14. Predicted (line) and observed (dots) 24-hr average PM_{10} chloride concentrations for June 23-25, 1987.

Figure A-15. Predicted (line) and observed (dots) 24-hr average nitric acid concentrations for June 23-25, 1987.

Figure A-16. Predicted (line) and observed (dots) 24-hr average ammonia concentrations for June 23-25, 1987.

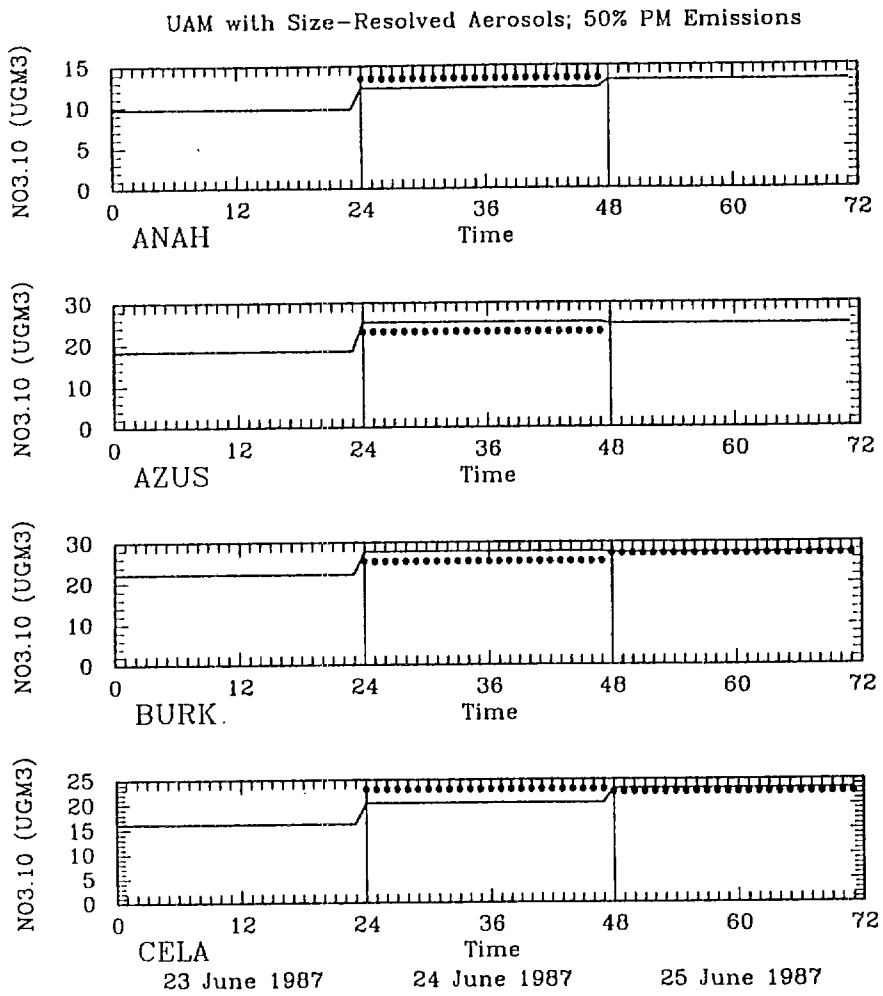
UAM with Size-Resolved Aerosols; 50% PM Emissions
NO3.10 (UGM3)
ANAH
AZUS
BURK
CELA
Time
23 June 1987
24 June 1987
25 June 1987

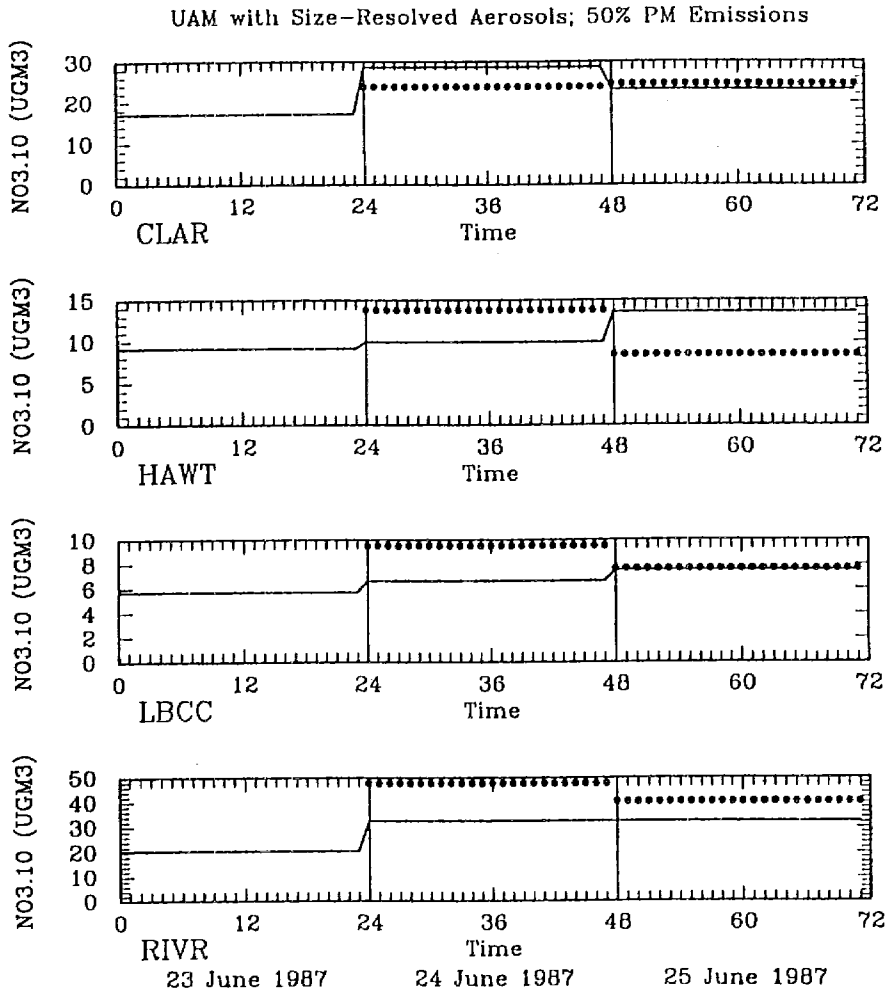
UAM with Size-Resolved Aerosols; 50% PM Emissions
NO3.10 (UGM3)
CLAR
HAWT
LBCC
RIVR
Time
23 June 1987
24 June 1987
25 June 1987

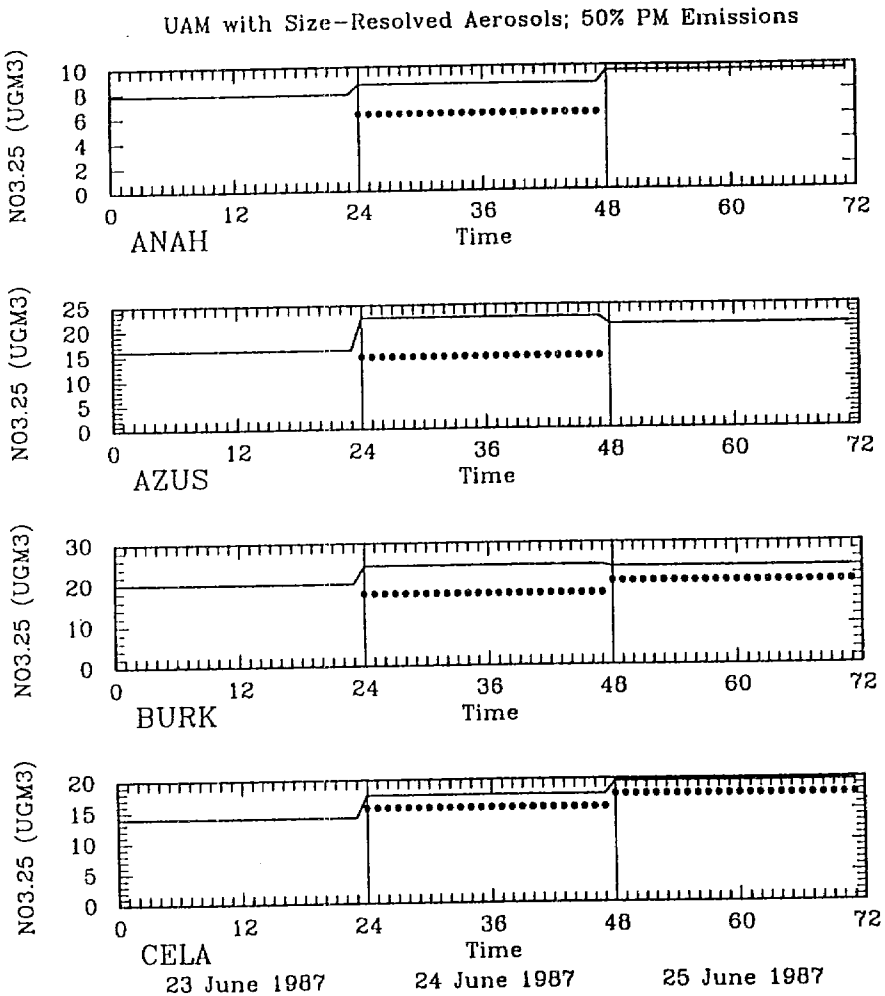
UAM with Size-Resolved Aerosols; 50% PM Emissions
NO3.25 (UGM3)
ANAH
AZUS
BURK
CELA
Time
0
12
24
36
48
60
72
23 June 1987
24 June 1987
25 June 1987

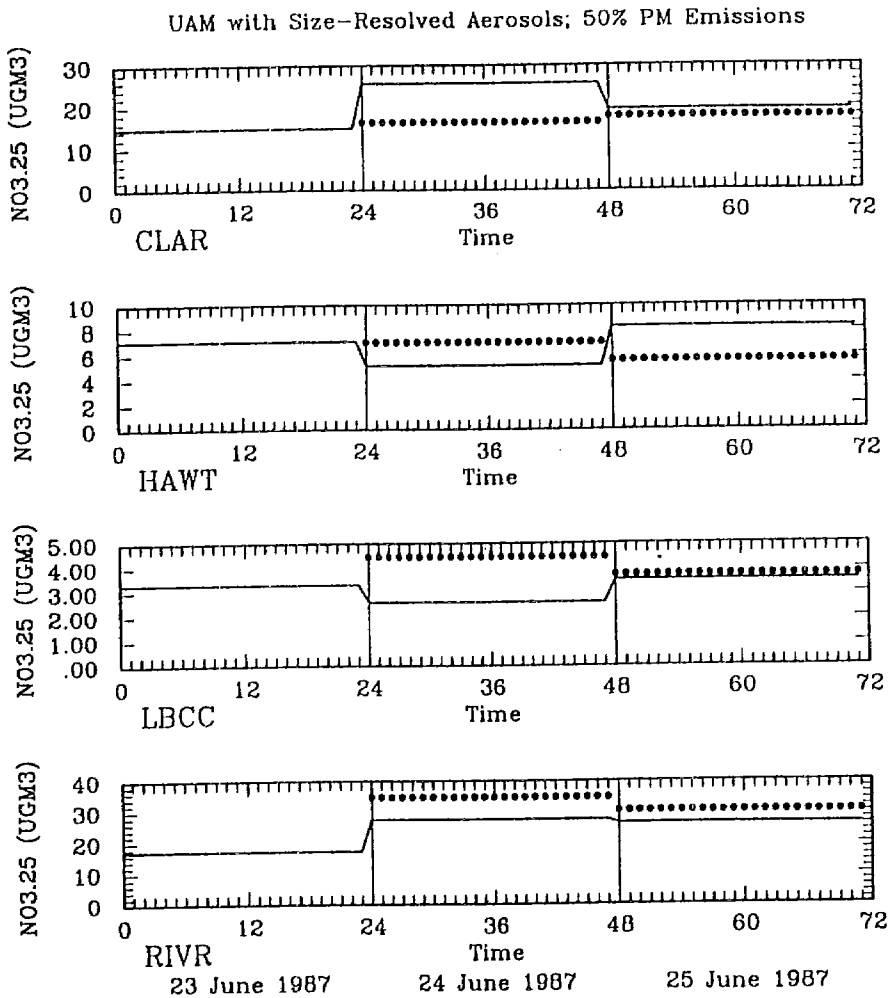
UAM with Size-Resolved Aerosols; 50% PM Emissions
NO3.25 (UGM3)
CLAR
HAWT
LBCC
RIVR
Time
0
12
24
36
48
60
72
23 June 1987
24 June 1987
25 June 1987

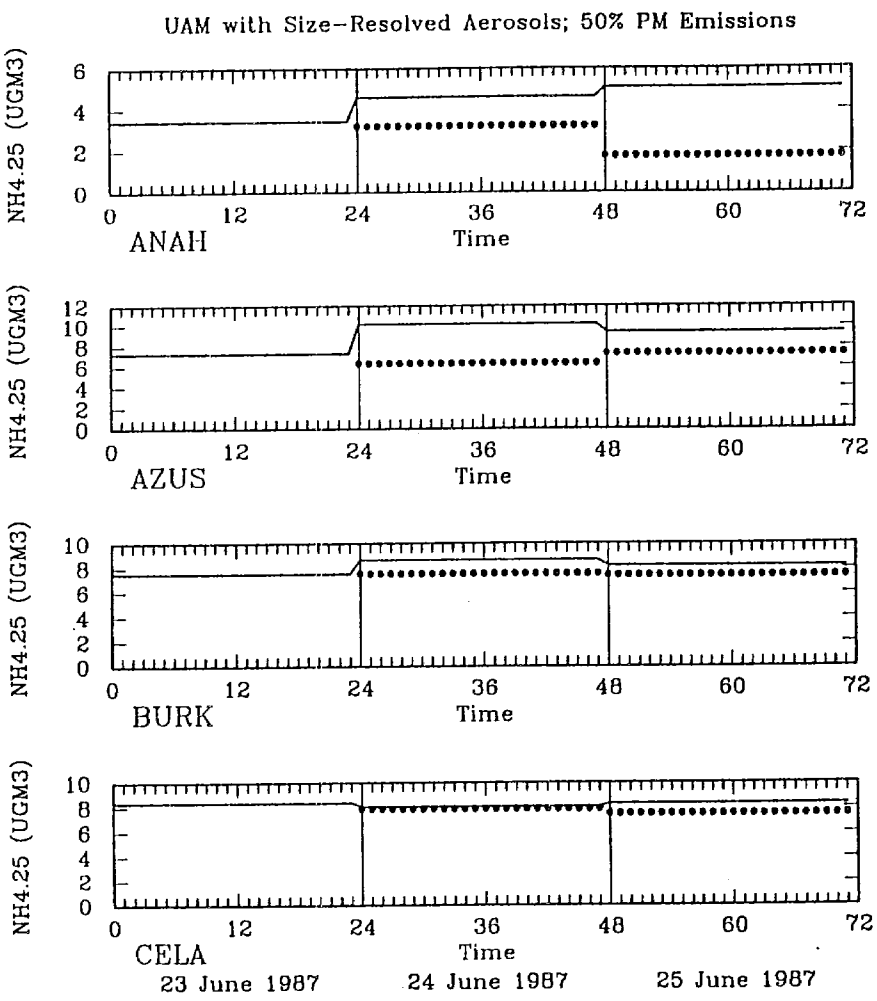
UAM with Size-Resolved Aerosols; 50% PM Emissions
NH4.25 (UGM3)
ANAH
AZUS
BURK
CELA
Time
23 June 1987
24 June 1987
25 June 1987

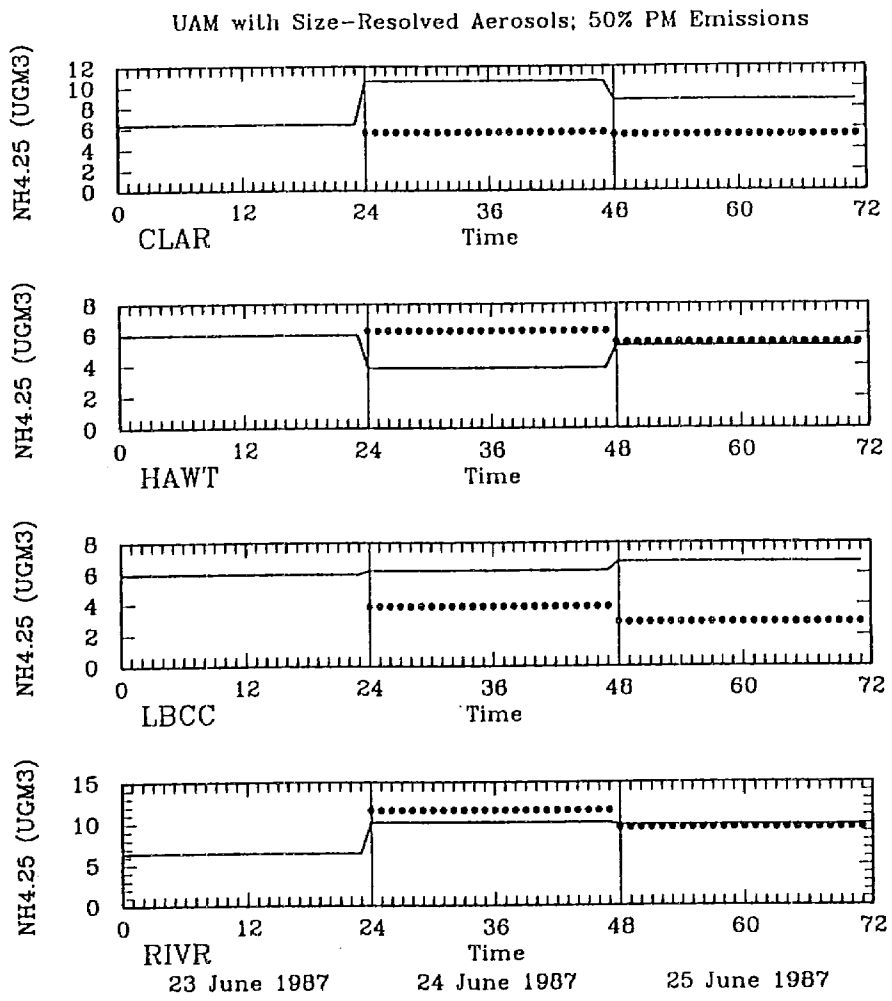
UAM with Size-Resolved Aerosols; 50% PM Emissions
NH4.25 (UGM3)
CLAR
HAWT
LBCC
RIVR
Time
23 June 1987
24 June 1987
25 June 1987

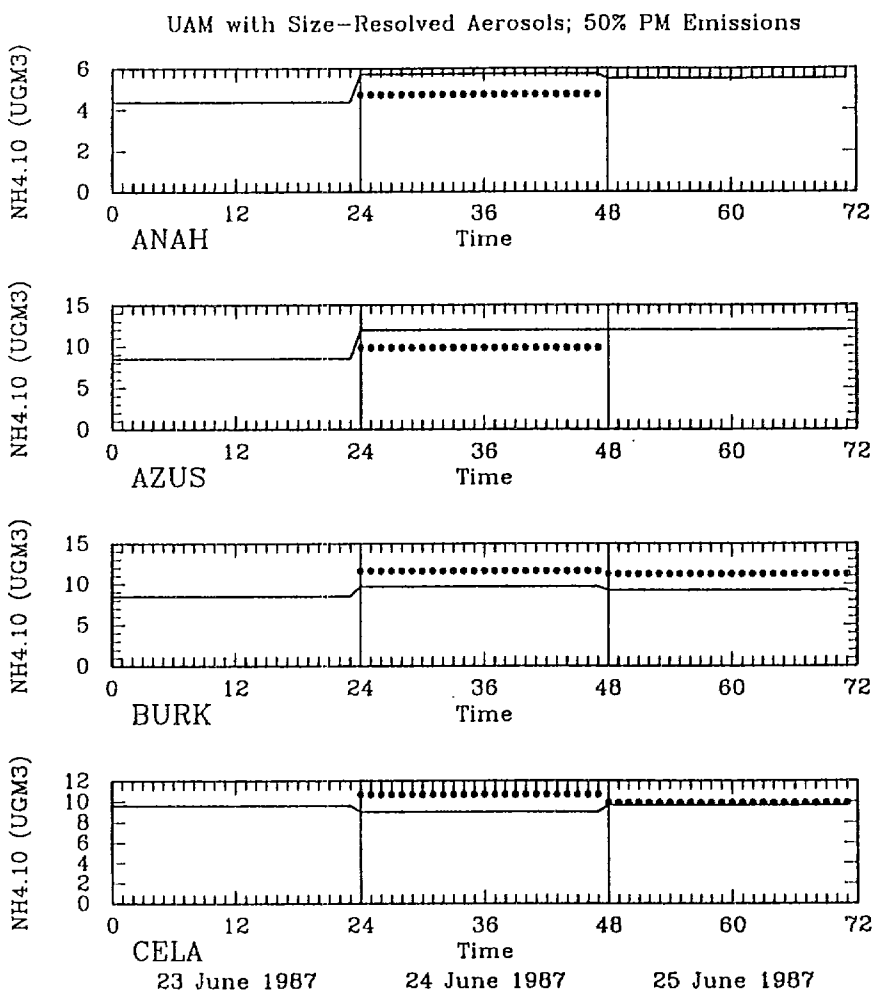
UAM with Size-Resolved Aerosols; 50% PM Emissions
NH4.10 (UGM3)
ANAH
AZUS
BURK
CELA
Time
23 June 1987
24 June 1987
25 June 1987

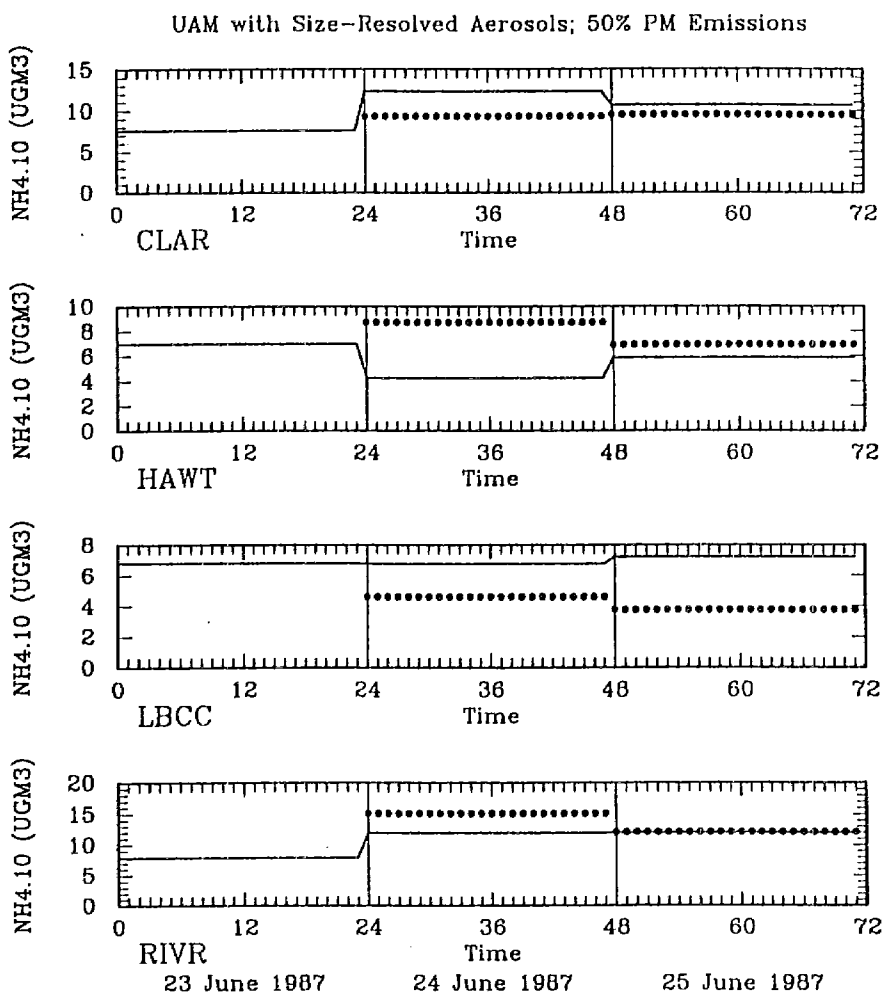
UAM with Size-Resolved Aerosols; 50% PM Emissions
NH4.10 (UGM3)
CLAR
HAWT
LBCC
RIVR
Time
23 June 1987
24 June 1987
25 June 1987

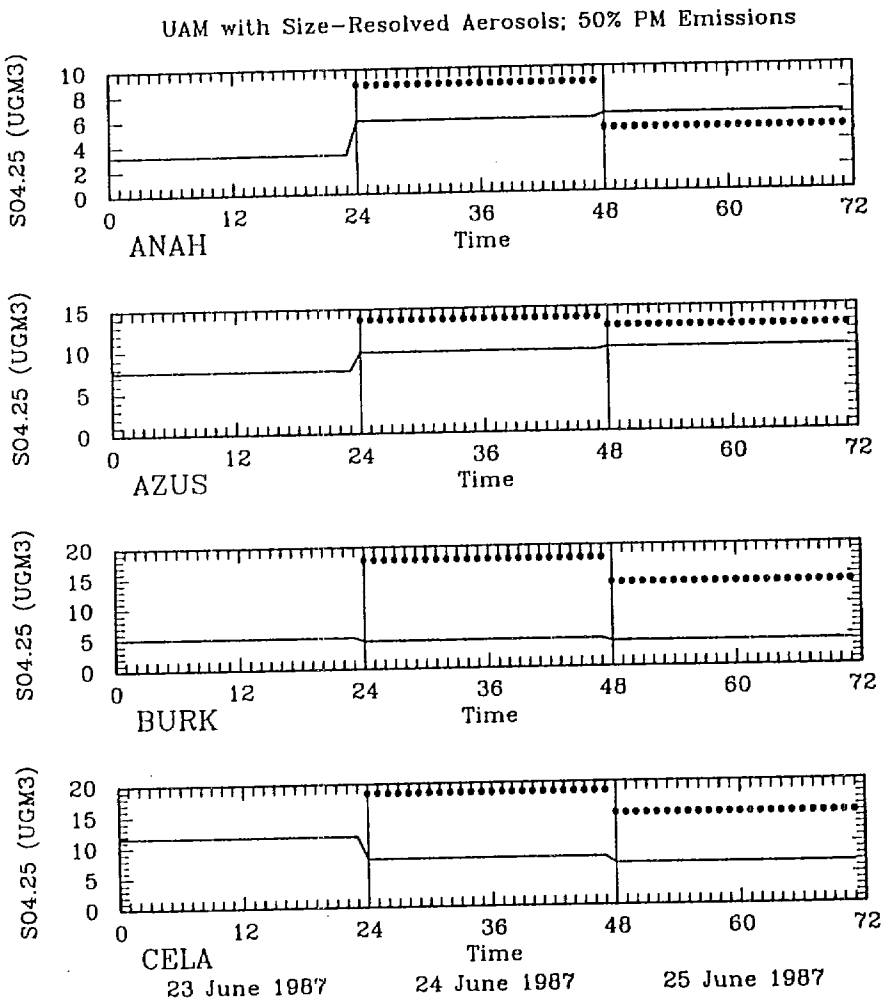
UAM with Size-Resolved Aerosols; 50% PM Emissions
SO4.25 (UGM3)
ANAH
AZUS
BURK
CELA
Time
23 June 1987
24 June 1987
25 June 1987

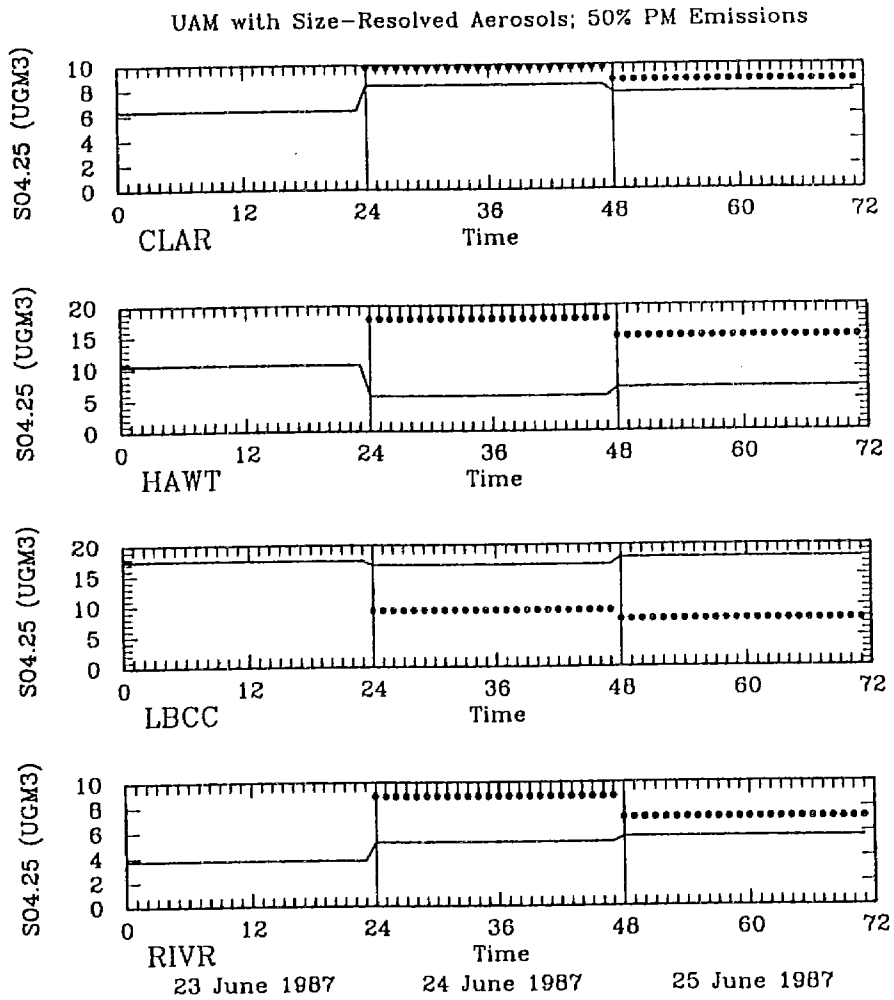
UAM with Size-Resolved Aerosols; 50% PM Emissions
SO4.25 (UGM3)
CLAR
HAWT
LBCC
RIVR
Time
23 June 1987
24 June 1987
25 June 1987

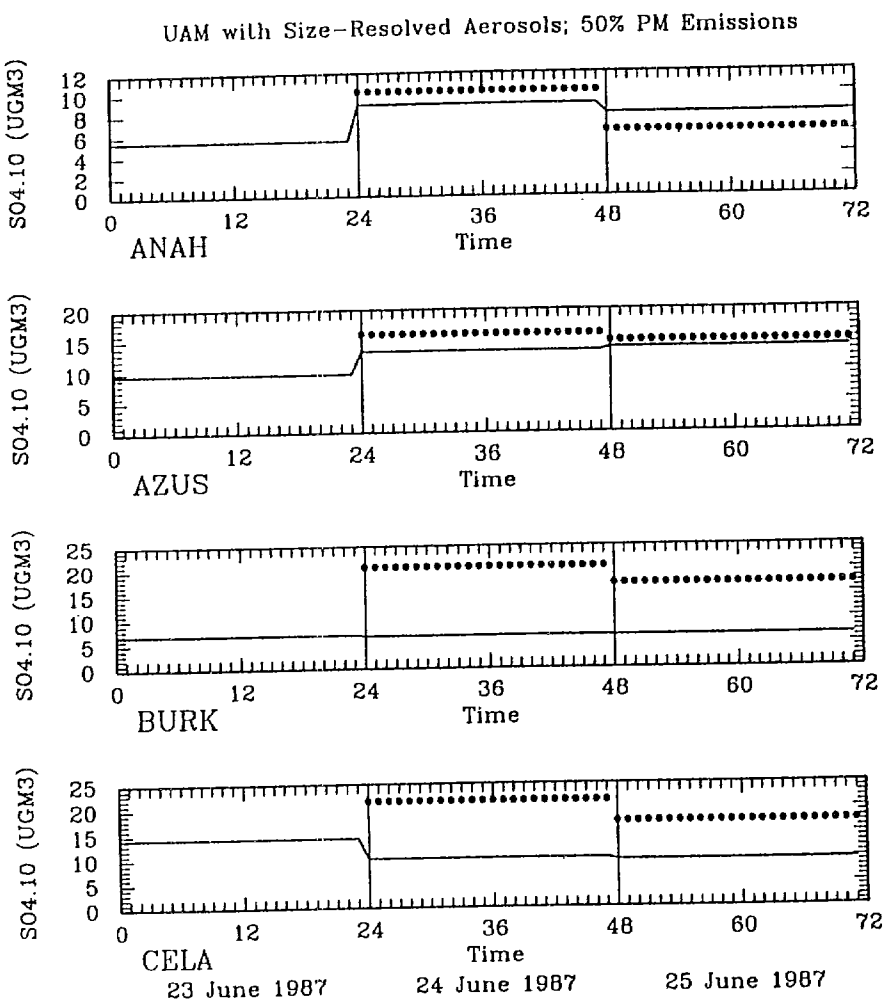
UAM with Size-Resolved Aerosols; 50% PM Emissions
SO4.10 (UGM3)
ANAH
AZUS
BURK
CELA
Time
23 June 1987
24 June 1987
25 June 1987

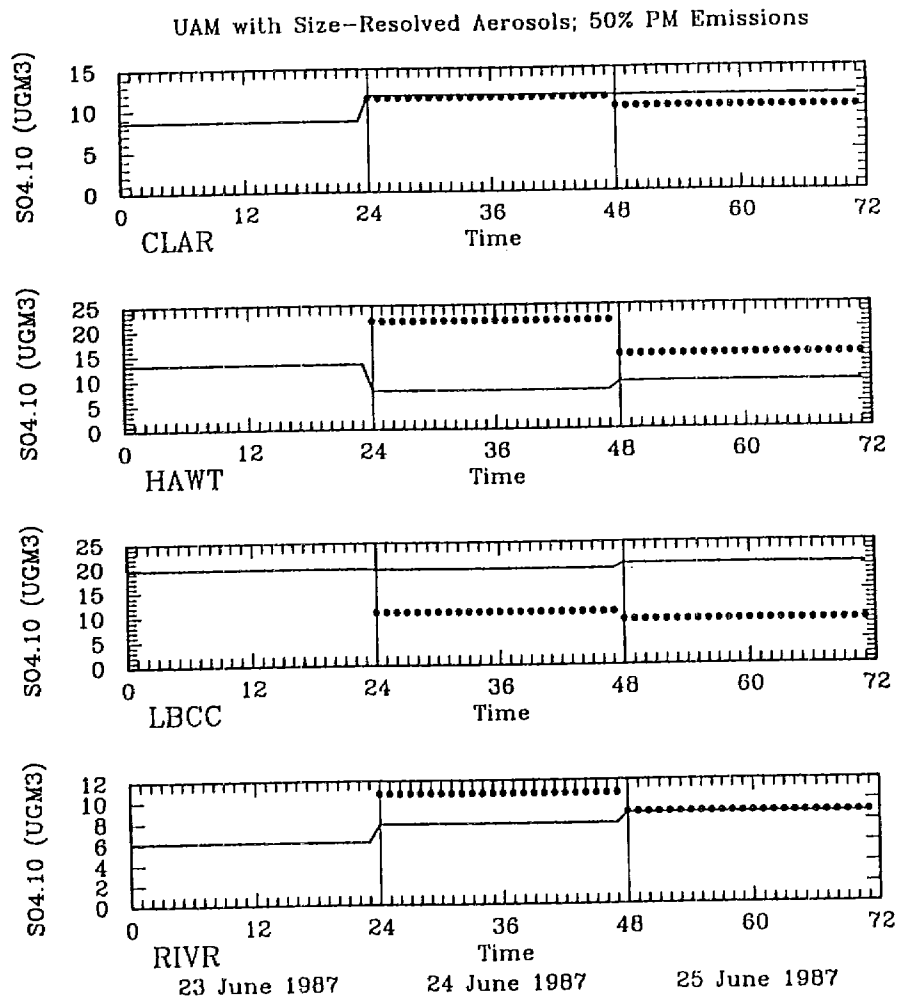
UAM with Size-Resolved Aerosols; 50% PM Emissions
SO4.10 (UGM3)
CLAR
HAWT
LBCC
RIVR
Time
23 June 1987
24 June 1987
25 June 1987

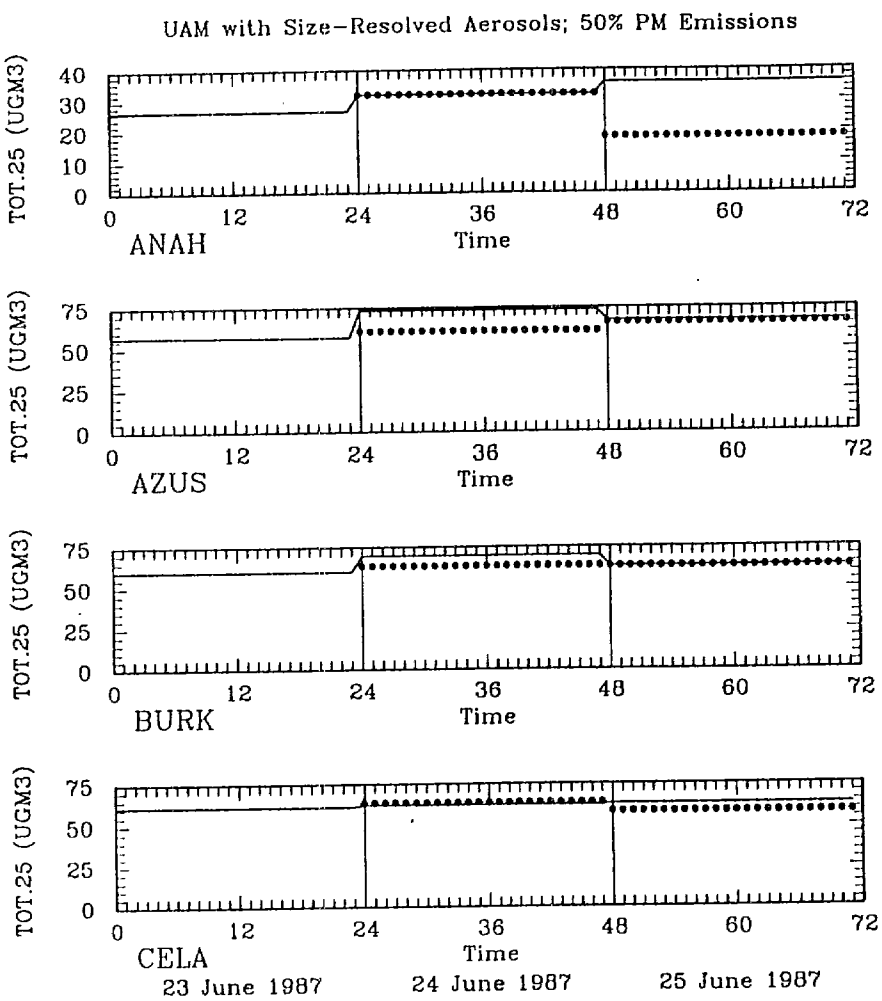
UAM with Size-Resolved Aerosols; 50% PM Emissions
TOT.25 (UGM3)
ANAH
AZUS
BURK
CELA
Time
23 June 1987
24 June 1987
25 June 1987

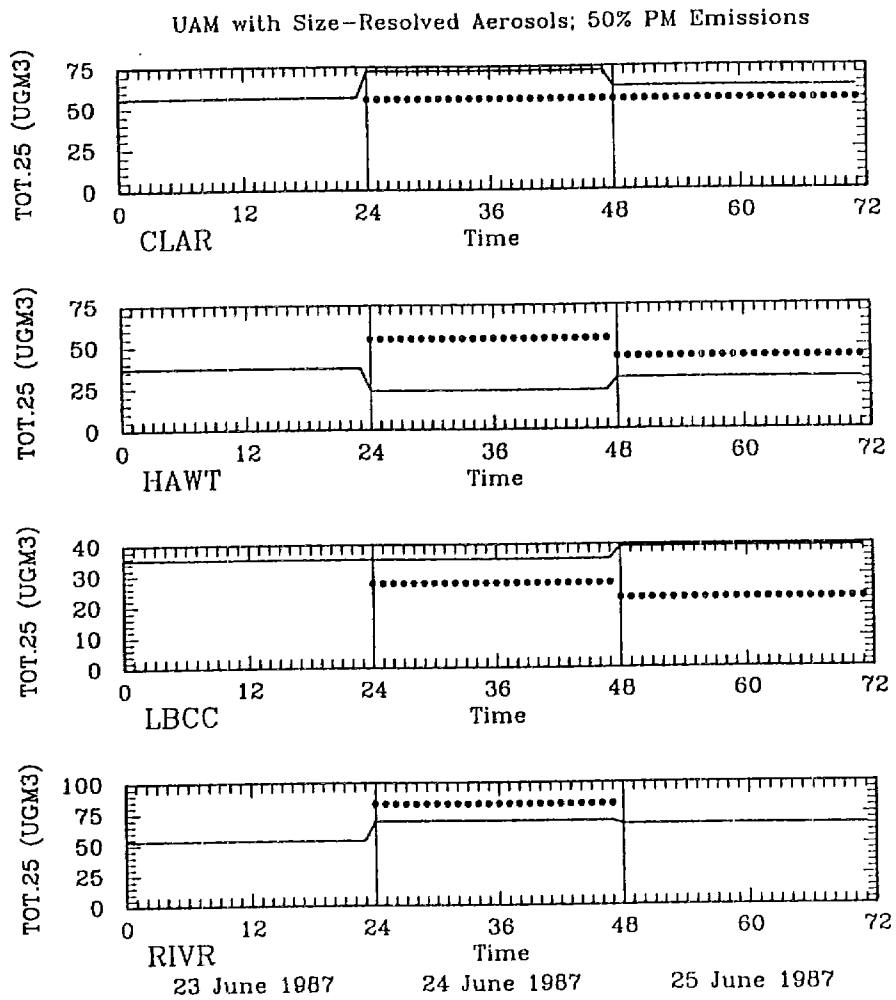
UAM with Size-Resolved Aerosols; 50% PM Emissions
TOT.25 (UGM3)
CLAR
HAWT
LBCC
RIVR
Time
23 June 1987
24 June 1987
25 June 1987

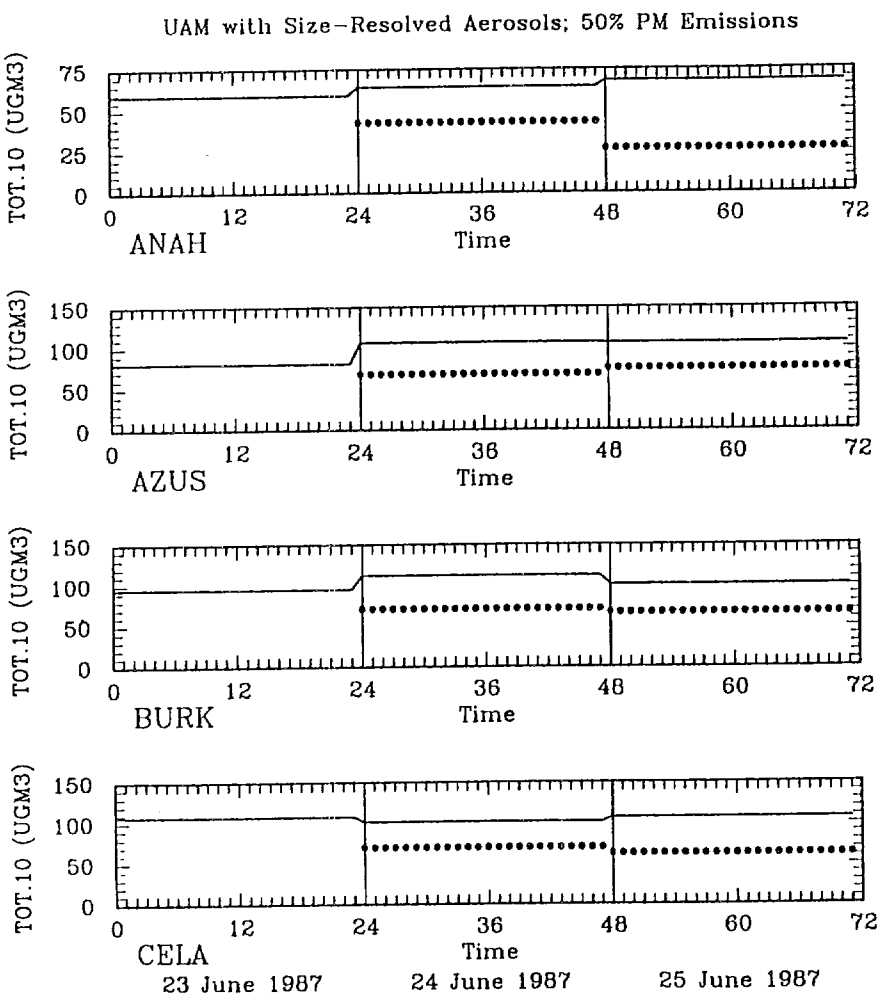
UAM with Size-Resolved Aerosols; 50% PM Emissions
TOT.10 (UGM3)
ANAH
AZUS
BURK
CELA
Time
0
12
24
36
48
60
72
23 June 1987
24 June 1987
25 June 1987

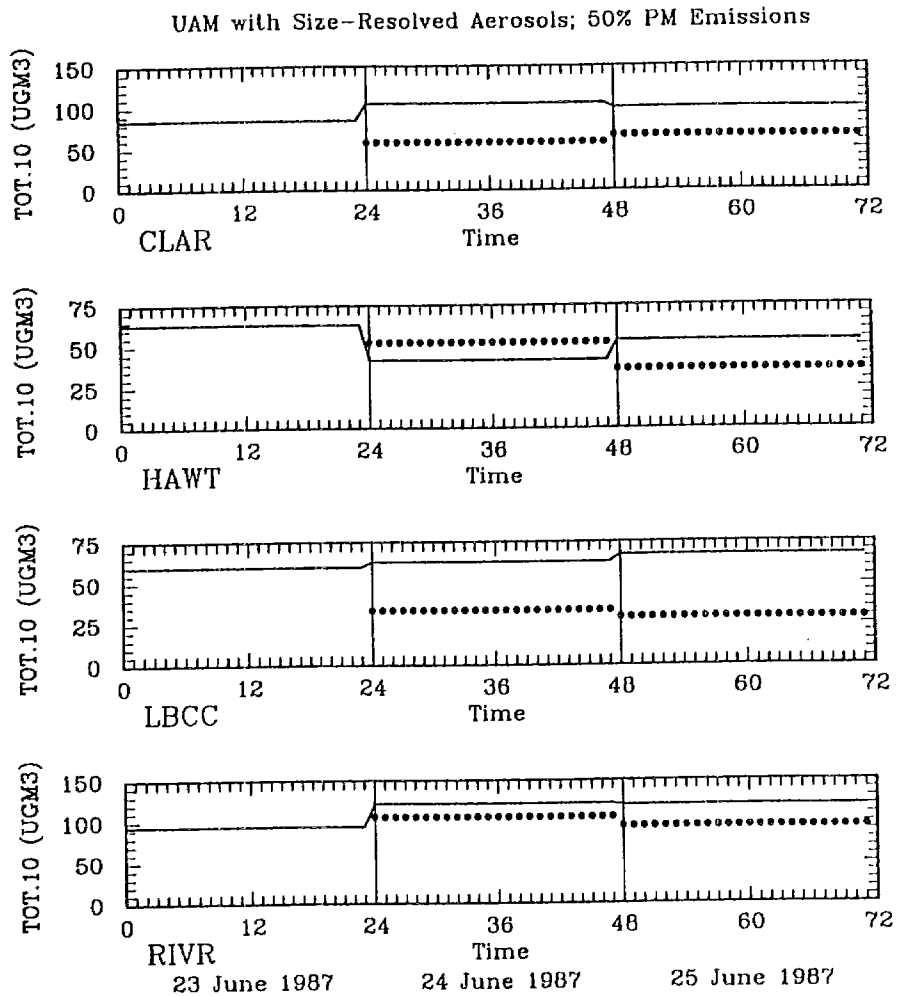
UAM with Size-Resolved Aerosols; 50% PM Emissions
TOT.10 (UGM3)
CLAR
HAWT
LBCC
RIVR
Time
0
12
24
36
48
60
72
23 June 1987
24 June 1987
25 June 1987

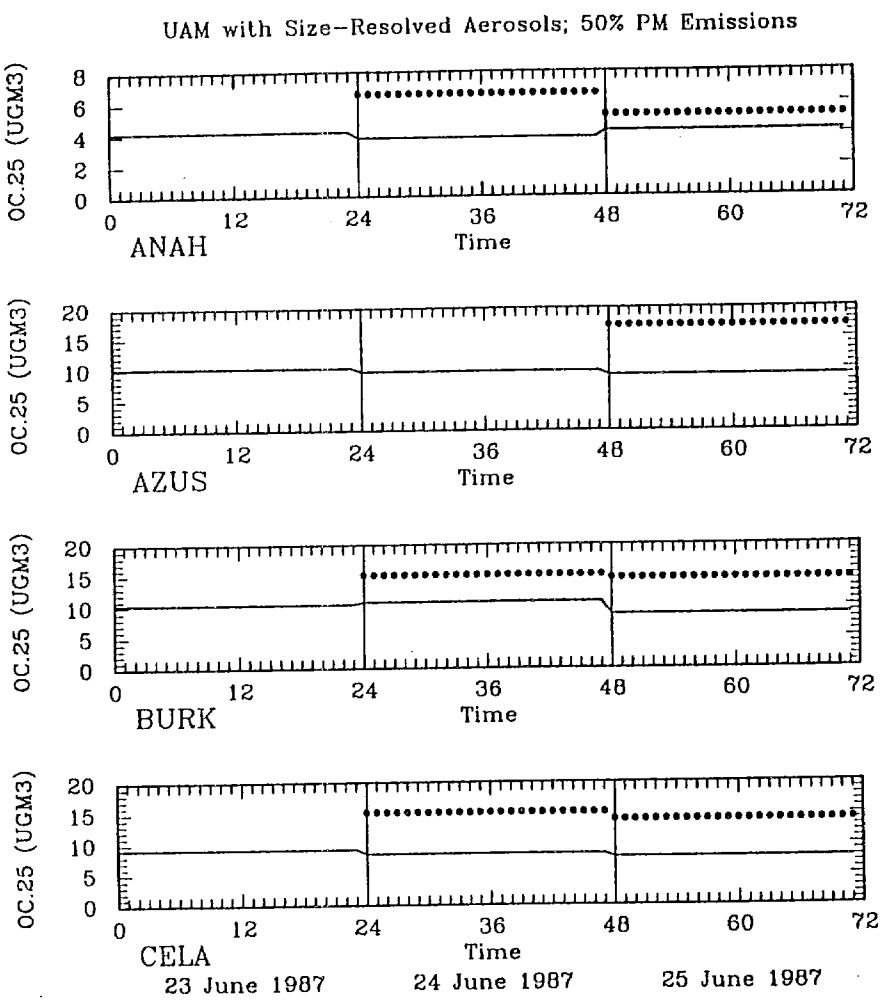
UAM with Size-Resolved Aerosols; 50% PM Emissions
OC.25 (UGM3)
ANAH
AZUS
BURK
CELA
Time
23 June 1987
24 June 1987
25 June 1987

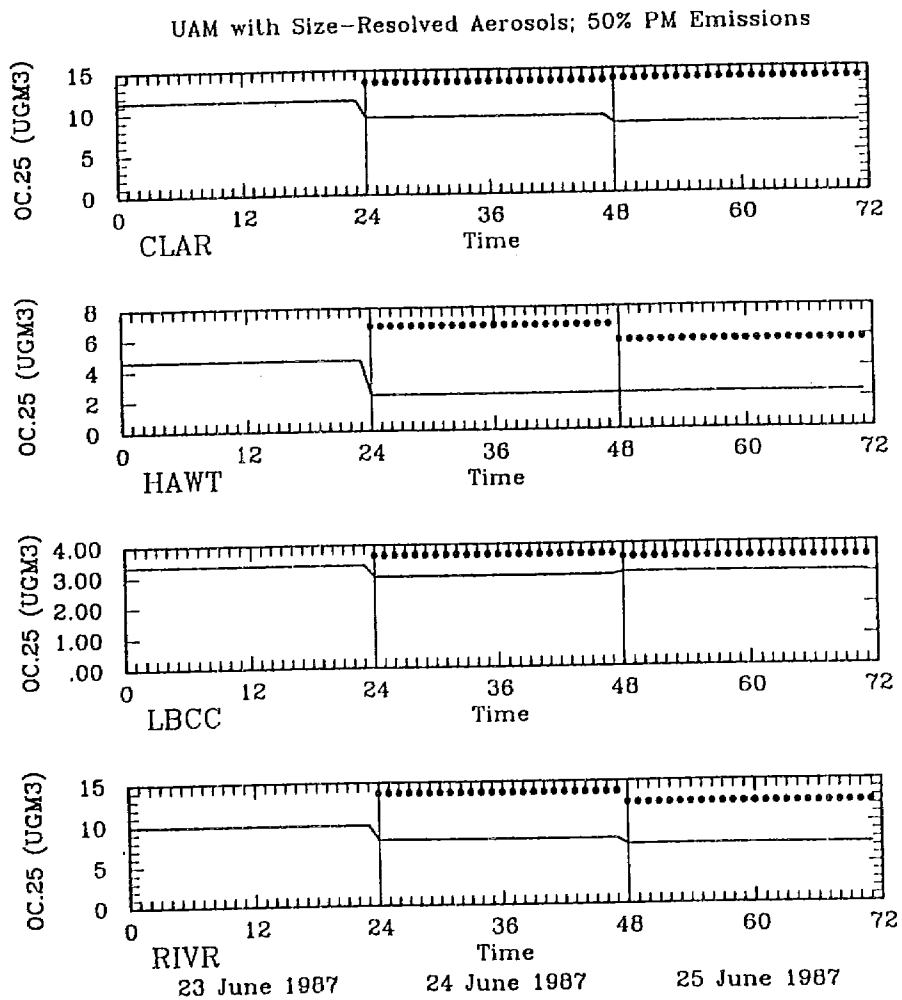
UAM with Size-Resolved Aerosols; 50% PM Emissions
OC.25 (UGM3)
CLAR
HAWT
LBCC
RIVR
Time
23 June 1987
24 June 1987
25 June 1987

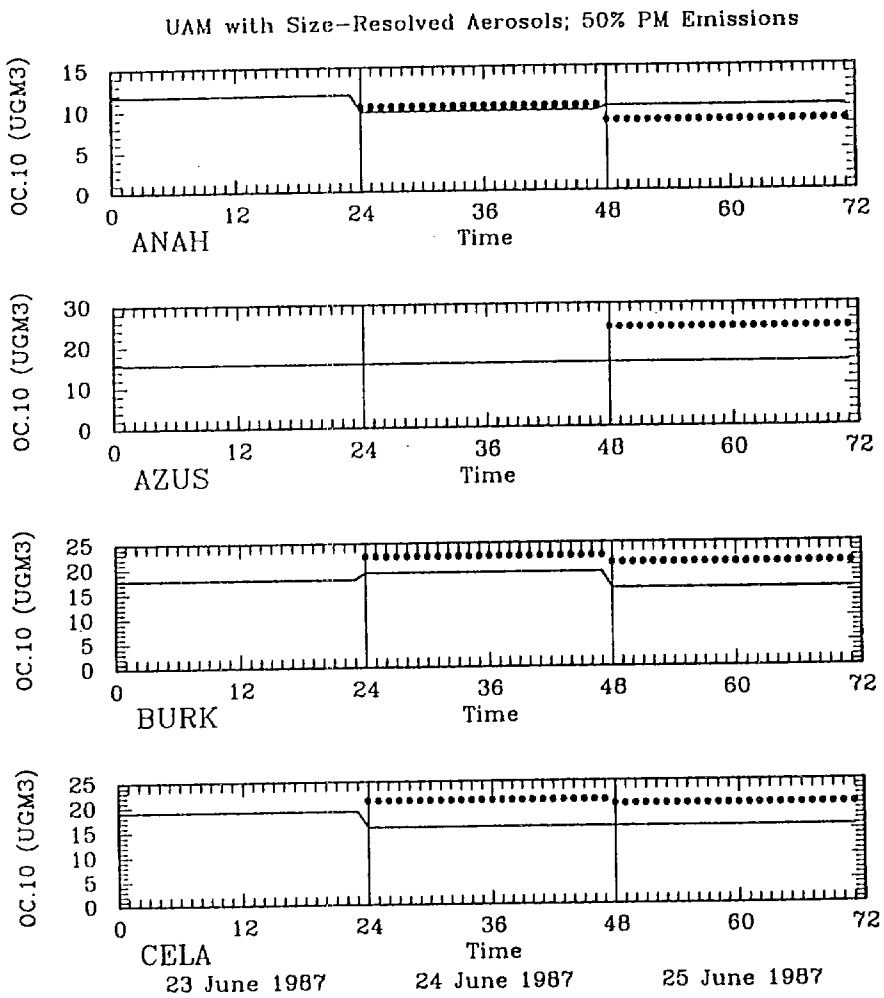
UAM with Size-Resolved Aerosols; 50% PM Emissions
OC.10 (UGM3)
ANAH
AZUS
BURK
CELA
Time
23 June 1987
24 June 1987
25 June 1987

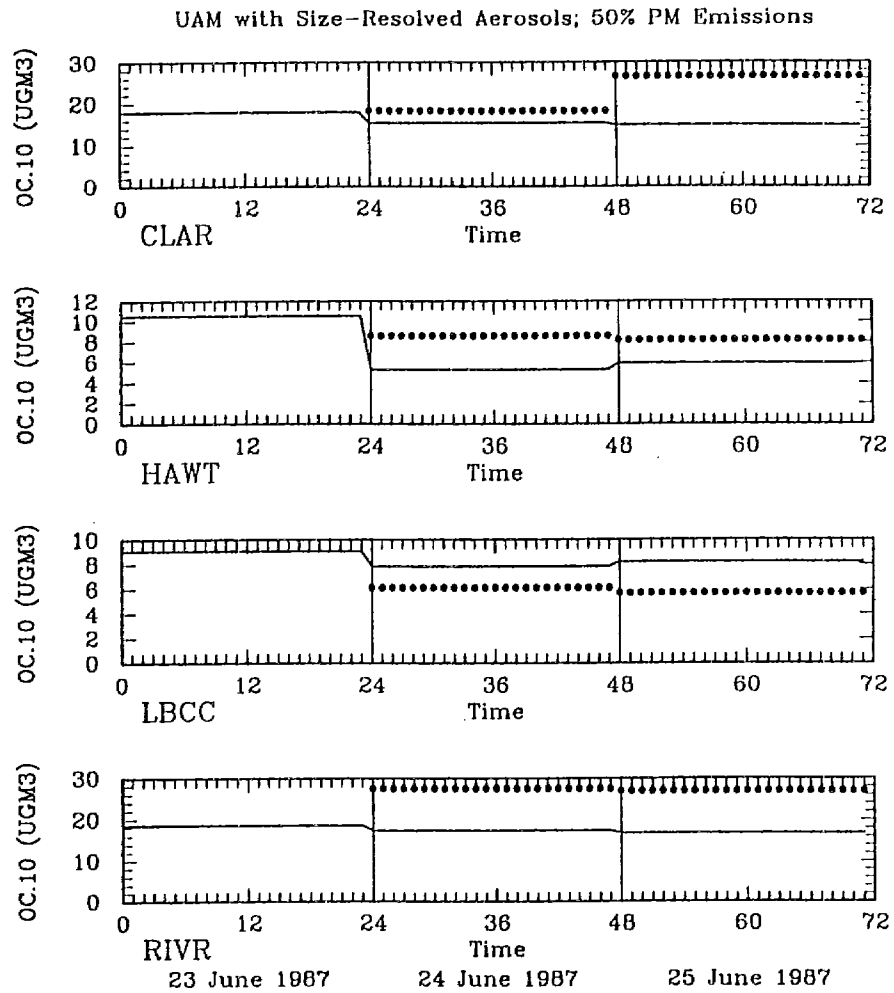
UAM with Size-Resolved Aerosols; 50% PM Emissions
OC.10 (UGM3)
CLAR
HAWT
LBCC
RIVR
Time
23 June 1987
24 June 1987
25 June 1987

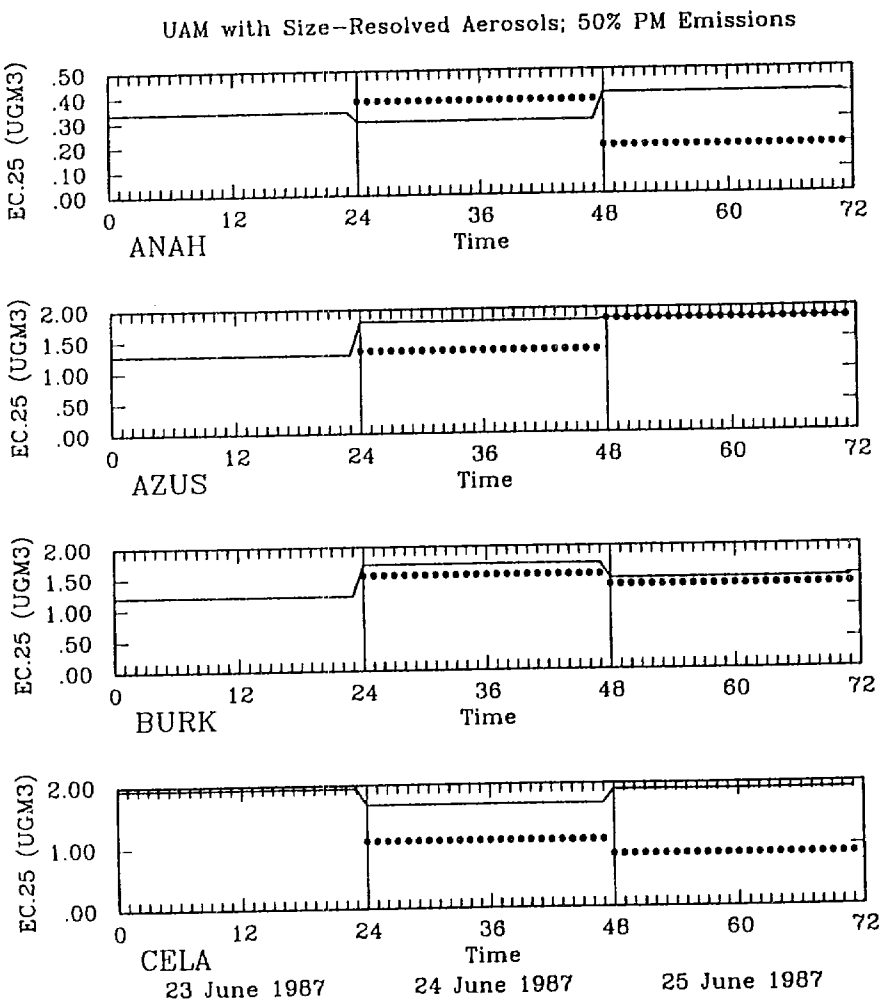
UAM with Size-Resolved Aerosols; 50% PM Emissions
EC.25 (UGM3)
ANAH
AZUS
BURK
CELA
Time
23 June 1987
24 June 1987
25 June 1987

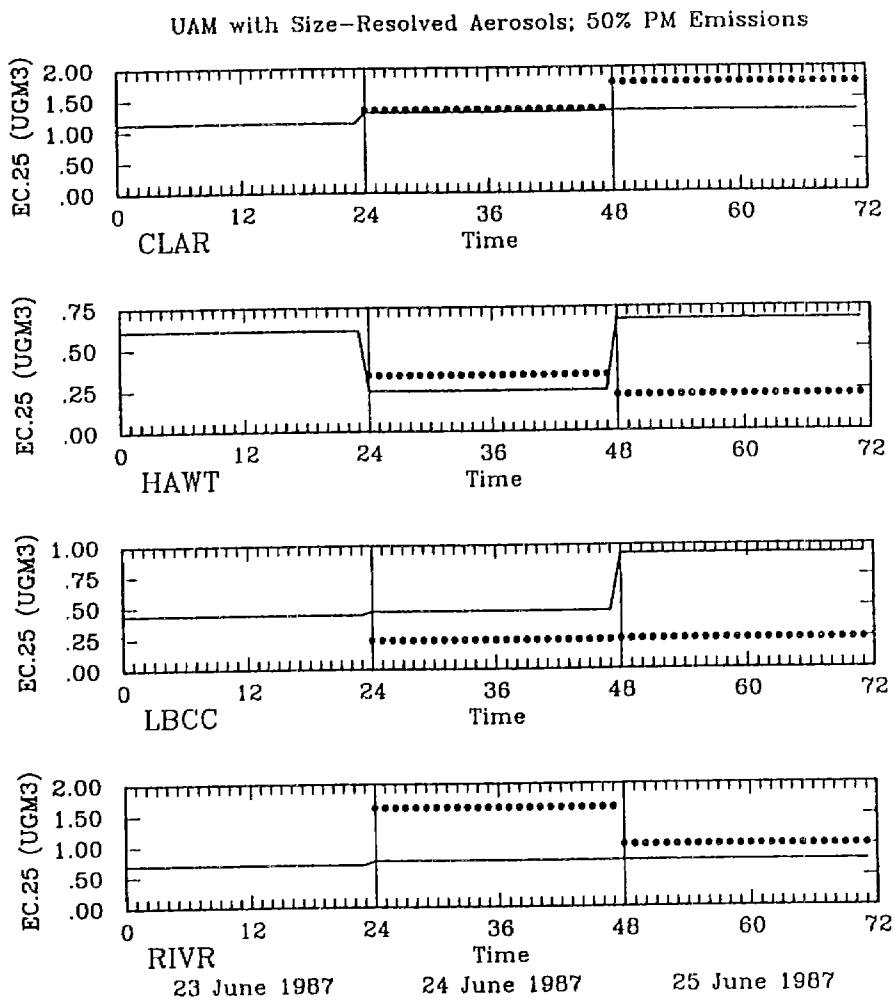
UAM with Size-Resolved Aerosols; 50% PM Emissions
EC.25 (UGM3)
CLAR
HAWT
LBCC
RIVR
Time
23 June 1987
24 June 1987
25 June 1987

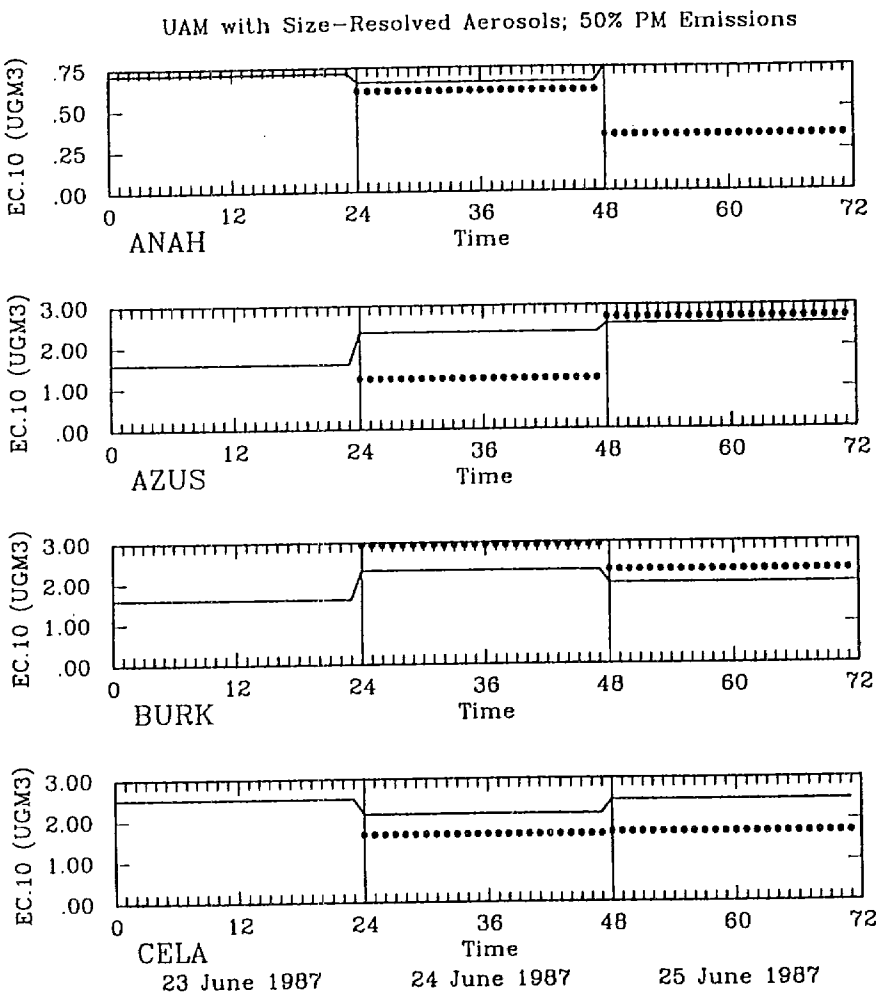
UAM with Size-Resolved Aerosols; 50% PM Emissions
EC.10 (UGM3)
.75
.50
.25
.00
0
12
24
36
48
60
72
Time
ANAH
3.00
2.00
1.00
.00
AZUS
BURK
CELA
23 June 1987
24 June 1987
25 June 1987

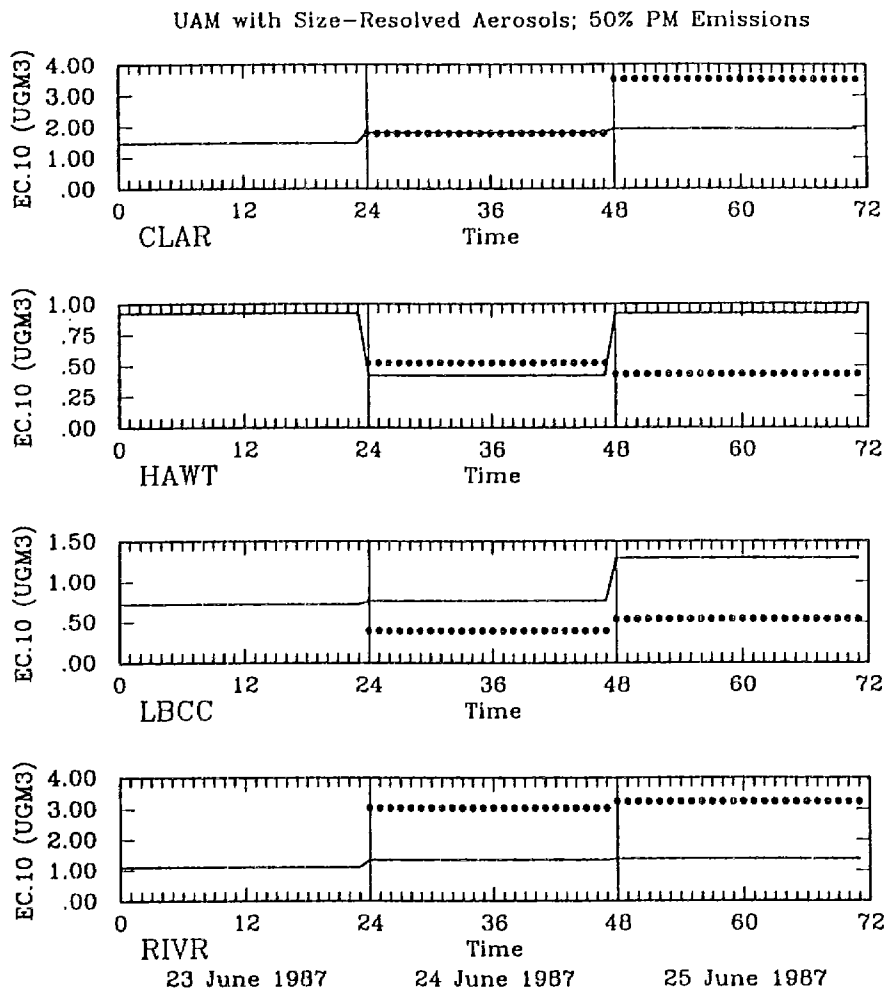
UAM with Size-Resolved Aerosols; 50% PM Emissions
EC.10 (UGM3)
4.00
3.00
2.00
1.00
.00
0
12
24
36
48
60
72
Time
CLAR
1.00
.75
.50
.25
.00
HAWT
1.50
1.00
.50
.00
LBCC
RIVR
23 June 1987
24 June 1987
25 June 1987

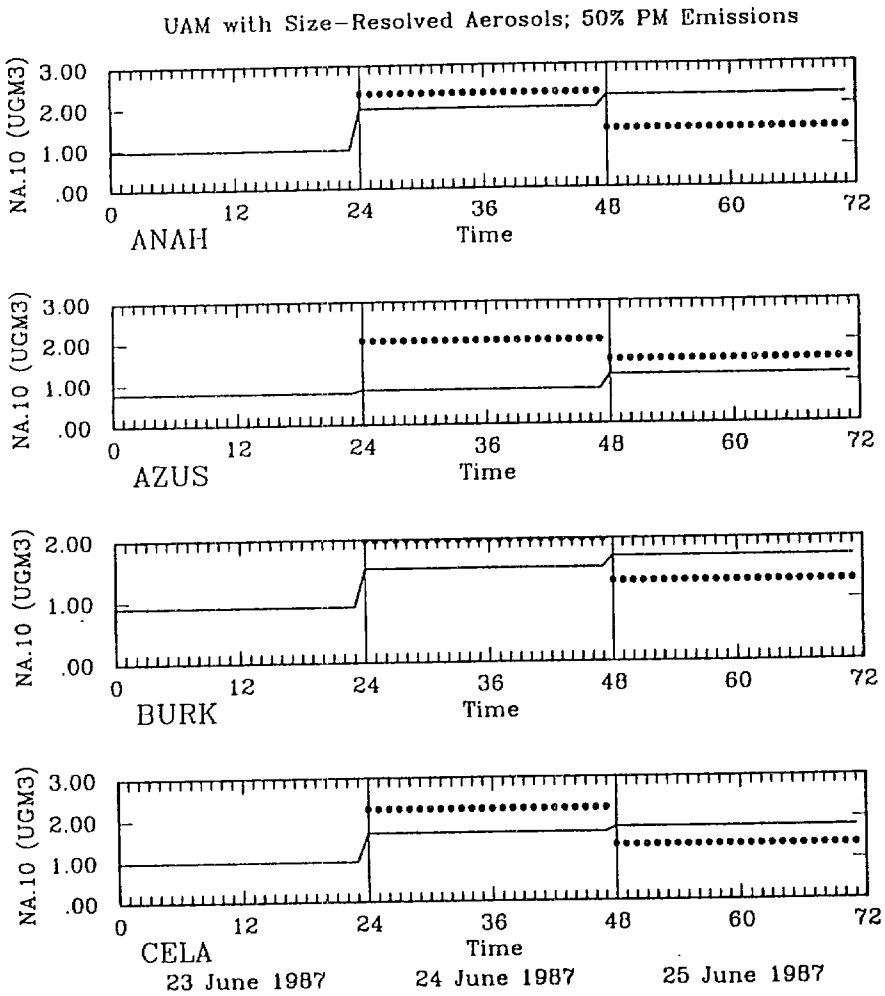
UAM with Size-Resolved Aerosols; 50% PM Emissions
NA.10 (UGM3)
3.00
2.00
1.00
.00
0
12
24
36
48
60
72
Time
ANAH
AZUS
BURK
CELA
23 June 1987
24 June 1987
25 June 1987

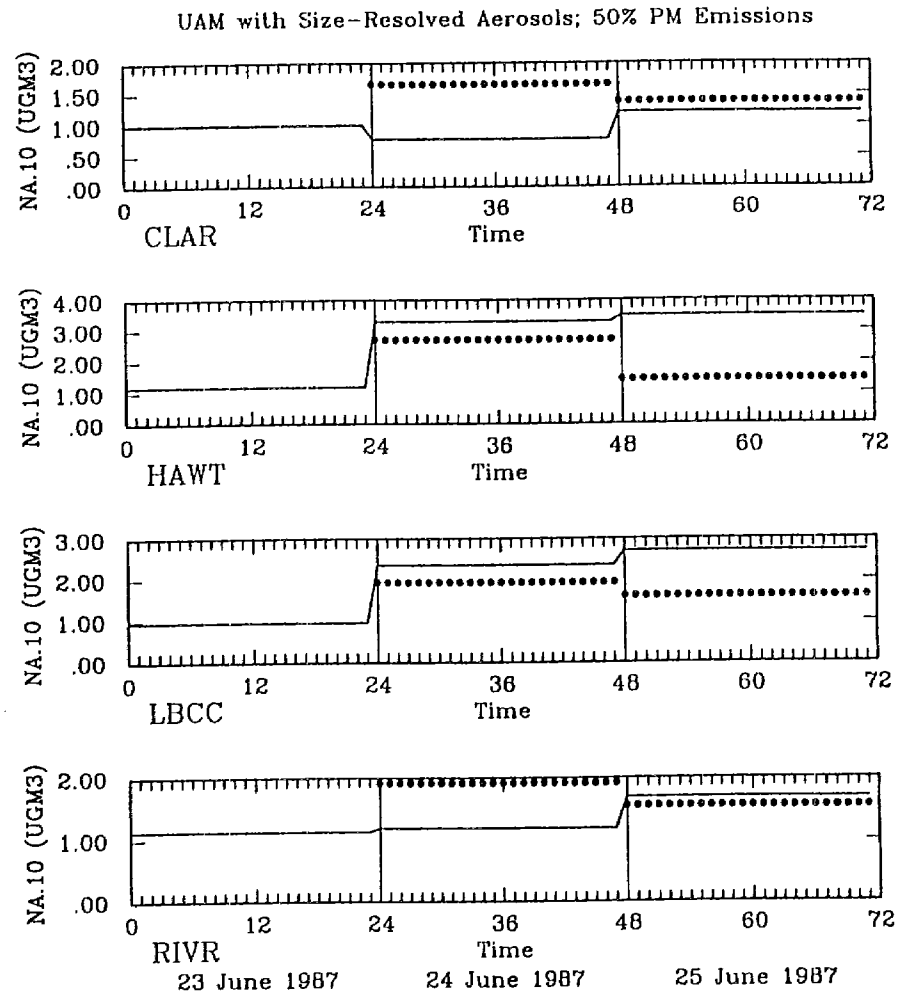
UAM with Size-Resolved Aerosols; 50% PM Emissions
NA.10 (UGM3)
2.00
1.50
1.00
.50
.00
4.00
3.00
0
12
24
36
48
60
72
Time
CLAR
HAWT
LBCC
RIVR
23 June 1987
24 June 1987
25 June 1987

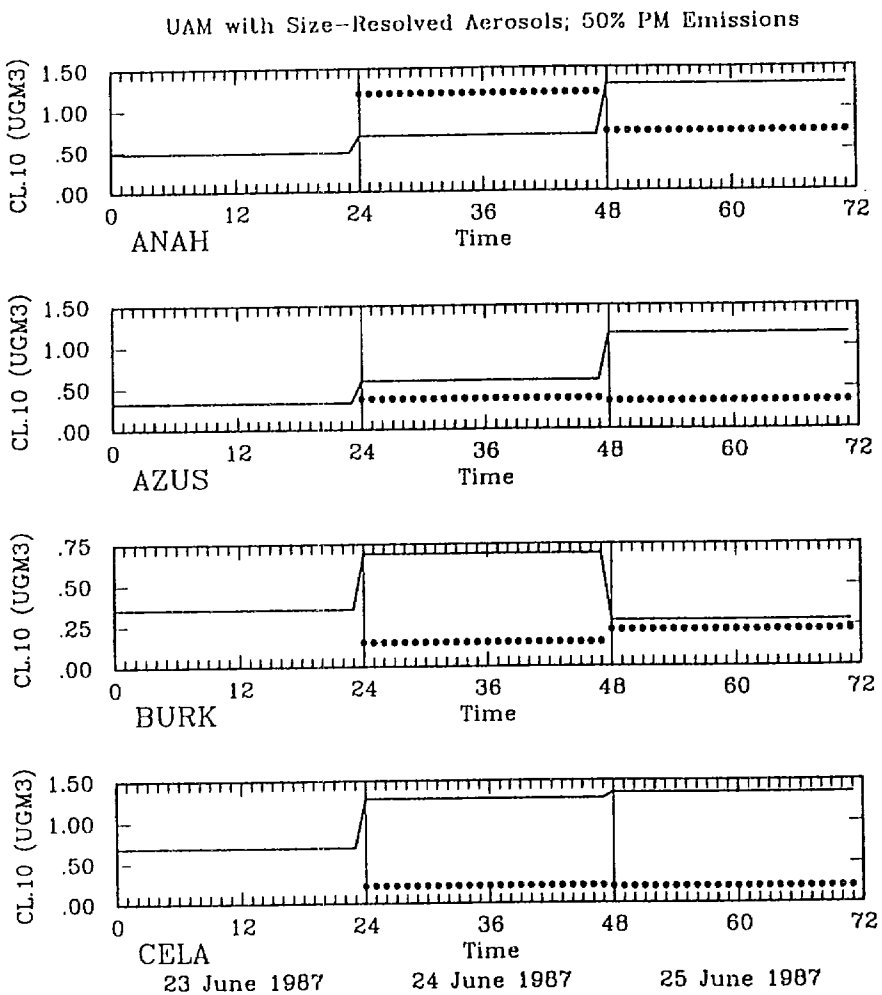
UAM with Size-Resolved Aerosols; 50% PM Emissions
CL.10 (UGM3)
1.50
1.00
.50
.00
0
12
24
36
48
60
72
Time
ANAH
AZUS
.75
.25
BURK
CELA
23 June 1987
24 June 1987
25 June 1987

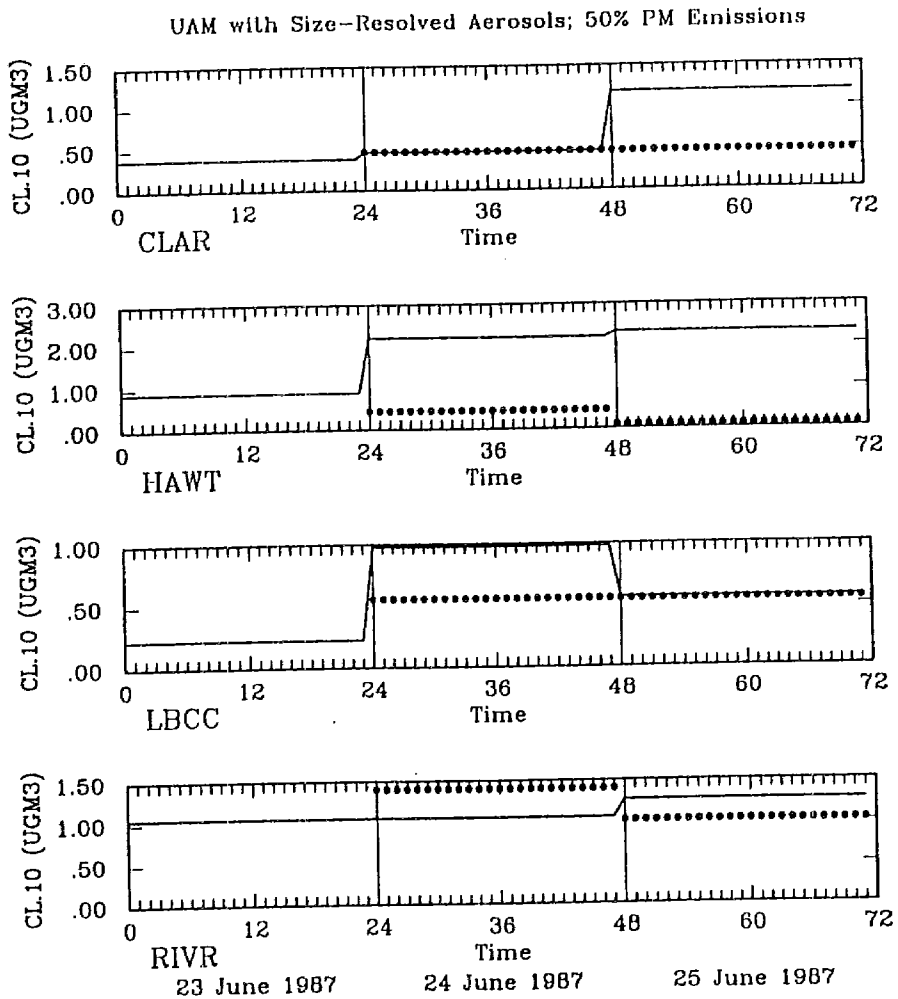
UAM with Size-Resolved Aerosols; 50% PM Emissions
CL.10 (UGM3)
1.50
1.00
.50
.00
0
12
24
36
48
60
72
Time
CLAR
3.00
2.00
HAWT
LBCC
RIVR
23 June 1987
24 June 1987
25 June 1987

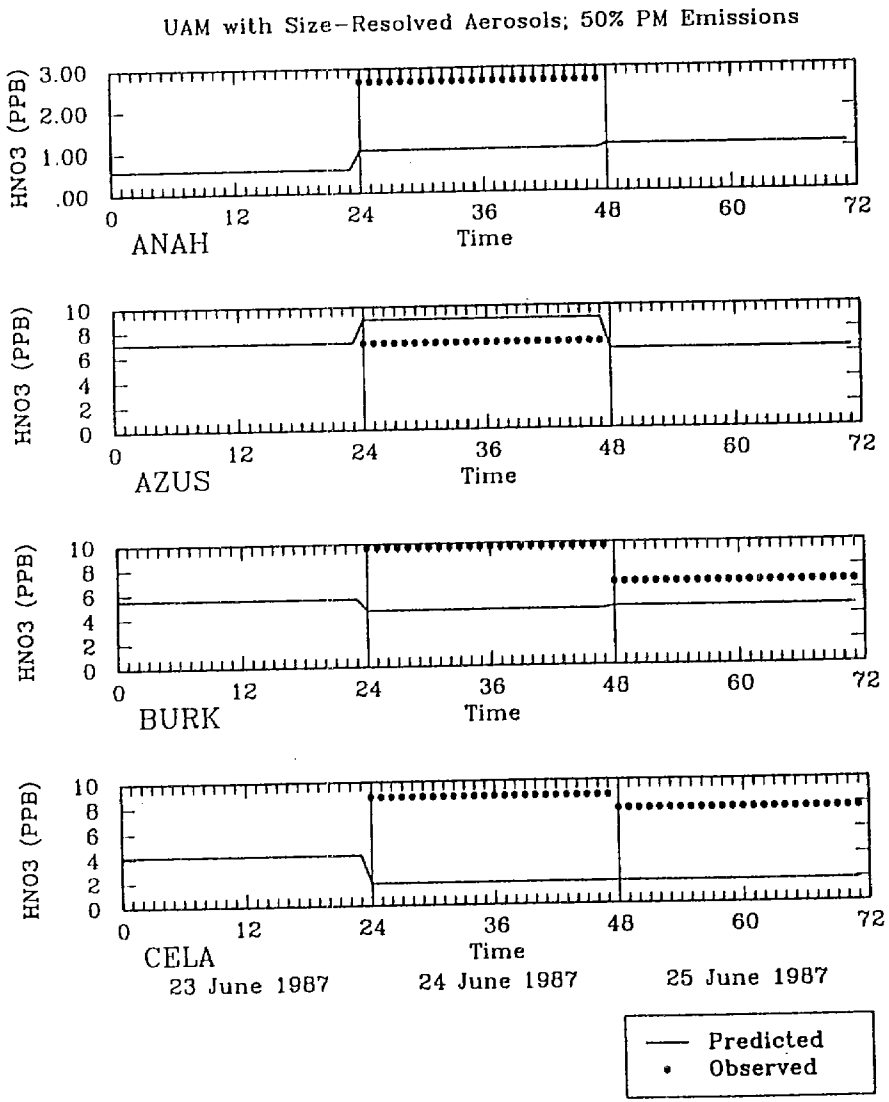
UAM with Size-Resolved Aerosols; 50% PM Emissions
HNO3 (PPB)
ANAH
AZUS
BURK
CELA
Time
23 June 1987
24 June 1987
25 June 1987
Predicted
Observed

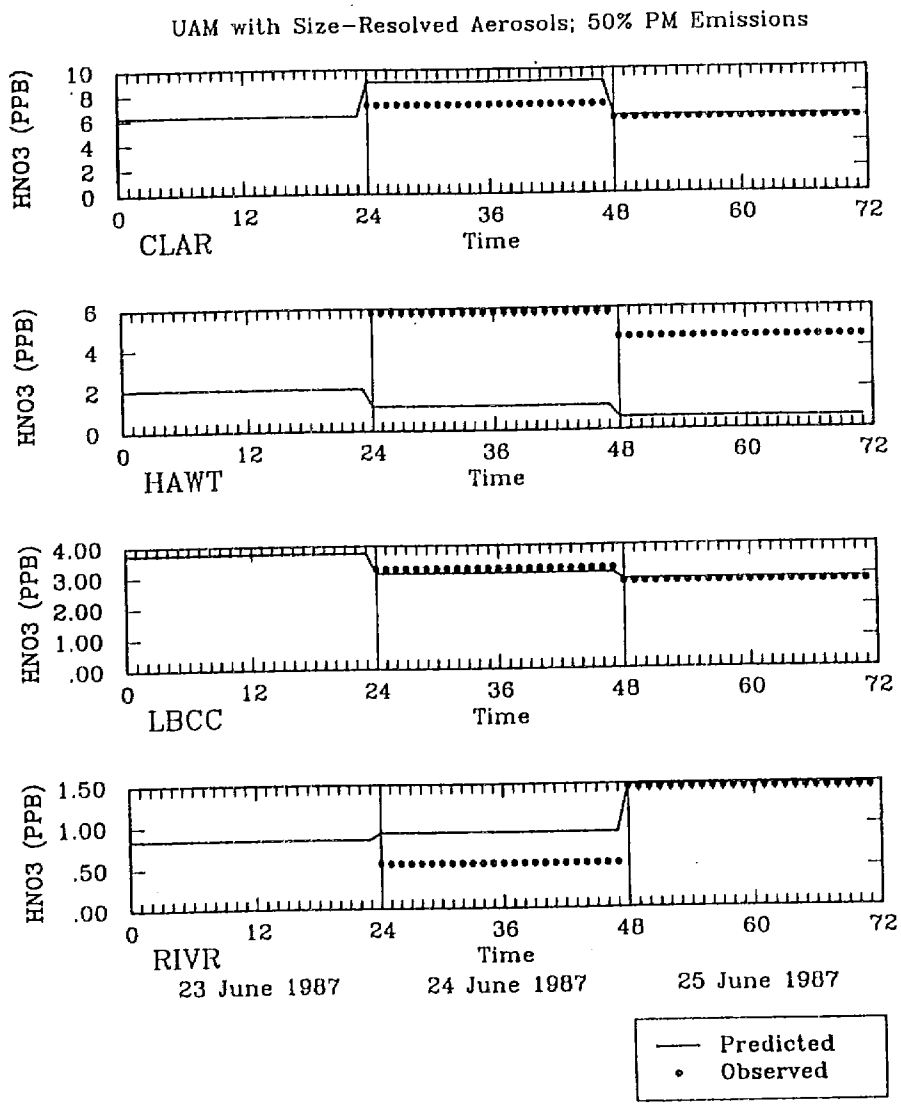
UAM with Size-Resolved Aerosols; 50% PM Emissions
HNO3 (PPB)
CLAR
HAWT
LBCC
RIVR
Time
23 June 1987
24 June 1987
25 June 1987
Predicted
Observed

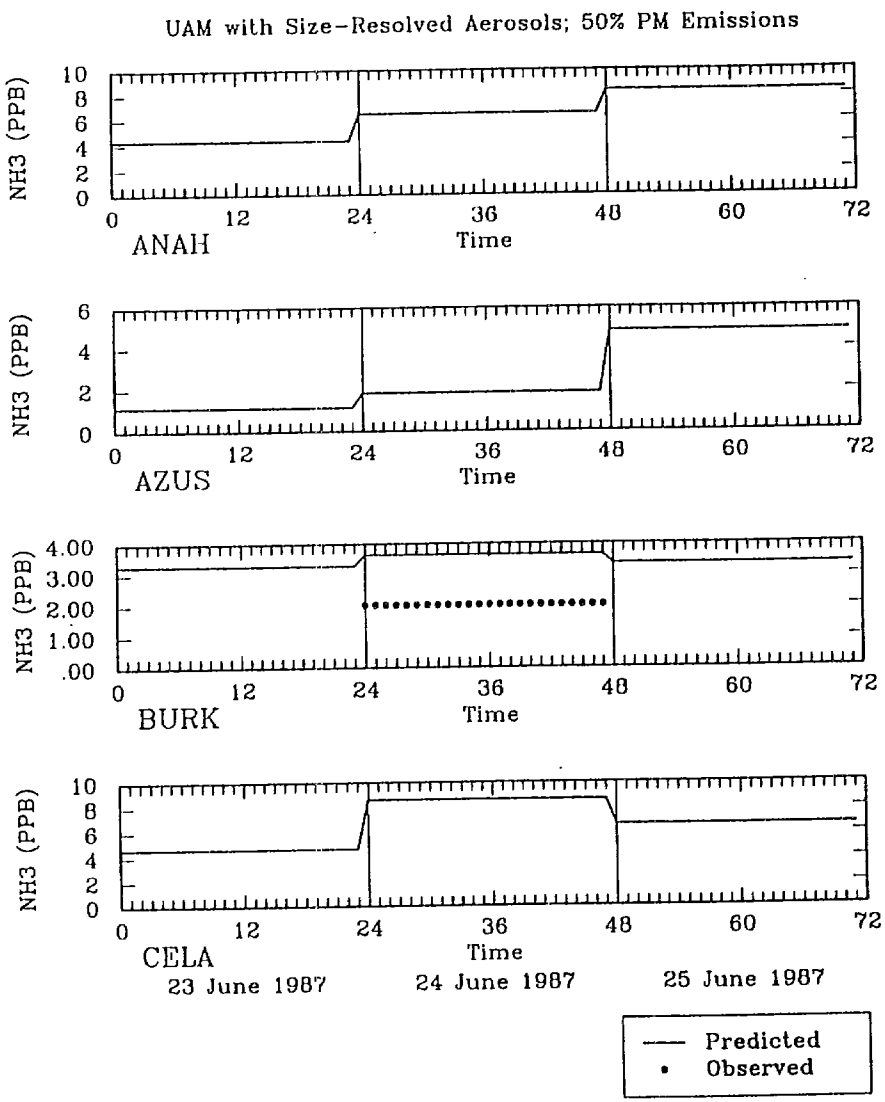
UAM with Size-Resolved Aerosols; 50% PM Emissions
NH3 (PPB)
ANAH
AZUS
BURK
CELA
Time
23 June 1987
24 June 1987
25 June 1987
Predicted
Observed

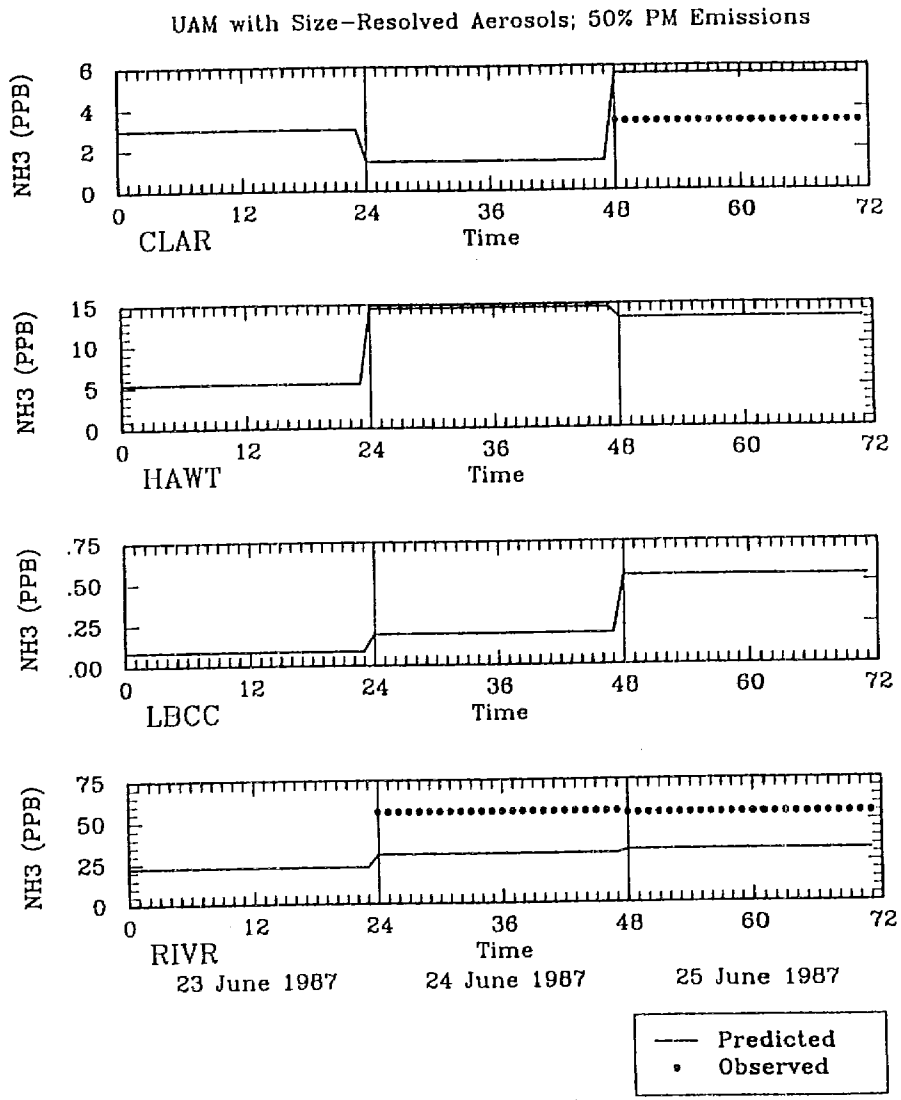
UAM with Size-Resolved Aerosols; 50% PM Emissions
NH3 (PPB)
CLAR
HAWT
LBCC
RIVR
Time
23 June 1987
24 June 1987
25 June 1987
Predicted
Observed

Appendix B

Station Plots for the December 10 and 11, 1987 Episode

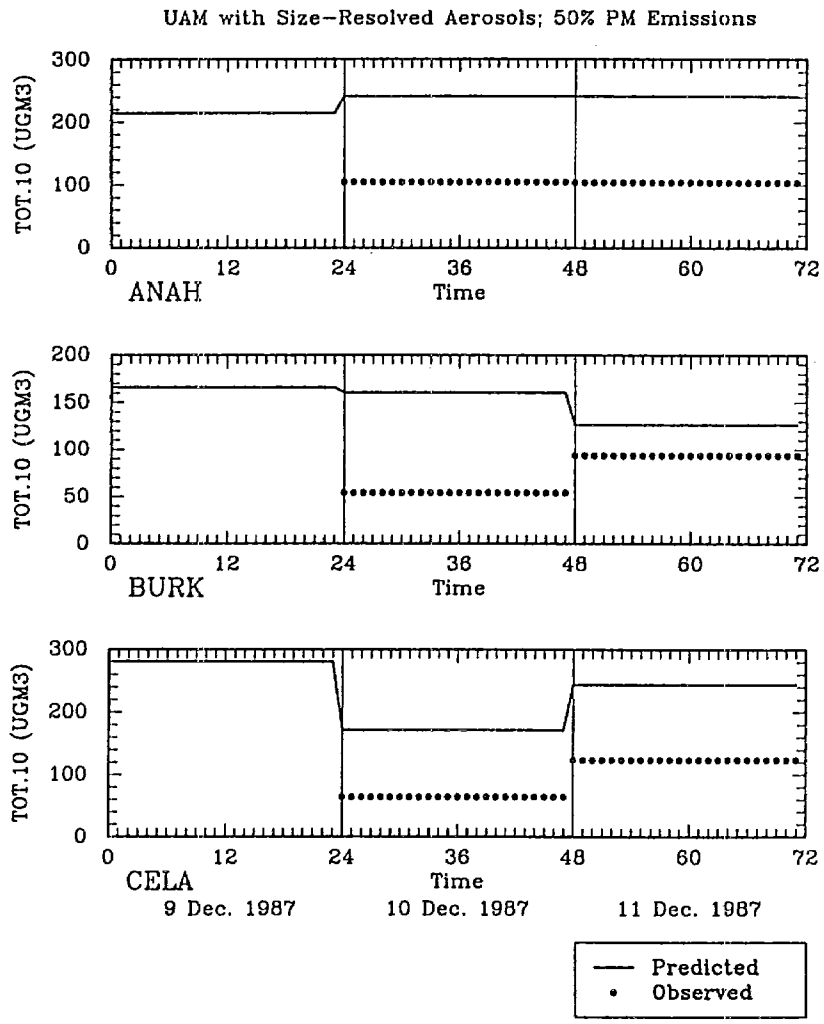
UAM with Size-Resolved Aerosols; 50% PM Emissions
TOT.10 (UGM3)
ANAH
BURK
CELA
Time
9 Dec. 1987
10 Dec. 1987
11 Dec. 1987
Predicted
Observed

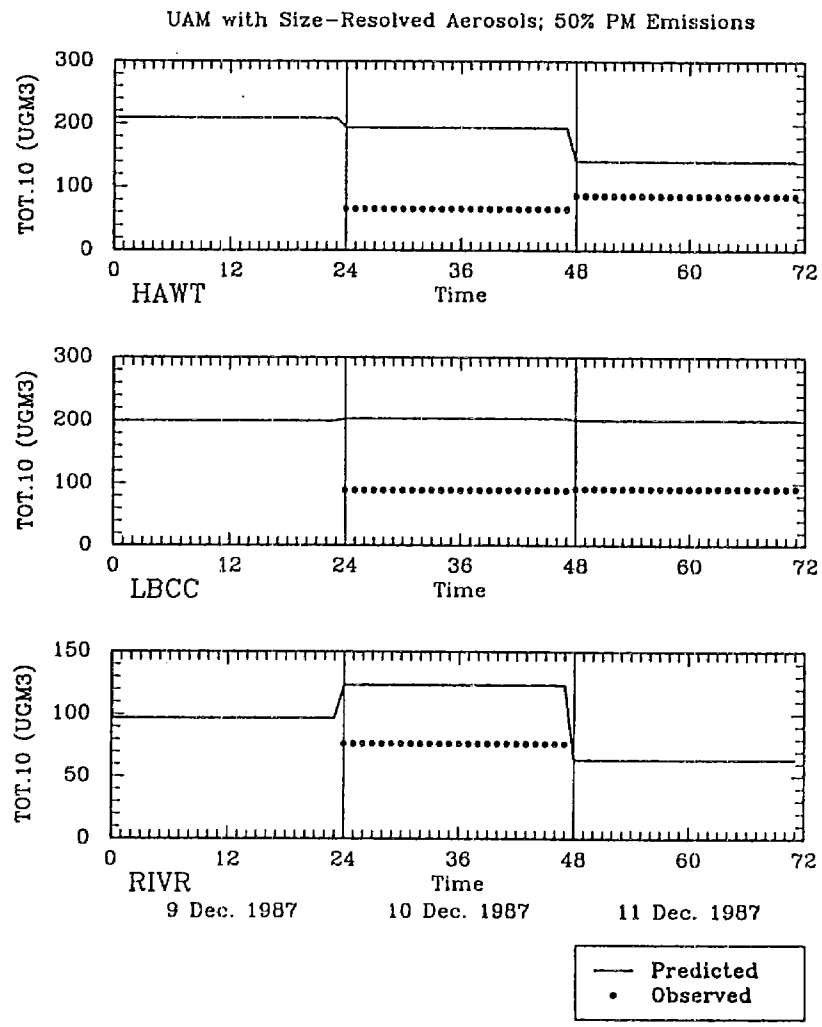
UAM with Size-Resolved Aerosols; 50% PM Emissions
TOT.10 (UGM3)
HAWT
LBCC
RIVR
Time
9 Dec. 1987
10 Dec. 1987
11 Dec. 1987
Predicted
Observed

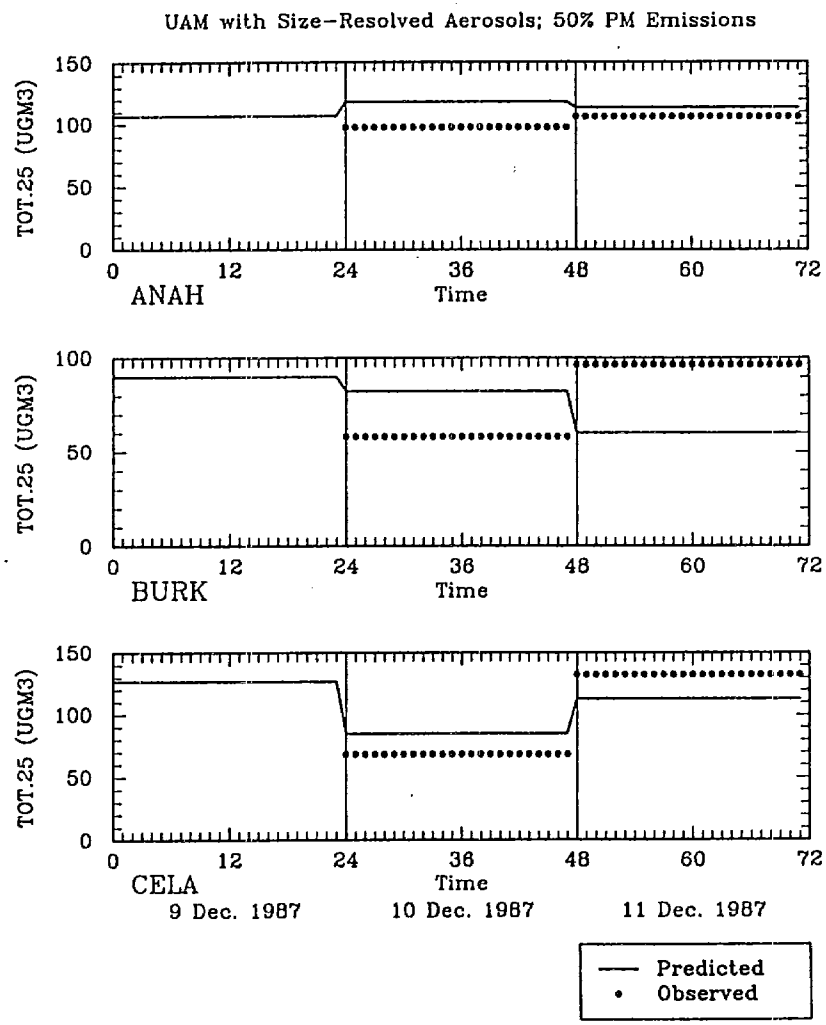
UAM with Size-Resolved Aerosols; 50% PM Emissions
TOT.25 (UGM3)
ANAH
BURK
CELA
Time
9 Dec. 1987
10 Dec. 1987
11 Dec. 1987
Predicted
Observed

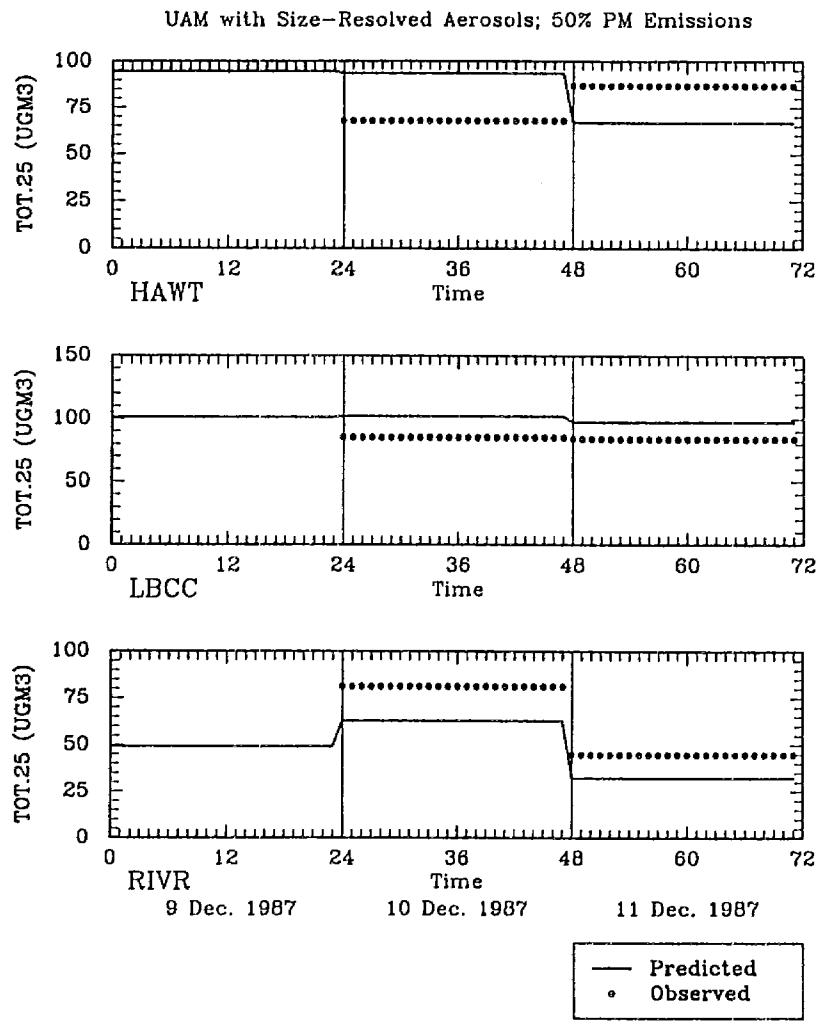
UAM with Size-Resolved Aerosols; 50% PM Emissions
TOT.25 (UGM3)
HAWT
LBCC
RIVR
Time
9 Dec. 1987
10 Dec. 1987
11 Dec. 1987
Predicted
Observed

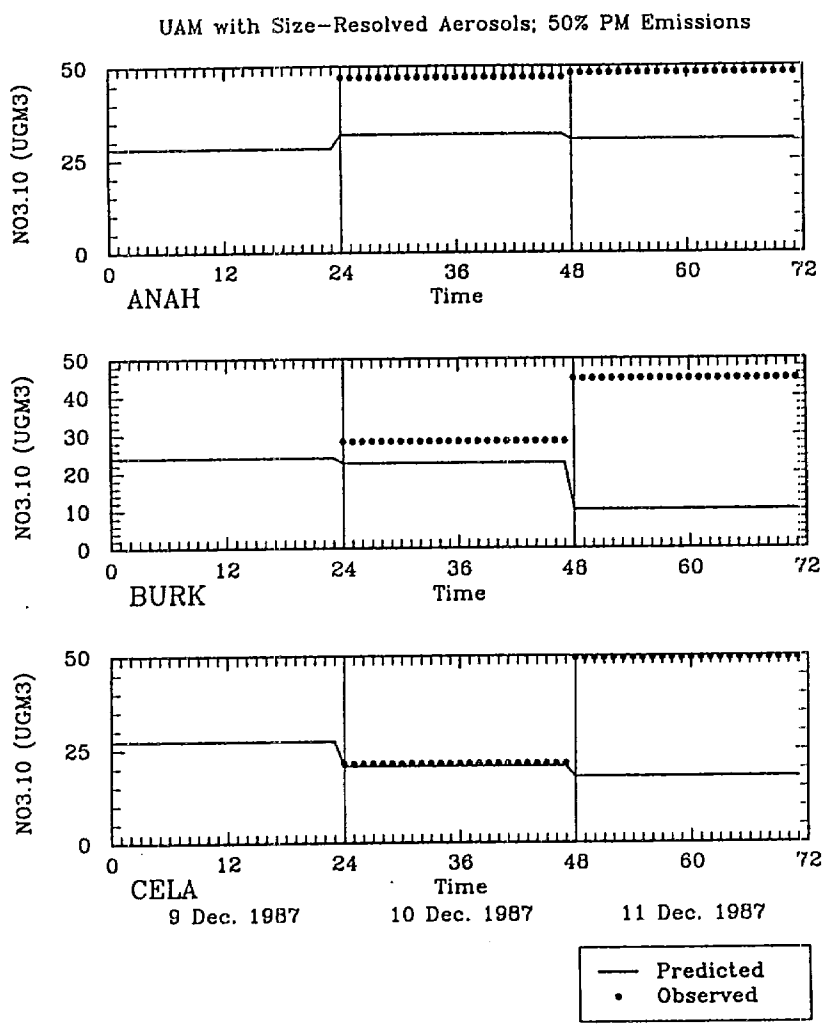
UAM with Size-Resolved Aerosols; 50% PM Emissions
NO3.10 (UGM3)
ANAH
BURK
CELA
Time
9 Dec. 1987
10 Dec. 1987
11 Dec. 1987
Predicted
Observed

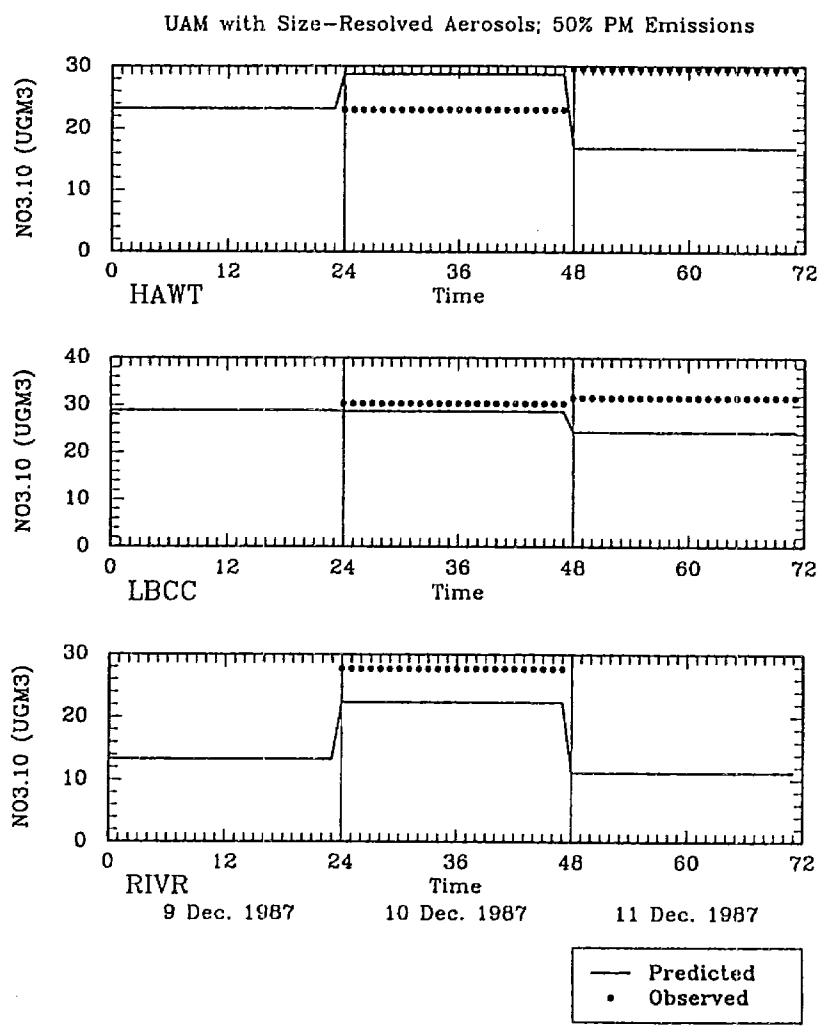
UAM with Size-Resolved Aerosols; 50% PM Emissions
NO3.10 (UGM3)
HAWT
LBCC
RIVR
Time
9 Dec. 1987
10 Dec. 1987
11 Dec. 1987
Predicted
Observed

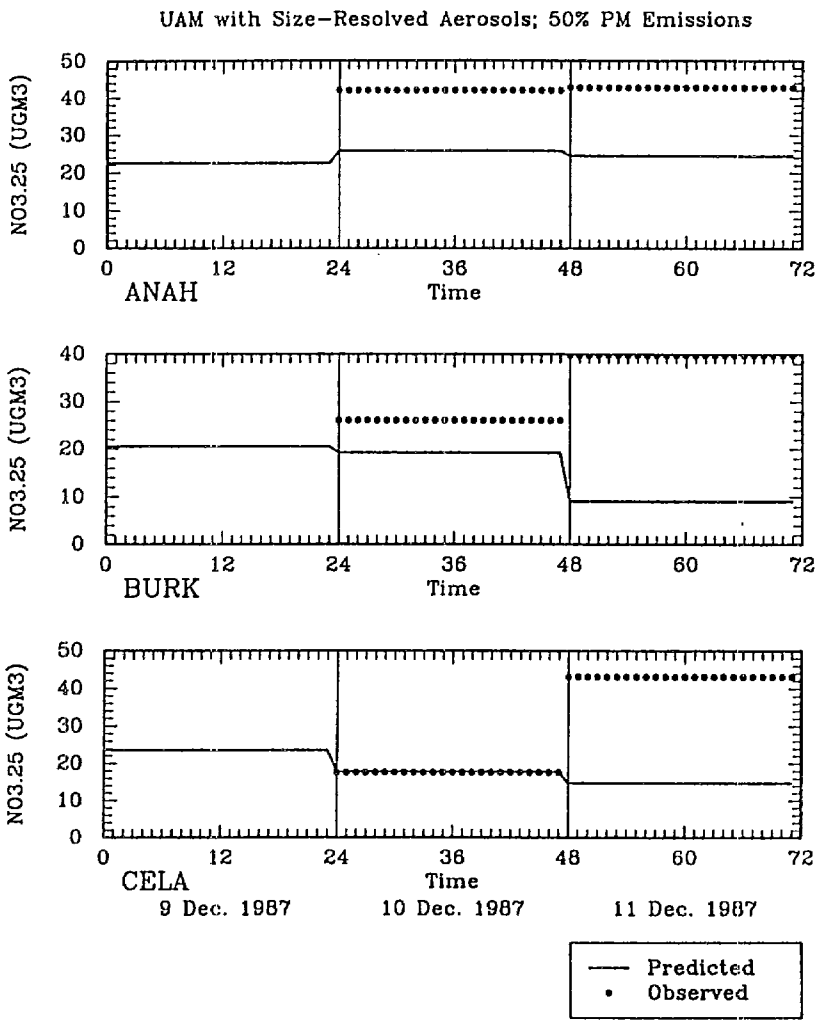
UAM with Size-Resolved Aerosols; 50% PM Emissions
NO3.25 (UGM3)
ANAH
BURK
CELA
Time
9 Dec. 1987
10 Dec. 1987
11 Dec. 1987
Predicted
Observed

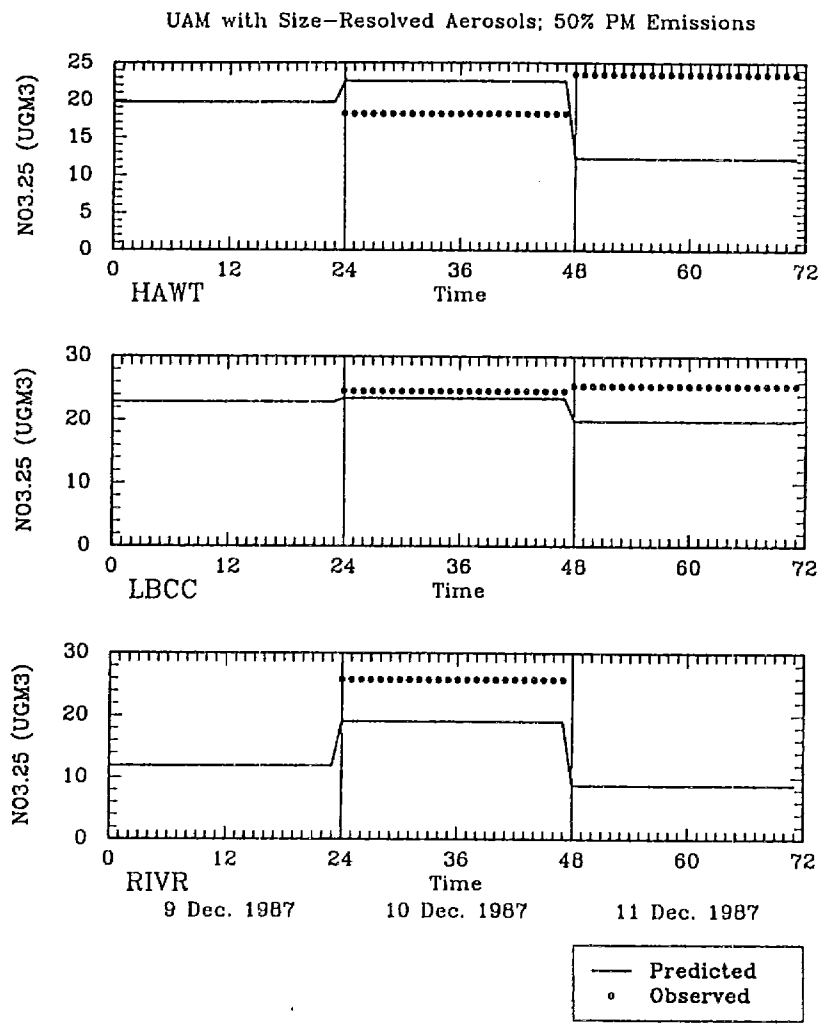
UAM with Size-Resolved Aerosols; 50% PM Emissions
NO3.25 (UGM3)
HAWT
LBCC
RIVR
Time
9 Dec. 1987
10 Dec. 1987
11 Dec. 1987
Predicted
Observed

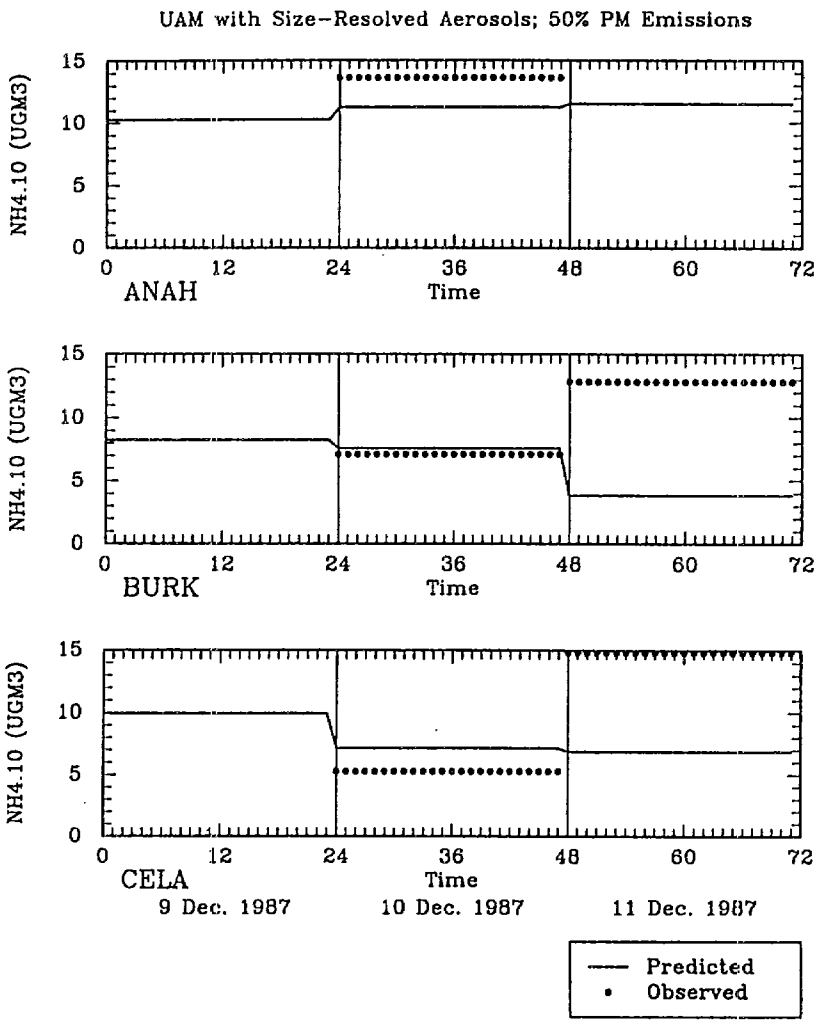
UAM with Size-Resolved Aerosols; 50% PM Emissions
NH4.10 (UGM3)
ANAH
BURK
CELA
Time
9 Dec. 1987
10 Dec. 1987
11 Dec. 1987
Predicted
Observed

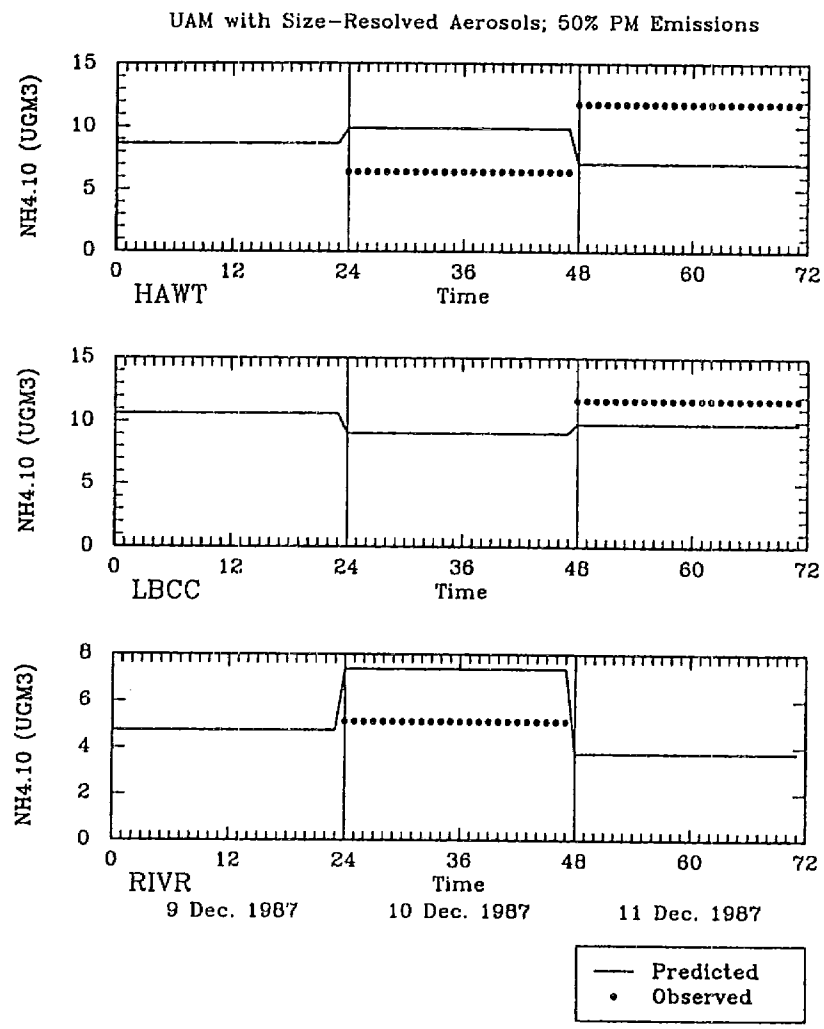
UAM with Size-Resolved Aerosols; 50% PM Emissions
NH4.10 (UGM3)
HAWT
LBCC
RIVR
Time
9 Dec. 1987
10 Dec. 1987
11 Dec. 1987
Predicted
Observed

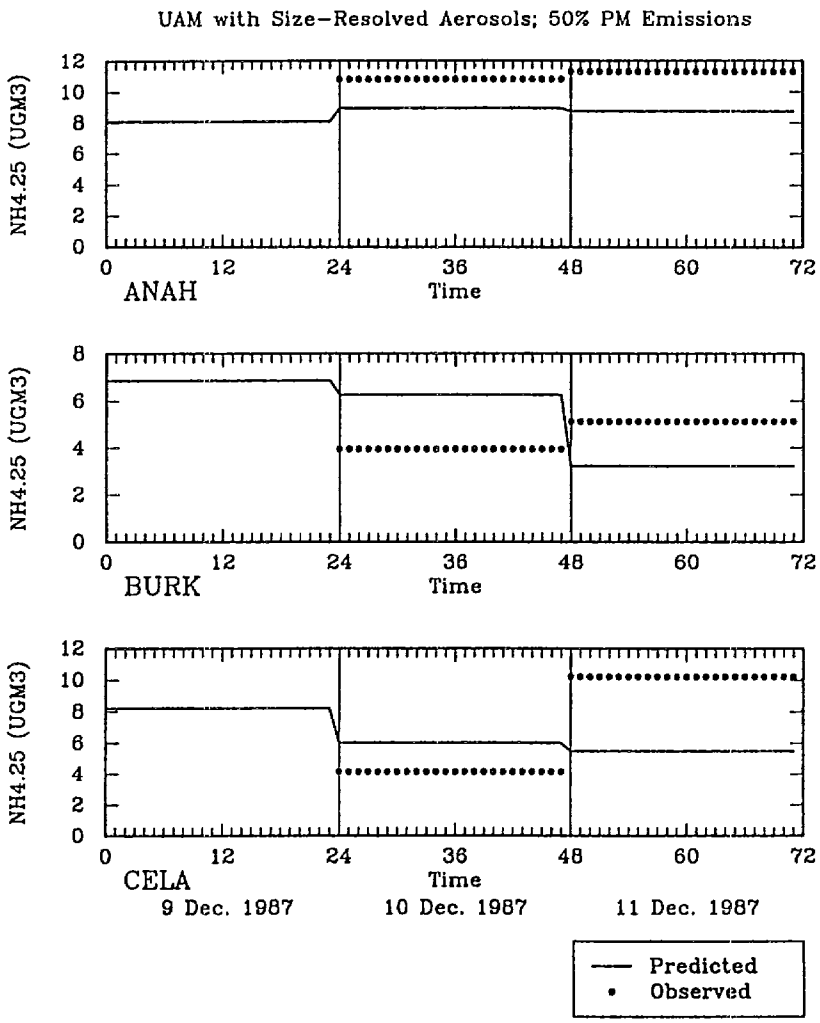
UAM with Size-Resolved Aerosols; 50% PM Emissions
NH4.25 (UGM3)
ANAH
BURK
CELA
Time
9 Dec. 1987
10 Dec. 1987
11 Dec. 1987
Predicted
Observed

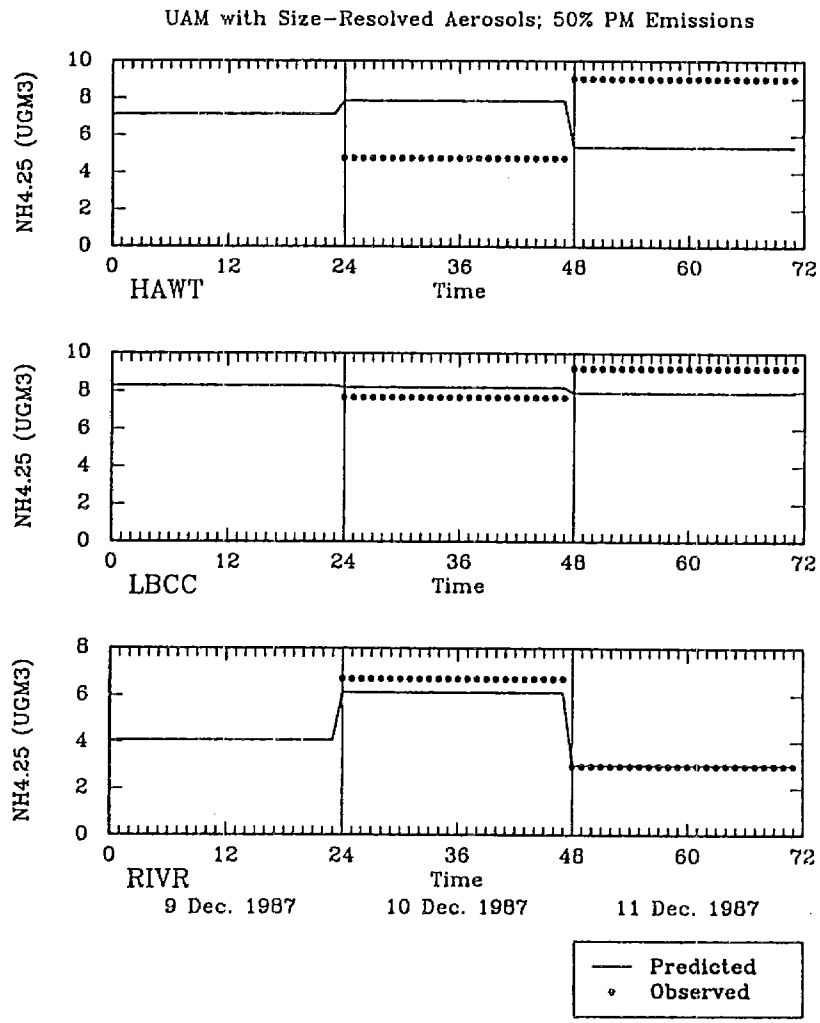
UAM with Size-Resolved Aerosols; 50% PM Emissions
NH4.25 (UGM3)
HAWT
LBCC
RIVR
Time
9 Dec. 1987
10 Dec. 1987
11 Dec. 1987
Predicted
Observed

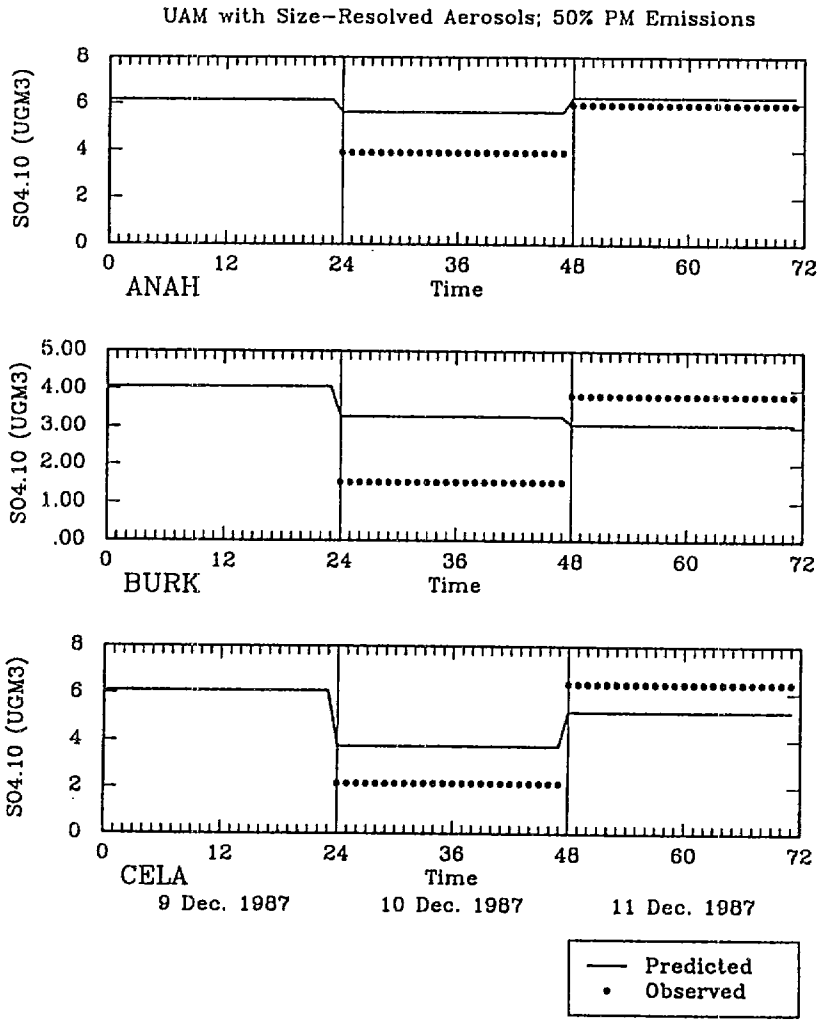
UAM with Size-Resolved Aerosols; 50% PM Emissions
SO4.10 (UGM3)
ANAH
BURK
CELA
Time
9 Dec. 1987
10 Dec. 1987
11 Dec. 1987
Predicted
Observed

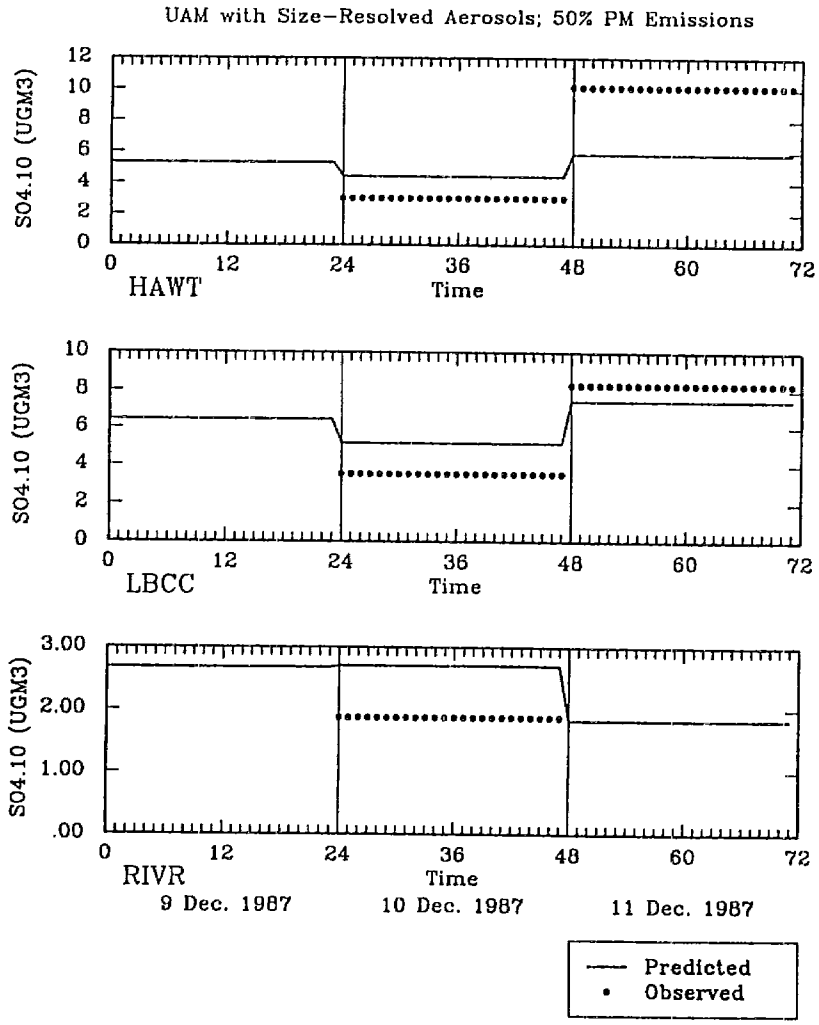
UAM with Size-Resolved Aerosols; 50% PM Emissions
SO4.10 (UGM3)
HAWT
LBCC
RIVR
Time
9 Dec. 1987
10 Dec. 1987
11 Dec. 1987
Predicted
Observed

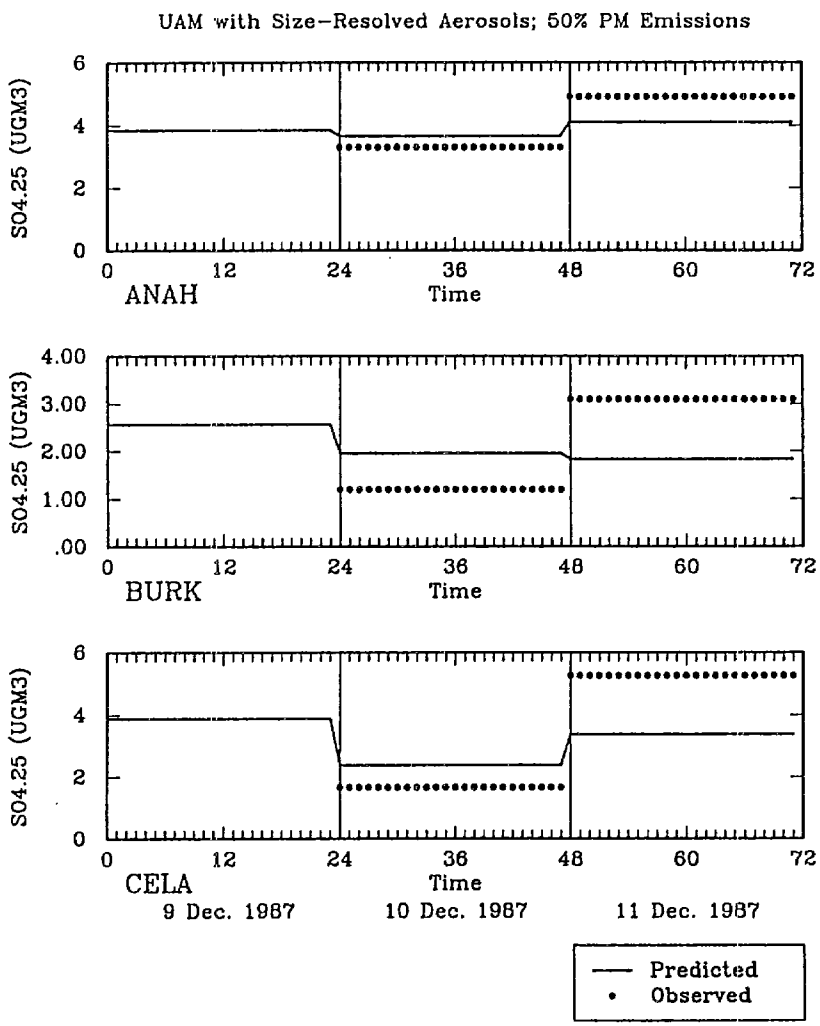
UAM with Size-Resolved Aerosols; 50% PM Emissions
SO4.25 (UGM3)
ANAH
BURK
CELA
Time
9 Dec. 1987
10 Dec. 1987
11 Dec. 1987
Predicted
Observed

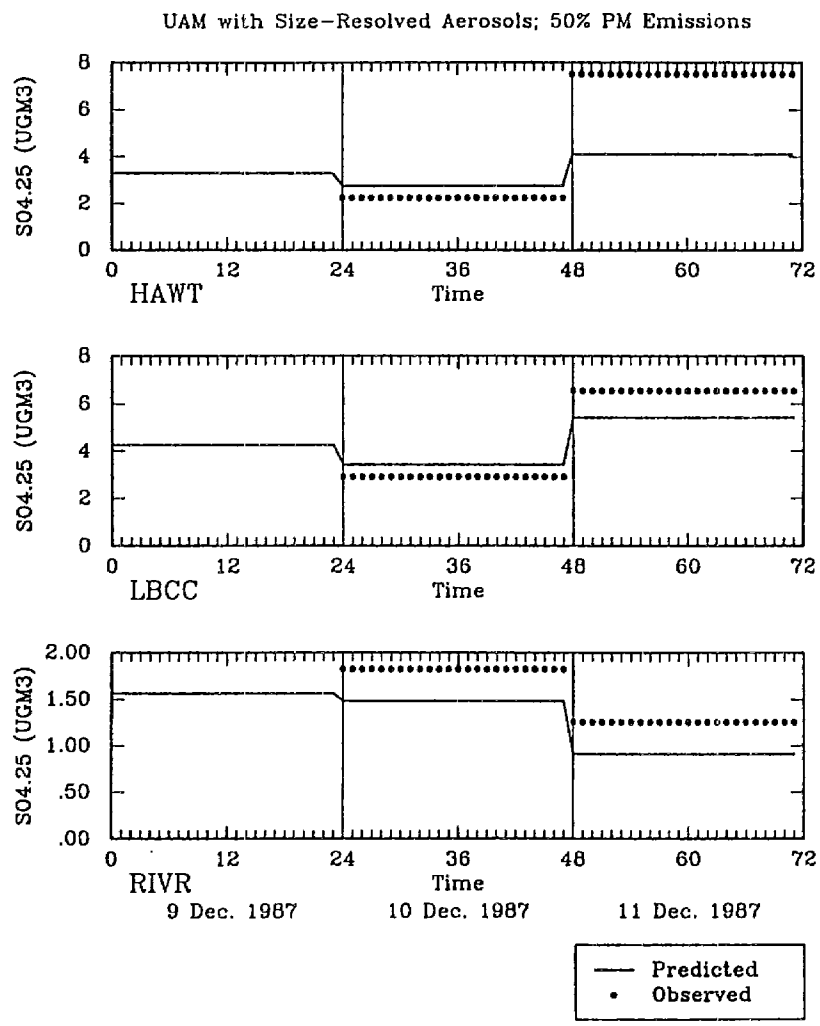
UAM with Size-Resolved Aerosols; 50% PM Emissions
SO4.25 (UGM3)
HAWT
LBCC
RIVR
Time
9 Dec. 1987
10 Dec. 1987
11 Dec. 1987
Predicted
Observed

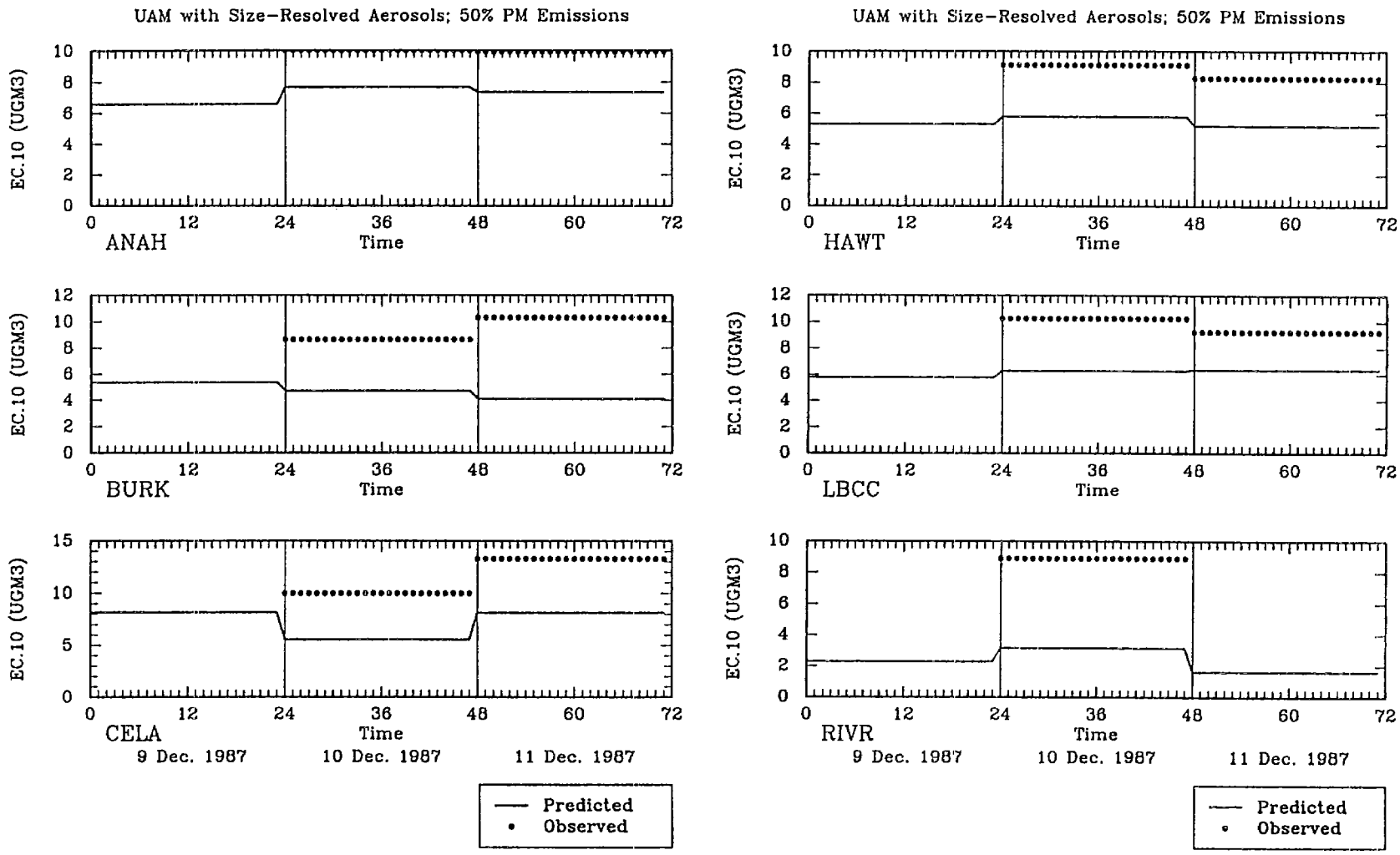
UAM with Size-Resolved Aerosols; 50% PM Emissions
EC.10 (UGM3)
ANAH
BURK
CELA
Time
9 Dec. 1987
10 Dec. 1987
11 Dec. 1987
Predicted
Observed
UAM with Size-Resolved Aerosols; 50% PM Emissions
HAWT
LBCC
RIVR

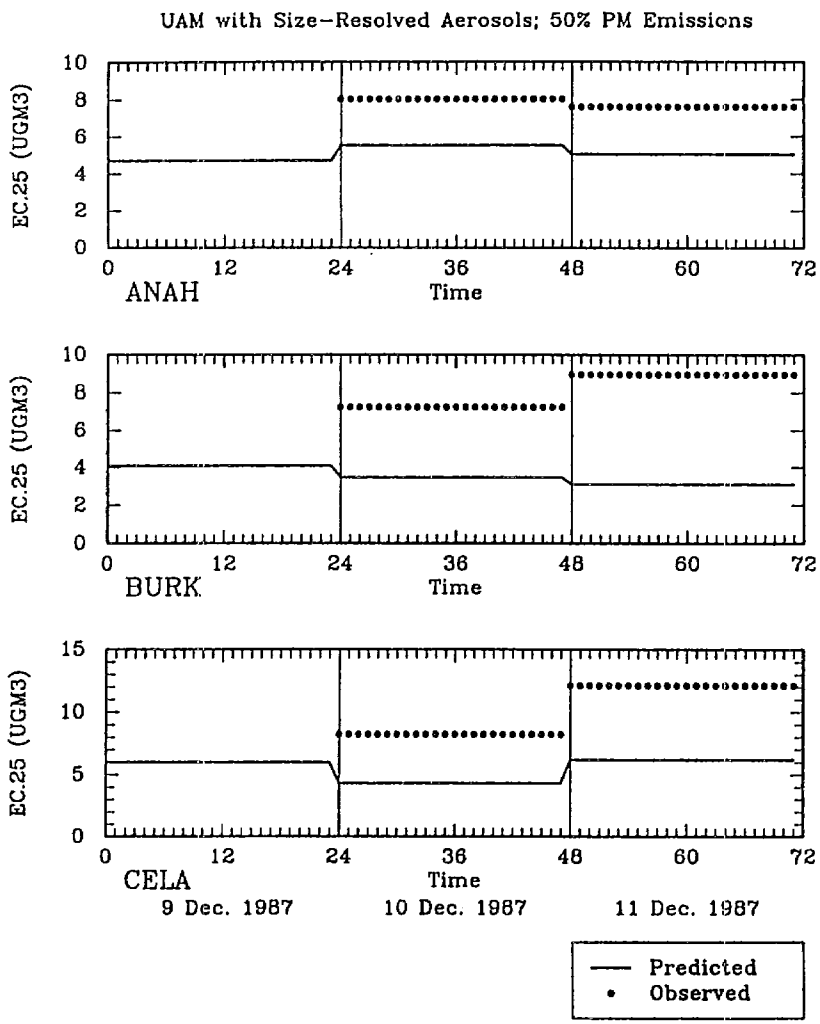
UAM with Size-Resolved Aerosols; 50% PM Emissions
EC.25 (UGM3)
ANAH
BURK
CELA
Time
9 Dec. 1987
10 Dec. 1987
11 Dec. 1987
Predicted
Observed

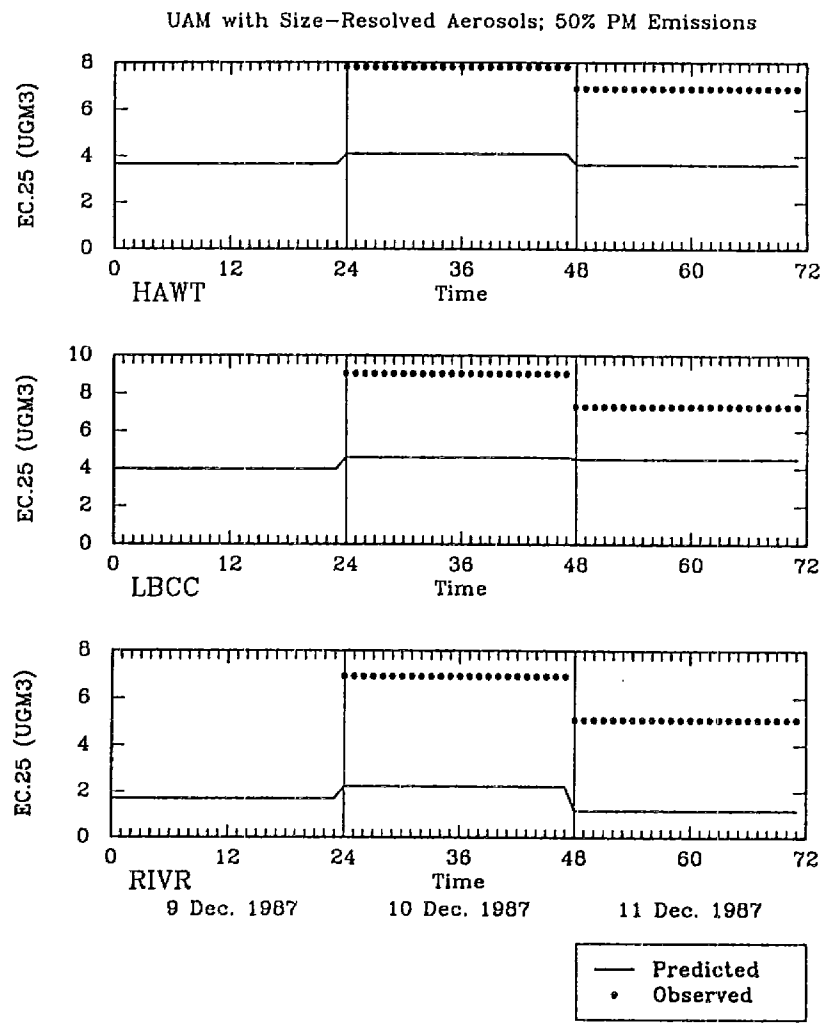
UAM with Size-Resolved Aerosols; 50% PM Emissions
EC.25 (UGM3)
HAWT
LBCC
RIVR
Time
9 Dec. 1987
10 Dec. 1987
11 Dec. 1987
Predicted
Observed

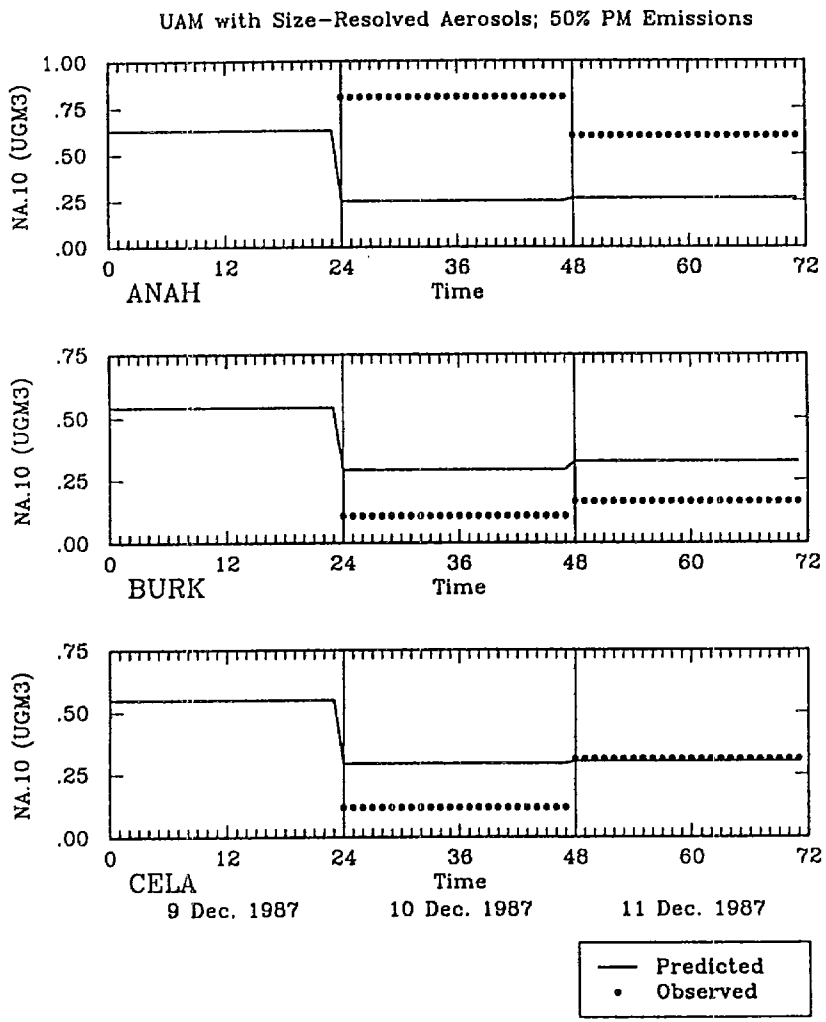
UAM with Size-Resolved Aerosols; 50% PM Emissions
NA.10 (UGM3)
1.00
.75
.50
.25
.00
0
12
24
36
48
60
72
ANAH
Time
.75
.50
.25
.00
BURK
.75
.50
.25
.00
CELA
9 Dec. 1987
10 Dec. 1987
11 Dec. 1987
Predicted
Observed

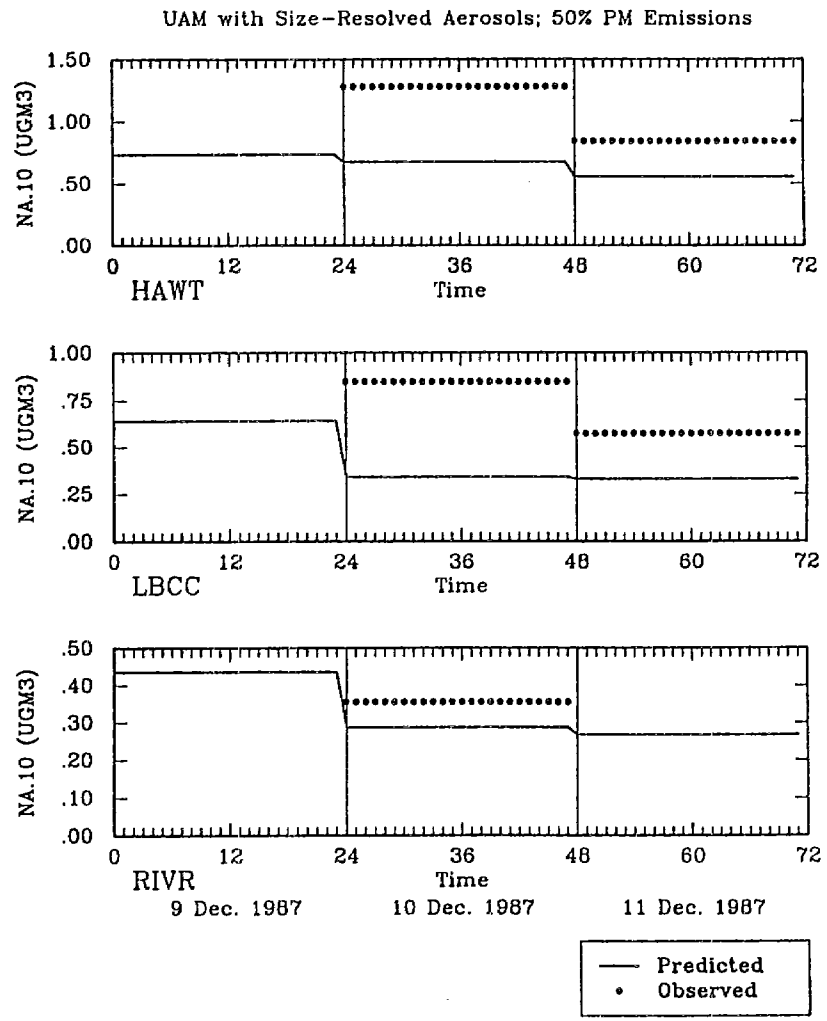
UAM with Size-Resolved Aerosols; 50% PM Emissions
NA.10 (UGM3)
1.50
1.00
.50
.00
0
12
24
36
48
60
72
HAWT
Time
1.00
.75
.50
.25
.00
LBCC
.50
.40
.30
.20
.10
.00
RIVR
9 Dec. 1987
10 Dec. 1987
11 Dec. 1987
Predicted
Observed

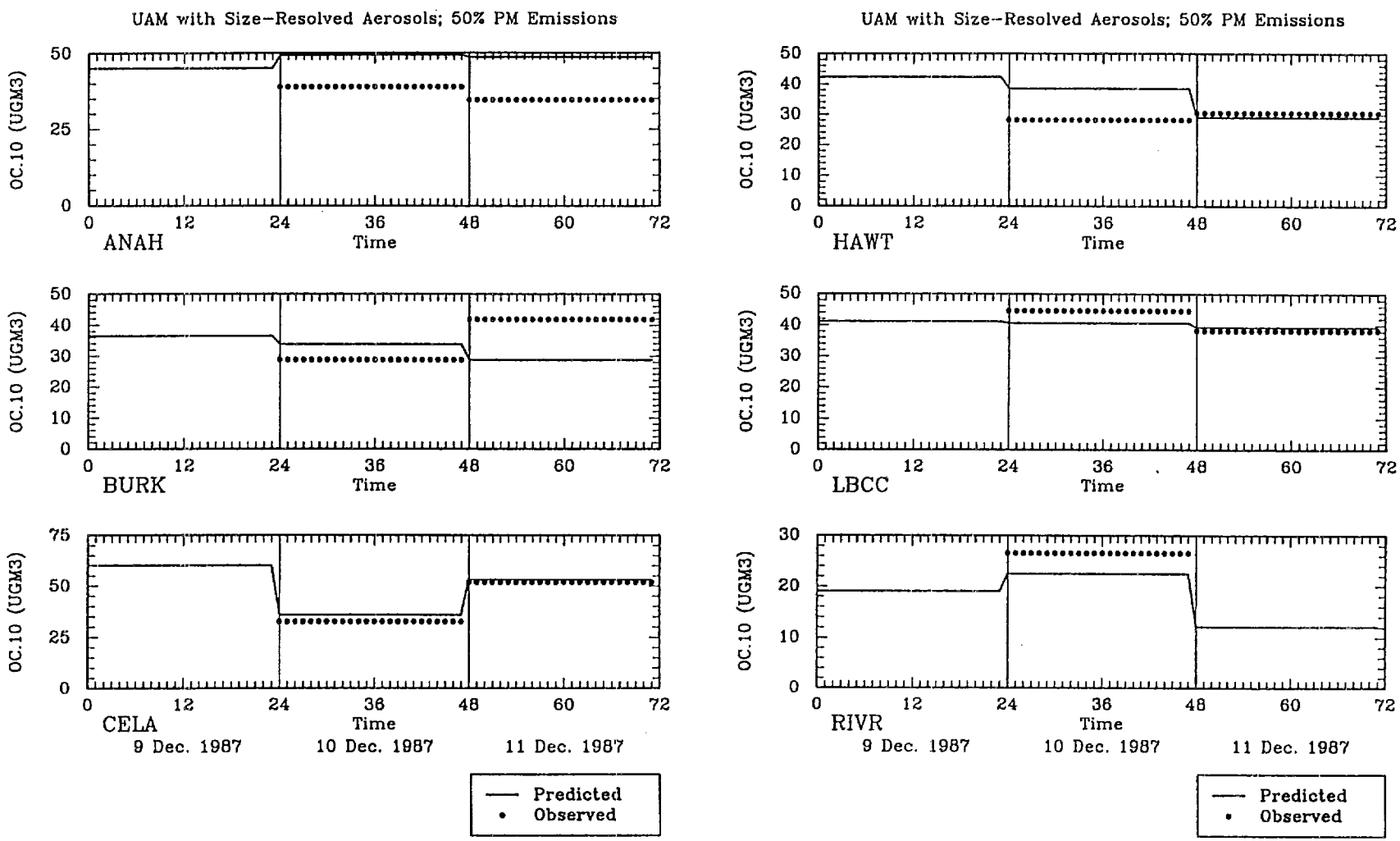
UAM with Size-Resolved Aerosols; 50% PM Emissions
OC.10 (UGM3)
ANAH
BURK
CELA
HAWT
LBCC
RIVR
Time
9 Dec. 1987
10 Dec. 1987
11 Dec. 1987
Predicted
Observed

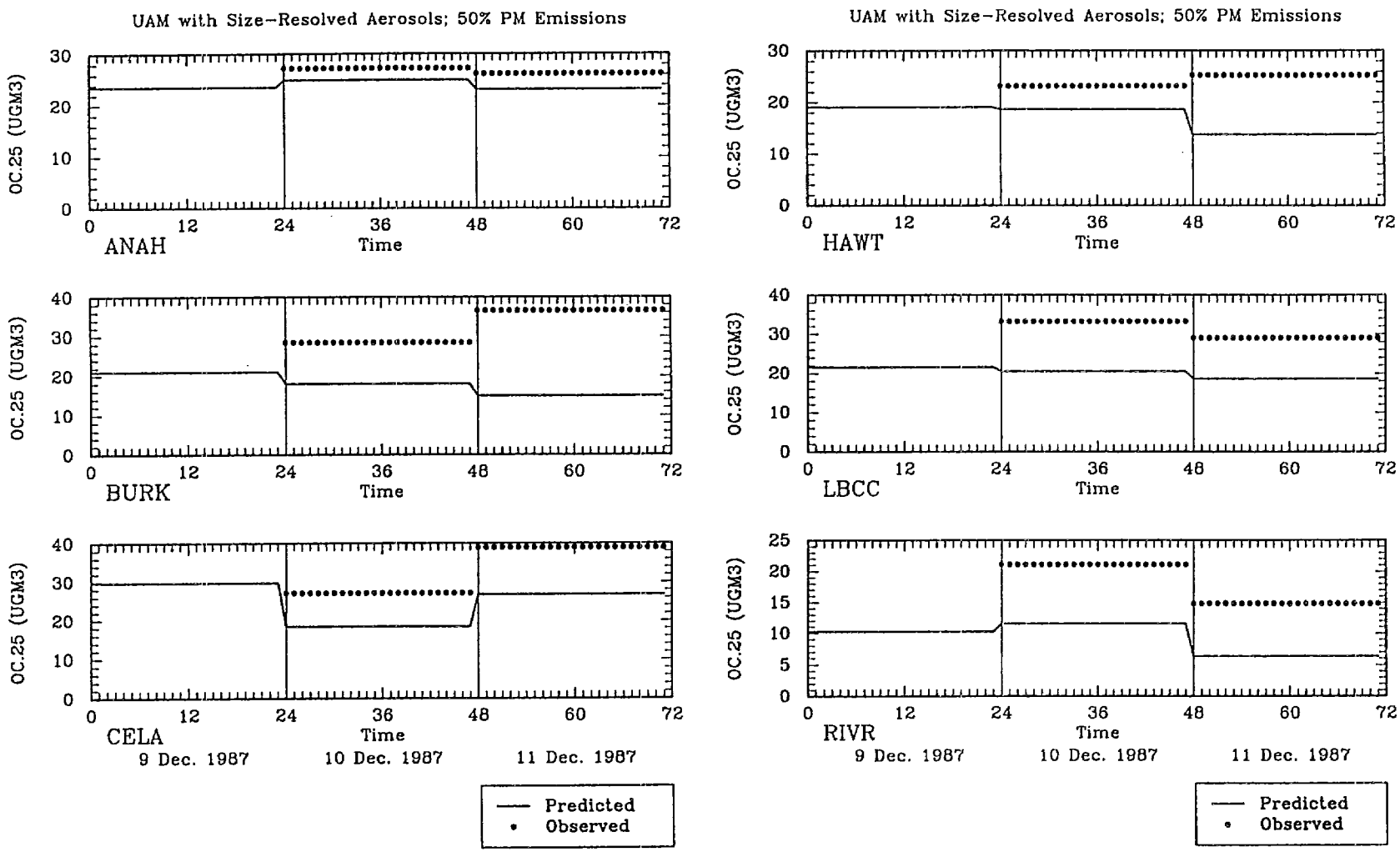
UAM with Size-Resolved Aerosols; 50% PM Emissions
OC.25 (UGM3)
ANAH
BURK
CELA
HAWT
LBCC
RIVR
Time
9 Dec. 1987
10 Dec. 1987
11 Dec. 1987
Predicted
Observed

Appendix C

Bimodal Character of Accumulation Mode Aerosol Mass Distributions in Southern California

Hering, S., Eldering, A., and Seinfeld, J.H. (1997) Bimodal character of accumulation mode aerosol mass distributions in Southern California, *Atmos. Environ.*, *31*, 1-11.

Pergamon

PII: S1352-2310(96)00175-6

Atmospheric Environment Vol. 31, No. 1, pp. 1-11, 1997
Copyright © 1996 Published by Elsevier Science Ltd
Printed in Great Britain. All rights reserved
1352-2310/97 $15.00 + 0.00

BIMODAL CHARACTER OF ACCUMULATION MODE AEROSOL MASS DISTRIBUTIONS IN SOUTHERN CALIFORNIA

SUSANNE HERING,* ANNMARIE ELDERING† and JOHN H. SEINFELD‡,§

*Aerosol Dynamics Inc., 2329 Fourth Street, Berkeley, CA 94710, U.S.A.; † Department of Civil and Environmental Engineering, University of Iowa, Iowa City, IA 52242-1527, U.S.A.; and ‡ Division of Engineering and Applied Science, California Institute of Technology, 104-44, Pasadena, CA 91125, U.S.A.

(*First received* 29 *February* 1996 *and in final form* 24 *May* 1996)

Abstract—Size-resolved measurements of fine particle chemical composition and physical measurements of fine particle size distributions obtained during the Southern California Air Quality Study (SCAQS) are compared. Number distributions of the ambient aerosols were measured using optical particle counters and electrical aerosol analyzers. Optical counter data are reduced using an ambient-based calibration. Mass size distributions are inferred from the sum of size-resolved chemical composition as measured by impactors. Optical counter data reduced with an ambient-based calibration compare well to impactor measurements. Both sets of data show that the accumulation mode of the total mass size distribution may be bimodal. Condensation and droplet modes previously identified in chemical species size distributions are frequently apparent in the total mass size distribution. Copyright © 1996 Published by Elsevier Science Ltd

Key word index: SCAQS, aerosols, mass distributions.

INTRODUCTION

In work in the 1970s, Whitby and coworkers showed that the volume or mass distribution of airborne particles is composed of several modes. They identified three modes: a coarse mode, an accumulation mode and a nuclei mode (Willeke and Whitby, 1975). The coarse mode, corresponding to particles above 2 μm in diameter, was associated with wind-blown dust and mechanically generated aerosols. The accumulation mode, corresponding to particles approximately 0.1 to 2 μm in diameter, was identified as particles originating from aged combustion sources and photochemical processes. A nuclei mode corresponding to particles below 0.1 μm was apparent in size distributions measured along freeways, and was attributed to fresh combustion sources.

More recently, impactor measurements of the size distribution of inorganic ion species have shown a bimodal character for these aerosols in the accumulation mode size range, that is for diameters between 0.1 and 1 μm. Hering and Friedlander (1982) identified two types of sulfur size distributions in the Los Angeles Basin, with typical modal diameters of 0.2 and 0.6 μm, respectively. The more predominant mode was that at 0.6 μm, and this was attributed to sulfates formed as the result of heterogeneous processes. The 0.2 μm mode was attributed to sulfates formed as the result of homogeneous gas phase reactions. John *et al.* (1990) observed similar modes in the nitrate, ammonium ion and sulfate size distributions measured in the Southern California Air Quality Study (SCAQS). He labeled these modes as "condensation" and "droplet". Similar multimodal character for carbon-containing particles and for sulfates and nitrates is evident in data reported by Sloane *et al.* (1991) for the Denver area.

Meng and Seinfeld (1994) examined the mechanisms of formation of the droplet mode. They showed that growth of condensation mode particles by accretion of water vapor or by gas-phase or aerosol-phase sulfate production cannot explain the existence of the droplet mode. Activation of condensation mode particles to form fog or cloud drops followed by aqueous-phase chemistry and fog evaporation was shown to be a plausible mechanism for formation of the droplet mode.

The question addressed in this paper is whether "condensation" and "droplet" modes are present in the total, physical size distribution, as well as in the size distribution of individual chemical constituents. More specifically, we ask how prevalent is the bimodal nature of the accumulation mode. The question is addressed through examination of size-resolved chemical composition and physical size

§ Author to whom correspondence should be addressed.

distribution data on fine ambient aerosols measured during the Southern California Air Quality Study (SCAQS). This data set includes number distributions measured using optical particle counters and electrical aerosol analyzers, size-resolved chemical composition obtained from impactors, and total fine particle chemical composition determined through filter measurements. To assess the ability to resolve the bimodal character of accumulation mode aerosol, we first examine the consistency among the data sets. We then analyze the accumulation mode size distributions, and changes in chemical composition as a function of size.

THE SCAQS DATA SET

For SCAQS, impactor and physical size distribution measurements were made in 1987 during 11 summer time intensive measurement days at the Claremont and Riverside sampling sites (Hering and Blumenthal, 1989). During six fall intensive measurement days, these size distributions were measured at Long Beach and downtown Los Angeles sampling sites. Impactor samples were collected over 4 h sampling periods during the day, beginning at 0600 local time, and then over a single 12 h period at night, beginning at 1800, giving four distributions per site per day. Physical size distributions were measured continuously, and were averaged over the impactor sampling periods. Additionally, total fine particle concentrations were measured by filter methods using the SCAQS sampler, which had the same daytime sampling periods as the impactors. As reported by Eldering *et al.* (1994), 80 to 95% of the gravimetrically measured PM 2.5 filter mass was chemically identified, depending on the site examined.

Physical size distributions of submicrometer aerosols were measured using an electrical aerosol analyzer (TSI model 3030, St Paul, Minnesota) and a 32-channel active scattering laser particle counter with a nominal size range from 0.09 to 3 μm (Particle Measuring Systems model ASASP-X, Boulder, Colorado). The electrical aerosol analyzer (EAA) and laser optical particle counter (OPC) sampled from a metal plenum. Both instruments were located inside a sampling trailer, and were not at ambient relative humidity. The EAA data were reduced using the manufacturer's published constants. The optical particle counter data were reduced using the ambient aerosol calibration data of Hering and McMurry (1991), as described below. This is similar to the method used by Eldering *et al.* (1994).

Size distributions of the inorganic ions were measured by John *et al.* (1990) using Berner impactors. Samples were collected on greased tedlar substrates, and analyzed by ion chromatography. Size distributions of carbonaceous aerosol were acquired by the University of Minnesota (McMurry, 1989) using the micro-orifice uniform deposit impactor (MOUDI) preceded by an AIHL cyclone (John and Reischl, 1980). Samples were collected on ungreased aluminum foil substrates which were not rotated during sampling, and were analyzed by heating the samples in contact with an MnO_2 catalyst and quantitating the evolved carbon dioxide (Mueller *et al.*, 1982).

COMPARISON OF IMPACTOR AND FILTER DATA

The concentration of fine particle ions and of organic and elemental carbon measured by impactor are compared to that measured by filtration using the SCAQS sampler (Fitz and Zwicker, 1988). With the SCAQS sampler, fine particle sulfate was measured on a 47 mm Teflon filter operated downstream of a Bendix cyclone. This same filter was also assayed for nitrate and ammonium ion, but these values were not used directly. Fine particle nitrate was measured by a nylon filter operated downstream of a MgO multiple tube denuder and an AIHL cyclone. The loss of nitrate from the Teflon filter was determined by comparison with the nylon filter value, and this difference was used to correct the ammonium ion concentration with the assumption that all of the volatilized nitrate was in the form of ammonium nitrate. Finally, carbonaceous aerosol concentrations are measured from a quartz fiber filter operated in parallel to the Teflon filter, downstream of the Bendix cyclone. Organic (OC) and elemental (EC) carbon were analyzed by the same method used for the impactor samples (Mueller *et al.*, 1982). Organic carbon (OC) concentrations were corrected for vapor adsorption on a sample-by-sample basis by subtraction of the organic carbon measured simultaneously on a quartz backup filter placed downstream of the Teflon filter.

To summarize, the formulas used to derive the airborne concentration of inorganic ions from the SCAQS sampler are as follows:

$$SO_4^{2-} = L_9(SO_4)$$

$$NO_3^- = L_3(NO_3)$$

$$NH_4^+ = L_9(NH_4) + 0.29[L_3(NO_3) - L_9(NO_3)]$$

$$OC = L_7(OC) - L_9(OC)$$

$$EC = L_7(EC)$$

where $L_9(SO_4)$, $L_9(NO_3)$ and $L_9(NH_4)$ refer to the sulfate, nitrate and ammonium ion concentrations on the fine particle Teflon filter, and $L_3(NO_3)$ is the nitrate concentration from the denuded fine particle nylon filter. $L_7(OC)$ and $L_7(EC)$ refer to organic and elemental carbon determinations on the parallel quartz filter, and $L_9(OC)$ is organic carbon on the quartz backup filter. (The designations L_3, L_7 and L_9 refer to the legs 3, 7, and 9 of the sampler, as defined by Fitz and Zwicker (1988).) The ammonium ion concentration inferred by this method agreed (absence of systematic bias) with that measured on an

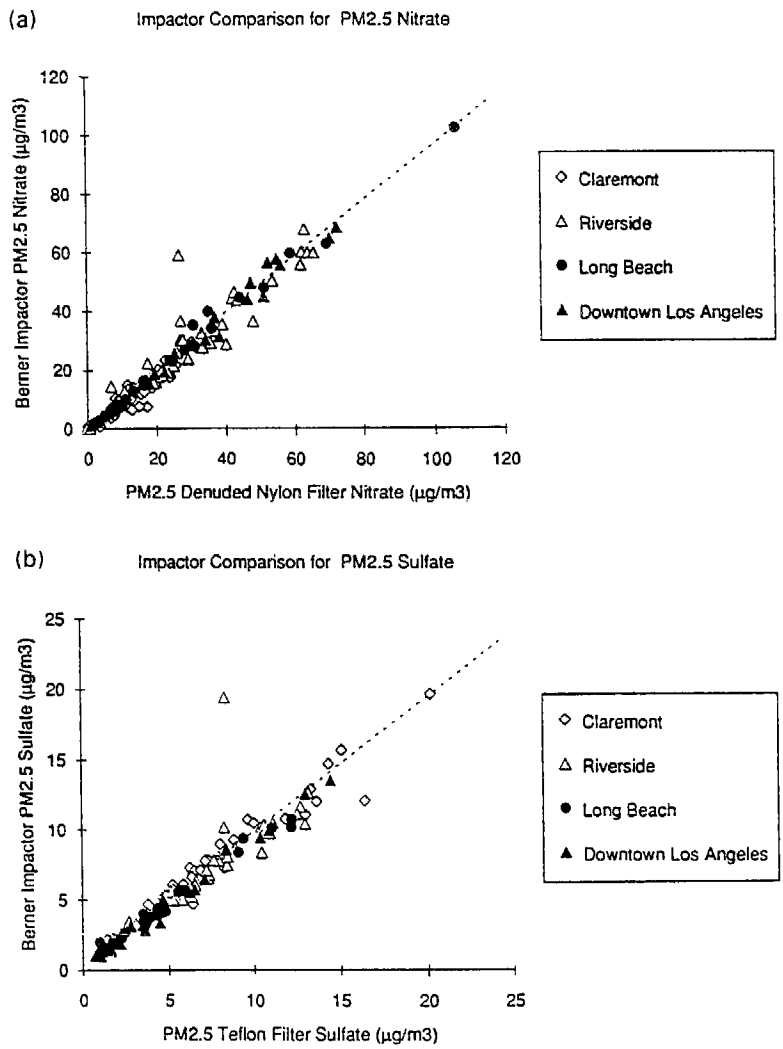

Fig. 1. Comparison of fine particle inorganic ion concentrations measured by Berner impactor (John *et al.*, 1990) and by the SCAQS denuder-filter sampler (Fitz and Zwicker, 1988). (a) Nitrate, (b) sulfate. The dashed line is the 1 : 1 correspondence.

oxalic acid filter downstream of an oxalic acid coated glass tube denuder at most sites. The sole exception was at Riverside, where the denuder became overloaded due to the high ammonia concentrations.

To compare the Berner impactor data to the filter data, the AIHL cylcone penetration efficiency curve was applied to the Berner size distribution data to obtain a size fraction equivalent to that measured on the filters. A cyclone penetration curve for a flow rate of 22 $\ell\,\mathrm{min}^{-1}$, as used in the SCAQS sampler, was interpolated from the data of John and Reischl (1980). Strictly speaking, the AIHL cyclone penetration curve only applied to the nitrate data, but this same curve was used to approximate the performance of the Bendix cyclone precut for ammonium ion and sulfate filter data. The penetration curves were applied to the inverted Berner impactor data, i.e. one which had been smoothed using a Twomey inversion algorithm to correct for cross sensitivity between impactor stages.

Scatter plots of ion data are shown in Fig. 1. The dashed line indicates a one-to-one correspondence. Aside from one outlier in the Riverside data, which occurred on the afternoon (2 p.m.) sample of 29 August 1987, the agreement is good. Mean concentration values from the filter and Berner impactor data, shown in Table 1, indicate no systematic bias in the methods. The precision between the two methods is indicated by the pooled standard deviation given in Table 1, which varies from 0.9 $\mu\mathrm{g\,m}^{-3}$ for sulfate to 3.5 $\mu\mathrm{g\,m}^{-3}$ for nitrate (the outlier was included in these statistics).

One expects agreement between filter and impactor methods for sulfate, a nonvolatile species. However, nitrate and ammonium ion concentration values can differ among methods due to volatilization. For

example, the mean nitrate concentration from the Teflon filter of the SCAQS sampler ($L_9(NO_3)$) is 17 $\mu g\,m^{-3}$, which is 28% lower than that from the nylon filter. Losses are especially pronounced in the summer samples at Claremont, for which the Teflon filter is 61% lower than the nylon filter, on average.

Table 1. Comparison of ion concentrations measured by Berner impactor and SCAQS filter sampler

Species	Mean value[a] Filter ($\mu g\,m^{-3}$)	Impactor ($\mu g\,m^{-3}$)	Standard deviation ($\mu g\,m^{-3}$)
Nitrate	23.7	23.0	3.5
Sulfate	6.4	6.4	0.9
Ammonium ion	8.8	9.6	1.7

[a] Grand mean for summer at Claremont and Riverside and for winter at Long Beach and Downtown Los Angeles.

The agreement between the impactor and the nylon filter value indicates that volatilization losses are not important in the Berner impactor. This is consistent with laboratory and field tests by Wang and John (1988) and Wall *et al.* (1988). If volatilization had occurred, one would expect it would be most severe for the smaller particle size cutpoint stages of the impactor which operate at reduced pressure. Such a bias would distort the size distribution to larger particle sizes. However, as no significant volatilization is seen by comparison with the nylon filter data, we conclude the Berner impactor ion size distributions are not likely to be distorted.

In contrast to the ion species, measurements for carbonaceous aerosols are more uncertain. The impactor data, shown in Fig. 2, are systematically lower

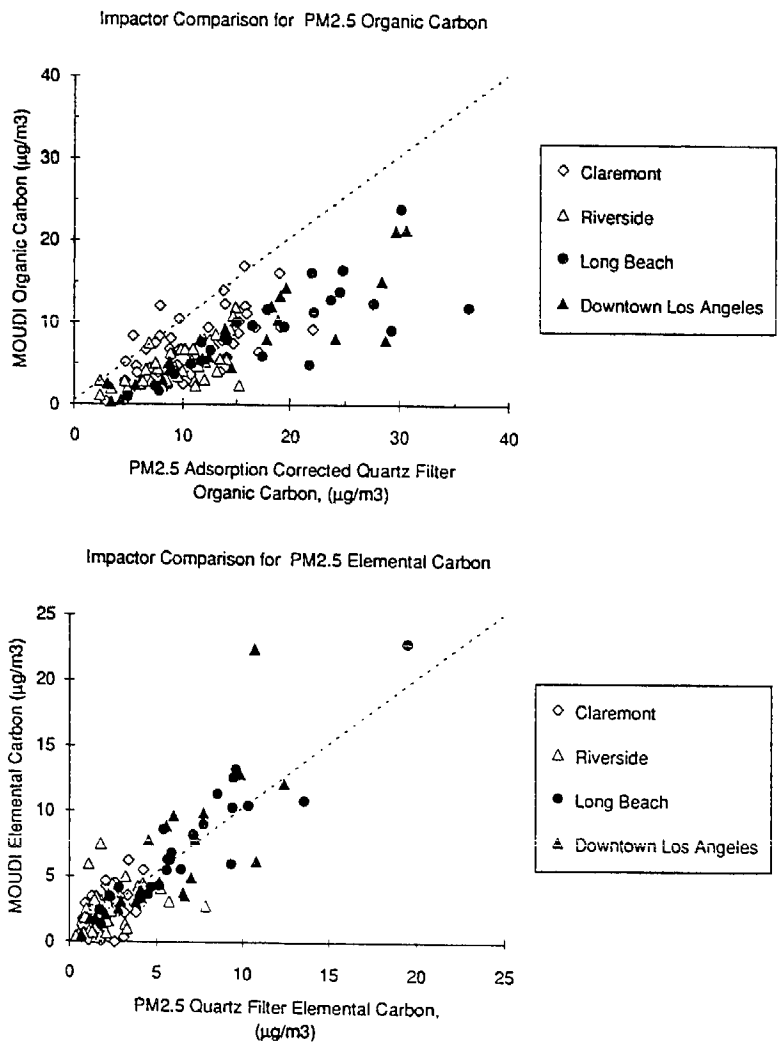

Fig. 2. Comparison of fine particle organic and elemental concentrations measured by the micro-orifice impactor and by adsorption corrected quartz filters. The dashed line is the 1 : 1 correspondence.

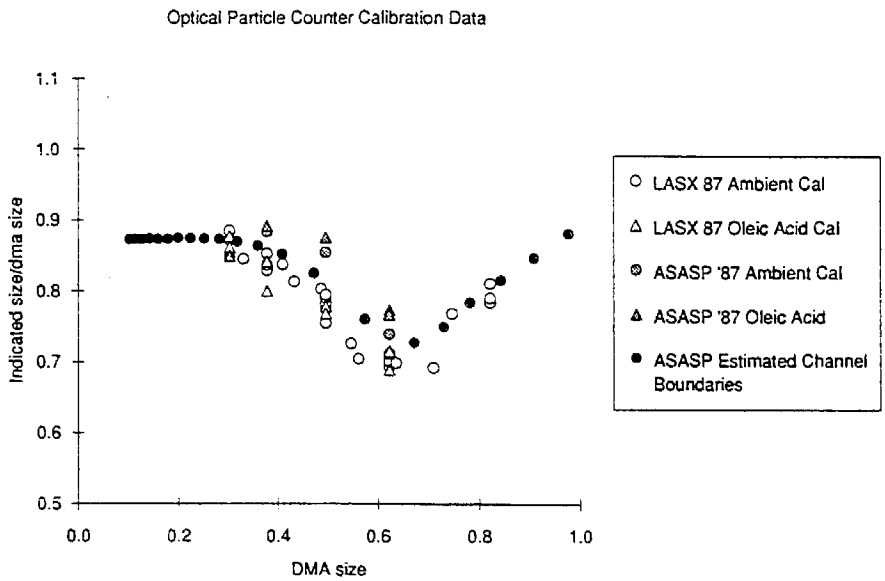

Fig. 3. Calibration data for the LAS-X and ASASP optical particle counter. 1987 data for the LAS-X are taken from Hering and McMurry (1990).

than those from absorption-corrected filter measurements from the SCAQS sampler. This difference persists for winter time samples as well as the summer samples. Thus it would seem unlikely that the difference is due to volatilization. In contrast, the elemental carbon data do not show a significant systematic difference, based on Student's t-test. The mean organic carbon concentrations measured by the MOUDI were lower than the mean adsorption corrected filter by 44%. Sampling artifacts with regard to carbon aerosol sampling are not fully understood, and it is not certain whether the greater error lies with the impactor or with the filter determinations.

OPTICAL PARTICLE CALIBRATION

The optical particle counters sized particles in the size range 0.1–3 μm, which is nearly the same size range measured by the impactors and is the size range corresponding to the accumulation mode. As such, the data from the optical counters are more critical to the analysis of the accumulation mode aerosols than those of the electrical aerosol analyzers, which measured over the size range 0.03–0.3 μm.

During SCAQS, Hering and McMurry (1991) calibrated a particle measuring systems model LAS-X optical counter with size classified ambient aerosols and compared the response with that for oleic acid aerosol (refractive index, $n = 1.43$) and polystyrene latex spheres ($n = 1.59$). The ambient and oleic acid aerosols were size classified using a differential mobility analyzer (TSI Model 3031, St Paul, Minnesota) and the LAS-X response was evaluated using a 1024 multichannel analyzer with a variable gain input amplifier. Pulse height voltages from size-classified particles were resolved within 5%. Both the LAS-X and the model ASASP used for the SCAQS site measurements have the same optical design, and use an active scattering HeNe laser with a wide angle collection of 35–120° for sizing particles in the 0.09–3 μm size range. The instruments differ in that LAS-X classifies particles into 16 size bins whereas the ASASP is a 32-channel instrument.

Calibration results from Hering and McMurry for ambient aerosols and oleic acid particles are shown in Fig. 3. These measurements were made in July 1987, at the Claremont sampling site. Results are presented as the ratio of the PSL-equivalent optical size to the actual geometric size of the particle as determined by the differential mobility analyzer. Also shown are four data points obtained at the same time for the ASASP optical counter used during SCAQS to measure size distributions aboard the aircraft operated by Sonoma Technology Inc. This instrument was exactly the same model as used at the ground-based sampling sites for SCAQS.

In general, the data show that ambient aerosols appear smaller optically than latex spheres, especially near 0.5 μm. The response is closer to that of oleic acid aerosols. Although only a few data points were taken with the ASASP, the response is similar in shape to that of the LAS-X. Since only one model of each instrument type is examined, it is not known whether this difference is due to the model or instrument variability. Based on these results, we have estimated the particle sizes corresponding to the 32 channels of the ASASP, as shown by the dark circles on Fig. 3. These points were obtained by following the dip in the LAS-X curve, but offsetting points slightly toward the values obtained from the ASASP. Extrapolation of the data to smaller and larger particle sizes was

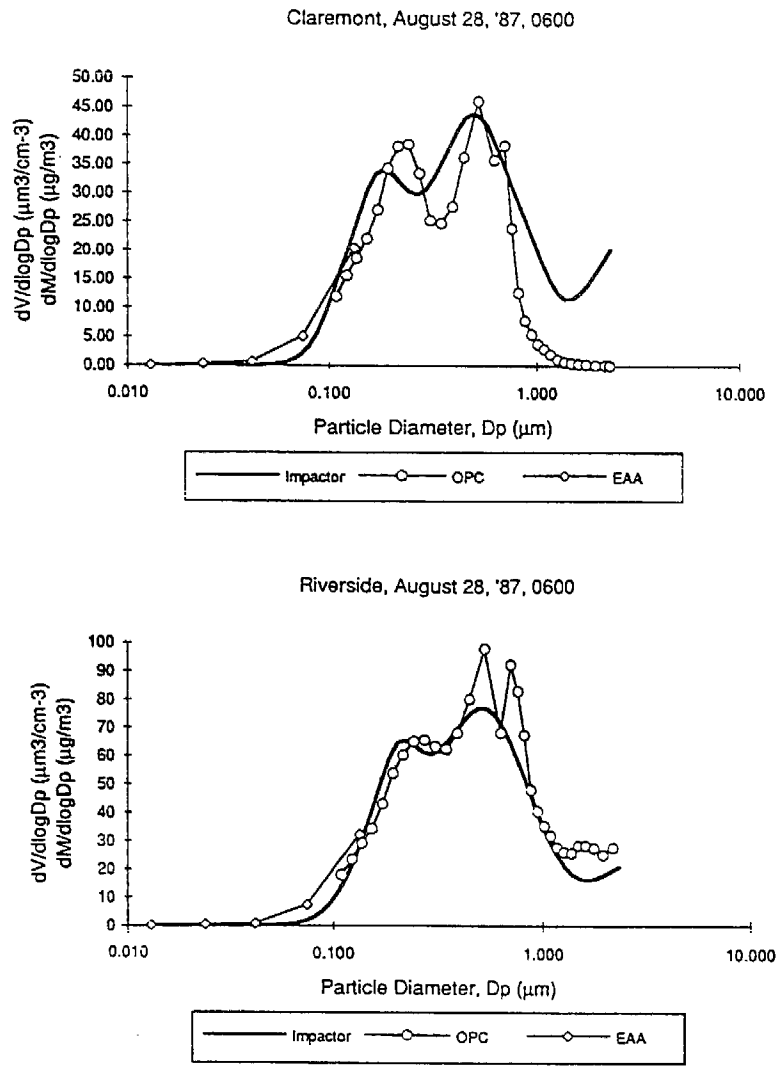

Fig. 4. Impactor mass distributions obtained by summing inorganic ions and carbon species and volume distributions from electrical aerosol analyzer (EAA) and optical particle counter (OPC) data for the 4 h period beginning at 0600 PDT on 28 August 1987 at Claremont and Riverside, California.

done on the basis of a recent calibration (February 1995) of the ASASP and LAS-X using dioctyl sebacate ($n = 1.45$).

SIZE DISTRIBUTION RESULTS

Volume distributions from the optical counter and electrical aerosol analyzer are compared with mass distributions obtained by summing chemical constituents measured by the impactors. The mass sum includes sulfate, nitrate, ammonium ion, elemental carbon, and organic carbon. Organic carbon was multiplied by a factor of 1.4 in order to estimate the mass of organic compounds present. The aerodynamic size from the impactors was converted to geometric (Stokes) diameters assuming a particle density of $1.5\ \mathrm{g\,cm^{-3}}$. The contribution from water associated with the aerosol is not included for the impactors, and likely is not seen in the optical counter data due to heating of the sample, as discussed by Eldering *et al.* (1994).

Figure 4 shows size distributions from Claremont and Riverside on 28 August, one of the study days modeled as part of this work. Both the impactor and the optical counter data show that the accumulation mode of the total size distribution is bimodal, with local maxima at about 0.25 and 0.65 μm. The fall samples tended to be unimodal, as seen in the example distribution from Long Beach for 10 December given in Fig. 5. These trends were observed throughout the

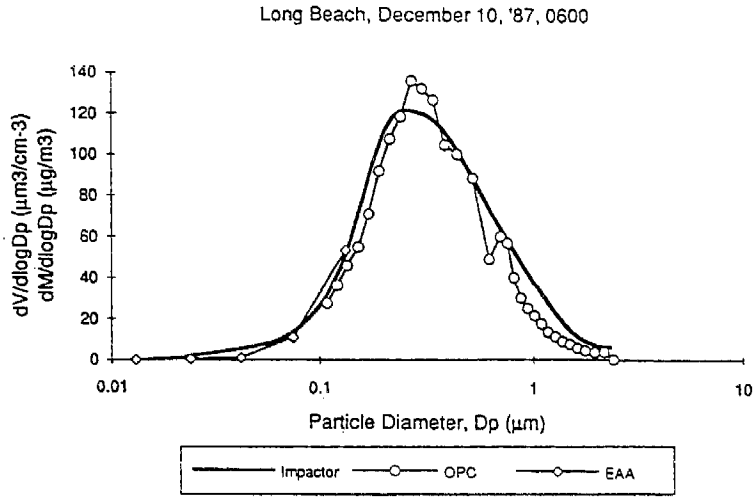

Fig. 5. Impactor and EAA-OPC size distributions for the 4 h period beginning at 0600 PST on 10 December 1987 at Long Beach, California (see caption for Fig. 4).

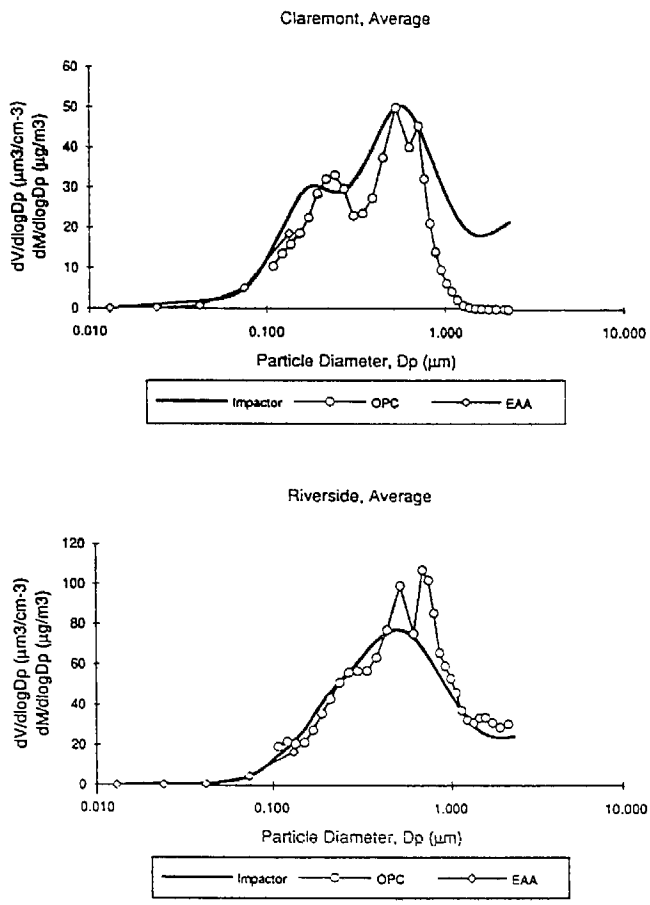

Fig. 6. Average of impactor mass distributions obtained by summing inorganic ions and carbon species and of volume distributions from electrical aerosol analyzer (EAA) and optical particle counter (OPC) data for Claremont and Riverside in the summer of 1987.

data set, as can be seen from the averaged size distributions presented in Figs 6 and 7 (averages of hourly size distribution measurements over 11 d in the summer and 6 d in the fall).

The aerosol mass from individual distributions as measured by the impactors are compared with the aerosol volume calculated from the combined EAA-OPC number distributions in Fig. 8. Likewise,

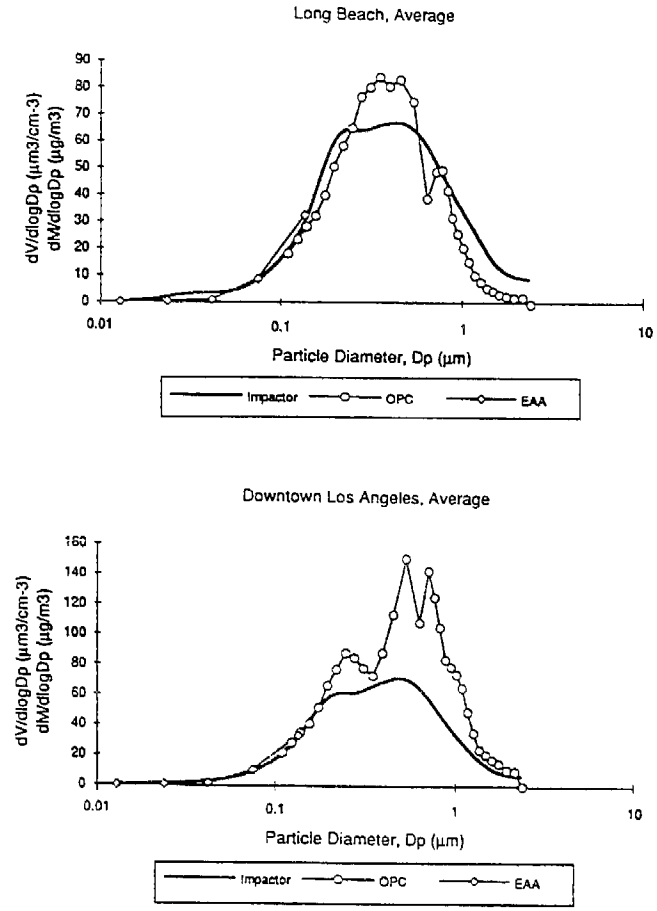

Fig. 7. Average of impactor mass distributions and EAA-OPC volume distributions for Long Beach and downtown Los Angeles for the fall of 1987.

Fig. 9 compares the geometric mean diameters from these two methods. These size distribution parameters are calculated for particles less than 2 μm in diameter. Systematic differences between these methods can be seen from the differences in the method mean values presented in Table 2. No systematic difference in the geometric mean diameters measured by these two methods is observed. The aerosol volume from the EAA-OPC measurements are systematically lower than that inferred from the impactor aerosol mass for summer time samples at Claremont. In contrast, the fall samples at downtown Los Angeles are biased in the opposite direction. It was found in reducing the optical counter data that the aerosol volume was quite sensitive to the exact calibration constants used for the channel boundaries, whereas the geometric mean size was not. As calibrations for the individual instruments were not available, it is likely that these discrepancies could be due to instrument variability.

CONDENSATION AND DROPLET MODES OF THE ACCUMULATION MODE

Inspection of individual measurement periods showed a remarkable consistency in the character of the size distributions by the impactor and EAA-OPC systems. Whenever bimodal character is observed in the impactor size distribution data, it was also seen in the EAA-OPC data. Occasionally the EAA-OPC data appeared bimodal when the impactor data did not. Because the impactor data exhibited weaker bimodal tendencies, these data were used to classify the distributions. Size distributions were classified as "distinctly bimodal" when the impactor distributions exhibited two distinct modes, separated by a local minimum. Using this criteria, 65% of the Claremont samples were distinctly bimodal, as compared to 33% for Riverside. For the fall samples, only 13% of the Long Beach and 8% of the downtown Los Angeles samples exhibited this distinctly bimodal

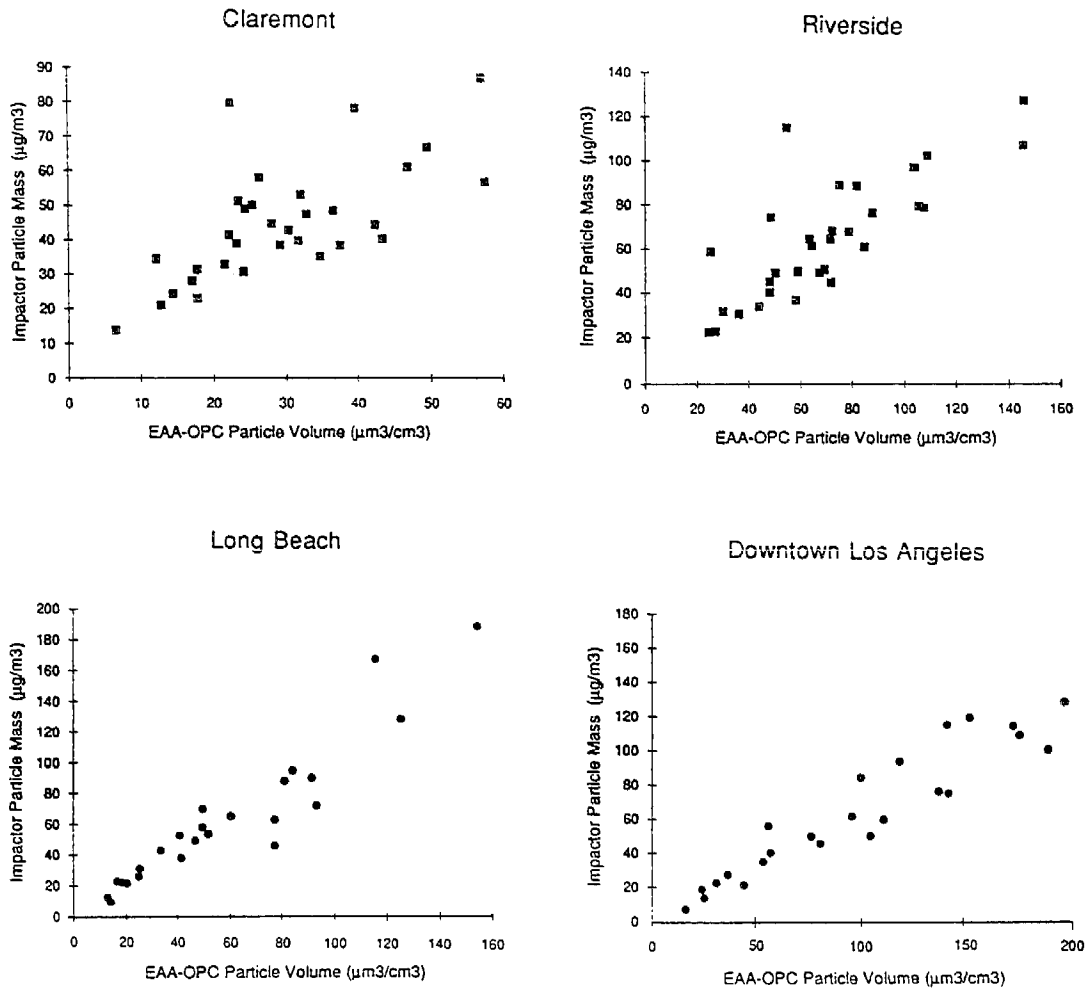

Fig. 8. Comparison of fine particle mass and fine particle volume obtained from impactor EAA-OPC size distributions measurements, respectively.

character. For other distributions, the maxima in the mass distribution corresponded to either the droplet or the condensation mode. These distributions were classified as "dominant condensation mode" or as "dominant droplet mode". Unimodal distributions with a maxima near the 0.4 μm saddle between the two modes were not observed.

Statistics for the droplet and condensation modes are summarized in Table 3. The two modes are characterized by a mode diameter which is the diameter at the local maximum in the size distribution. The mode diameter for the droplet mode varied from a minimum of 0.46 μm to a maxima of 0.90 μm, with a grand average of 0.65 μm. The mode diameter for the condensation mode varied from 0.10 to 0.39 μm, with an average value of 0.26 μm.

For bimodal distributions, the average chemical composition of each mode is calculated by simply splitting the distribution at the saddle point between the two modes, and calculating the average composition above and below the saddle point. Other distributions are classified as either "condensation" or "droplet", and their average chemical composition is averaged into the values in Table 3. No effort has been made to deconvolute the distributions, or to account for condensation or droplet mode shoulders observed for some distributions. For all sites, and for both seasons, nitrates comprise the largest fraction of the droplet mode. The condensation mode is dominated by organic carbon at Claremont. For the summer site at Riverside, and for both fall sampling sites, organic carbon and nitrate are of comparable concentrations in the condensation mode.

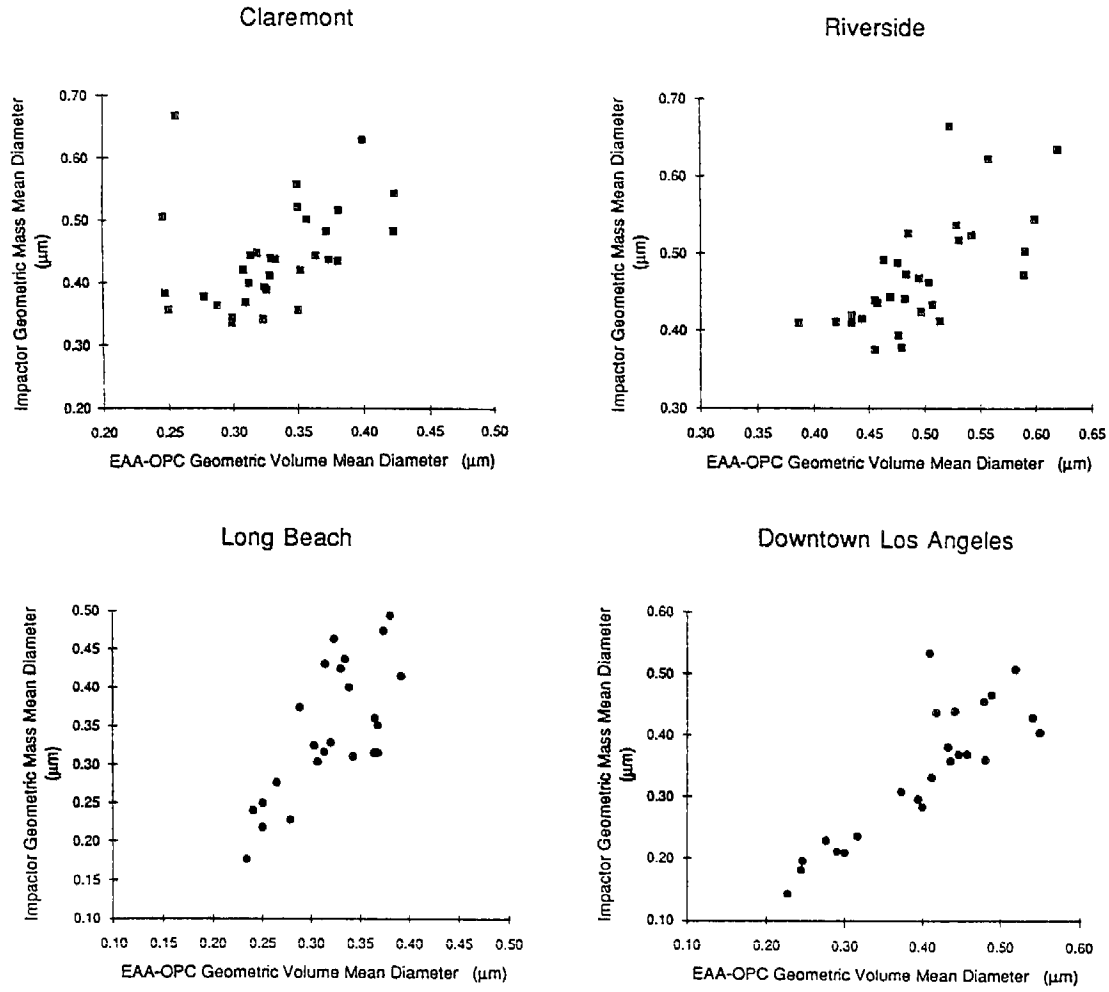

Fig. 9. Comparison of geometric mean diameter for particles below 2 μm obtained from impactor EAA-OPC size distribution measurements.

Table 2. Comparison of size distribution parameters from combined impactor and optical counter—electrical aerosol analyzer measurements

	Aerosol mass ($\mu g\, m^{-3}$)	Aerosol volume ($\mu m^3\, m^{-3}$)	Mean diameter (μm)
Claremont			
Combined impactor	45		0.44
Optical counter & EAA		29	0.34
Riverside			
Combined impactor	66		0.47
Optical counter &EAA		71	0.51
Long Beach			
Combined impactor	64		0.35
Optical counter &EAA		60	0.32
Downtown Los Angeles			
Combined impactor	65		0.36
Optical counter & EAA		97	0.40

SUMMARY

The structure of the size distribution of accumulation mode aerosols in the South Coast Air Basin of California was investigated by examination and comparison of species size distributions from impactors and physical size distributions obtained by electrical mobility and optical particle counters. Similar trends are observed in both sets of measurements, in that the accumulation mode is frequently bimodal. The condensation and droplet modes previously identified in chemical species size distributions have now been confirmed in the total volume or mass distribution.

Acknowledgements—This work was supported by the State of California Air Resources Board contract 92-311. We wish to acknowledge valuable comments by Walter John and Peter McMurry.

Table 3. Mode statistics and average chemical composition

Site Season	Claremont summer	Riverside summer	Long Beach fall	Los Angeles fall
Statistics				
No. of distributions	43	43	24	24
% Distinct bimodal distr.	65	33	13	8
% Dominant droplet mode	21	47	33	46
% Dominant cond. mode	14	21	54	46
Droplet mode diameter (μm)	0.69 ± 0.09	0.61 ± 0.14	0.62 ± 0.13	0.65 ± 0.11
Condensation mode diameter (μm)	0.23 ± 0.03	0.25 ± 0.10	0.30 ± 0.04	0.26 ± 0.03
Average composition of condensation mode				
Organic carbon (%)	43 ± 19	28 ± 23	29 ± 13	31 ± 12
Elemental carbon (%)	13 ± 05	8 ± 06	13 ± 06	22 ± 11
Ammonium ion (%)	12 ± 05	17 ± 09	16 ± 06	9 ± 06
Nitrate (%)	16 ± 10	36 ± 20	34 ± 13	31 ± 16
Sulfate (%)	16 ± 10	11 ± 08	7 ± 03	6 ± 03
Average composition of droplet mode				
Organic carbon (%)	20 ± 09	12 ± 10	15 ± 07	15 ± 03
Elemental carbon (%)	5 ± 04	4 ± 05	8 ± 04	8 ± 02
Ammonium ion (%)	19 ± 03	20 ± 04	19 ± 02	19 ± 02
Nitrate (%)	32 ± 10	48 ± 12	43 ± 12	48 ± 08
Sulfate (%)	23 ± 07	15 ± 04	14 ± 11	10 ± 07

REFERENCES

Eldering A., Cass G. R. and Moon K. C. (1994) An air monitoring network using continuous particle size distribution monitors connecting pollutant properties to visibility via Mie scattering calculations. *Atmospheric Environment* **28**, 2733–2749.

Fitz D. and Zwicker J. (1988) Design and testing of the SCAQS sampler. Final report to the California Air Resources Board, contract A6-077-32, AeroVironment report no. AV-FR-87/649.

Hering S. V. (1990) Southern California Air Quality Study Aerosol Data Management Report. California Air Resources Board contract A832-086, Sacramento, California.

Hering S. V. and Blumenthal D. L. (1989) Southern California Air Quality Study Description of Measurement Activities. California Air Resources Board contract A5-157-32, Sacramento, California.

Hering S. V. and Friedlander S. K. (1982) Origins of aerosol sulfur size distributions in the Los Angeles Basin. *Atmospheric Environment* **16**, 2647–2656.

Hering S. V. and McMurry P. H. (1991) Response of a PMS LAS-X laser optical particle counter to monodisperse atmospheric aerosols. *Atmospheric Environment* **25A**, 463–468.

John W. and Reischl G. (1980) A cyclone for size selective sampling of ambient air. *J. Air Pollut. Control Ass.* **30**, 872–876.

John W., Wall S. M., Ondo J. L. and Winklmayr W. (1990) Modes in the size distributions of atmospheric inorganic aerosol. *Atmospheric Environment* **24A**, 2349–2359.

McMurry P. H. (1989) Organic and elemental carbon size distributions of Los Angeles aersols measured during SCAQS. Final report to Coordinating Research Council, project SCAQS-6-1, Particle Technology Laboratory report no. 713.

Meng Z. and Seinfeld J. H. (1994) On the source of the submicrometer droplet mode of urban and regional aerosols. *Aerosol Sci. Technol.* **20**, 253–265.

Mueller P. K., Fung K. K., Heisler S. L., Grosjean D. and Hidy G. M. (1982) In *Particulate Carbon: Atmospheric Life Cycle* (edited by Wolff G. T. and Klimisch T. L.). Plenum Press, New York.

Sloane C. S., Watson J., Chow J., Pritchett L. and Richards L. W. (1991) Size segregated fine particle measurements by chemical species and their impact on visibility impairment in Denver. *Atmospheric Environment* **25A**, 1013–1024.

Wall S. M., John W. and Ondo J. L. (1988) Measurement of aerosol size distributions for nitrate and major ionic species. *Atmospheric Environment* **22**, 1649–1656.

Wang H. C. and John W. (1988) Characteristics of the Berner impactor for sampling inorganic ions. *Aerosol Sci. Technol.* **8**, 157–172.

Willeke K. and Whitby K. T. (1975) Atmospheric aerosols: size distribution interpretation. *J. Air Pollut. Control Ass.* **25**, 529–534.

Appendix D

Systematic Bias in the Measurement of $PM_{2.5}$

Final Report

Submitted to
Prof. John Seinfeld

California Institute of Technology
Purchase Order No. PC149952
issued as subcontract under
California Air Resources Board
Contract No. 93-304

Prepared by
Susanne Hering
Aerosol Dynamics Inc.
2329 Fourth St.
Berkeley, CA 94710

March 1996

Systematic Bias in the Measurement of $PM_{2.5}$

Introduction

Over the past year the US Environmental Protection Agency has reviewed the air quality criteria for particulate matter, and is considering the adaptation of a new, fine particle standard. Should a new standard be promulgated, one of the most important issues will be the measurement technology which would become the reference method. Currently, EPA is considering a gravimetric method for quantifying fine particles. Particles below a specified size cut at about 2.5 μm would be collected on a Teflon filter, equilibrated and weighed.

It is well known that systematic biases exist in the quantification of airborne particle concentrations by gravimetric mass determination. Many studies have shown that particle nitrates, which are a major component of fine particles in California and the Western US are easily volatilized from Teflon filters. This would mean a systematic bias in the reference method likely to be proposed for fine particles.

This report examines data from the 1987 Southern California Air Quality Study to quantify the magnitude of nitrate losses, and how their loss affects gravimetric mass determinations. This study includes simultaneous measurements by different methods for evaluating nitrate losses. It should be noted that the data examined here are for with short sampling duration, 4 to 7 hours, with immediate retrieval of samples at the end of collection period. As such, the losses found here represent a lower limit for what would be expected for 24-hr sampling, with retrieval of the sample one or more days after collection.

Comparison of SCAQS Measurements for Fine Particle Nitrate

The three measurements of fine particle nitrate available for comparison in the SCAQS are: (1) a $PM_{2.5}$ Teflon filter, (2) a $PM_{2.5}$ denuded nylon filter and (3) impactor size distributions from the Berner impactor. The filter samples were part of the SCAQS sampler and were operated on all intensive sampling days at 9 sites in the summer and 6 sites in the fall. The nylon filter samples were preceded by an AIHL-design cyclone, the Teflon filter was preceded by a Bendix 240 cyclone. The impactor was operated at 3 sites in the summer and 2 sites in the fall. The AIHL cyclone penetration efficiency curve has been applied to the impactor size distributions to obtain an equivalent $PM_{2.5}$ size fraction, as described by Hering et al (1996).

Comparisons at Sites with Impactor Data
In our previous work, the impactor nitrate and sulfate values were compared to the $PM_{2.5}$ values for nitrated from the denuded nylon filter, and the $PM_{2.5}$ sulfate from the Teflon filter sulfate. The mean sulfate concentration from the impactor agreed with that from the Teflon filter to within 4% for summer and fall sampling. The mean impactor nitrate agreed to within 3% of the denuded nylon filter value for the fall, while summer time impactor nitrate values were 7% lower, on average.

Scatter plots for comparing values for the nitrate concentration measured by the impactor and denuded nylon filter are shown in Figures 1a and 2a for fall and summer sites, respectively. Figures 1b and 2b show the analogous comparison between nitrate collected on the Teflon filter and that from the denuded nylon filter. In contrast to the impactor data, the Teflon filter nitrate values are consistently lower than those from the denuded nylon. Discrepancies are not as large for fall sampling periods (Figure 1) as for the summer (Figure 2).

Figure 3 shows the same comparisons for summer time measurements at Claremont, wherein data are segregated by the time of day the samples were collected. Morning sampling refers to those collected between 0600 and 1000 PDT, day time samples were collected from 1000 to 1400, and from 1400 to 1800 PDT. Night time samples were collected from 1800 to 0100, and 0100 to 0600. Clearly, the largest discrepancies are found for the daytime sampling. Similar trends were observed at all sites with impactor measurements, as shown by the graphs in Appendix A. Because good agreement is found for sulfate, and because lower values relative to the nylon filter are found during the hottest periods of the day, the discrepancies shown in Figure 3 are attributed to volatilization of nitrate during sampling.

Comparisons at all SCAQS Sites
Whereas impactor measurements were only made at selected sites, the SCAQS sampler was operated at all sites. Data from each sampling period at each site are shown in Appendix B. Each of these graphs shows the same trend as shown for Claremont in Figure 3b, namely losses are most pronounced for the summer time samples collected during the day (1000 to 1400 PDT and 1400 to 1800 PDT).

Average results from all of the Basin summer and fall sites are shown in Figure 4. For the summer, denuded nylon filter nitrate is Teflon filter values are higher by a factor of two or more at all sites except Rubidoux. Rubidoux data show a smaller percentage loss, but because the nitrate concentrations at this site are so large the loss expressed as $\mu g/m^3$ is similar to that seen at the other non-coastal sites of Central LA, Burbank, Azusa and Claremont.

The percentage of nitrate lost for daytime and night time sampling are shown in Figure 5 for both summer and fall periods. Summer daytime losses are in the

range from 80% to 90% for all sites but Rubidoux. Nighttime losses at these sites are in the 40% to 60% range. These results are similar to that reported by John et al (1988) for measurements made at Claremont in the summer of 1985. SCAQS fall samples show the same trends, but with marked lower losses of 25% to 40% in the daytime and 15 to 20% at night. The percentage losses at Rubidoux were consistently the lowest percentage, perhaps attributable to the high ammonia levels observed at this site.

Comparison with $PM_{2.5}$ Mass

Nitrate lost from the Teflon filters during sampling reduces the mass measured gravimetrically. In SCAQS this loss was corrected for by adding the volatilized nitrate, assumed to be ammonium nitrate, to the measured gravimetric mass to obtain $PM_{2.5}$ mass. The average mass of ammonium nitrate lost at each site for each season is shown in Figure 6. Average summer and fall losses ranged from 5 to 11 $\mu g/m^3$, except at Rubidoux, where fall losses were negligible. The amount lost on an individual sampling period ranged from 0 to 54 $\mu g/m^3$, as shown in Table 1. The corresponding fraction of the volatilized-corrected $PM_{2.5}$ mass is as high as 65% in the summer, and as high as 40% in the fall, with mean values of 15% and 9% respectively.

The magnitude of the error associated with a simple gravimetric mass measurement is better illustrated by the ratio of the mass of ammonium nitrate lost to the measured gravimetric mass. This is shown in Figure 7 for each site, averaged over summer and fall seasons. These data have been screened to exclude periods with nitrate concentrations $< 2\ \mu g/m^3$, and to exclude the small number of the periods for which the sum of species exceeded the volatilized corrected mass determination. On average, errors from volatilization were 20% of the gravimetric mass in the summer, and 11% in the fall, as shown in Table 1. The error in individual values ranged over 100%, but as exemplified by the Long Beach data shown in Figure 8, most gravimetric mass values were within 30% of the volatilzed-corrected mass determination. However, we note that the largest errors occurred for events of high concentration.

Implications

For criteria pollutants such as ozone or carbon monoxide, the parameter which is measured is clearly defined in terms of the gas phase concentration of a specific, known chemical compound. In contrast, $PM_{2.5}$ is a complex mixture of particles of different sizes, morphologies and chemical composition. For regulatory purposes the definition of what comprises $PM_{2.5}$ will be determined by the measurement method selected by EPA. In contrast to gaseous criteria pollutants, the $PM_{2.5}$ measurement methodology will be an integral part of the new standard, as currently formulated.

There are many implications should EPA choose to adopt a definition of $PM_{2.5}$ which does not accurately reflect the mass concentration of airborne particles below 2.5 μm. Two of the more significant implications are, as follow:

(1) Systematic biases in the reference method are likely to result in biases in control strategies. If nitrate concentrations are consistently under-reported while the concentration of nonvolatile substances such as soil dust and sulfates are not, then control strategies would selectively emphasize sources of nonvolatile species. As such, the issue of measurement bias in an air quality standard could be very important from the perspective of the cost of inappropriate controls.

(2) Monitoring networks will not be able to take advantage of innovations in particle measurement technology. Automated, semi-continuous particle characterization methods are attractive from the point of view of providing a more complete data set at lower operating costs. While it is possible for different methodologies to agree with an accurate measure of fine particles (as demonstrated here in the comparison of nitrate data from impactors and denuded nylon filters), it is nearly impossible to replicate a measurement bias under a variety of atmospheric conditions.

Recommendations

To better determine the expected losses from the methodology under consideration at EPA, further work is needed to assess nitrate losses in 24-hour sampling networks, such as that collected at CIT, and more recently by SCAQMD. The quantified losses could be modeled using the theories for losses such as that developed by Zhang and McMurry (1991), thereby allowing this work to provide a basis for predicting losses in other conditions. It would also be very useful to examine data sets outside of California.

References

Hering, S. V., Eldering, A., Seinfeld, J. H. (1996) Bimodal character of accumulation mode aerosols in southern California, submitted to *Atmos Environ*.

John W., Wall S. and Ondo, J. L. (1988), A new method for nitric acid and nitrate aerosol measurement using the dichotomous sampler, *Atmos Environ* 22 1627-1636.

Zhang X. Q., and McMurry P. H. (1991) Theoretical analysis of evaporative losses of adsorbed or absorbed species during atmospheric aerosol sampling, Environ. Sci. Technol. 14: 266-277.

Table 1. PM-2.5 Nitrate Losses from Teflon Filters in SCAQS [Excluding Rubidoux]

Ammonium Nitrate Loss	range	mean
Summer	0-54 µg/m3	8 µg/m3
Winter	0-46 µg/m3	7 µg/m3

As percent of NO3-	range	mean
Summer	0-100%	61%
Winter	0- 89%	22%

As Percent of Mass	range	mean
Summer	0-65%	15%
Winter	0-41%	9%

As Percent of Gravimetric Mass	range	mean
Summer	0-169 %	20%
Winter	0- 70 %	11%

Table 1-Summary Table, 3/9/96

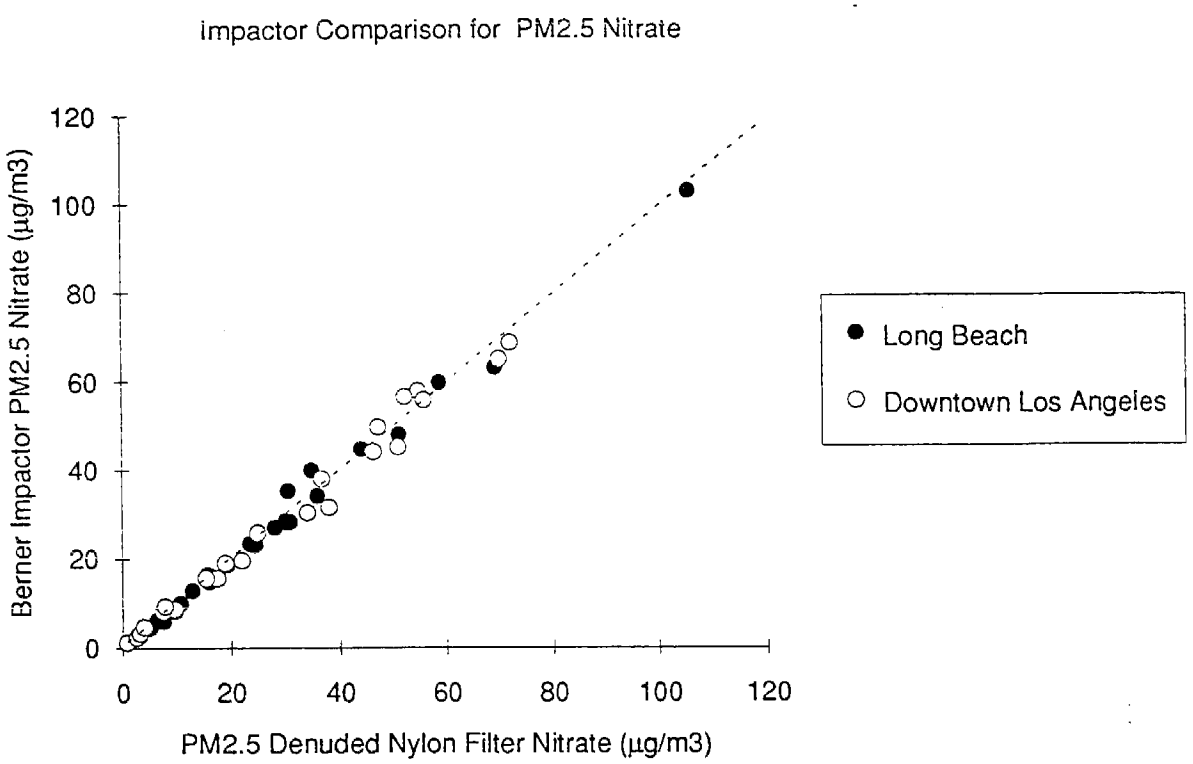

Figure 1a. Comparison of $PM_{2.5}$ nitrate measured by impactor and denuded nylon filter for fall SCAQS.

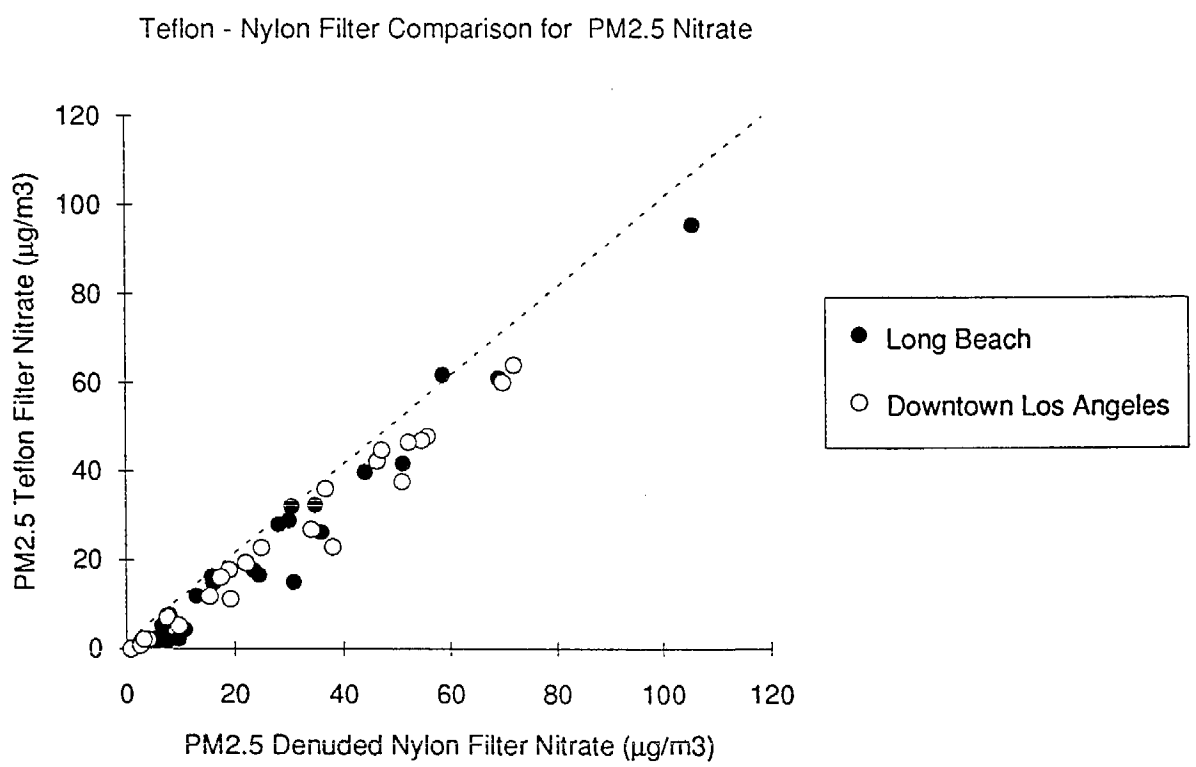

Figure 1b. Comparison of $PM_{2.5}$ nitrate measured by Teflon filter and denuded nylon filter for fall SCAQS.

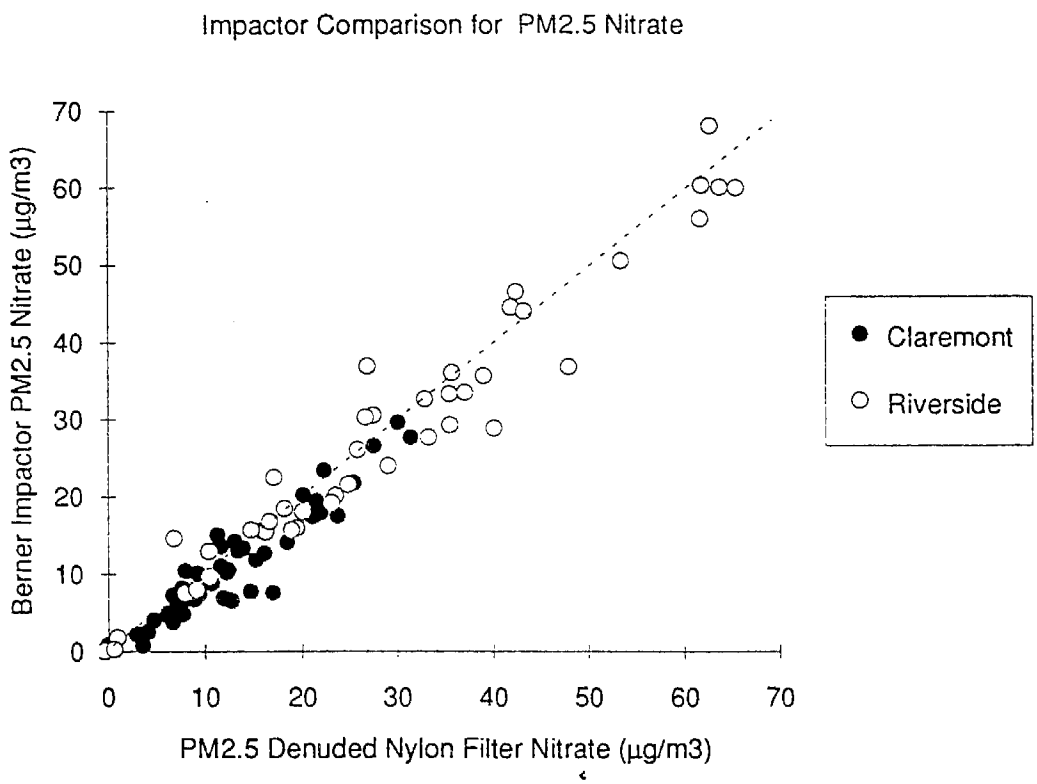

Figure 2a. Comparison of $PM_{2.5}$ nitrate measured by impactor and denuded nylon filter for summer SCAQS.

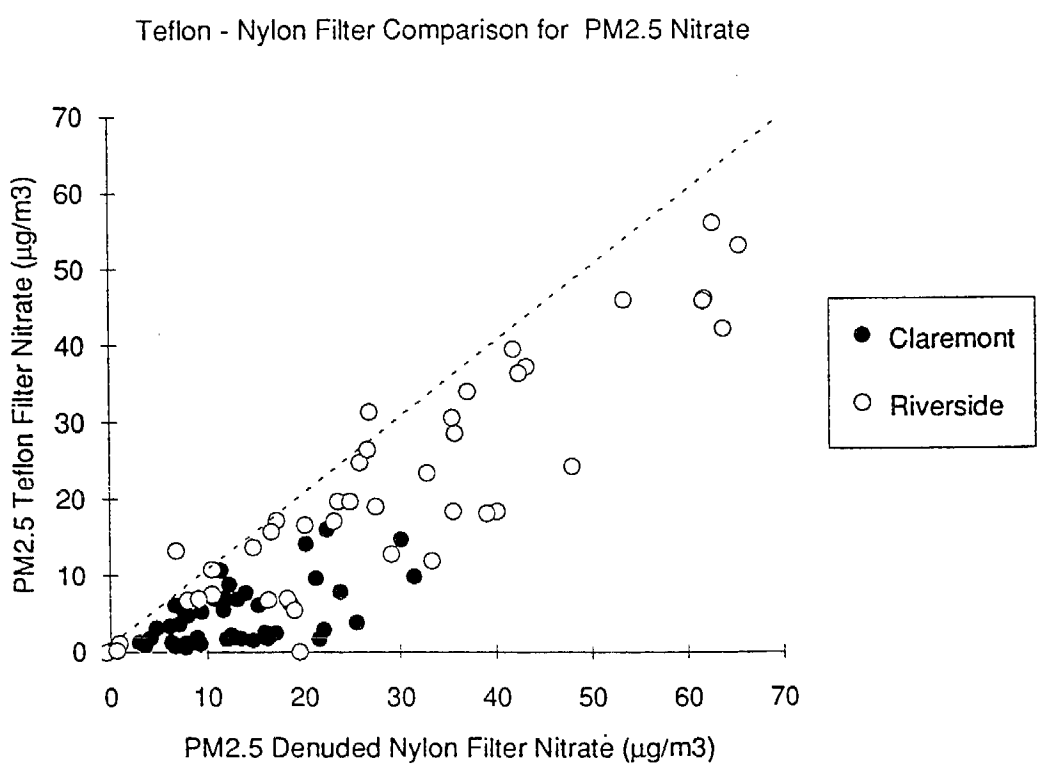

Figure 2b. Comparison of $PM_{2.5}$ nitrate measured by Teflon filter and denuded nylon filter for summer SCAQS.

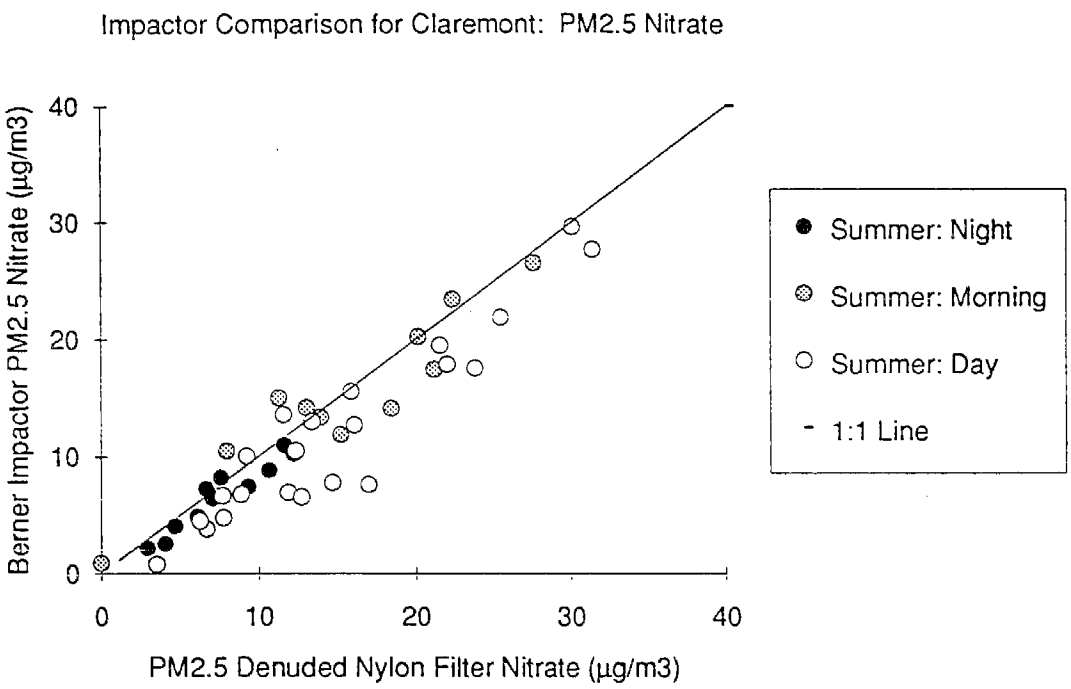

Figure 3a. Comparison of summer SCAQS $PM_{2.5}$ nitrate measured by impactor and denuded nylon filter for different times of day at Claremont.

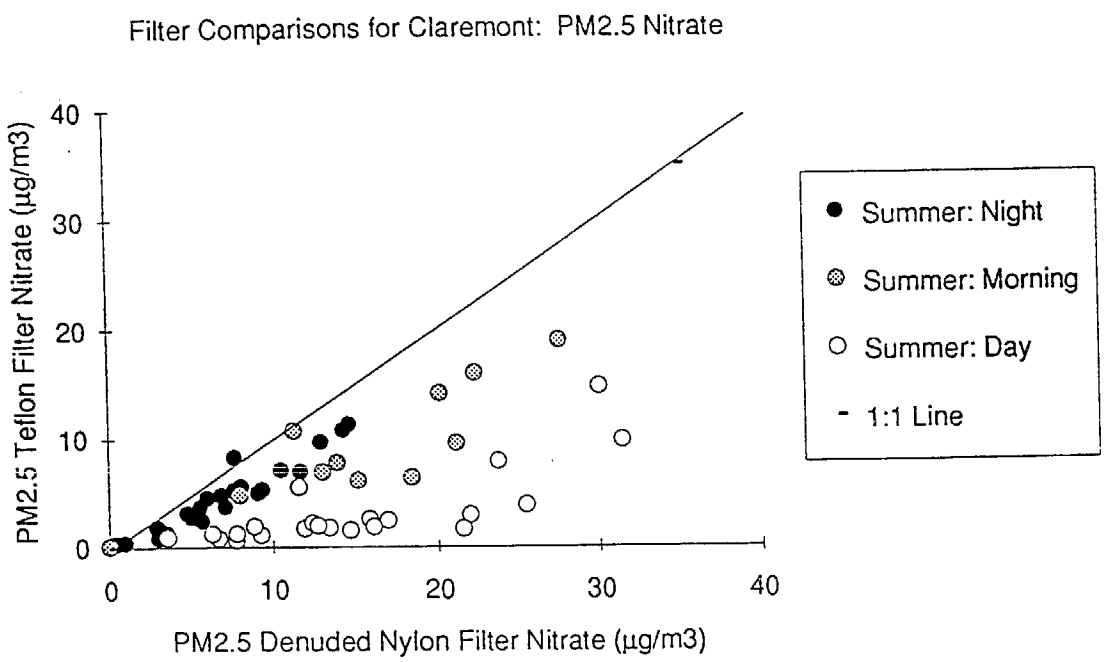

Figure 3b. Comparison of summer SCAQS $PM_{2.5}$ nitrate measured by Teflon filter and denuded nylon filter for different times of day at Claremont.

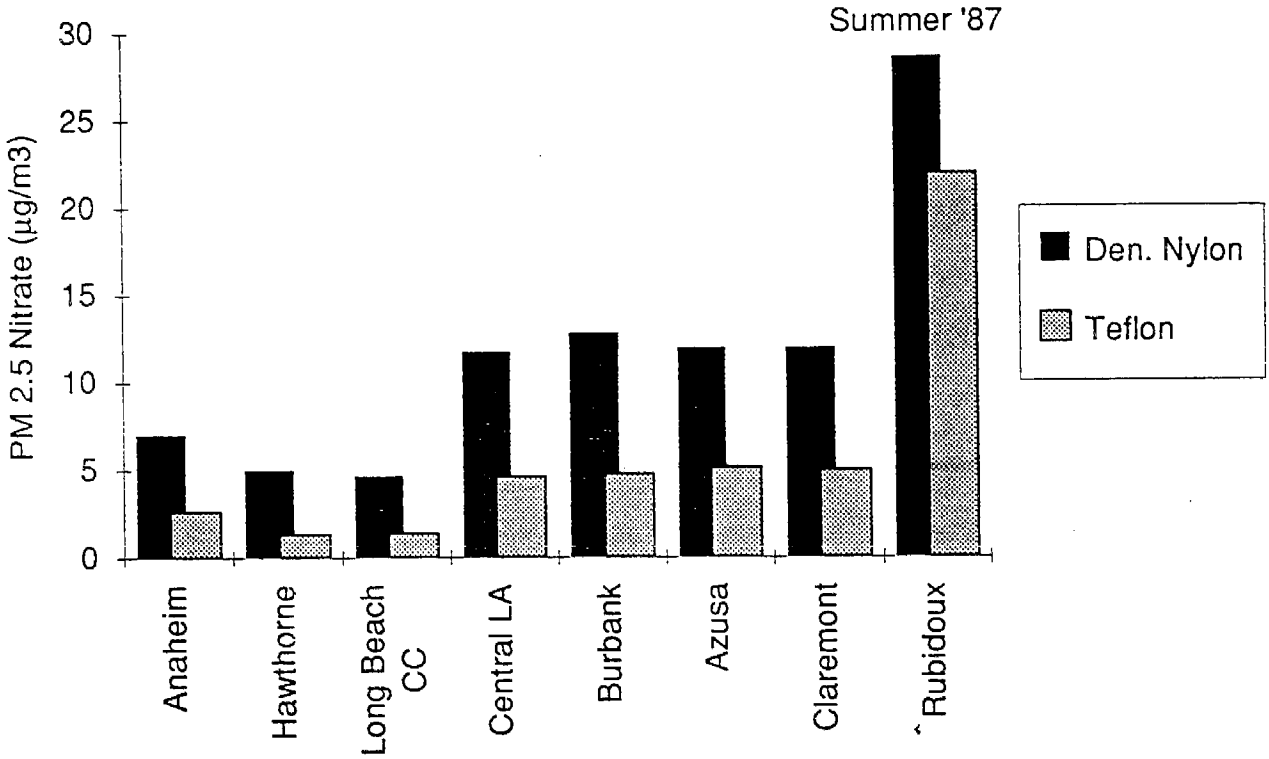

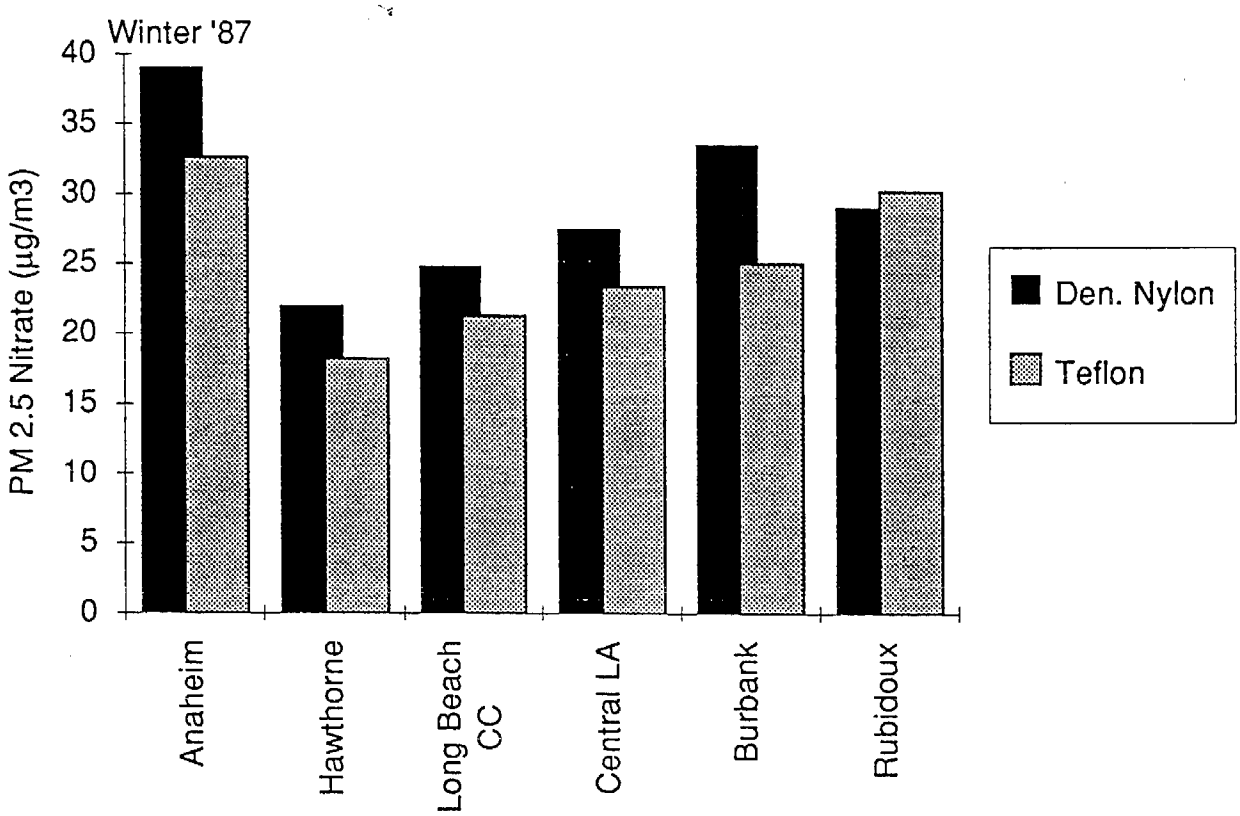

Figure 4. Comparison of average of denuded nylon filter and Teflon filter $PM_{2.5}$ nitrate for each summer and fall site during SCAQS.

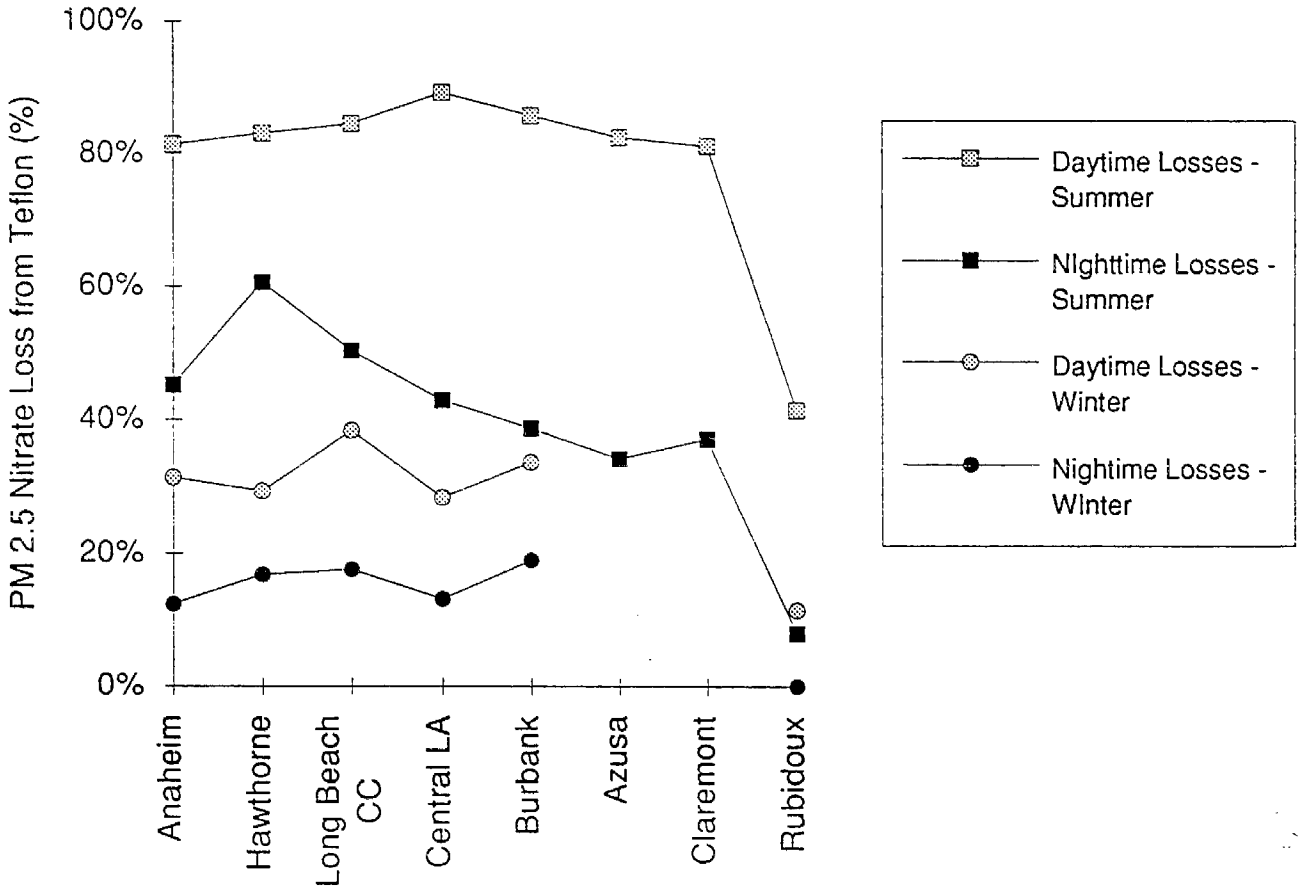

Figure 5. Fraction of nitrate lost from $PM_{2.5}$ Teflon filters during SCAQS.

% of nitrate lost, 3/8/96

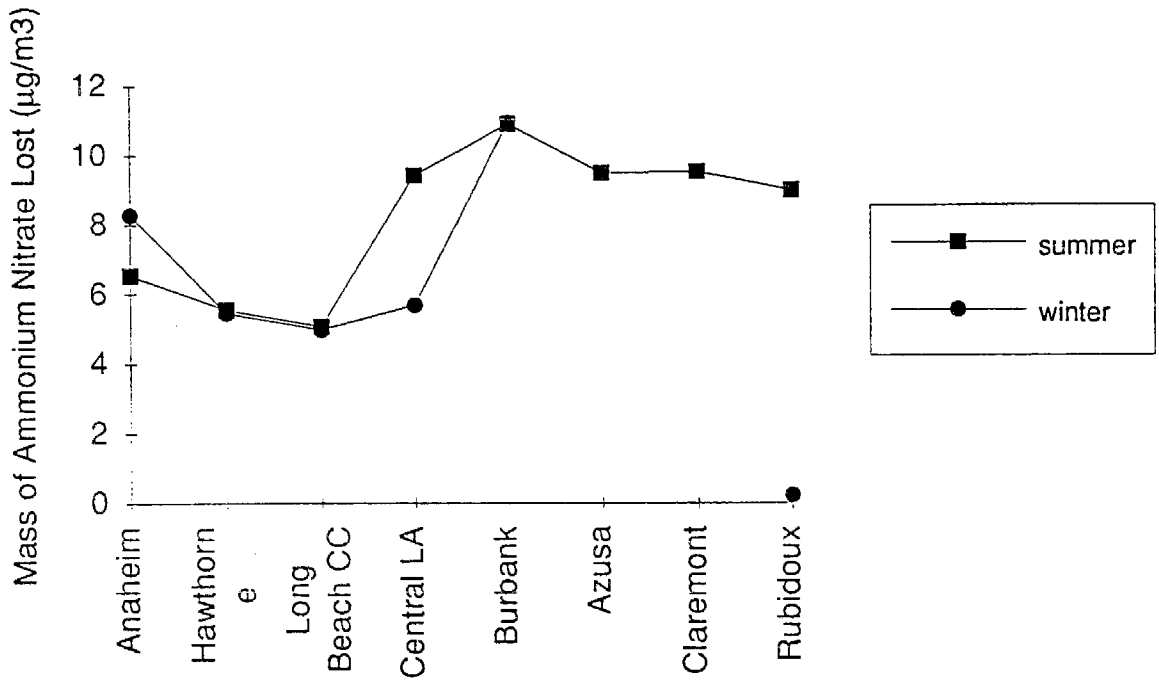

Figure 6. Mass of ammonium nitrate lost from $PM_{2.5}$ Teflon filters.

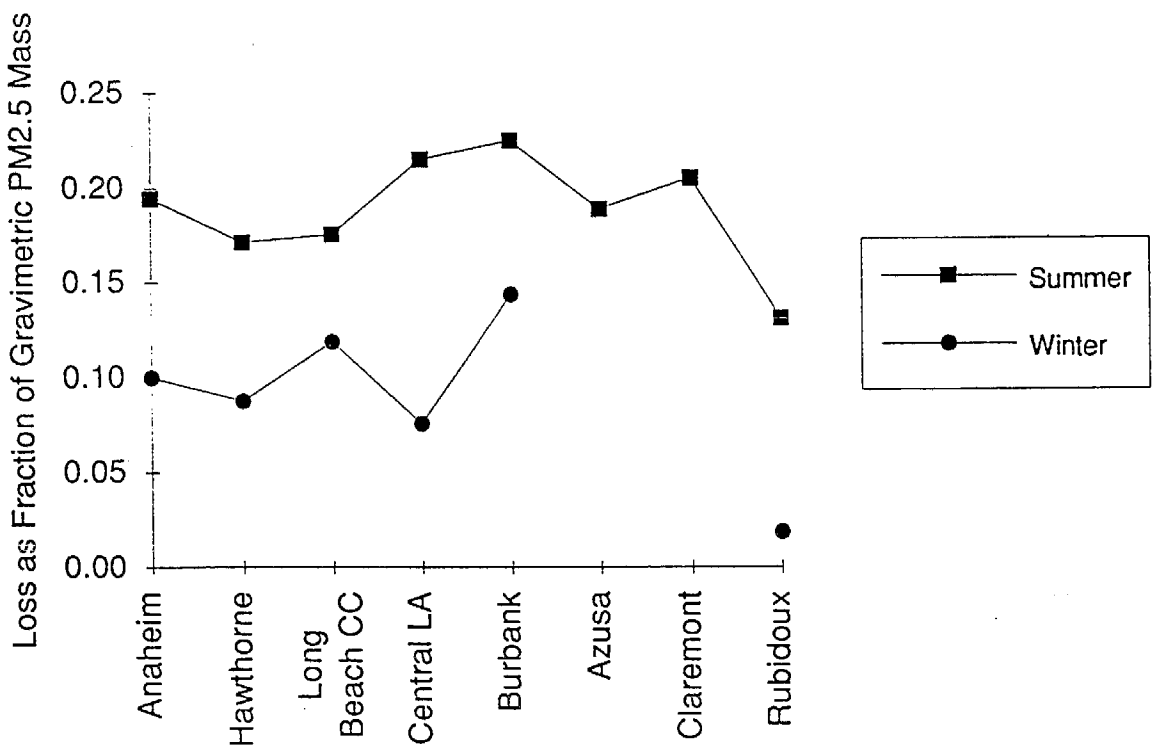

Figure 7. Ratio of the ammonium nitrate loss from $PM_{2.5}$ filters to the gravimetric mass on the Teflon filter.

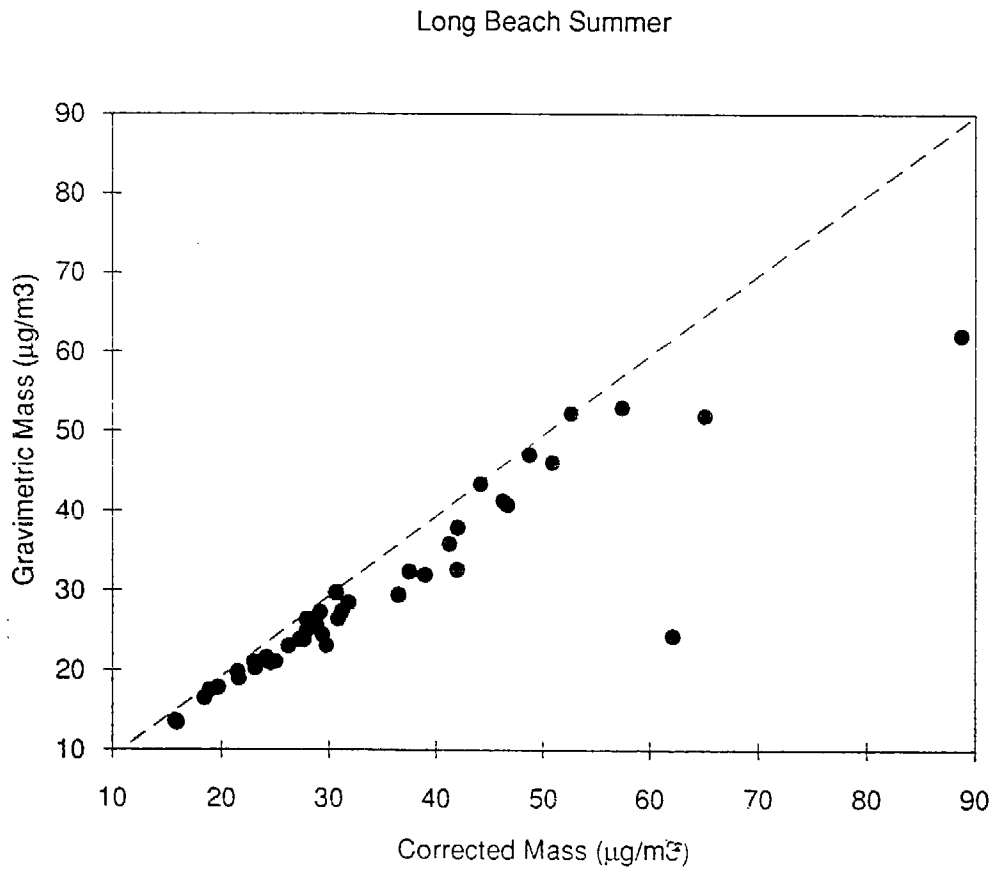

Figure 8. Comparisons of gravimetric mass to volatilized-corrected gravimetric mass for summer measurements at the Long Beach City College site.

long beach corr vs grav mass, 3/8/96

Appendix A

Scatter Plots of $PM_{2.5}$ Sulfate and Nitrate Measured by Impactor and by the SCAQS Sampler

Impactor Comparison for Claremont: PM2.5 Sulfate

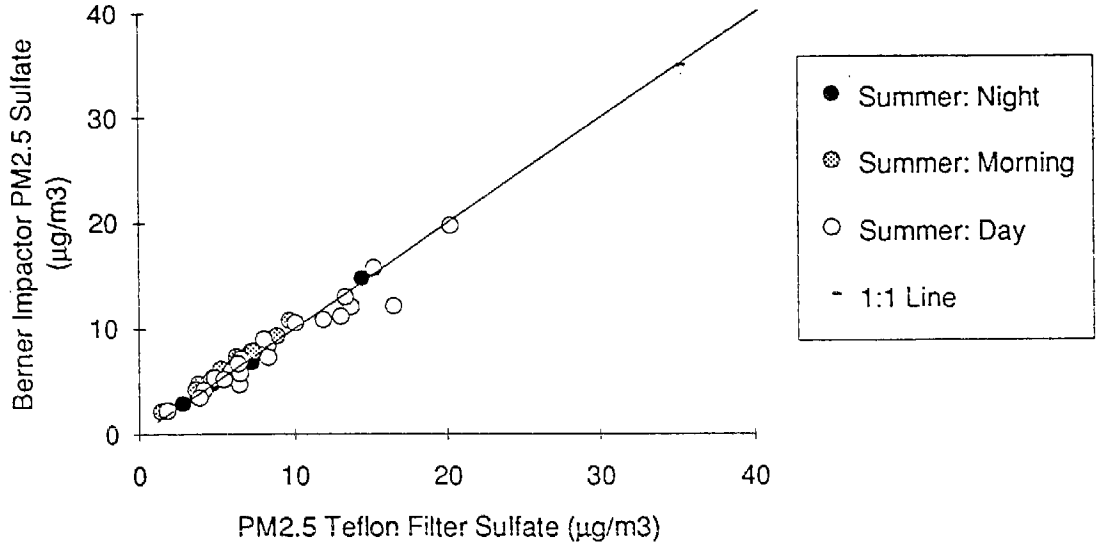

Impactor Comparison for PM2.5 Sulfate for Rubidoux - Summer

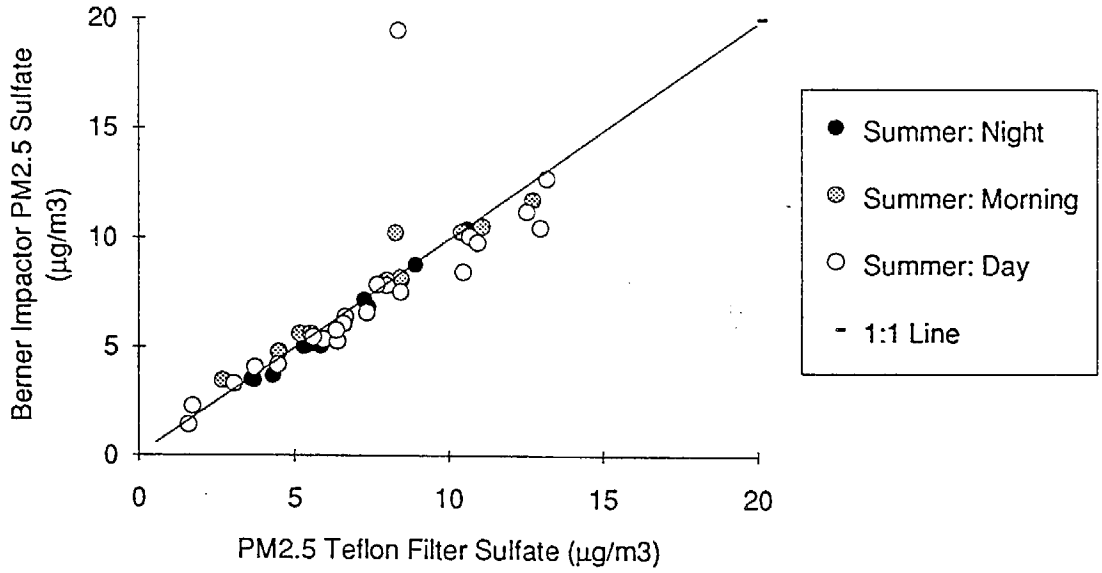

Impactor Comparison for PM2.5 Sulfate for Long Beach - Summer

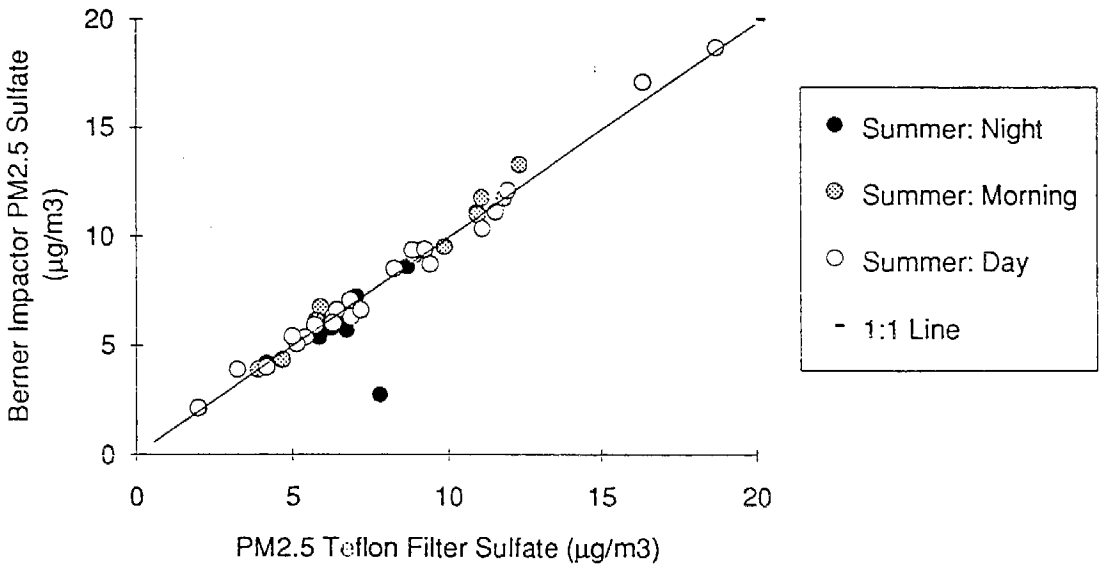

Impactor Comparison for PM2.5 Sulfate for Long Beach -Winter

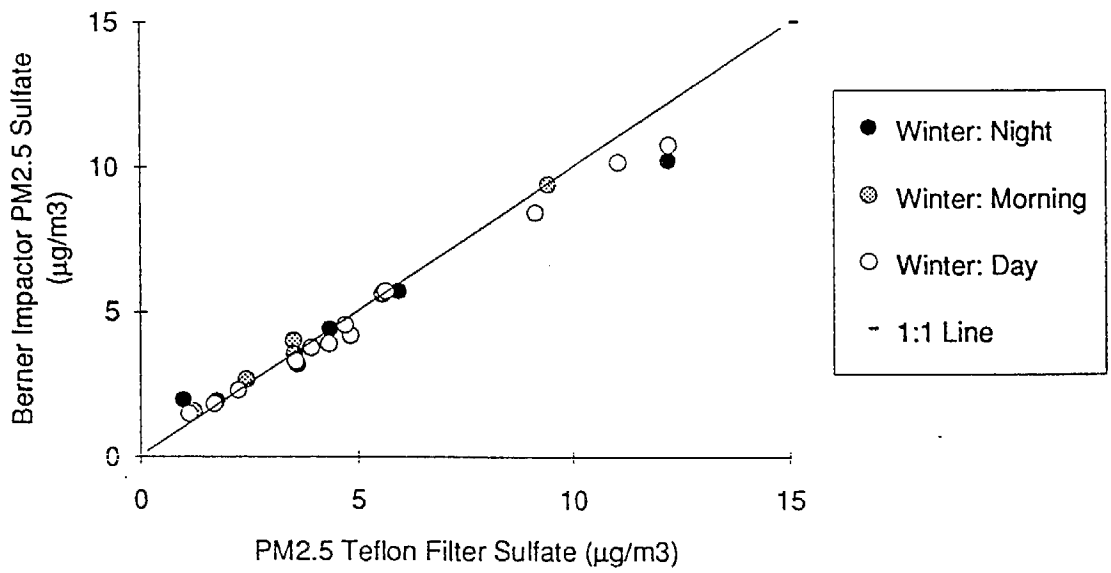

Impactor Comparison for PM2.5 Sulfate for Central Los Angeles - Winter

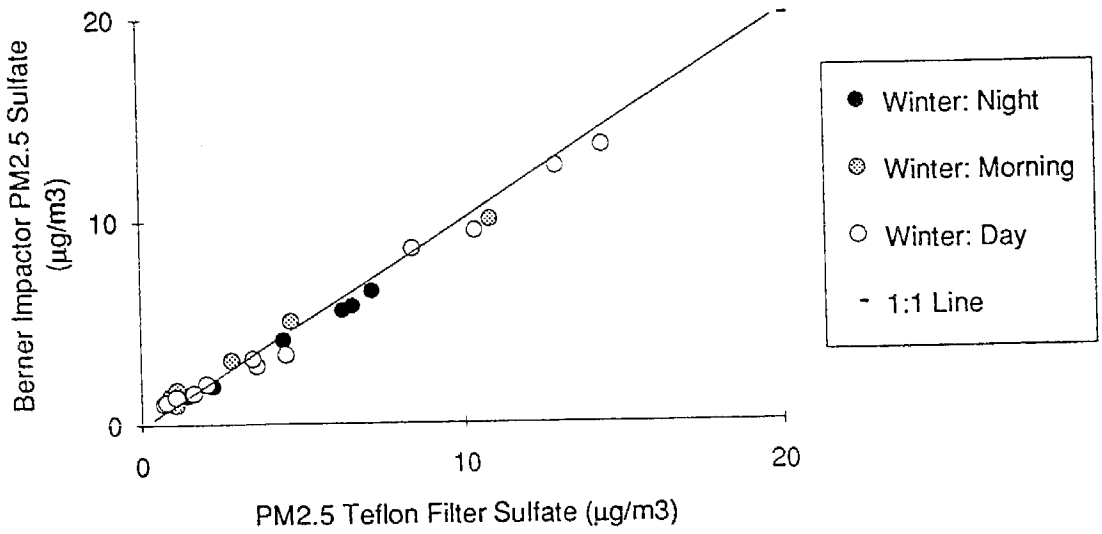

Imp-so4-CELA Win, 9/22/95

Impactor Comparison for Claremont: PM2.5 Nitrate

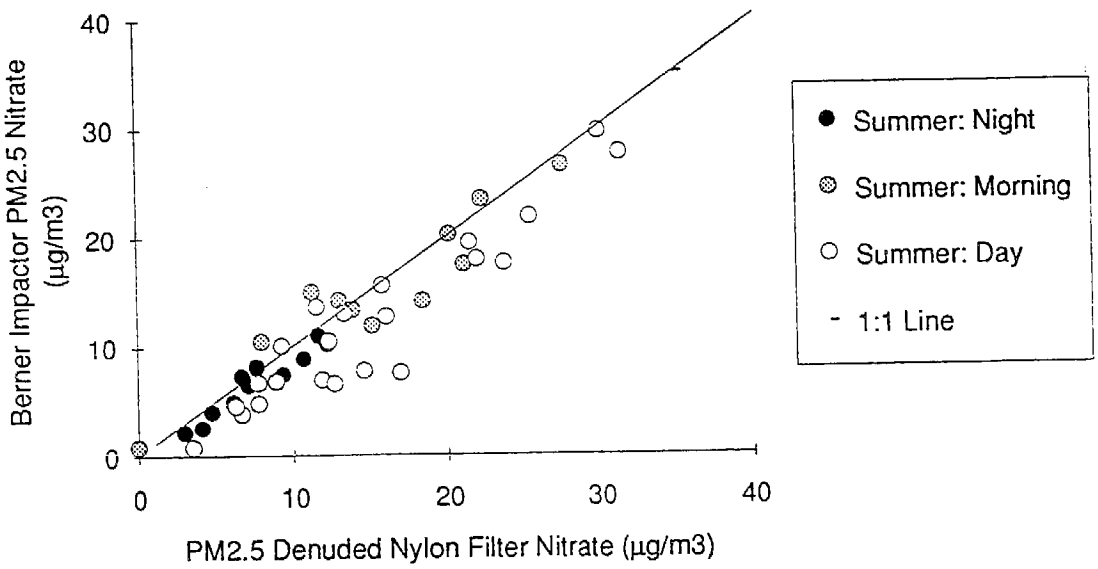

FIlter Comparison for PM2.5 NItrate at Claremont- Summer

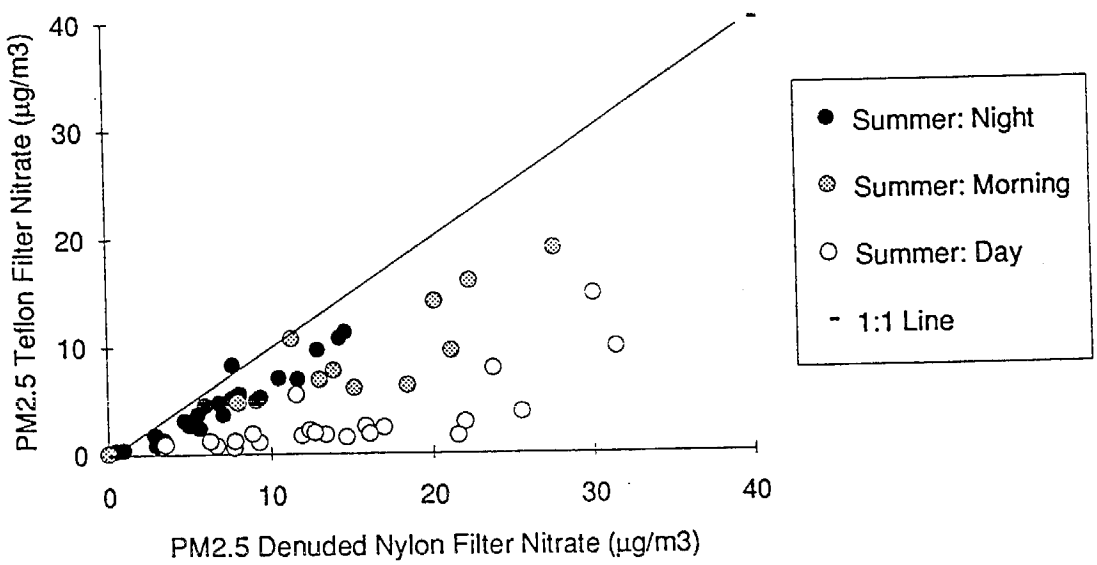

Impactor Comparison for PM2.5 Nitrate for Rubidoux - Summer

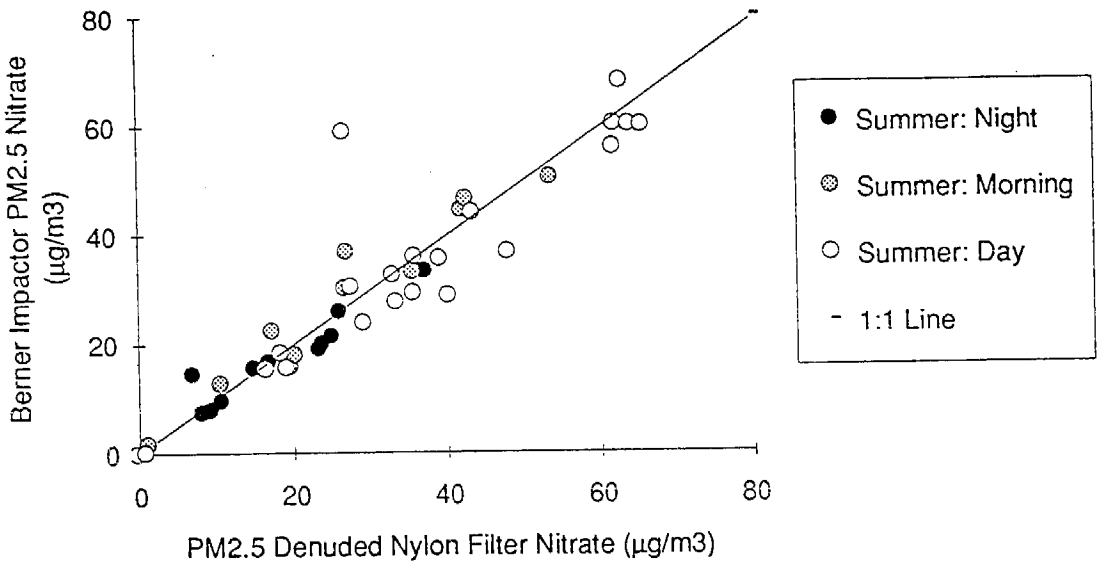

Filter Comparison for PM2.5 Nitrate at Rubidoux - Summer

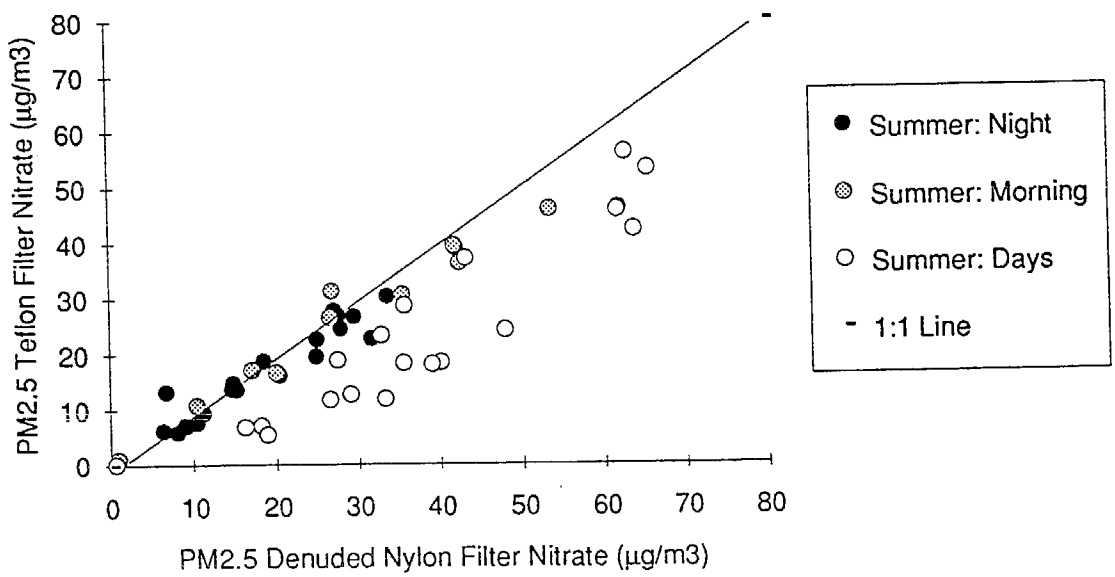

Impactor Comparison for PM2.5 Nitrate at Long Beach - Summer

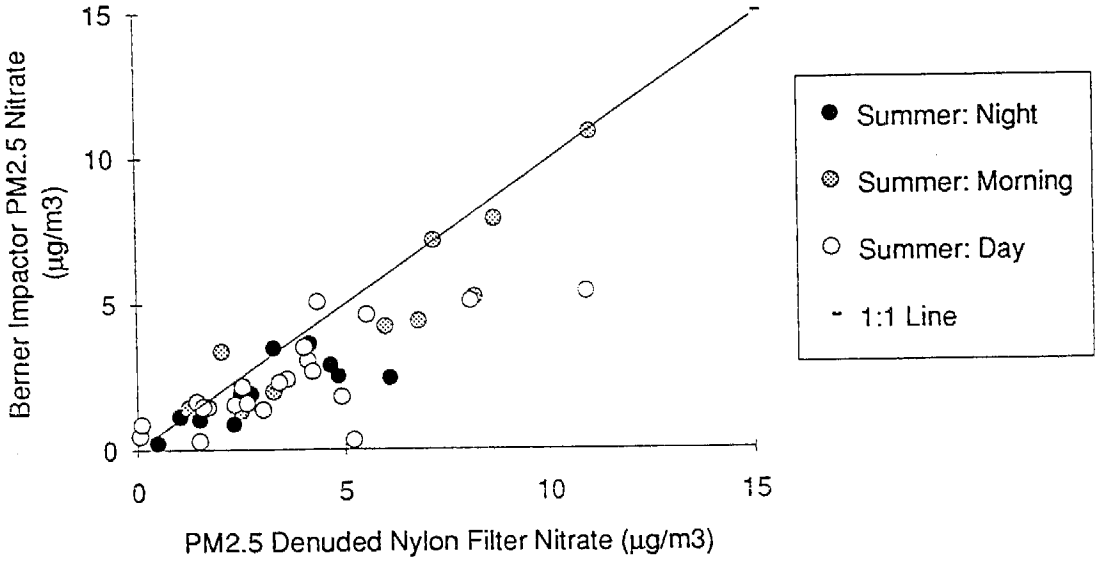

FIlter Comparison for PM2.5 Nitrate at Long Beach - Summer

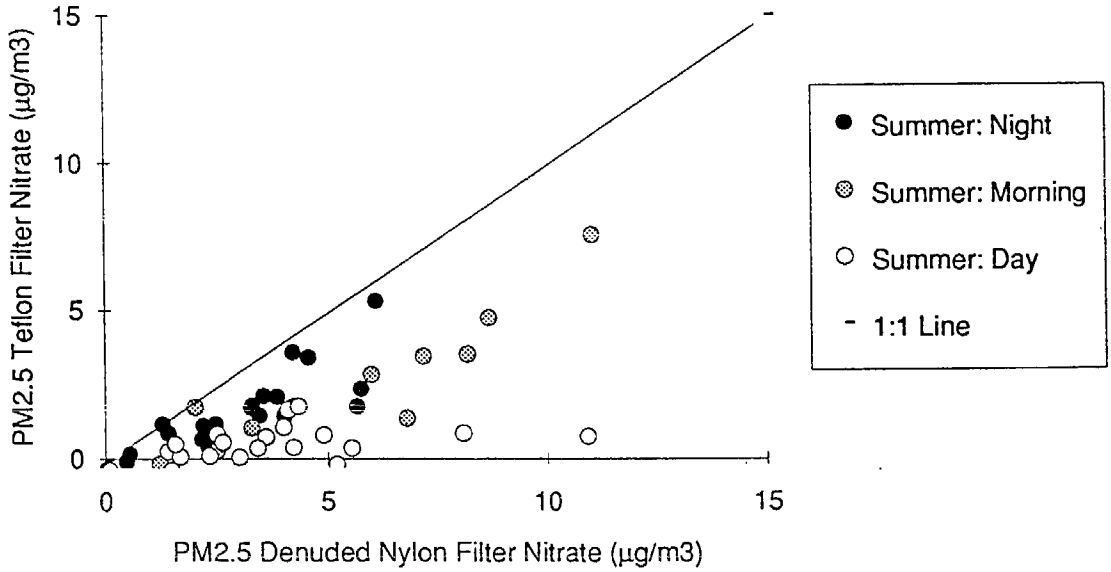

Impactor Comparison for PM2.5 Nitrate for Long Beach -Winter

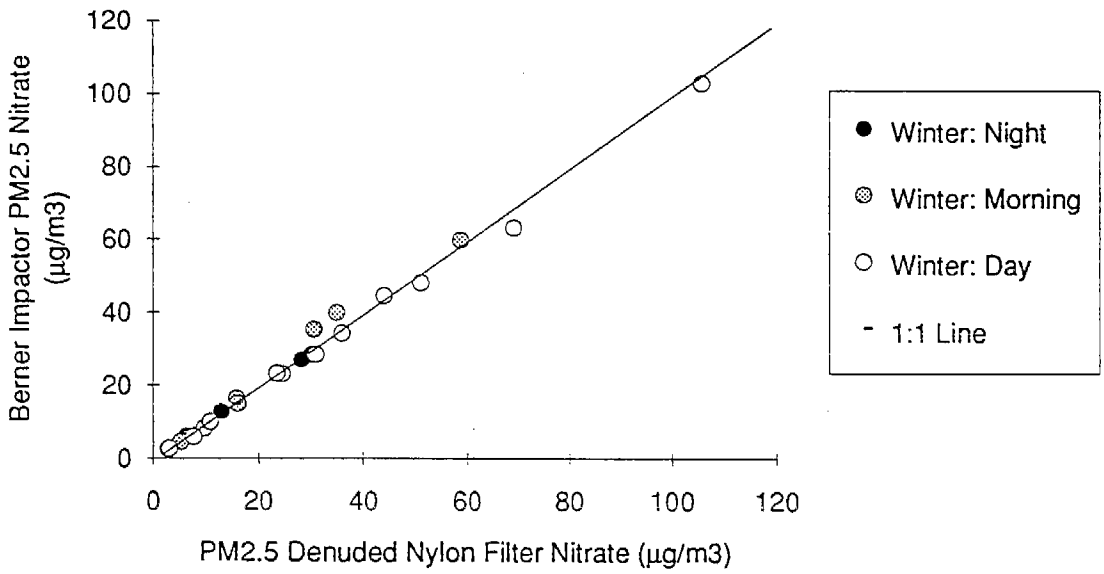

Filter Comparison for PM2.5 Nitrate at Long Beach - Winter

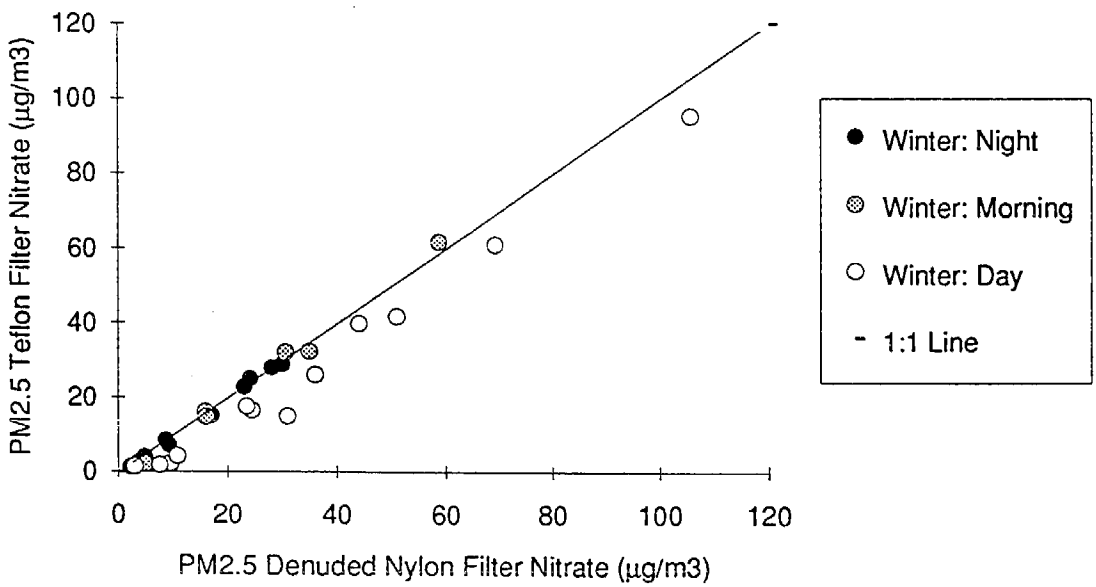

Impactor Comparison for PM2.5 Nitrate at Central Los Angeles - Winter

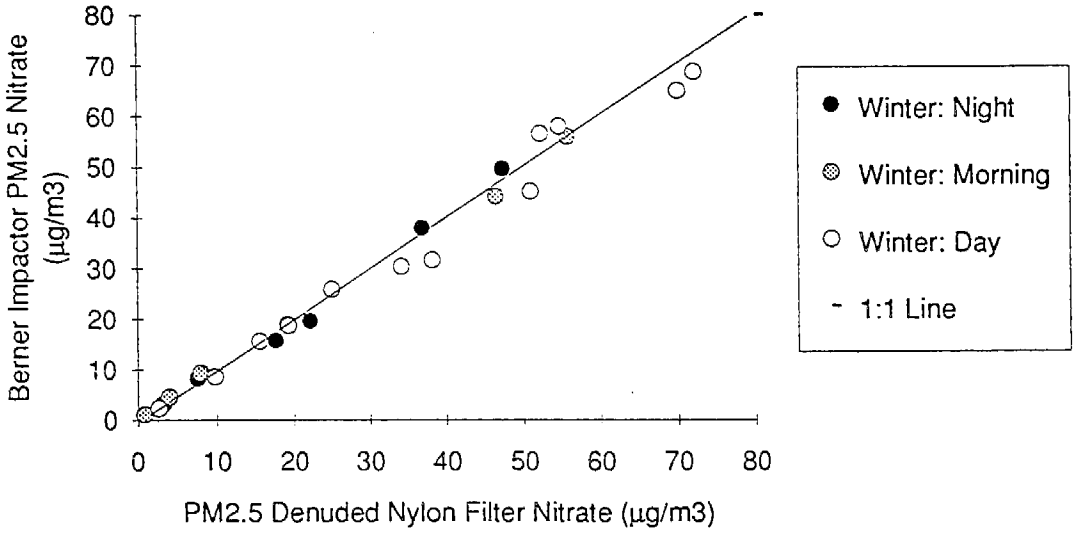

Filter Comparison for PM2.5 Nitrate at Central Los Angeles - Winter

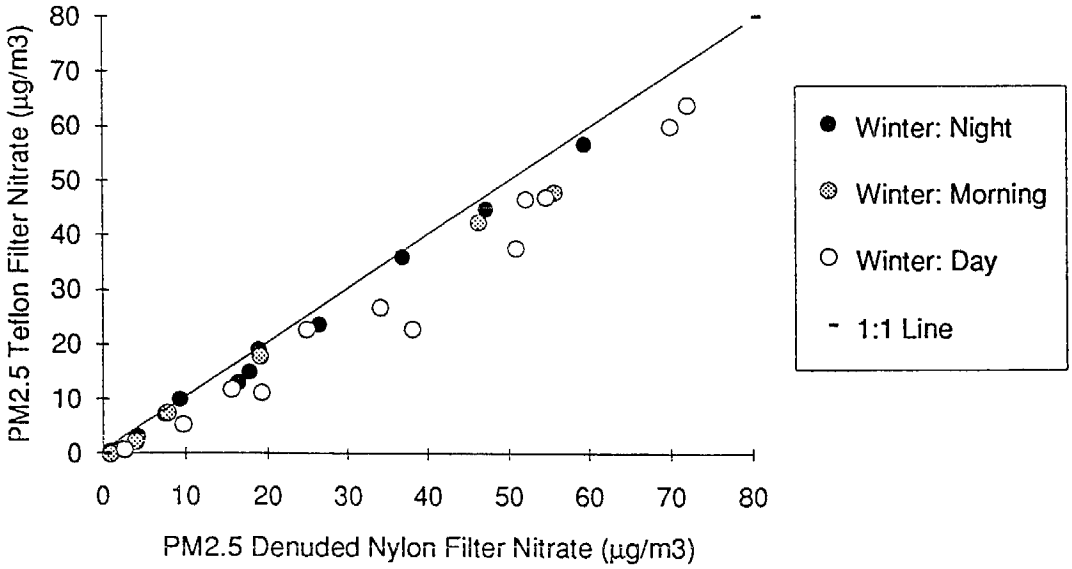

Appendix B

Scatter Plots of $PM_{2.5}$ Nitrate on Teflon Filters and Denuded Nylon Filters

Anaheim: Summer

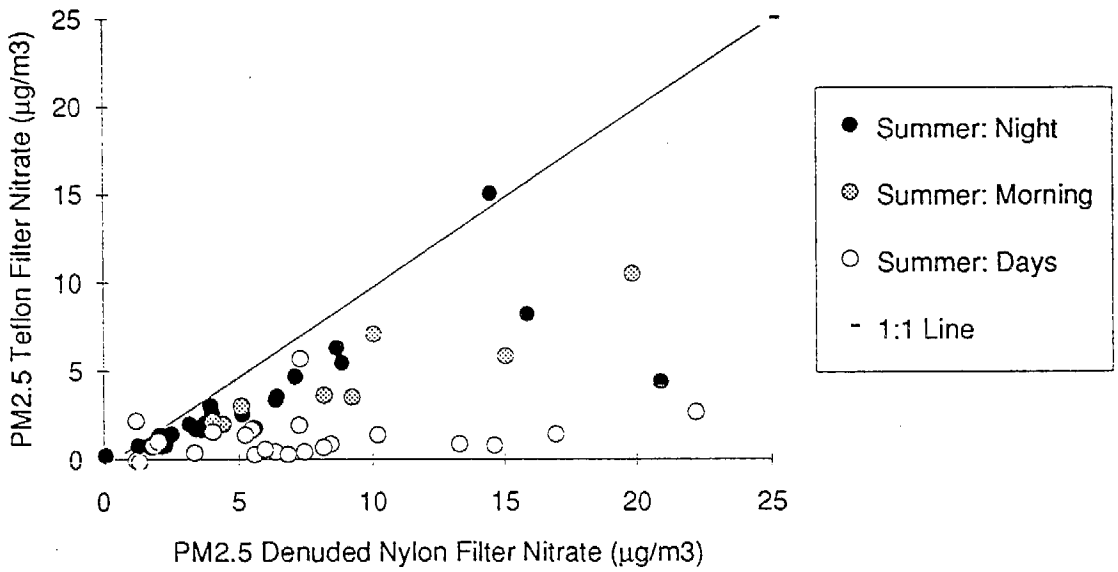

Anaheim: Winter

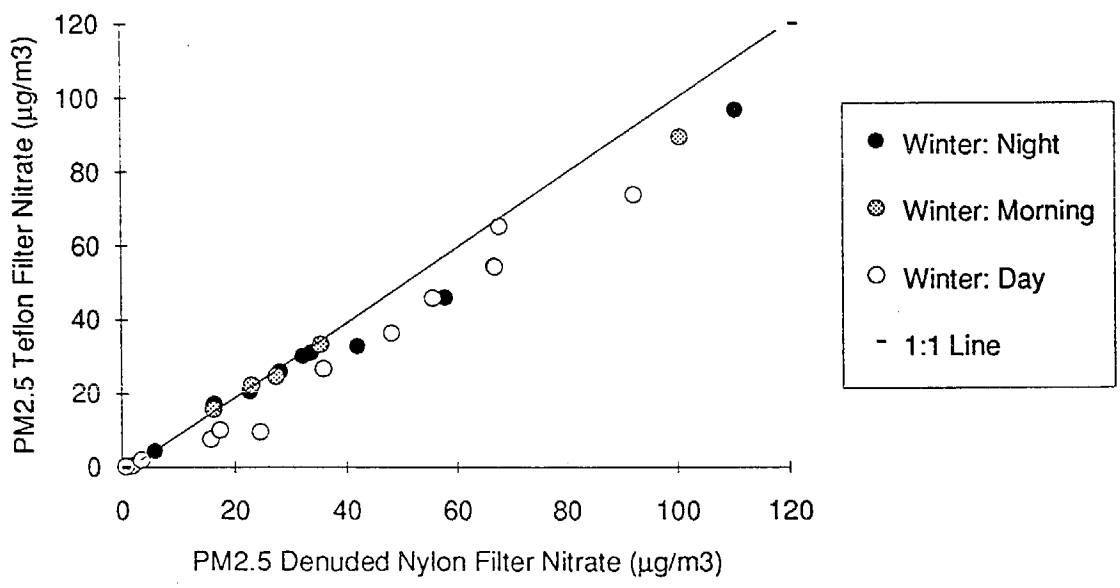

Hawthorne: Summer

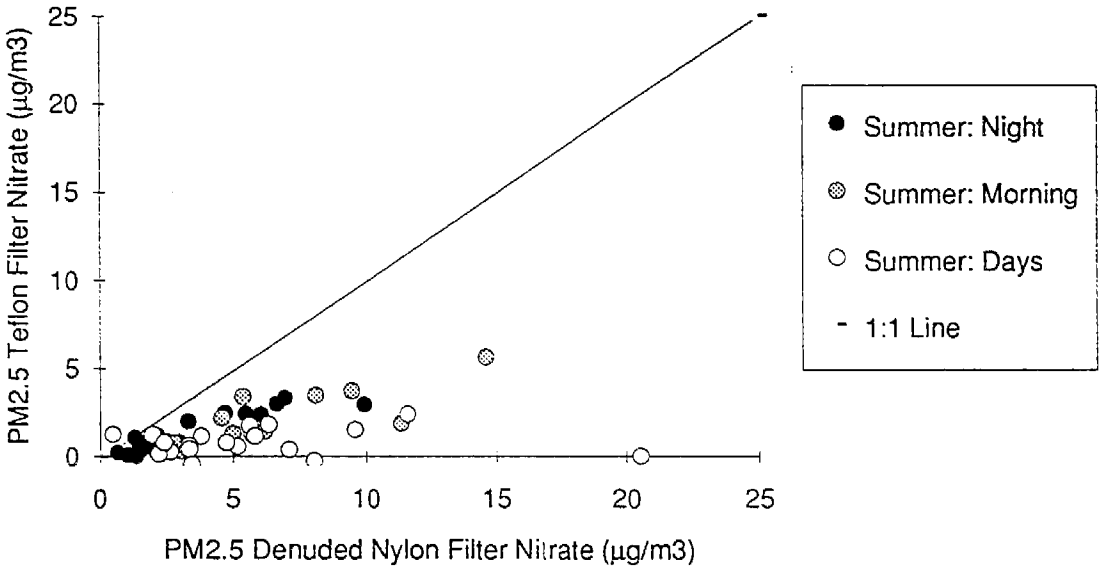

Hawthorne: Winter

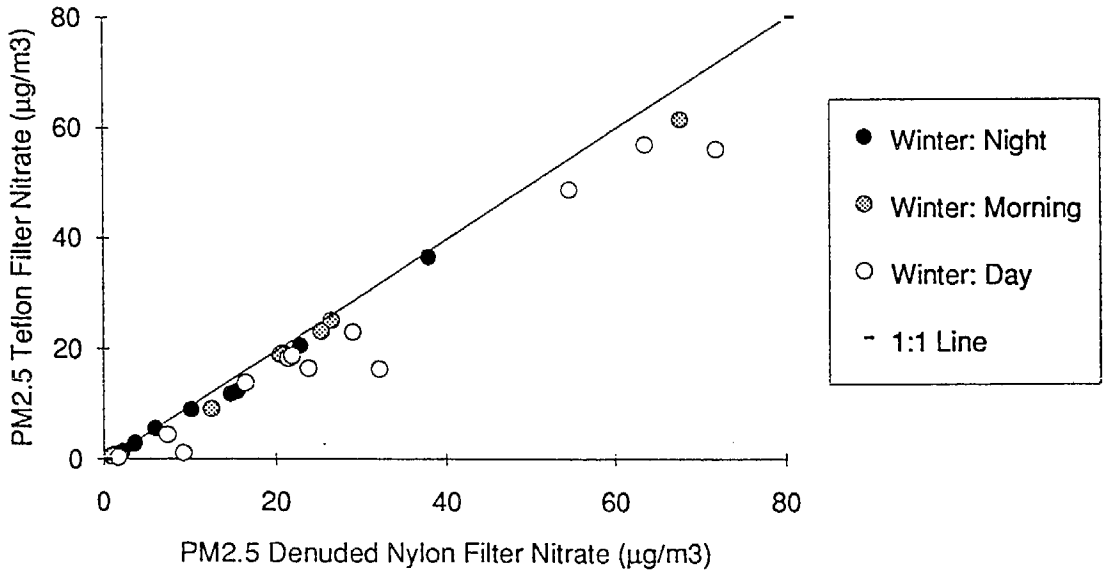

Long Beach CC: Summer

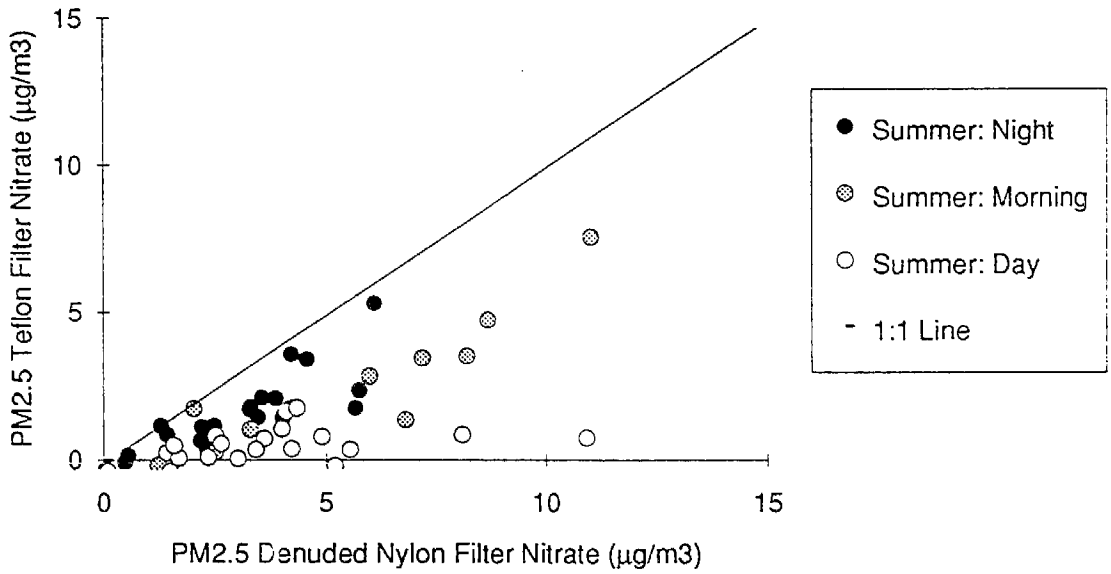

Long Beach CC: Winter

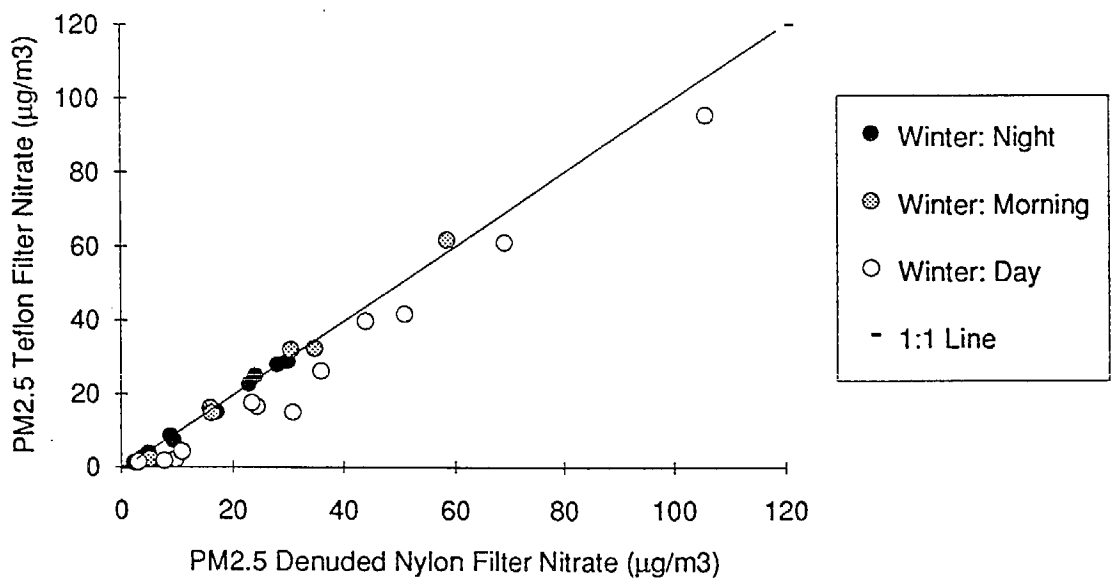

Central Los Angeles: Summer

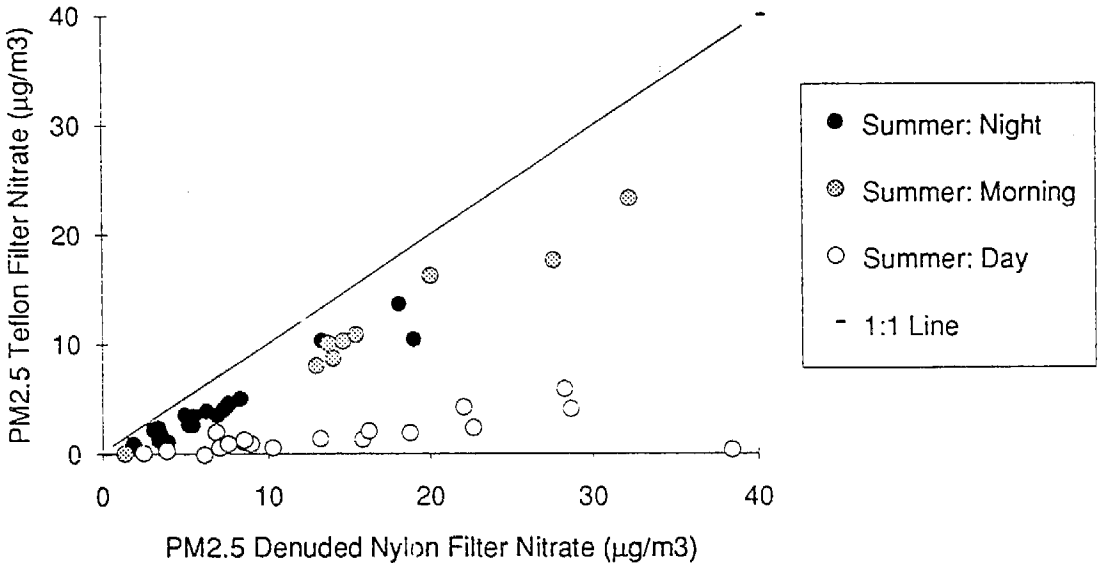

Central Los Angeles: Winter

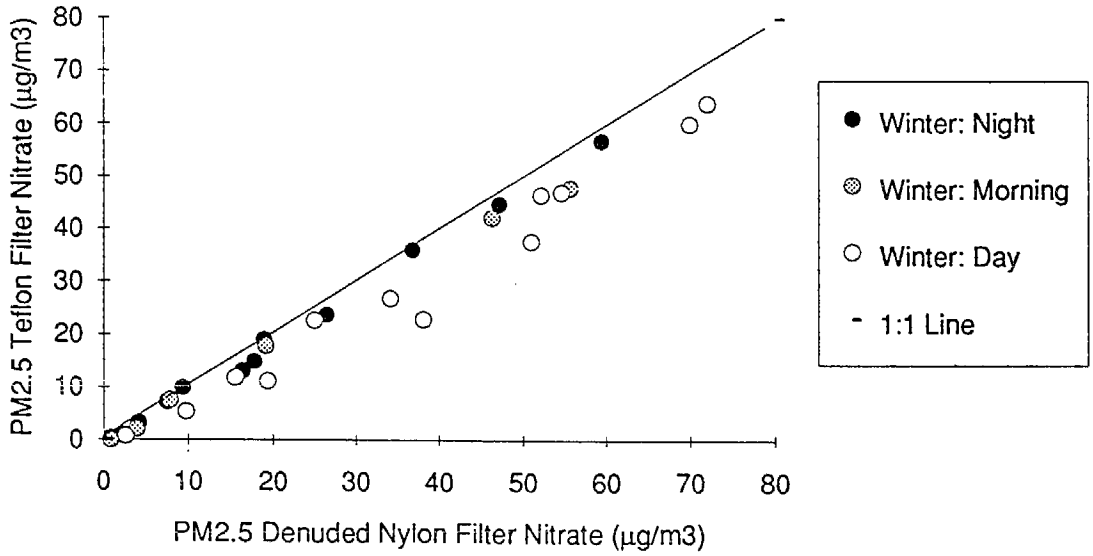

Burbank: Summer

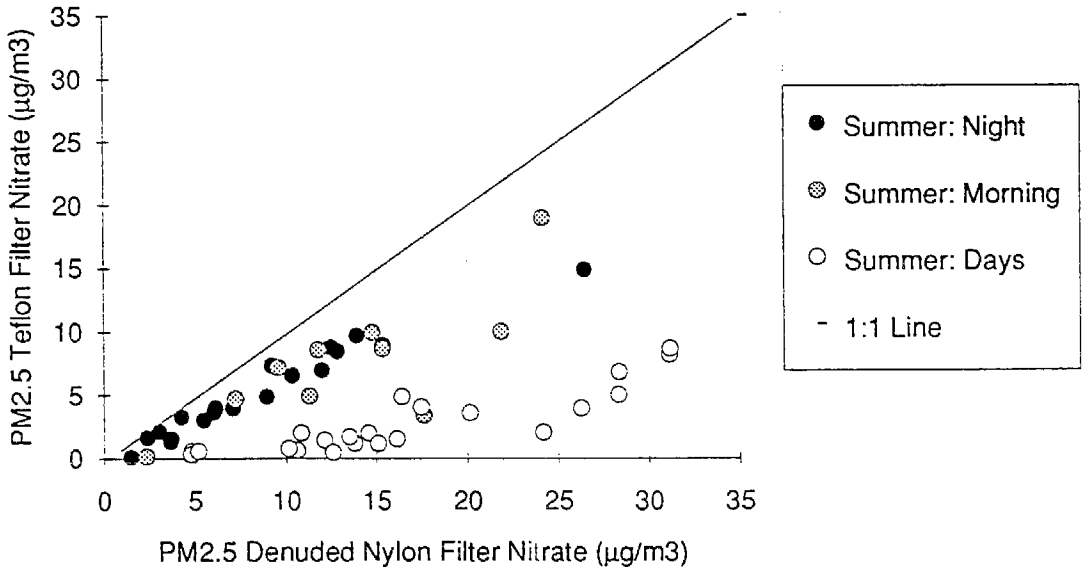

Burbank: Winter

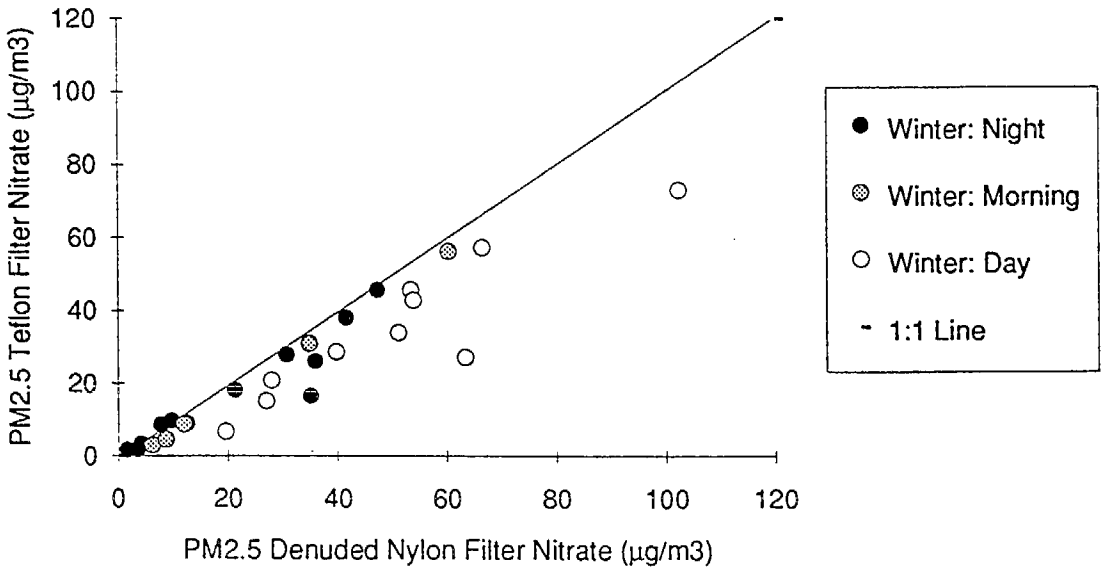

Claremont: Summer

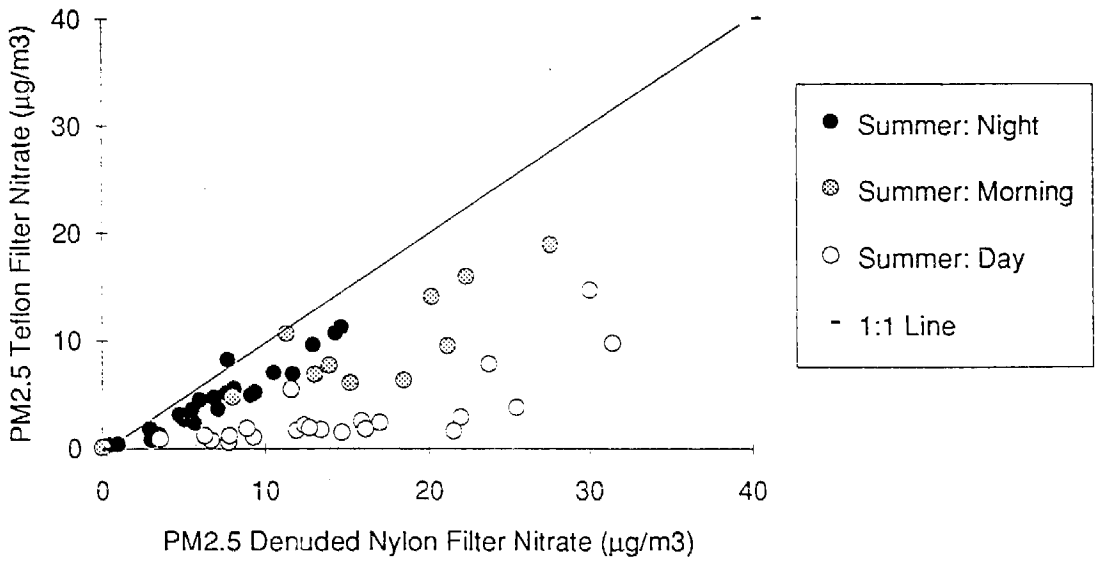

Azusa: Summer

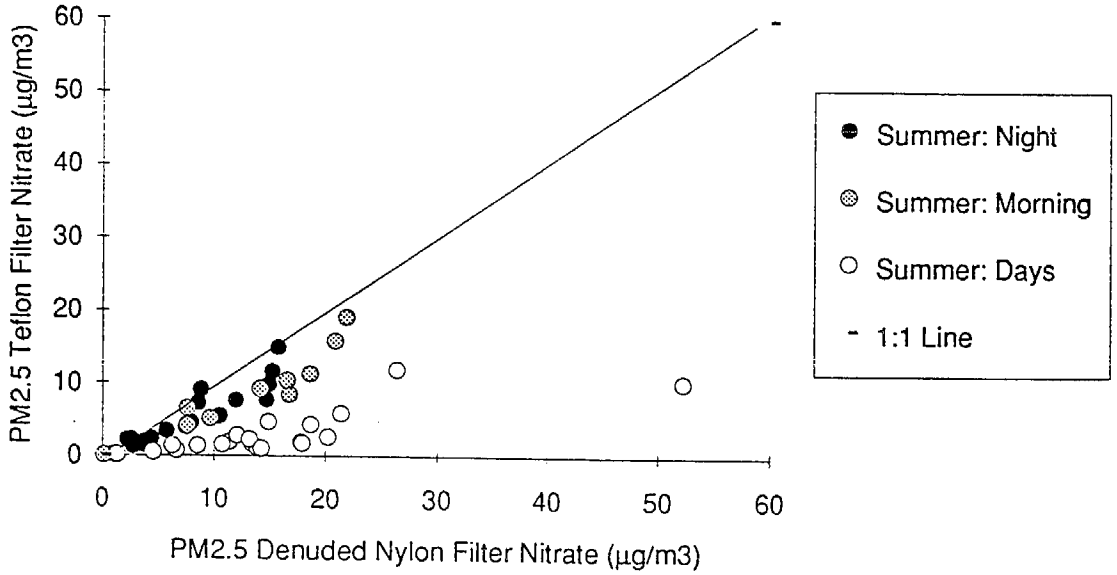

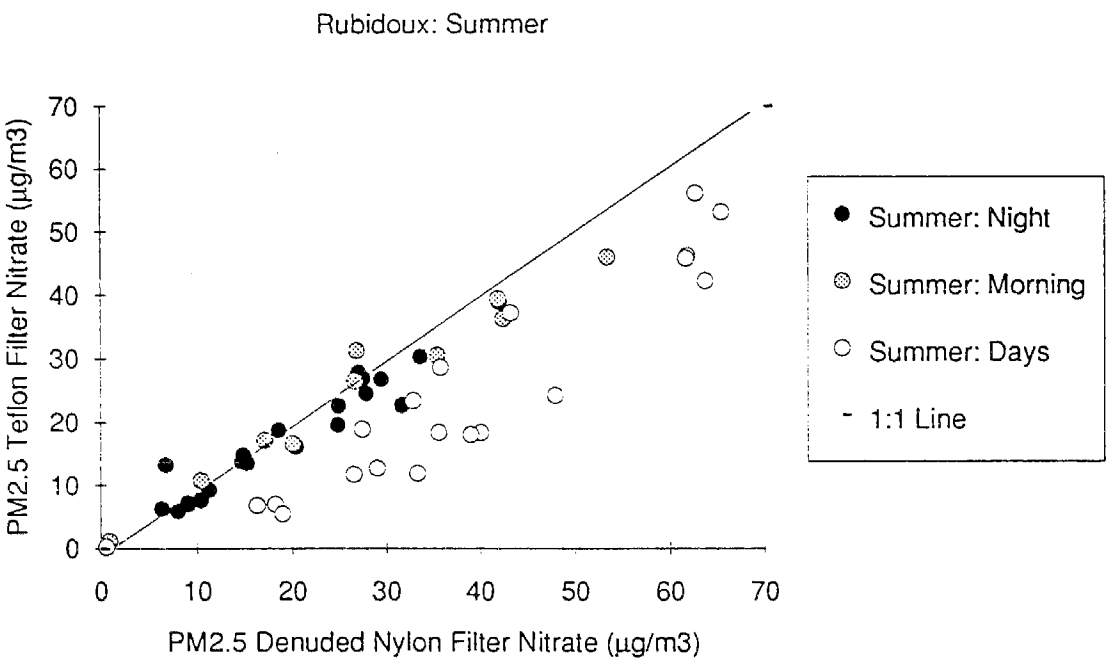
Rubidoux: Summer
PM2.5 Teflon Filter Nitrate (µg/m3)
PM2.5 Denuded Nylon Filter Nitrate (µg/m3)
0
10
20
30
40
50
60
70
Summer: Night
Summer: Morning
Summer: Days
1:1 Line

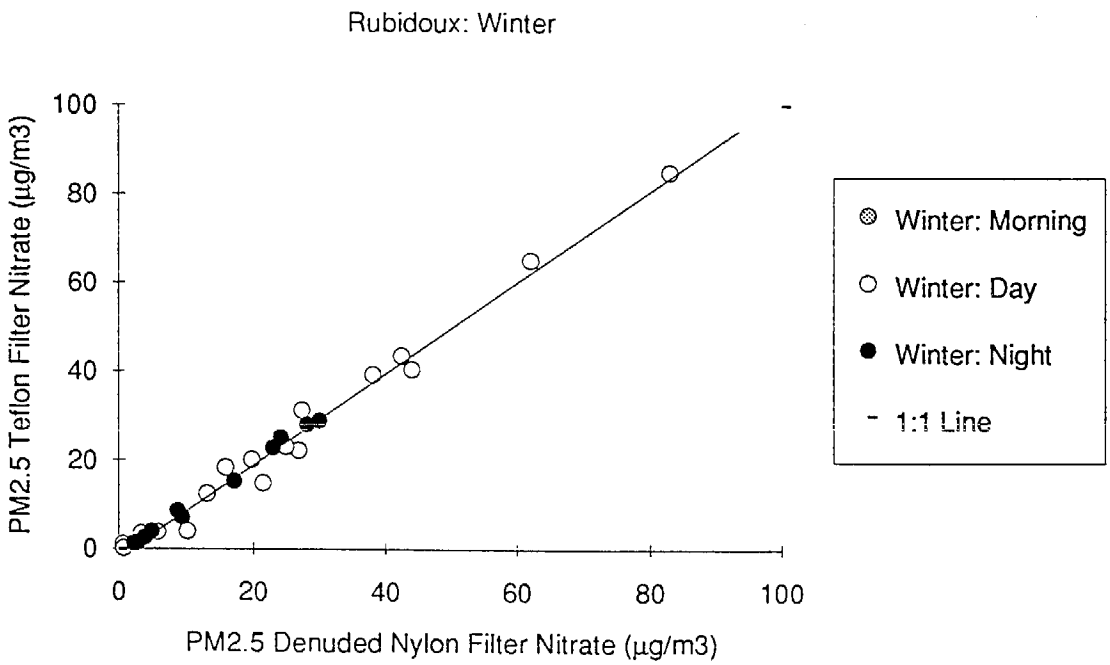
Rubidoux: Winter
PM2.5 Teflon Filter Nitrate (µg/m3)
PM2.5 Denuded Nylon Filter Nitrate (µg/m3)
0
20
40
60
80
100
Winter: Morning
Winter: Day
Winter: Night
1:1 Line

Appendix E

EQUIL2.1 USER'S GUIDE

1. Introduction

EQUIL2.1 is an updated version of the aerosol equilibrium model EQUIL developed by Pilinis and Seinfeld. It partitions the volatile aerosol species (nitrate, ammonium and chloride) between the gas and aerosol phases and calculates the appropriate amount of liquid water assuming thermodynamic equilibrium.

The code can be incorporated in a 1D or 3D atmospheric photochemical model or it can be used interactively for the simulation of experimental data or sensitivity analysis.

2. Files

EQUIL2_1. F : Main fortran code for EQUIL2.1. This file is needed for the incorporation of EQUIL2_1.F in a 1-D or 3-D photochemical model.

EQSUBS.F. Fortran code with the subroutines used by EQUIL2.1. This file is needed for the incorporation of EQUIL2_1.F in a 1-D or 3-D photochemical model.

DRIVER.F : Thus is the driver for the equilibrium program, so that the program can run interactively. It performs a single or multiple aerosol calculations prompting each time the user for the input values and then providing the answers on the screen.

The code has been compiled and tested on HP 9000, IBM RISC 6000 and DEC Alpha workstations with and without optimization.

3. Using EQUIL2.1 for Interactive Calculations

All three files have to be compiled, linked and executed. The code requests from the user the necessary input data for the partitioning of the volatile aerosol species between the aerosol and

gas phases. A sample input and a sample output are presented in Tables 1 and 2, respectively.

As shown in these two tables the inputs to the code are the temperature in Kelvin, the relative humidity (from 0.0 to 1.0), and the total concentrations of the various species in $\mu g/m^3$. The requested concentrations include *both the aerosol and gas-phase* concentrations of each species

Sulfates should be inserted as sulfuric acid (MW=98), while total NH_3+NH_4 as NH_3 (MW=17), HNO_3 + NO_3 as HNO_3 (MW=63) and HCl + Cl as HCl (MW=36.5). Once the necessary inputs are read by the program they are reported for verification and then the program proceeds in the calculation of the minimum of the Gibbs free energy.

Table 1: Sample Input to EQUIL2.1

```
   Insert ambient temperature ( K)
298.0
   Insert ambient Relative Humidity ( 0-1 scale)
0.9
   Insert Na concentration ( in micrograms m-3)
2.3
 Insert aerosol sulfate conc. (micrograms m-3 of H2SO4)
9.8
   Insert (NH3+NH4) concentration ( in micrograms m-3)
1.7
   Insert (HNO3+NO3) concentration ( in micrograms m-3)
6.3
   Insert (HCl+Cl) concentration ( in micrograms m-3)
3.55
```

The output (Table 2) includes

(a) The seven input values (relative humidity, temperature, equivalent Na, sulfuric acid, ammonia, nitric acid and HCl). These concentrations include both the aerosol and gas phase concentrations of a species.

(b) The calculated gas-phase concentrations of HCl, HNO_3 and NH_3 in $\mu g\ m^{-3}$.

(c) The total chloride, nitrate, ammonia and sulfate in the aerosol phase in $\mu g\ m^{-3}$. These species may in their ionic form or part of salt.

(d) The total aerosol mass in $\mu g\ m^{-3}$.

(e) The total dry aerosol mass (=total mass-water) in $\mu g\ m^{-3}$.

(f) The concentrations in $\mu g\ m^{-3}$ of the twelve aerosol species predicted by the model.

Table 2: Sample output from the model

```
relative humidity   = 0.900
temperature         = 298.0
equivalent Na       = 2.300
sulfuric acid       = 9.800
ammonia             = 1.700
nitric acid         = 6.300
     HCl            = 3.550

HCl                 .34149E+01
HNO3                .54707E+01
NH3                 .00000E+00

total Cl      =     .13508E+00 micrograms m-3 HCl
total NO3     =     .82934E+00 micrograms m-3 HNO3
total NH4     =     .17000E+01 micrograms m-3 NH3
total SO4     =     .98000E+01 micrograms m-3 H2SO4
[tot. aer.]   =     .52348E+02 micrograms m-3
[tot. aer.]-[H2O] = .14848E+02 micrograms m-3

NH4NO3              .00000E+00
NaHSO4              .00000E+00
NH4HSO4             .00000E+00
(NH4)3H(SO4)2       .00000E+00
NA2SO4              .00000E+00
NANO3               .00000E+00
NACl                .00000E+00
(NH4)2SO4           .00000E+00
NH4Cl               .00000E+00
liquid H2O          .37501E+02
NH4                 .18000E+01
H2SO4aq             .00000E+00
HSO4                .68582E+00
SO4                 .89212E+01
NO3                 .81617E+00
Na                  .23000E+01
Cl                  .13138E+00
```

4. Model Overview

A wide range of phases and compounds may be present in the aerosol. EQUIL2.1 uses our understanding of the corresponding thermodynamics to simplify the minimization calculation. A series of cases have been identified, and are described by appropriate submodules of EQUIL2.1. This makes the code a lot more complicated, but also more efficient. The details of the way EQUIL2.1 handles these chemical regimes are presented in the attached flow-chart.

The program starts by determining whether the atmospheric system under consideration is sodium rich or not. If not EQUIL2.1 determines whether the system is sulfate deficient or sulfate rich. The crucial parameter for this determination is the ratio $R = (NH_3+Na) / H_2SO_4$ on a molar basis. The system is sulfate deficient if $R > 2$, while the system is sulfate rich for $R < 2$. In the sulfate deficient case sulfates can be assumed to be completely neutralized, since there is an abundance of ammonia and sodium chloride. The sulfate rich case can be divided into two subcases. When $1 < R < 2$, part of the sulfates are neutralized, while the rest of it reacts to produce HSO_4^-. When $R < 1$, part of the sulfates remains as H_2SO_4, while the rest of it reacts to produce HSO_4^-. The distribution of sulfates among the possible ions depends on thermodynamic equilibrium.

Another important variable is the relative humidity of deliquescence. Nine deliquescence relative humidities are employed by the code, corresponding to the nine thermodynamically possible solids. For relative humidities above its deliquescence relative humidity the solid may not exist, because only its aqueous solution is thermodynamically possible. On the other hand for relative humidities below the deliquescence relative humidity the solid may or may not exist. Finally, for relative humidities below the lowest deliquescence relative humidities of the salts involved the aerosol is assumed to be dry. Thus the entire range of relative humidities can be divided in several regimes (see flow chart). For more information the reader can consult the papers by Pilinis and Seinfeld describing the principles of the operation of the original EQUILIB code.

5. Use of EQUIL2.1 as a Module in a 3D Model

EQUIL2.1 (files *EQUIL2_1.F and EQSUBS.F*) can be used as a module in atmospheric models

for the partitioning of volatile species (ammonia, nitric and hydrochloric acid) between the gas and aerosol phases and the estimation of the aerosol liquid water content. The main code should call subroutine EQUILIB, the main subroutine of EQUIL2_1.F. All communications with the main code are done through the arguments of this subroutine

```
subroutine      equilib(temp1,rh,w1,rwater,ammon,sodium,
                 sulfate,nitrate,chloride,hno3,nh3,rhcl,rna2so4,rnh42s4,
                rnh4cl,rnacl,rnano3,rnh4no3,bisulf,clc,rh2so4,cnh4hso4,rnahso4)
```

All the arguments are real numbers and w1 is a vector with 5 rows. Table 3 explains the meaning of each of the above variables. Note that all the concentrations are in $\mu g/m^3$.

The input variables describe the sum of a gas and aerosol-phase species concentration, and these species have often different molecular weights. EQUIL2_1 for compatibility reasons with the original EQUIL1.0 is using the same conventions. Ammonia, sulfuric, nitric, and hydrochloric acid should be passed to EQUILIB as *the equivalent concentrations of the corresponding gases*. Therefore sulfate should be passed to EQUILIB as equivalent H_2SO_4 (MW=98). Finally sodium should be passed to EQUILIB as equivalent NaCl (MW=58.5). Note that this is just a convention and EQUILIB uses only the sodium in the calculations. The chloride included in w1(1) is neglected in the calculations. The chloride information is passed to EQUILIB through w1(5).

Interpretation of the output is straightforward, as the twenty reported concentrations refer to specific compounds with a unique molecular weight. Note that there is a one to one correspondence between aerosol species and reported concentrations. For example, sulfate is the mass concentration of SO_4^{2-}, an ionic species in solution. It does not include sulfate in other forms, i.e. ammonium sulfate, HSO_4^-, etc. For all the species concentrations the corresponding molecular weight is used.

All the variables are real, single precision and the species concentrations are all in $\mu g\ m^{-3}$.

Table 3: Input and Output Variables for Subroutine EQUILIB

VARIABLE	EXPLANATION AND UNITS	COMMENTS
INPUT VARIABLES		
temp1	Temperature (in K)	atmospheric temperature
rh	Relative Humidity (0-1 scale)	scale is from 0.0 to 1.0
w1(1)	Na concentration ($\mu g/m^3$)	sodium expressed as equivalent NaCl (MW=58.5)
w1(2)	total H_2SO_4 and SO_4^{2-} concentration	total sulfate expressed as equivalent H_2SO_4 (MW=98)
w1(3)	total NH_3 + NH_4 concentration	total ammonia expressed as equivalent NH_3 (MW=17)
w1(4)	total NO_3 + HNO_3 concentration	total nitrate expressed as equivalent HNO_3 (MW=63)
w1(5)	total Cl + HCl concentration ($\mu g/m^3$)	total chloride expressed as equivalent HCl (MW=36.5)
OUTPUT VARIABLES		
rwater	H_2O concentration ($\mu g/m^3$)	aerosol liquid water
ammon	NH_4^+ concentration ($\mu g/m^3$)	aerosol ammonium in solution
sulfate	SO_4^{2-} concentration ($\mu g/m^3$)	aerosol sulfate
nitrate	NO_3^- concentration ($\mu g/m^3$)	aerosol nitrate
chloride	Cl^- concentration ($\mu g/m^3$)	aerosol chloride
hno3	HNO_3 concentration (gas) ($\mu g/m^3$)	gas-phase nitric acid
nh3	NH_3 concentration (gas) ($\mu g/m^3$)	gas-phase ammonia
rhcl	HCl concentration (gas) ($\mu g/m^3$)	gas-phase hydrochloric acid
rna2so4	Na_2SO_4 (s) concentration ($\mu g/m^3$)	solid salt
rnh42s4	$(NH_4)_2SO_4$ (s) concentration ($\mu g/m^3$)	solid salt
rnh4cl	NH_4Cl (s) concentration ($\mu g/m^3$)	solid salt
rnacl	NaCl (s) concentration ($\mu g/m^3$)	solid salt
rnano3	$NaNO_3$ (s) concentration ($\mu g/m^3$)	solid salt
rnh4no3	NH_4NO_3(s) concentration ($\mu g/m^3$)	solid salt
bisulf	HSO_4 concentration ($\mu g/m^3$)	aerosol bisulfate
clc	$(NH_4)_3H(SO_4)_2$(s) concentration ($\mu g/m^3$)	solid salt
rh2so4	H_2SO_4 concentration ($\mu g/m^3$)	aerosol sulfuric acid
cnh4hso4	NH_4HSO_4 (s) concentration ($\mu g/m^3$)	solid salt
rnahso4	$NaHSO_4$(s) concentration ($\mu g/m^3$)	solid salt
sodium	Na^+ concentration ($\mu g/m^3$)	

6. Testing of EQUIL2.1

The original code (EQUIL1.0) was developed in 1986 by Drs. Pilinis and Seinfeld for the VAX VMS system and has been used since then in a variety of applications. The code used a series of machine dependent FORTRAN statements that could be misinterpreted by some UNIX Fortran compilers. A series of minor problems associated with the code response in some unique atmospheric situations was fixed by EQUIL2.0 in 1994 but the code remained compatible with only the VAX VMS system.

In version EQUIL2.1 the VAX specific parts of the code have been rewritten and the EQUIL2.1 can be compiled (with and without) optimization in HP, IBM and DEC workstations. The code was evaluated by comparing its results with the results of the previous simulations. A suite of roughly 5,000 simulations was run covering the whole range of typical atmospheric conditions.

Comparing EQUIL1.0, EQUIL2.0 and EQUIL2.1 running in the same platform we noticed the following. The results were exactly the same for more than 95% of the cases. The small differences in the remaining 5% of the cases (usually of the order of 1 or 2 $\mu g\ m^{-3}$) were mostly attributed to the correction of problems of the previous versions. We examined these cases one by one and verified that EQUIL2.1 gives the correct results. Actually EQUIL2.0 gives exactly the same results for all these cases when run in the interactive mode in any platform. The problems of EQUIL2.0 in these cases appeared to be related to the way that UNIX compilers keep old variables in memory and the non-standard coding used in EQUIL2.0 and have been corrected.

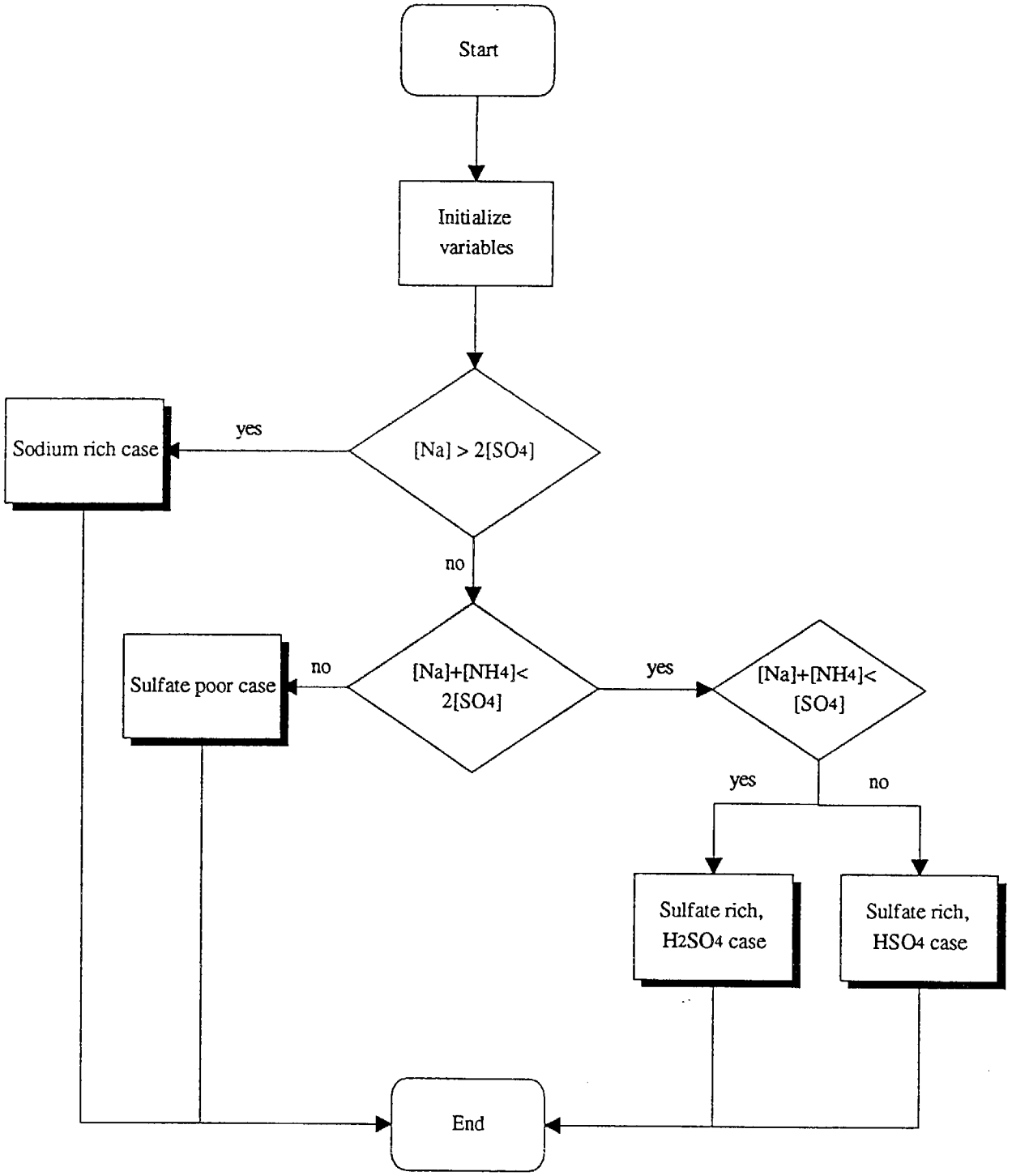

Main flow chart

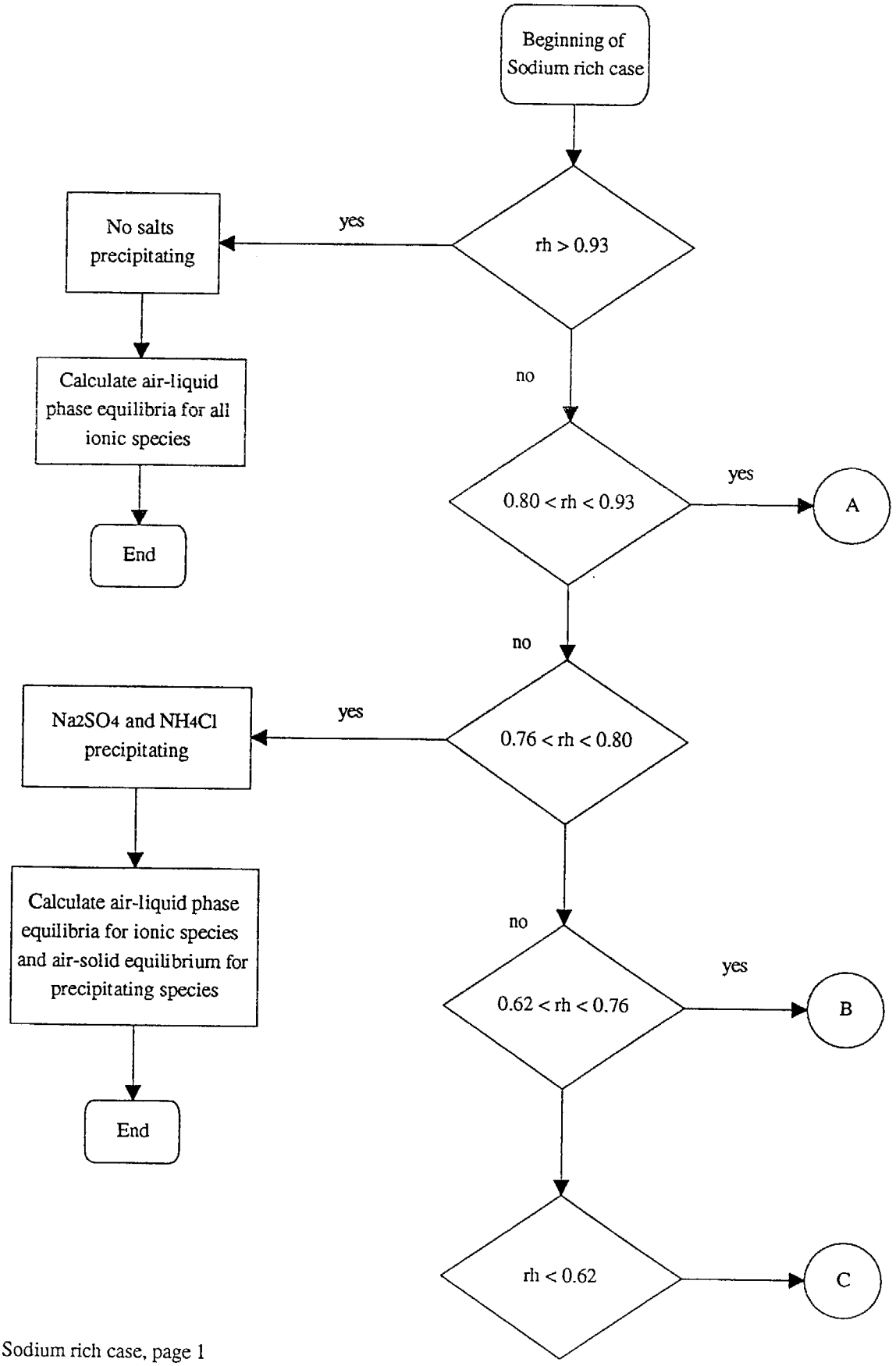

Sodium rich case, page 1

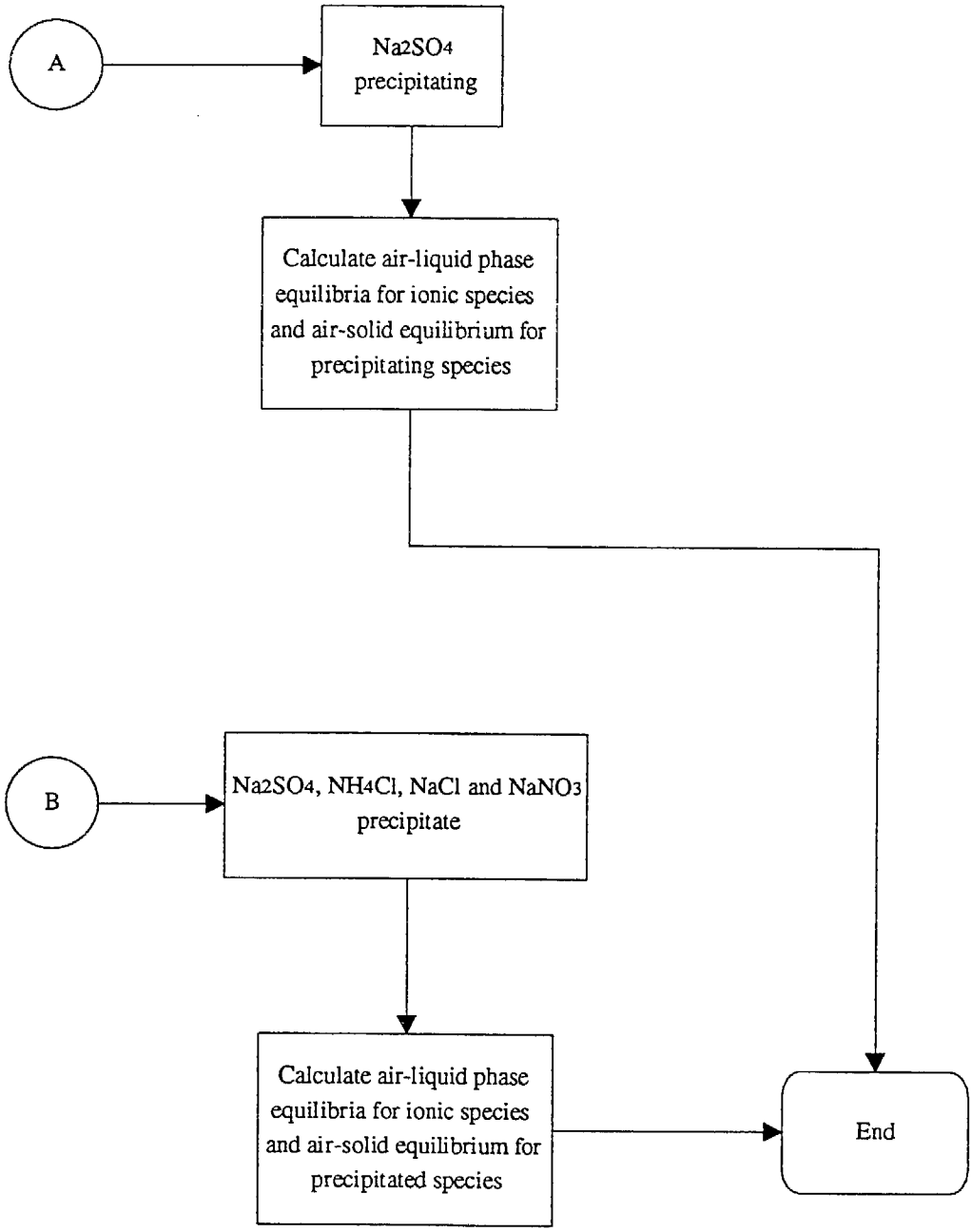

Sodium rich case, page 2

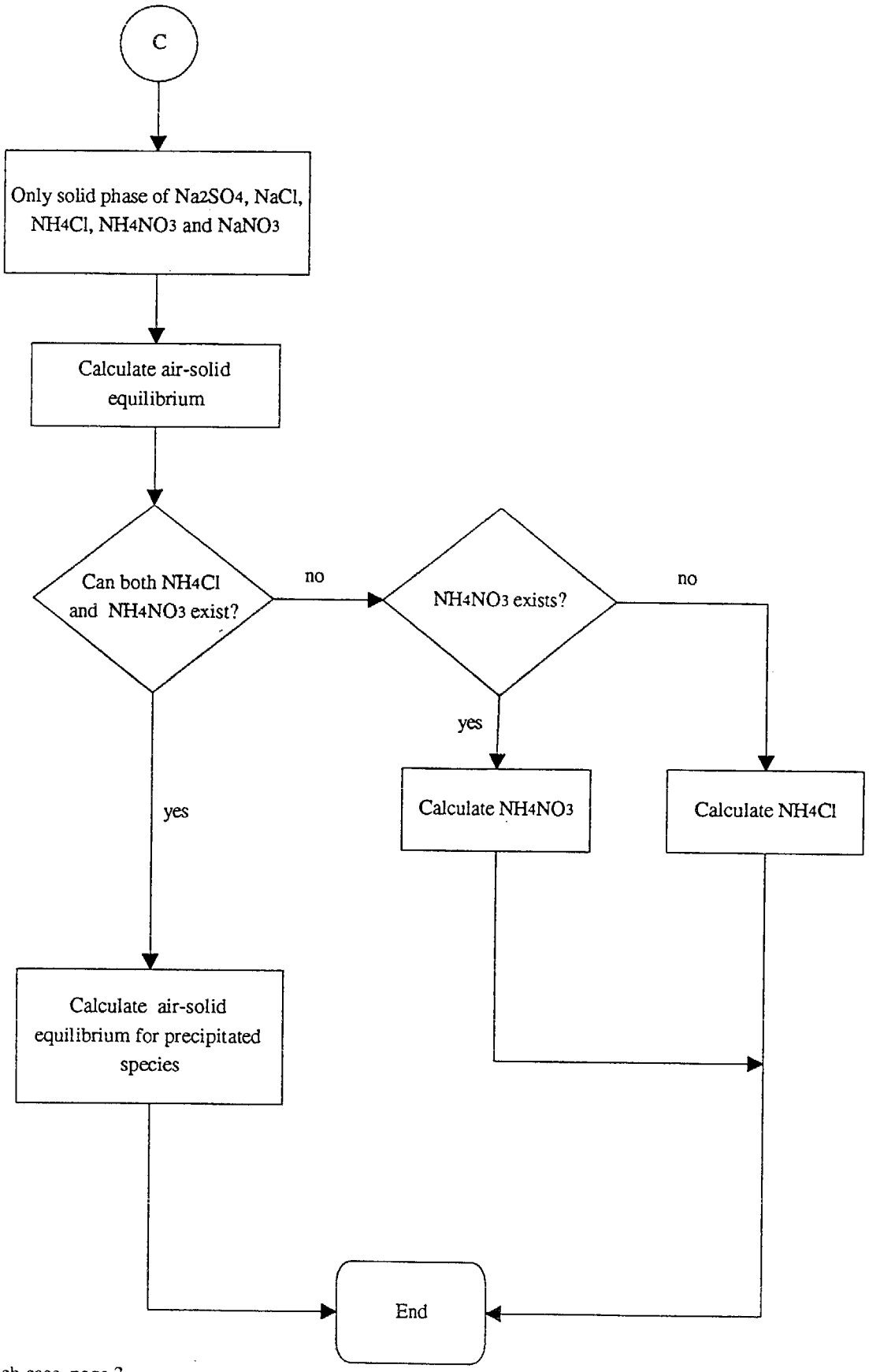

Sodium rich case, page 3

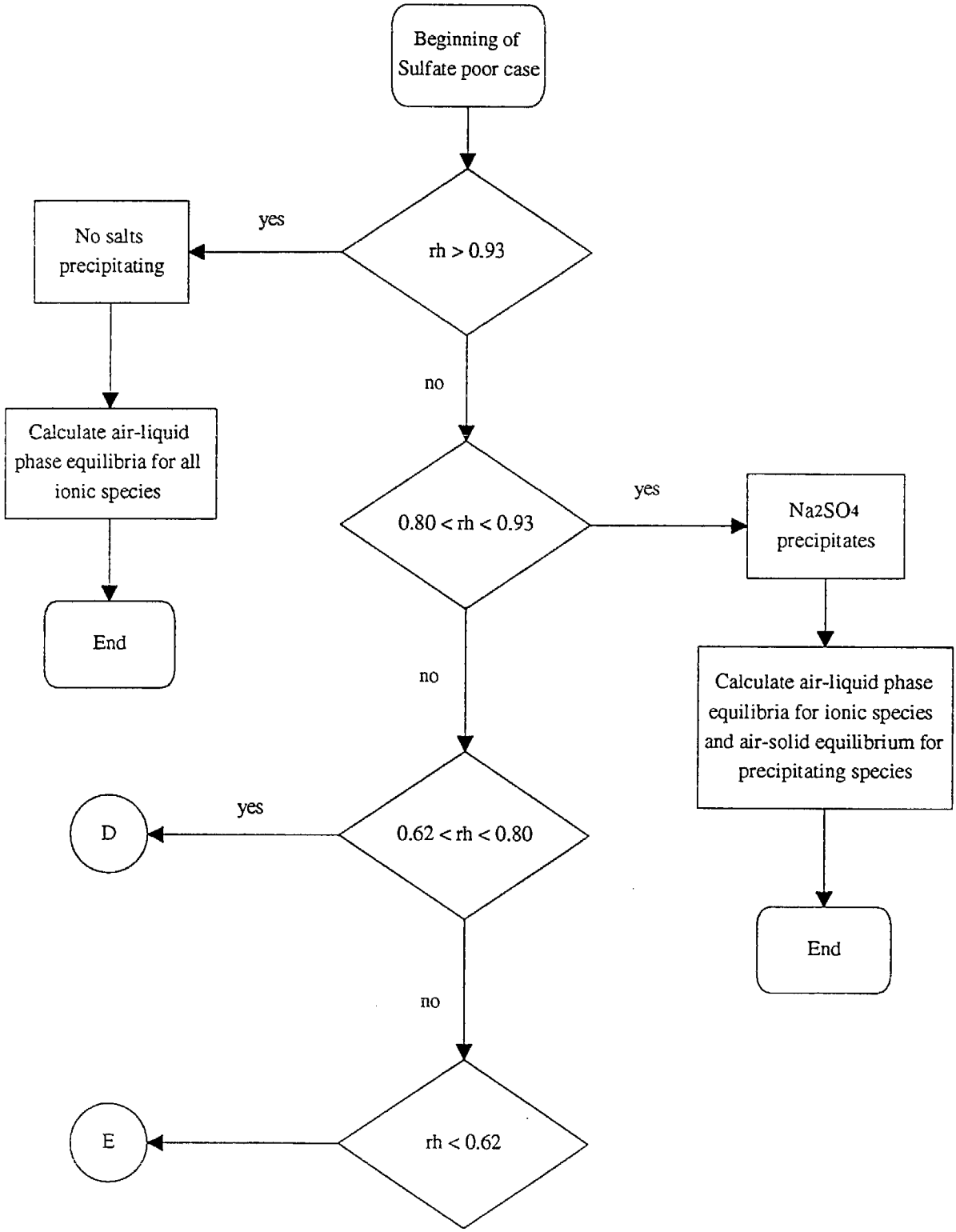

Sulfate poor case, page 1

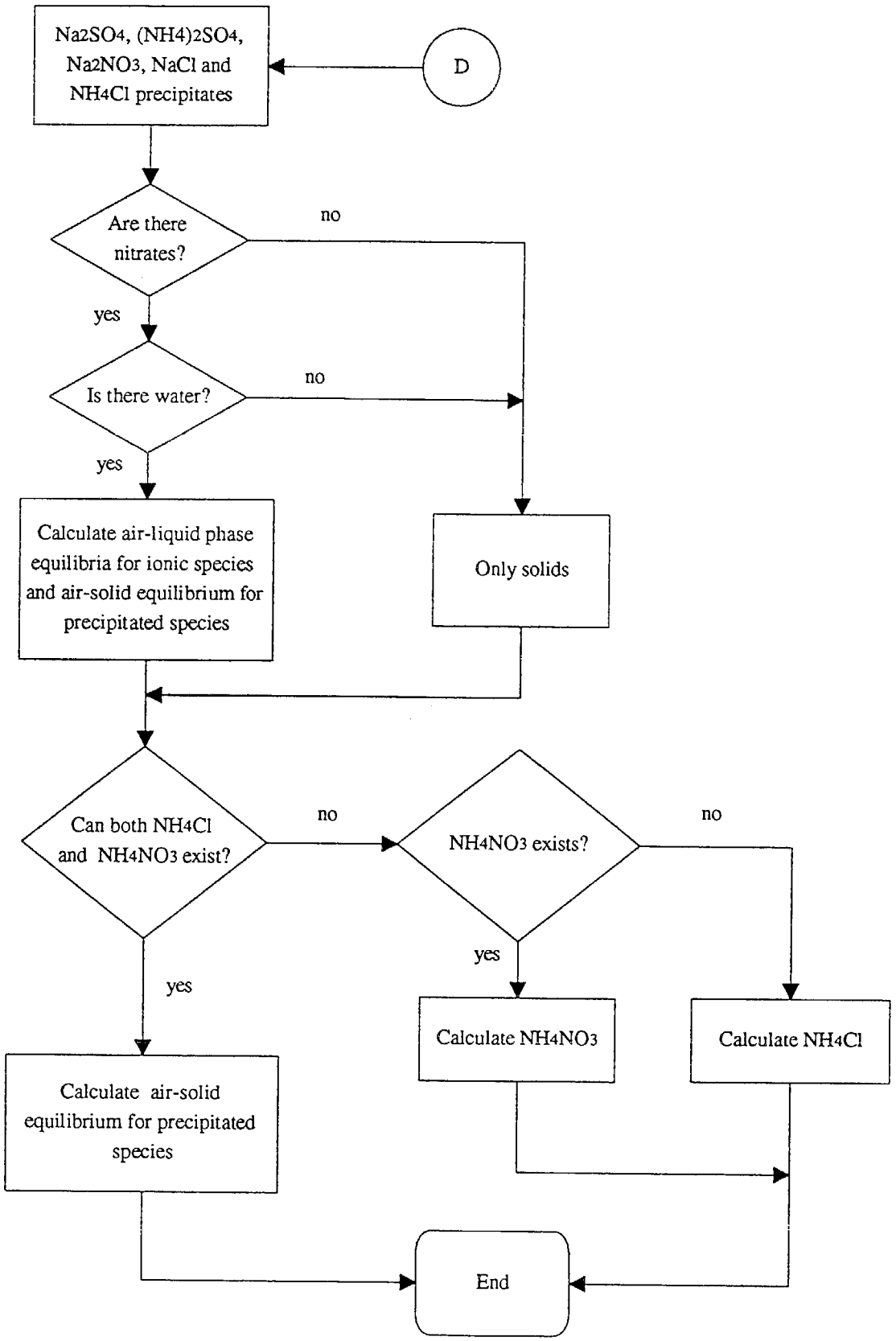

Sulfate poor case, page 2

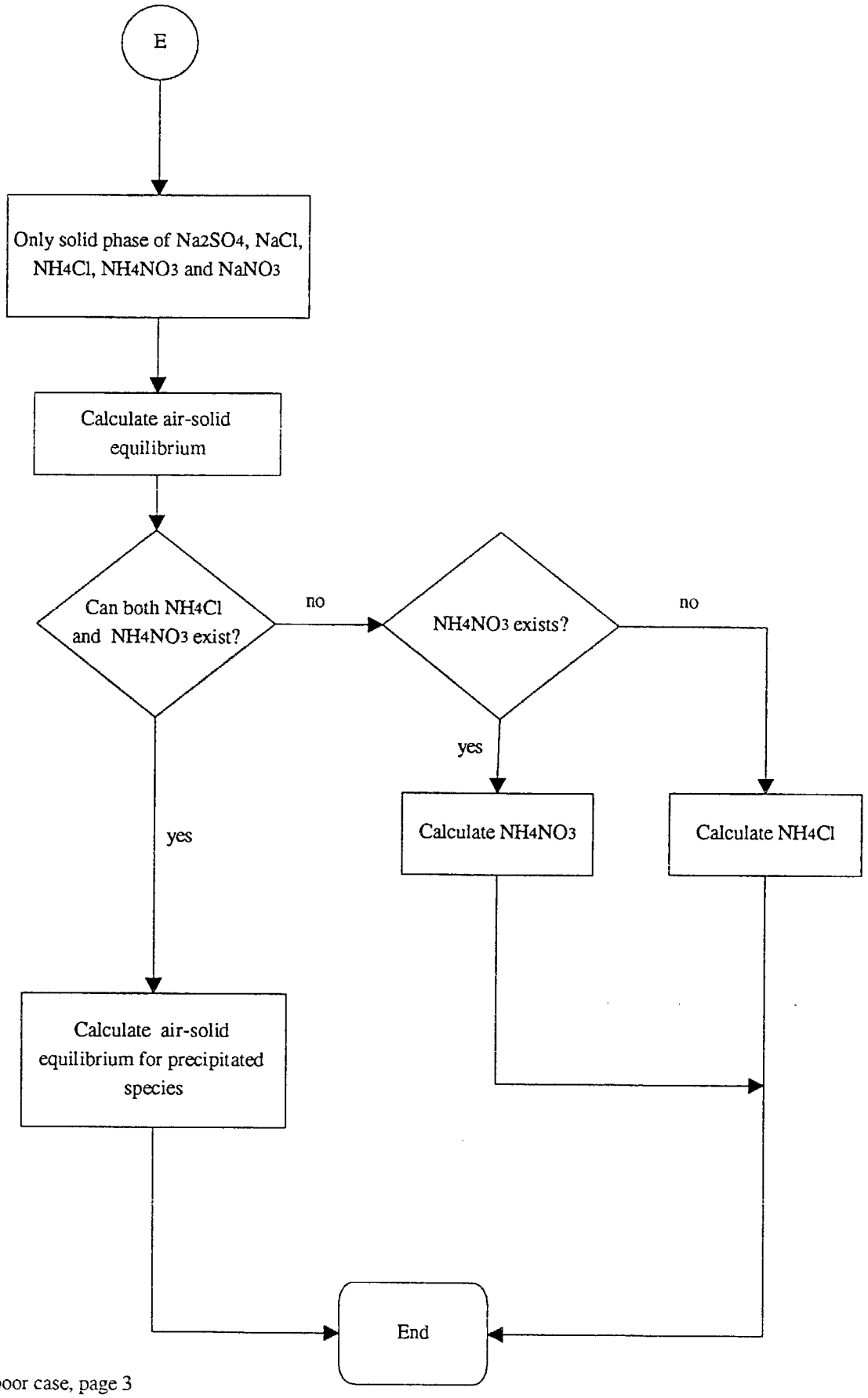

Sulfate poor case, page 3

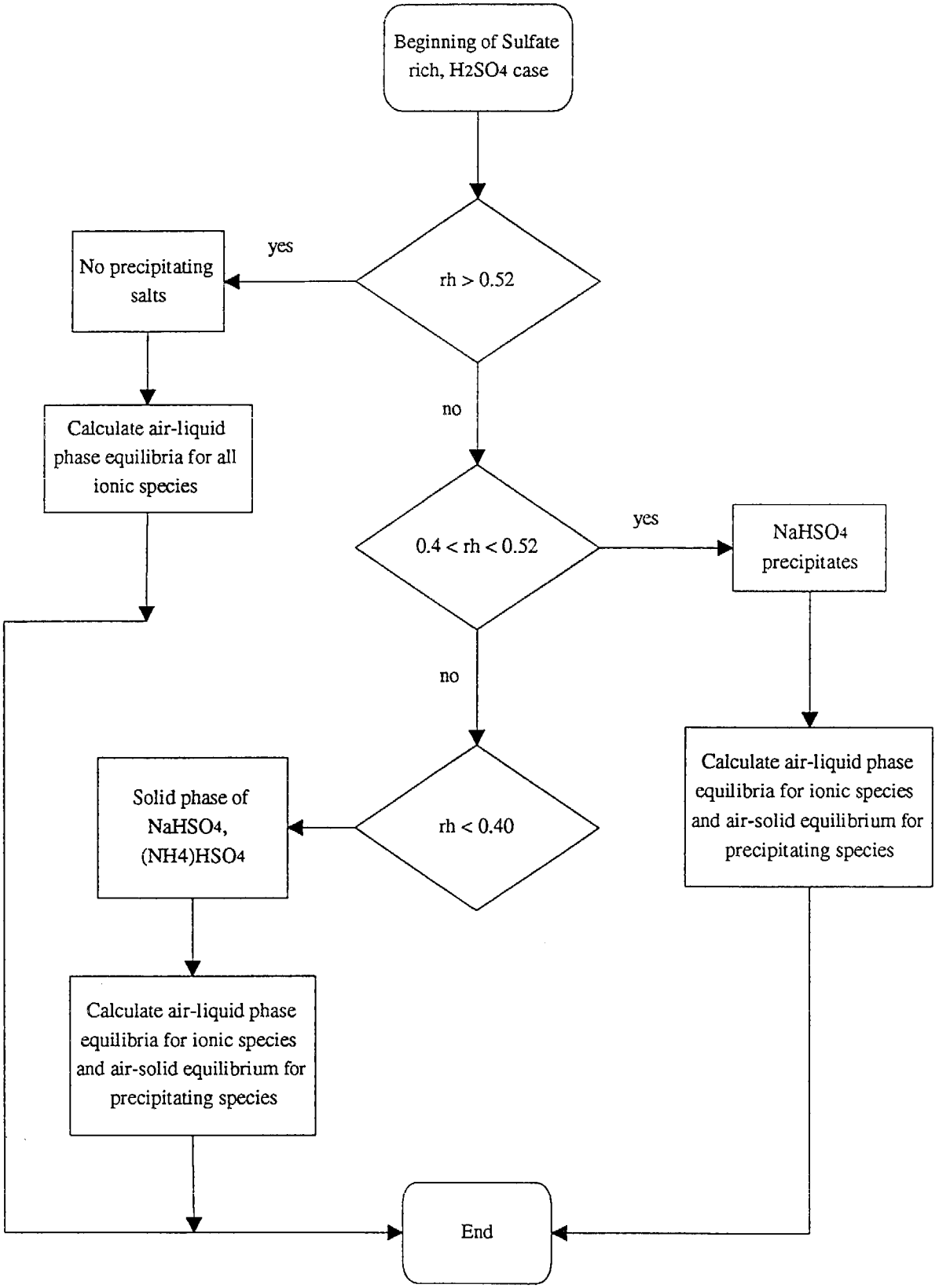

Sulfate rich, H_2SO_4 acidity case

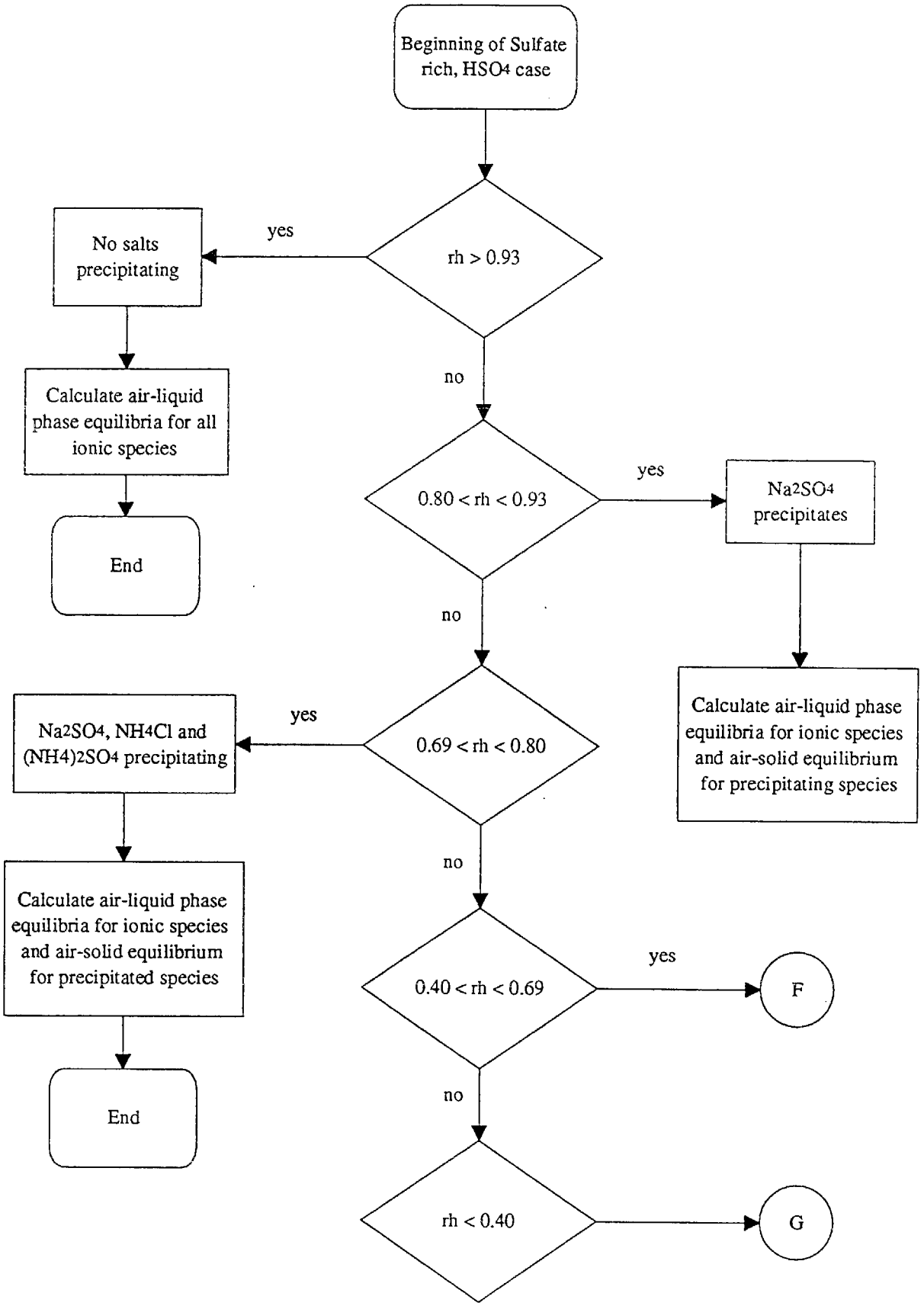

Sulfate rich, HSO4 acidic case, page 1

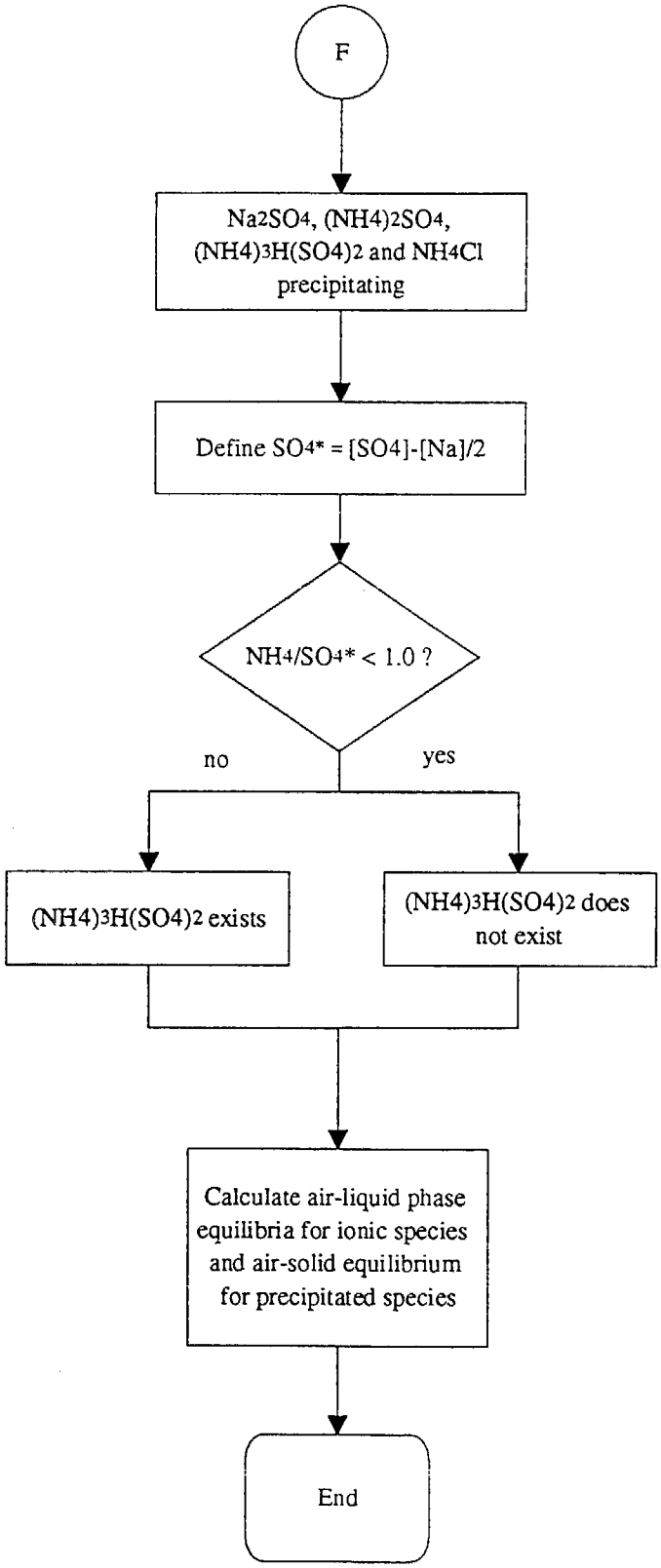

Sulfate rich, HSO_4 acidic case, page 2

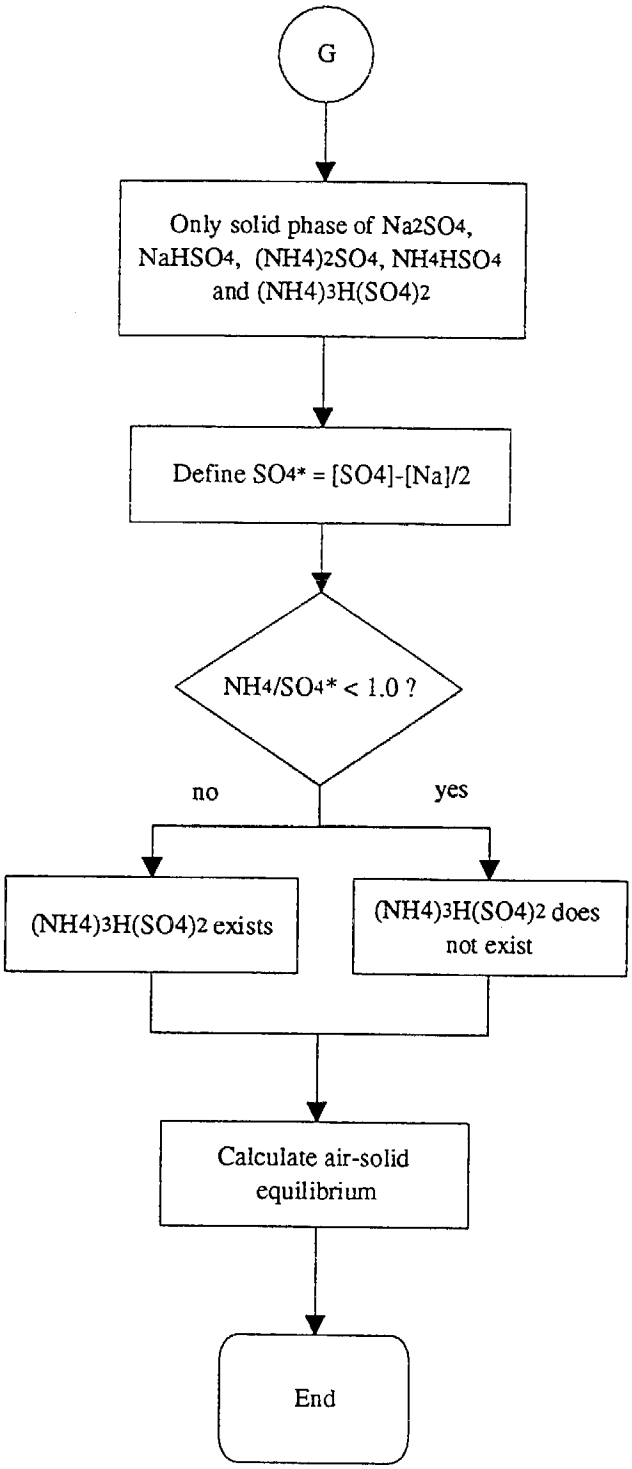

Sulfate rich, HSO4 acidic case, page 3

Appendix F

Modelling Urban and Regional Aerosols - I. Model Development

Wexler, A.S., Lurmann, F.W., and Seinfeld, J.H. (1994) Modelling urban and regional aerosols - I. Model development, *Atmospheric Environment, 28*, 531-546.

Pergamon

Atmospheric Environment Vol. 28, No. 3, pp. 531–546, 1994
Copyright © 1994 Elsevier Science Ltd
Printed in Great Britain. All rights reserved
1352-2310/94 $6.00+0.00

MODELLING URBAN AND REGIONAL AEROSOLS—I. MODEL DEVELOPMENT

ANTHONY S. WEXLER
Department of Mechanical Engineering, University of Delaware, Newark, DE 19716, U.S.A.

FREDRICK W. LURMANN
Sonoma Technology, Inc., Santa Rosa, CA 95403, U.S.A.

and

JOHN H. SEINFELD
Department of Chemical Engineering, California Institute of Technology, Pasadena, CA 91125, U.S.A.

(*First received* 22 *April* 1993 *and in final form* 3 *August* 1993)

Abstract—The partial differential equation that describes the size and composition distribution of atmospheric particles is stated. The equation describes the processes that may influence the particulate size and composition, namely emissions, deposition, advection, turbulent diffusion, condensation, evaporation, coagulation, nucleation, settling and heterogeneous chemical reactions. Each term in the equation is analysed to estimate its influence on the overall distributions under typical urban conditions. Numerical methods are developed to solve the equation in conjunction with an Eulerian gas-phase model.

Key word index: Aerosol model, aerosol size distribution, aerosol composition distribution.

INTRODUCTION

Mathematical models of urban air pollution have been instrumental in identifying source–receptor relationships, and developing optimum emission control strategies for ozone and other gas-phase pollutants (National Research Council, 1991). Particulate pollutants are also ubiquitous in urban areas, but the physical and chemical principles that govern the formation and removal of aerosols are considerably more varied and complex than those determining gas-phase behavior. The first generation of aerosol models assumed thermodynamic equilibrium between the gas and aerosol phases for the volatile compounds to predict the total particulate mass (Russell and Cass, 1986; Bassett *et al.*, 1991) and the particle size and composition distribution (Hogo *et al.*, 1985; Pilinis and Seinfeld, 1988).

Departures from equilibrium between gas and particulate phases for the volatile compounds have been observed by Tanner (1982) near New York City and Allen *et al.* (1989) in England. Recently we showed that equilibrium may not hold in the presence of low aerosol loading, in agreement with these observations. In addition, we showed that even when equilibrium holds, the size distribution of the secondary compounds cannot be predicted by thermodynamic considerations alone; gas–aerosol transport must also be considered (Wexler and Seinfeld, 1990). During the Southern California Air Quality Study (SCAQS), John and co-workers (John *et al.*, 1990, and references therein) measured the size distribution of inorganic compounds, including volatile ammonium nitrate, with an eight-stage impactor. By analysing the size distribution of ammonium and nitrate in these samples we were able to show that departures from equilibrium exist in the South Coast Air Basin (SoCAB) of California, and that these departures are correlated to our predictions (Wexler and Seinfeld, 1992).

The current paper is part one of a two-part series. Our goal in this paper is the development of a size-resolved multicomponent model of urban and regional atmospheric aerosols. The primary assumption in this work is that the aerosol is internally mixed, that is, all the particles of a given size have the same composition. Due to limitations in current instrumentation little information is available about the degree of mixing of aerosol particles. A few investigators (Covert and Heintzenberg, 1984; McMurry and Stolzenburg, 1989) have shown that ambient aerosol particles are not internally mixed with respect to their hygroscopic properties. However, due to lack of further information, it is prudent for the purposes of model development to assume that the aerosol particles are internally mixed. That is, the particle composition is only a function of particle size. In essence, the model attempts to predict impactor-based measurements of particle composition by mixing the particles of a given size. Although we expect a range of compositions for particles of the same size, as of yet the body of available data is not sufficient to support development of a non-internally mixed aerosol model.

Ambient aerosol particles contain water and water-soluble inorganic compounds, elemental carbon, organic compounds and crustal material. The source of NaCl, elemental carbon, crustal material and a portion of the organics is typically direct emission. Most of the ammonium and nitrate, and the remaining organic compounds derive from gas-to-particle conversion processes. The aerosol-phase sulfate is derived from condensation of gas-phase sulfate or from aerosol-phase oxidation of SO_2 in fogs. To develop a model of the particulate concentrations of these compounds, we begin by stating the governing partial differential equation for aerosol compounds. The processes considered are advection, turbulent diffusion, condensation and evaporation, coagulation, nucleation, aerosol-phase chemical reactions, gravitational settling, emissions and deposition. We examine each of these processes to determine when and if each plays a significant role in the alteration of the composition or size of the particles.

The resulting governing equation is used in conjunction with a host gas-phase model to predict both the gas-phase pollutant concentrations and the size and composition of particulate pollutants. Numerical methods are developed for solving the condensation and evaporation terms. The remaining terms are solved using numerical methods available in the host gas-phase model. The result is a model of gas and aerosol processes that can predict both the composition and size distribution of atmospheric aerosols. In part II we use the model in conjunction with the Urban Airshed Model (UAM) (Gery *et al.*, 1989) to predict the size and composition of the aerosol in the SoCAB, and compare these predictions to data from SCAQS.

MULTICOMPONENT INTERNALLY MIXED AEROSOL DYNAMICS

In an Eulerian frame of reference, the particle size and composition distribution is influenced by emission and deposition, condensation and evaporation, advection and diffusion, coagulation, nucleation, gravitational settling, and aerosol-phase chemical reactions. The general dynamic equation that describes the composition of an internally mixed aerosol over time is

$$\begin{aligned}
&\frac{\partial q_i(m,\mathbf{x},t)}{\partial t} \quad \text{(local rate of change)}\\
&+(\mathbf{V}(\mathbf{x},t)-V_s(m)\mathbf{k})\cdot\nabla q_i(m,\mathbf{x},t)\\
&\text{(spatial advection and gravitational settling)}\\
&=H_i(m,\mathbf{x},t)q(m,\mathbf{x},t)-\frac{\partial(mq_iH)}{\partial m} \quad \text{(cond./ evap.)}\\
&+\int_0^m \Gamma(m',m-m',\mathbf{x},t)q_i(m',\mathbf{x},t)\frac{q(m-m',\mathbf{x},t)}{m-m'}\mathrm{d}m'\\
&\text{(coag. in)}\\
&-q_i(m,\mathbf{x},t)\int_0^\infty \Gamma(m',m,\mathbf{x},t)\frac{q(m',\mathbf{x},t)}{m'}\mathrm{d}m'\\
&\text{(coag. out)}\\
&+\nabla\cdot(\mathbf{K}(\mathbf{x},t)\nabla q_i(m,\mathbf{x},t)) \quad \text{(spatial diffusion)}\\
&+E_i(m,\mathbf{x},t) \quad \text{(emissions)}\\
&+R_i(m,\mathbf{x},t) \quad \text{(chemical reaction)}\\
&+N_i(m,\mathbf{x},t) \quad \text{(nucleation)} \qquad (1)
\end{aligned}$$

where $q(m,\mathbf{x},t)$ is the total mass distribution such that $q_i(m,\bar{z},t)\mathrm{d}m$ is the mass concentration of species $i(i=1,\ldots,s)$ in the mass range $[m,m+\mathrm{d}m]$ and $\Sigma_{i=1}^s q_i=q$, m_i is the mass of species i in an individual particle of total mass $m=\Sigma_{i=1}^s m_i$, $H_i=(1/m)\mathrm{d}m_i/\mathrm{d}t$ is the inverse of the characteristic time for particle growth due to condensation or evaporation of species i and $\Sigma_{i=1}^s H_i=H$, $\Gamma(m',m)=\Gamma(m,m')$ is the binary coagulation coefficient, $\mathbf{x}$ is the spatial coordinate vector, t is time, $\mathbf{V}$ is the wind velocity vector, V_s is the settling velocity, $\mathbf{k}$ is the unit vector in the vertical direction, $\mathbf{K}(\mathbf{x},t)$ is the turbulent diffusivity tensor, and E_i, R_i and N_i are, respectively, the emissions, reaction, and nucleation rates of species i in the mass range m to $m+\mathrm{d}m$. Note that the functions $H_i(m)$ and $R_i(m)$ are not explicitly dependent on composition, yet the condensation and reaction terms must depend on particle composition. Since the aerosol is assumed to be internally mixed, the composition is a unique function of size, $q_i=q_i(m)$, and thus the composition dependence of these terms can be evaluated. The condensation, evaporation, and coagulation terms are derived in Pilinis (1990). The spatial advection and diffusion terms are stated in Pilinis and Seinfeld (1988) without proof, and are therefore worthy of discussion.

In equation (1) the spatial advection and diffusion terms transport particle composition in proportion to the mass concentration of each component. Since other formulations based on transport proportional to number concentration or water concentration have been proposed (Carmichael *et al.*, 1986), these terms deserve some discussion. Consider two adjacent parcels of air containing identical number concentrations, or as in Carmichael's model, water concentrations. Diffusion will transport particles from one cell to the other, with no net change in number concentration or water concentration. Now consider what happens if these particles contain other compounds, such as ammonium sulfate, in different concentrations; the number or water concentration will not change due to diffusion, but the composition of the particles does due to the spatial gradient in the ammonium sulfate concentration. Thus models that diffuse aerosol proportional to the number concentration or water concentration will assume zero diffusion, when in reality the diffusion may be quite significant. The issue is somewhat confused by the internally mixed aerosol assumption; unless coagulation occurs, particles of composition A diffusing into a parcel containing par-

ticles of composition B do not alter particle composition in the parcel, but the internally mixed aerosol models report that they do. Nevertheless, diffusion and advection are significant physical processes that must be represented as accurately as possible. The representation chosen here is for diffusion to be proportional to the concentration of each species in mass per unit volume of atmosphere. Thus any gradient, be it in number, mass of water, or mass of another component, results in a diffusional flux.

The primary assumption in the derivation of equation (1) is that the aerosol is internally mixed, that is, all particles of a given size have the same composition. There are a number of reasons for making this assumption. First, there is little experimental data on the external mixing characteristics of atmospheric particles and most of the data address the hygroscopic mixing properties of the particles (Covert and Heintzenberg, 1984; McMurry and Stolzenburg, 1989). Second, to model an internally mixed aerosol requires one independent variable, the size m, to describe the composition. A general multicomponent model requires one independent variable for each aerosol species (Kim and Seinfeld, 1990). This is prohibitive in computer time and memory use for an airshed model—the goal of this work is to develop a practical size-resolved model. Third, the particle emissions data are not sufficiently detailed to warrant a more detailed model. Currently particle emissions data for the SoCAB are reported in only four size sections. One of the sections is larger than 10 μm, so is not relevant to PM_{10} modelling, and the remaining three sections each have uniform composition and only cover the larger particle size range (<1, 1–2.5, 2.5–10 μm).

Equation (1), referred to as the internally mixed aerosol dynamic equation (IMADE), describes the processes that affect the size and composition of aerosol particles in the atmosphere. In subsequent sections we will develop methods for solving for IMADE.

IMPORTANT PHYSICAL PROCESSES: TERM-BY-TERM ANALYSIS OF EQUATION (1)

Given the internally mixed aerosol assumption, equation (1) is a comprehensive statement of the physical and chemical processes that govern the size and composition of atmospheric aerosols. Since the primary goal of this work is to describe the processes that significantly influence the aerosol size and composition in the urban and regional atmosphere, it is important that we examine the IMADE to identify if and when each of the terms may significantly affect the size or composition of aerosols under typical urban and regional conditions. Terms that are not likely to be significant can be eliminated from the IMADE, increasing the computational efficiency of its solution. In this examination we focus our attention on ambient atmospheric processes and exclude the special mixing conditions and higher concentrations that occur in plumes. Current gas-phase models do not typically handle plume chemistry, and since our goal is to produce an aerosol airshed model, we also neglect the special physical and chemical processes that occur in plumes.

Furthermore, we restrict our attention to the lower relative humidity conditions indicative of aerosol particles and do not consider fog or cloud droplets where the physical and chemical processes are substantially different. Significant aerosol transformation takes place in fogs and clouds, so an airshed model that accurately simulates both low and high relative humidity cases must take into account the processes pertinent to the prevailing meteorological conditions in order to accurately predict, for instance, sulfate concentrations. The restriction to lower humidity cases is an effort to do the subject justice in a work of reasonable length, not to diminish the importance of the higher relative humidity conditions. Quantitative comparison of terms is done for conditions prevalent in the SoCAB.

CONDENSATION AND EVAPORATION

Modelling of condensation and evaporation is essential to discerning the impact of gas-to-particle conversion. This term could be eliminated from consideration if circumstances are such that the aerosol is composed mostly of primary species—that is, atmospheric transformation of the primary gaseous emissions does not lead to a significant mass of condensible species compared to the mass of primary aerosol emissions—but under typical inland conditions in the SoCAB, for example, up to 70% of organics (Turpin and Huntzicker, 1991) and 90% of inorganics (Eldering *et al.*, 1991) can be of secondary origin. Thus, the condensation and evaporation term will rarely be insignificant when compared to other terms in the IMADE under virtually any atmospheric condition.

Although condensation of secondary species or evaporation of volatile species certainly affects the aerosol size distribution and composition, not all particle sizes are equally affected. The H_i^{-1} are the characteristic times for the condensation/evaporation processes and when these terms are sufficiently large, they can be safely neglected as the condensation or evaporation process is too slow compared to other processes. H_i can be estimated from mass flux to a single particle (Wexler and Seinfeld, 1990) which gives

$$H_i = \frac{1}{m}\frac{\mathrm{d}m_i}{\mathrm{d}t} = \frac{2\pi D_p D_i}{m}\frac{\Delta C_i}{\frac{2\lambda}{\alpha_i D_p}+1} \tag{2}$$

where $\Delta C_i = C_{\infty,i} - C_{s,i}$ is the difference in concentration of species i between the ambient, $C_{\infty,i}$, and particle surface, $C_{s,i}$, α_i is the accommodation coefficient,

D_p is the particle diameter, D_i is the molecular diffusivity, and λ is the mean free path.

Water transport between the particle and the gas phase is fast compared to the transport of pollutant species, because (1) the vapor-phase concentrations of water are so much higher than that of the pollutant species, and (2) H_i is proportional to these vapor-phase concentrations. As a result, water can be assumed to be in equilibrium between the vapor and condensed phases. Departures from equilibrium have been observed in nephelometers due to a hysteresis between deliquescence and efflorescence (Rood *et al.*, 1987, 1989; Shaw and Rood, 1990), but this has not been observed in the atmosphere.

Assuming equilibrium for water, two sets of cases arise. In the first set, the aerosol is a single aqueous phase. In such cases the water content of the aerosol has been modelled by the ZSR relation (Wexler and Seinfeld, 1991, and references therein)

$$m_w = \sum_i \frac{1000 m_i}{M_i m_{0,i}(r.h.)} \tag{3}$$

where m_i and m_w were defined previously, M_i is the molecular weight of species i, and $m_{0,i}$ is the molality of species i in a single-solute solution with water activity equal to *r.h.* Thus water condensation or evaporation is a result of (a) condensation or evaporation of inorganic species which result in changes to m_i and (b) changes in ambient *r.h.* which result in changes to $m_{0,i}$. Differentiating this expression with respect to time and combining with the definition of H_i gives

$$\begin{aligned} H_w &= \frac{1}{m}\frac{\mathrm{d}m_w}{\mathrm{d}t} \\ &= \frac{1}{m}\frac{\partial m_w}{\partial t} + \frac{1}{m}\frac{\partial r.h.}{\partial t}\frac{\partial m_w}{\partial r.h.} \\ &= \sum_i \frac{1000 H_i}{M_i m_{0,i}(r.h.)} \\ &\quad - \frac{1000}{m}\frac{\partial r.h.}{\partial t}\sum_i \frac{m_i}{M_i m_{0,i}^2(r.h.)}\frac{\partial m_{0,i}(r.h.)}{\partial r.h.}. \end{aligned} \tag{4}$$

The IMADE is an expression for the mass concentration, q_i, but equation (4) is in terms of the single particle mass, m_i. Multiplying both the numerator and denominator of the second term on the right-hand side of equation (4) by the particle number concentration n, and noting that $q = nm$ and $q_i = nm_i$ (Pilinis, 1990) gives

$$\begin{aligned} H_w &= \sum_i \frac{1000 H_i}{M_i m_{0,i}(r.h.)} \\ &\quad - \frac{1000}{q}\frac{\partial r.h.}{\partial t}\sum_i \frac{q_i}{M_i m_{0,i}^2(r.h.)}\frac{\partial m_{0,i}(r.h.)}{\partial r.h.} \end{aligned} \tag{5}$$

which is an expression for the change in water content of an aqueous-phase aerosol due to (1) condensation or evaporation of water-soluble inorganics, and (2) simultaneous changes in ambient *r.h.* This expression is sufficient for calculation of H_w for particles composed of a single aqueous-phase.

In the second set, the particle is a solid or a solid phase of species i in equilibrium with an aqueous phase. Condensation or evaporation of species i results in increases or decreases of the solid-phase mass of species i and no change in the water content of the aerosol. Changes in the ambient relative humidity may or may not change the aerosol mass of water. If the *r.h.* is sufficiently below the deliquescence point of the particle, modest increases in *r.h.* will not result in any appearance of an aqueous-phase in the particle. If the particle is composed of a mixed solid–aqueous phase, increases in *r.h.* cause some or all of the solid phase(s) to dissolve. An implicit assumption in the use of equation (5) is all the particle electrolytes are in the aqueous phase, which is clearly violated here. As a result of these difficulties, the water content changes of aerosols containing a solid phase are calculated in an *ad hoc* manner discussed in the numerical methods section.

Equations (2) and (5) are used to calculate the instantaneous rates of evaporation and condensation of condensible (e.g. H_2SO_4) and volatile (e.g. HNO_3 and H_2O) species. The molecular mean free path, λ, is about 0.065 μm under typical ambient conditions, and the molecular diffusivity is about 0.1 $cm^2 s^{-1}$ for the species of interest here. It should be noted that these equations can be evaluated using meteorological data, and gas- and particulate-phase concentration data.

The surface accommodation coefficient, α_i, is the fraction of condensing molecules that stick upon colliding with the particle surface. In general, the value of α_i depends on the colliding species, and on the surface of the aerosol particle. For collision of the highly soluble organic species considered here, the accommodation coefficient on pure water is typically 0.01 to 0.1 (Van Doren *et al.*, 1991; Van Dingenen and Raes, 1991). If the particle is coated with an organic surface layer, the accommodation coefficient is probably decreased (Gill *et al.*, 1983; Wexler and Seinfeld, 1990). The effects of changes in the accommodation coefficient are twofold. First, if α_i is near unity the condensation is characterized as primarily continuum and is proportional to D_p, whereas if α_i is small the condensation is primarily free molecular and is proportional to D_p^2. Thus the magnitude of α_i affects the size distribution of condensing species. Second, the magnitude of α_i affects the rate at which equilibration between the gas and aerosol phases takes place. Since very little quantitative information is available regarding α_i in the atmosphere, a constant value is assumed for all species and for all particle sizes, and since the maximum α of these compounds on pure water is typically about 0.1 and the minimum α for heavily coated particles is probably about 0.001, we choose the geometric mean, $\alpha_i = 0.01$, for all species and particle sizes.

GRAVITATIONAL SETTLING

Vertical transport of aerosol particles is governed by turbulent diffusion, advection and gravitational settling. It is expected that for the smallest aerosol particles settling will be negligible compared to vertical turbulent diffusion, but for particles sufficiently large it will be significant. In addition, settling of the larger particles may significantly influence their dry deposition. Among previous urban aerosol models, only UAM-AERO (Hogo *et al.*, 1985) considered gravitational settling and for only the two largest particle sizes.

Compared to dry deposition

Gravitational settling substantially influences surface deposition if the settling velocity, V_s, is significant compared to the deposition velocity in the absence of settling, V_d. For particle diameters much greater than the mean free path of air, the settling velocity is given by

$$V_s = \frac{D_p^2 \rho_p g}{18\mu} \tag{6}$$

where D_p is the particle diameter, ρ_p is its density, $g = 9.8\ \mathrm{m\,s^{-2}}$ is the gravitational constant, and μ is the viscosity of air (Seinfeld, 1986). The deposition velocity can be estimated as (Seinfeld, 1986)

$$V_d = \left(\frac{\kappa^2 V(z_1)}{\ln z_1/z_0}\right)\left(\ln\frac{z_1}{z_0} + 2.6\right)^{-1} \tag{7}$$

where $\kappa = 0.4$ is von Karman's constant, $V(z_1)$ is the average wind speed at reference height z_1, and z_0 is the roughness height. We will assume that particle settling may affect deposition when $V_s > V_d/10$, which gives

$$D_p > \sqrt{\left(\frac{1.8\mu}{\rho_p g}\frac{\kappa^2 V(z_1)}{\ln z_1/z_0}\right)\left(\ln\frac{z_1}{z_0} + 2.6\right)^{-1}}. \tag{8}$$

Evaluating this expression for $z_1 \sim 10$ m, $z_0 \sim 2$ m, $V(z_1) \sim 3\ \mathrm{m\,s^{-1}}$, $u \sim 2 \times 10^{-5}\ \mathrm{kg\,m\,s^{-1}}$, and $\rho_p \sim 1000\ \mathrm{kg\,m^{-3}}$, we find that for particle diameters greater than about 10 μm, settling may affect deposition.

Compared to vertical turbulent diffusion

Gravitational settling may also affect the concentration profile due to enhanced vertical transport in the air above the surface, and the effect of settling is expected to be most important for the larger particles. Consider surface emission of coarse particles. If we consider vertical transport terms only, the IMADE reduces to

$$-V_s \frac{\partial q_i}{\partial z} = K_{zz}\frac{\partial^2 q_i}{\partial z^2} \tag{9}$$

whose solution for constant K_{zz} is

$$\left.\frac{\partial q_i}{\partial z}\right|_z = \left.\frac{\partial q_i}{\partial z}\right|_{z=0} \exp\left(-\frac{V_s}{K_{zz}} z\right). \tag{10}$$

The concentration profile that results from solving equations (9) and (10) depends on the specific boundary conditions employed, but in general, exponentially decays with height. The characteristic height, K_{zz}/V_s, determines whether diffusion, settling, or both are important. Specifically, if K_{zz}/V_s is much greater than the height of the lowest computational cell, Δz, the concentration profile can be considered uniform with z and settling can be ignored. Thus we assume that the flux due to gravitational settling can be neglected if the Peclet number, $V_s \Delta z/K_{zz}$, is less than 0.1, which gives

$$D_p < \sqrt{\frac{18\mu}{\rho_p g}\frac{K_{zz}}{10\Delta z}} \sim \sqrt{3.7 \times 10^{-9}\ \mathrm{m\text{-}s}\frac{K_{zz}}{\Delta z}}. \tag{11}$$

Under typical daytime conditions in the SoCAB, the atmosphere below the inversion is unstable and the turbulent diffusivity is greater than about $30\ \mathrm{m^2\,s^{-1}}$. For cell heights of 200 m, equation (11) becomes $D_p < 20\ \mu$m. Thus under unstable atmospheric conditions particles less than about 20 μm are not significantly affected by settling compared to turbulent diffusion. Under nighttime conditions, the atmosphere is stably stratified or neutral with a turbulent diffusivity greater than only $1\ \mathrm{m^2\,s^{-1}}$, so particles less than about 4 μm are not significantly affected by settling.

Thus we find that gravitational settling does not significantly affect particle dry deposition, since those of atmospheric interest are typically less than 10 μm. We also find that under very stably stratified conditions, the concentration distribution of particles between 4 and 10 μm is affected by gravitational settling. In the airshed model and subsequent considerations of atmospheric processing of aerosols, we neglect the effect of settling for a number of reasons. First, the stratification must be extreme to obtain diffusivities as low as $1\ \mathrm{m^2\,s^{-1}}$, and we do not expect these conditions to occur frequently in the SoCAB. Second, typical airshed models use only five cells to simulate vertical concentration gradients so complex vertical profiles are not well represented due to the coarseness of the grid, and associated numerical diffusion and dispersion. Third, only the particles in the 4–10 μm size range are affected, which is relatively narrow considering we are simulating particle sizes that typically span three decades in diameter. As a consequence, gravitational settling is neglected.

COAGULATION

Coagulation is the process whereby two particles collide and combine to form a larger particle. Previous atmospheric aerosol models have included the ability to compute coagulation (e.g. Pilinis and Seinfeld, 1988; Hogo *et al.*, 1985). In this section we evaluate the rate that coagulation alters the size and composition of aerosol particles, and thereby assess

when and if coagulation is a relevant process in the urban or regional atmosphere. Three physical processes may result in coagulation of particles in the atmosphere: Brownian motion, gravitational settling, and turbulent shear. Each of these processes may be enhanced by the van der Waals force.

Brownian coagulation

Particles undergo random motion due to haphazard collisions with surrounding molecules. This random process is called Brownian motion and its relevance to coagulation is that it results in random collisions of particles with each other. In the treatment to follow we assume that all collisions of particles result in coagulation. This serves to overestimate the rate of coagulation, but since the sticking coefficient is not well known for atmospheric particles, a better estimate is not available.

The coagulation coefficient ranges from about $10^{-9}\,\mathrm{cm^3\,s^{-1}}$ for particles of similar size to nearly $10^{-5}\,\mathrm{cm^3\,s^{-1}}$ for 0.01 μm diameter particles coagulating with 10 μm ones (Seinfeld, 1986; p. 396). Coincident with this dramatic change in coagulation coefficient is a commensurate variation in the number of particles with particle size. Therefore we examine coagulation of both similar and dissimilar size particles.

The particles of interest here have a range of diameters from 0.01 to 10 μm, and consequently a range of individual particle masses that spans nine orders of magnitude, so small particles coagulating with large ones will not substantially alter the mass of the large particles, but instead primarily act to reduce the mass and number of small particles. With this in mind, we assess the importance of coagulation of dissimilar particles by identifying and evaluating the time scale for depletion of small particles due to coagulation on large particles.

The coagulation coefficient due to Brownian diffusion is $\Gamma_{bd}=2\pi(D_{pl}+D_{ps})(D_l+D_s)\beta$, where D_{pl} and D_{ps} are the diameters of large and small particles, respectively, D_l and D_s are the diffusivities of large and small particles, respectively, and β is a correction factor that accounts for non-continuum effects when the radius of one or both particles is on the order of, or less than, the mean free path of air molecules in the atmosphere (Seinfeld, 1986).

For coagulation of small particles on large ones $D_{pl}+D_{ps}\sim D_{pl}$ and $D_l+D_s\sim D_s$, so the coagulation coefficient becomes $\Gamma_{bd}=2\pi D_{pl}D_s\beta$. The rate of increase in the mass of a large particle due to coagulation with small particles is then

$$J=2\pi D_{pl}D_s\beta q^s \tag{12}$$

where q^s is the mass concentration of small particles. The rate of depletion of the mass of the small particles due to coagulation with larger particles is the integral of equation (12) over all the larger particles

$$\frac{\mathrm{d}q^s}{\mathrm{d}t}=-2\pi D_s q^s\int\beta D_{pl}n(D_{pl})\mathrm{d}D_{pl}. \tag{13}$$

We can now define the time scale for depletion of the mass of small particles due to Brownian coagulation, τ_{bd}, as

$$\tau_{bd}=\left|\frac{1}{q^s}\frac{\mathrm{d}q^s}{\mathrm{d}t}\right|^{-1}=\left|-2\pi D_s\int\beta D_{pl}n(D_{pl})\mathrm{d}D_{pl}\right|^{-1} \tag{14}$$

which has a similar form as the time scale for condensation (Wexler and Seinfeld, 1990, 1992) and is independent of q^s.

To estimate the size of τ_{bd}, let us assume that the coagulation properties of the aerosol in the large-particle size range can be approximated by an equivalent monodisperse aerosol, so that

$$\tau_{bd}=[2\pi D_s\hat{\beta}\hat{D}_{pl}\hat{n}]^{-1} \tag{15}$$

where $\hat{D}_{pl}$ and $\hat{n}$ are the equivalent monodisperse diameter and number of the large particles, respectively, and $\hat{\beta}$ is the equivalent non-continuum correction. Using the large-particle mass loading, $\hat{m}_p=(\pi/6)\times\rho_p\hat{n}\hat{D}_{pl}^3$, to eliminate the number of large particles one obtains

$$\tau_{bd}=\frac{\hat{D}_{pl}^2\rho_p}{12D_s\hat{\beta}\hat{m}_p}. \tag{16}$$

Typical SoCAB aerosol size distributions exhibit two large particle modes — one in the 1–10 μm range and another in the 0.1–1 μm range—of similar mass loadings. Considering that the time constant in equation (16) depends on the square of the large-particle diameter, the 0.1–1 μm mode will preferentially scavenge the small particles. Evaluating equation (16) with $D_{pl}=0.3$ μm, the geometric mean diameter of the large particles, $\rho_p=1\,\mathrm{g\,cm^{-3}}$, the minimum density, $D_s=5\times10^{-4}\,\mathrm{cm^2\,s^{-1}}$, the diffusivity of 0.01 μm particles, $\hat{\beta}=0.65$, the non-continuum correction for coagulation of 0.01 μm particles on 0.3 μm ones, and $\hat{m}_p=50\,\mu\mathrm{g\,m^{-3}}$ (Wexler *et al.*, 1992), a high mass loading in this size range for the SoCAB, we obtain a value of τ_{bd} over 1 h. Coagulation of 0.01 μm particles on particles in the 1–10 μm range would take significantly longer.

Coagulation of similar sized particles may also alter the size distribution of particles. The time constant for self-coagulation of a monodisperse size distribution is $\tau_{sc}=2/\Gamma_{bd}\hat{n}$ (Seinfeld, 1986; p. 413), which can be written in terms of the particle mass loading as $\tau_{sc}=\pi\hat{D}_p^3\rho_p/3\Gamma_{bd}\hat{m}_p$. For self-coagulation, the coagulation coefficient is relatively independent of particle size and equal to $10^{-9}\,\mathrm{cm^3\,s^{-1}}$. Evaluating for $\hat{m}_p=10\,\mu\mathrm{g\,m^{-3}}$ and 0.1 μm gives $\tau_{sc}>1$ d. For 1–10 μm particles with mass loadings on the order of 100 $\mu\mathrm{g\,m^{-3}}$, τ_{sc} is much longer since the time constant increases as the cube of diameter and is only inversely proportional to mass

loading. Particles on the order of 0.01 μm may have significant coagulation. If the mass loading of these particles is greater than 0.25 $\mu g\,m^{-3}$, the time constant is less than 1 h.

Van der Waals forces enhance coagulation beyond that predicted by the above analyses, but for the smallest particles ($\sim$0.01 μm) this effect provides at most a factor of two, and for particles greater than 0.1 μm, the enhancement is less than 10% (Marlow, 1981). In opposition, particle bounce will tend to reduce the coagulation rate by some unknown quantity. Since (1) the characteristic time for coagulation due to Brownian motion is most certainly greater than 1 h, (2) a high mass loading and low density were assumed, and (3) other processes such as emissions and turbulent diffusion are expected to alter the small particle mass loading on shorter time scales, we deduce that coagulation is not a significant aerosol process under all but the most extreme conditions.

Gravitational settling and turbulent shear

Particles fall due to gravitational settling, and since the settling velocity is dependent on the particle size, particles of disparate size may collide and coagulate. The coagulation coefficient due to gravitational settling is approximately the relative area swept out by the settling particles, $\Gamma_{gs}=(\pi/4)D_{pl}^2(V_l-V_s)$ (Seinfeld, 1986; p. 400), where V_l and V_s are the settling velocities of the larger and smaller particles, respectively. Using a similar argument as employed for Brownian diffusion, we find that the time constant for coagulation due to settling is $\tau_{gs}=\frac{2}{3}2\hat{D}_{pl}\rho_p/3\hat{V}_l\hat{m}_p$. Evaluating τ_{gs} with a reasonable minimum for $\hat{D}_{pl}(\sim 0.1\ \mu m)$ and reasonable maximums for $\hat{V}_l(\sim 0.003\ m\,s^{-1})$ and $\hat{m}_p(\sim 50\ \mu g\,m^{-3})$ gives a τ_{gs} of many days and thus this process can be neglected.

The coagulation coefficient due to turbulent shear is $\Gamma_{ts}=\pi\sqrt{\varepsilon_k/120\nu}\ (D_{p1}+D_{p2})^3$, where $\sqrt{\varepsilon_k/\nu}$ is the characteristic turbulent shear rate at the length scales relevant to particle coagulation (Seinfeld, 1986; p. 400). In contrast to Brownian diffusion and gravitational settling, coagulation due to turbulent shear is greatest when both particles are as large as possible. If D_{p1} is equal to D_{p2}, the coagulation coefficient is $\Gamma_{ts}=8\pi\sqrt{\varepsilon_k/120\nu}\,D_p^3$. Employing the same substitutions as with Brownian and gravitational coagulation, the time scale for turbulent shear is $\tau_{ts}=\rho_p/(48\hat{m}_p\sqrt{\varepsilon_k/120\nu})$ which when evaluated for a typical shear rate of $\sqrt{\varepsilon_k/\nu}=10\ s^{-1}$ (Seinfeld, 1986; p. 400) and the maximum reasonable mass loading gives $\tau>2\times10^8$ s, or several years. We can conclude that turbulent shear does not cause coagulation. Thus, Brownian diffusion is the dominant coagulating process, but it operates so slowly that it can be neglected. Thus in the current model, coagulation will not be included.

NUCLEATION

For homogeneous nucleation to occur at a significant rate the partial pressure of the nucleating species must be sufficiently high to exceed its saturation vapor pressure. Below the so-called critical saturation ratio, nucleation does not occur to any significant extent, whereas above this ratio the rate may be substantial. It is believed that significant nucleation may occur both in concentrated sources (e.g. Hildemann *et al.*, 1989) and in the clean troposphere (Shaw, 1989). In this section we will identify ambient conditions in the SoCAB where nucleation may occur and estimate the effect of these nucleii on the composition and size distribution of aerosol compounds.

Gas-phase compounds such as sulfuric acid or condensible organics that form in the atmosphere may be removed by condensation on pre-existing aerosols, deposition to the surface, or formation of new particles via nucleation. The ambient concentration is shaped by a competitive process between formation and removal. The concentration, C_i, of a condensible compound in a parcel of air in contact with the surface is

$$\frac{dC_i}{dt}=P_i-T_{a,i}C_i-\frac{V_d}{L}C_i \tag{17}$$

where P_i is the production rate of i, $T_{a,i}$ is the rate of transport between the gas- and aerosol-phases of i, L is the ratio of the volume of the parcel to its deposition surface area, which will be taken equal to the inversion height, and V_d is the deposition velocity.

The production rate P_i is dependent on the gas-phase concentration of precursor species (such as SO_2 for H_2SO_4 production) and their chemical transformation rates. The aerosol transport rate is given by

$$T_{a,i}=\int_0^\infty \frac{2\pi n D_p D_i dD_p}{\frac{2\lambda}{\alpha_i D_p}+1} \tag{18}$$

which is the inverse of the characteristic time for transport between the gas and aerosol phases (Wexler and Seinfeld, 1922). The deposition velocity is examined later in this work when boundary conditions are discussed.

As an estimate of the gas-phase concentration of gas-phase precursors to nucleation, we can set the time derivative term in equation (17) to zero to obtain a steady state estimate of the ambient concentrations, $C_{ss,i}$

$$C_{ss,i}=\frac{P}{T_{a,i}+V_d/L} \tag{19}$$

Let us consider sulfuric acid nucleation and use equation (19) to estimate the gas-phase concentration of H_2SO_4(g), assuming nucleation is absent. Other nucleation paths such as via ammonia may be important (Kiang *et al.*, 1975), but will not be considered here. In the urban environment, gas-phase oxidation

of sulfur dioxide to sulfuric acid may occur over a number of pathways, but the accepted range is 0.5–2% h^{-1} (Seinfeld, 1986). Although higher oxidation rates have been observed in fogs and clouds, sulfuric acid formed in the aqueous phase will not lead to homogeneous nucleation. The current model does not handle plumes, so the higher oxidation rates observed in these situations are not considered here.

During SCAQS ambient levels of SO_2 were measured at nine sites during eight episodes. SO_2 concentrations typically range from 1 to 10 $\mu g\,m^{-3}$, except in Long Beach where levels were often over 15 and reached 30 $\mu g\,m^{-3}$ (Hering, 1990). Taking a typical oxidation rate of 1% h^{-1}, we find that the production rate is typically 0.01–0.1 $\mu g\,m^{-3}\,h^{-1}$, but can reach about 0.3 $\mu g\,m^{-3}\,h^{-1}$ at Long Beach.

In previous work we examined the likely range of the time constant $T_{a,i}^{-1}$, which in that work we termed τ_∞ (Wexler and Seinfeld, 1990). It was found to vary from a few seconds for heavily polluted inland conditions, where a large aerosol loading presented ample opportunity for condensation, to more than a day for less polluted conditions typical of coastal areas of the SoCAB. Long Beach is relatively close to the coast and would be expected to have a time constant, τ_∞, on the order of an hour.

The deposition time constant is L/V_d. The inversion height, L, is of the order of 1000 m or 10^5 cm. Although the deposition velocity has not been measured for H_2SO_4(g), that for SO_2(g) can be taken as a lower bound. Sehmel (1980) reviewed the literature on SO_2(g) deposition rates and found a range of 0.1–10 cm s^{-1}. Taking the rate for H_2SO_4(g) as 10 cm s^{-1}, the deposition time constant is about 10^4 s, or about 3 h. Thus, in lightly polluted areas where the ambient time constant is of the order of 1 h, deposition to the surface and deposition to existing aerosols are competing processes that operate over similar time scales. For areas with a higher aerosol loading, the aerosol time constant is shorter and deposition to the surface can be ignored. Note that an important assumption in this analysis is that the condensing species, H_2SO_4(g), is accommodated well on both the existing aerosol particles and the surface. This is probably a reasonable assumption for this compound, but may not be reasonable for others.

Evaluating equation (19) gives $C_{ss,H_2SO_4} \sim 0.3$ $\mu g\,m^{-3} \sim 2 \times 10^9$ molecules cm^{-3} for Long Beach. Jaecker-Voirol and Mirabel (1989) calculate the heteromolecular nucleation rate for sulfuric acid and water under typical atmospheric conditions. For an ambient H_2SO_4(g) concentration of 2×10^9 molecules cm^{-3} and an ambient temperature of 298 K, significant nucleation can occur for relative humidities greater than 60%, whereas at 273 K nucleation is always significant. SO_2 concentrations of 30 $\mu g\,m^{-3}$ were only observed occasionally during SCAQS, and the aerosol condensation time constant may be significantly shorter than 1 h, both factors serving to decrease the predicted H_2SO_4(g) concentration proportionally. For ambient H_2SO_4(g) concentrations one order of magnitude lower, significant nucleation does not occur at 298 K and occurs only above 40% *r.h.* at 273 K. Note that at lower ambient temperatures the oxidation rate of SO_2(g) is observed to be lower (Seinfeld, 1986), and at higher relative humidities aerosol scavenging and aqueous-phase oxidation of H_2SO_4(g) may significantly deplete the SO_2(g) concentration, both factors again serving to decrease the nucleation rate. Furthermore, temperatures of 273 K do not frequently occur in the SoCAB.

It appears that nucleation may form new particles under conditions of low aerosol loading, and high ambient SO_2(g) concentrations. Do these nucleii significantly effect the ambient size and composition distribution of aerosol particles? One way to address this question is to estimate the possible fate of such particles between the time of nucleation and when their size is significant. Hamill (1975) has estimated the rate of growth of freshly nucleated H_2SO_4–H_2O aerosol particles of atmospheric relevance. Using Hamill's work with a concentration of 2×10^9 molecules cm^{-3} and 80% *r.h.*, we estimate that freshly nucleated particles will grow to 0.01 μm in about 400 s. This growth time scale is an order of magnitude faster than the condensation or deposition time scales, so we conclude that the nucleii will not be substantially removed from the atmosphere before they grow to significant size. If the H_2SO_4(g) concentration is reduced due to the nucleation process, the growth time scale may be somewhat longer.

In contrast, the coagulation time scale for nucleii can be thought of in terms of the condensation time scale. Nucleii coagulating on larger particles may be considered analogous to condensation, where the diffusivity of the nucleii must be used instead of the molecular diffusivity. The coagulation time scale derived previously is valid here, but must be evaluated under the current conditions: small particles, and a long condensation time scale. Since the condensation time scale is inversely proportional to the diffusivity, and the diffusivity is inversely proportional to the square of the diameter of the nucleii, the time scale for coagulation of nucleii on large particles is about $\tau_\infty (D_p/d)^2$, where d is the diameter of typcial condensing molecules, and D_p is the diameter of coagulating nucleii. Since the nucleii are at least an order of magnitude larger than typical molecules, their coagulation time scale is long indeed and is expected to remove an insignificant number of nucleii.

Thus we find that under specific conditions, nucleation may produce H_2SO_4–H_2O nucleii that rapidly grow to a size where they may affect the composition and size distribution of the aerosol. In a subsequent section we discuss how nucleation is modelled.

CHEMICAL REACTION

There are few data on the rate or occurrence of chemical reactions in or on aerosol particles in the

atmosphere. The two reactions that will be considered here are oxidation of SO_2 to sulfuric acid and reaction of N_2O_5 with particulate water to form nitric acid. In fog and cloud droplets, S(IV) compounds are oxidized to S(VI) compounds, but the rate of this reaction is limited by the water available in the aerosol phase. Depending on the *r.h.* and electrolyte content of the aerosol, the liquid water content may range from 0 to 100 $\mu g\,m^{-3}$. The liquid water content of fogs is about 100–1000 $mg\,m^{-3}$, or at least 1000–times greater than that of aerosols. At low liquid water contents we can consider the SO_2 oxidation rate to be limited by the available liquid water, so that the aerosol oxidation rate is at least three orders of magnitude less than the aqueous-phase oxidation rate (Pandis *et al.*, 1992).

This argument, although rough, can be bolstered for the SoCAB as follows. Under coastal conditions, the ambient air is cool and relatively humid, but the aerosol loading is small. Due to the low aerosol loading, the time scale for mass transfer of SO_2(g) from the gas to particle phase is long (Wexler and Seinfeld, 1990) which limits any heterogeneous oxidation that may occur. As the air mass is advected inland, the aerosol loading increases due to emissions, but the temperature increases resulting in a reduced relative humidity, and a concomitant reduction in the liquid water content of the aerosol. At inland conditions sufficient surface area for rapid mass transfer of SO_2(g) to the particle phase is present, but there is insufficient liquid water to dissolve significant quantities of SO_2.

The scenario just outlined applies to the usual conditions in the summer in southern California, but other conditions more conducive to aerosol oxidation of SO_2(g) may occur, especially in the winter and at night. These conditions are usually associated with fogs, which are not treated in the current model.

A number of investigators have modelled reaction of N_2O_5 with particulate water to form nitric acid (e.g. Russell *et al.*, 1985; Li *et al.*, 1993) and found that the heterogeneous pathways may be significant compared to the homogeneous ones. The upper limit of the rate constant for the homogeneous reaction $N_2O_5 + H_2O \rightarrow 2HNO_3$ is estimated to be $k = 1.9 \times 10^{-6}\,ppm^{-1}\,min^{-1}$ (Tuazon *et al.*, 1983; Atkinson *et al.*, 1986) The atmospheric concentration of H_2O depends on the relative humidity and temperature, but is generally in the range of 4×10^3–4×10^4 ppm. Using the upper limit for the rate constant and water concentration gives a minimum characteristic time for conversion of N_2O_5 to HNO_3 by homogeneous pathways of 13 min. If the rate constant or water concentration are lower, the time constant will be correspondingly higher.

Competing with the homogeneous reaction is gas-to-particle conversion of N_2O_5 and subsequent reaction with H_2O(l) to form particulate phase HNO_3. If we assume that N_2O_5 is rapidly converted to HNO_3 at the droplet surface, the surface partial pressure of N_2O_5 is negligible and the characteristic time for condensation is T_a^{-1} given by equation (17). In previous work we have examined the size of this characteristic time and found it to vary from a few seconds to more than a day for conditions in the SoCAB depending on aerosol size and mass loading. N_2O_5 forms from reaction of NO_2 with NO_3. Since the nitrate radical is rapidly photolysed, NO_3 exists only in substantial concentrations at night. Also, NO emissions at night reduce O_3 below the inversion, which severely limits the amount of NO_3 that may be formed near the surface (Russell *et al.*, 1985). Thus N_2O_5 is expected to form at night and aloft, where the aerosol loadings are expected to be lower than near the surface. These lower loadings result in a longer characteristic time for condensation, which limits the heterogeneous reaction rate. Although this argument is qualitative, it indicates that homogeneous formation of HNO_3 from N_2O_5 and H_2O is likely to be more important than the heterogeneous process as has been shown via simulation by others (Russell *et al.*, 1985; Li *et al.*, 1993). Since the heterogenous formation rates of both sulfuric and nitric acid seem low compared to competing homogeneous rates, they are not considered in this model.

BOUNDARY AND INITIAL CONDITIONS

In the previous sections we showed that gravitational settling, coagulation, and aerosol-phase chemical reactions can be neglected under conditions typical of the SoCAB. These simplifications reduce the IMADE to

$$\begin{aligned}
&\frac{\partial q_i(m,\mathbf{x},t)}{\partial t} \quad \text{(local rate of change)}\\
&+\mathbf{V}(\mathbf{x},t)\cdot\nabla q_i(m,\mathbf{x},t) \quad \text{(spatial advection)}\\
&=H_i(m,\mathbf{x},t)q(m,\mathbf{x},t)-\frac{\partial(mq_iH)}{\partial m} \quad \text{(cond./evap.)}\\
&+\nabla\cdot(\mathbf{K}(\mathbf{x},t)\nabla q_i(m,\mathbf{x},t)) \quad \text{(spatial diffusion)}\\
&+E_i(m,\mathbf{x},t) \quad \text{(emissions)}\\
&+N_i(m,\mathbf{x},t) \quad \text{(nucleation).}
\end{aligned} \tag{20}$$

This is a partial differential equation for the s aerosol species in one temporal, three spatial, and one size coordinate. The initial aerosol concentrations are generally derived from observational data. In the vertical coordinate, the boundary conditions specify no diffusion of species through the inversion and dry deposition at the surface. In the horizontal directions, the boundary conditions typically specify background species concentrations; the boundaries must be drawn sufficiently far from the region of interest that backwash flows do not leave the modelling region. These boundary conditions are the same as those used to model gas-phase species, except that the deposition of aerosol species is dependent on the size of the aerosol particles.

Earlier in this work, we estimated the deposition velocity to assess its magnitude relative to that of gravitational settling. Here we describe the more complete formulation for dry deposition used in the model. The boundary conditions for aerosol particle deposition specify the flux at the surface, F

$$F_i(m)=K_{zz}(\mathbf{x}_1)\left(\frac{\partial q_i}{\partial z}\right)_{x=x_1}=V_d q_i(m,\mathbf{x}_1,t) \quad (21)$$

where K_{zz} is the turbulent diffusivity, $\mathbf{x}_1=(x,y,z_1)$ is an arbitrary position above the surface and V_d is the deposition velocity. For particles the deposition velocity is given by

$$V_d=(r_a+r_s+r_a r_s V_s)^{-1}+V_s \quad (22)$$

where r_a is the atmospheric resistance and r_s is the surface layer resistance (Slinn and Slinn, 1980; Pleim *et al.*, 1984). The atmospheric resistance is given by

$$r_a=(\kappa u_*)^{-1}[\ln(z_1/z_0)+\phi_H] \quad (23)$$

where $\kappa=0.4$ is von Karman's constant, u_* is the friction velocity, z_0 is the roughness height, and ϕ_H is the stability correction factor (Wesely and Hicks, 1977). The surface resistance is given by

$$r_s=(Sc^{-2/3}+10^{-3/St})^{-1} \quad (24)$$

where $St=(V_s/g)(u_*^2/\nu)$ is the Stokes number of the particle, $Sc=\nu/D$ is the Schmidt number, g is the gravitational acceleration, ν is the viscosity of air, and D is the particle diffusivity (Pleim *et al.*, 1984). These formulae for aerosol deposition are employed in the model to estimate surface removal of aerosol compounds.

The remaining boundary conditions are concerned with the aerosol size distribution. During the course of growth and evaporation, aerosol particles become substantially altered in size. A size range must be chosen that sufficiently extends beyond the particle sizes of interest so that these growth and shrinkage processes are adequately modelled. This is analogous to choosing a spatial domain sufficiently beyond the domain of primary concern, so that backwash flows may be taken into account. Unfortunately, this requirement can substantially increase the computational burden of the aerosol module.

Let us first consider the smallest particle size boundary, and label its diameter $D_{p,\min}$. Since particles smaller than $D_{p,\min}$ are not considered in the model, no particles can grow to this size. There are three sources for these particles; they may be emitted, homogeneous nucleation and subsequent growth may introduce new H_2SO_4–H_2O particles, and particles may evaporate water or volatile pollutants and shrink to this size. Freshly nucleated particles that have grown to $D_{p,\min}$ are treated similar to emissions of $D_{p,\min}$ particles; both are introduced into the smallest particle size section.

If $D_{p,\min}$ particles shrink, we reduce the particle mass in the $D_{p,\min}$ particle size, but do not move the particles in size space. When H is negative, we retain the $H_i q$ term in the IMADE, but set the $\partial m q_i H/\partial m$ term to zero for the smallest section. In effect, this formulation conserves mass when particles would shrink out of the domain by artificially coagulating particles so the single-particle mass does not fall below $D_{p,\min}$. Most ambient aerosol size distributions show extremely small mass in the small-particle size range, so this boundary condition should not adversely bias the predicted size distributions.

The $D_{p,\max}$ boundary is analogous to the one at $D_{p,\min}$. Particles greater than $D_{p,\max}$ are not considered in the model, so particles cannot shrink to this size. Particles are added to the largest size bin by growth or direct emission. There are two reasonable options for particles that grow out of the largest size bin. First, these particles can be considered to have deposited to the surface, or settled into the next lower spatial cell, since gravitational settling becomes more significant for larger particles. Or second, these particles can be kept in the largest size bin, analogous to what was done for shrinkage of the smallest particles. Although there may be substantial mass in the largest particles, due to gravitational settling their lifetime in the atmosphere is short. In order to isolate deposition in the spatial boundary conditions, and vertical transport in the diffusion operator, we have chosen the second approach: the particle mass that grows out of the modelling domain is retained in the largest size bin. This in effect splits large particles into smaller ones so they do not become greater than $D_{p,\max}$. Once again this process may be simulated by setting the $\partial m q_i H/\partial m$ term to zero for the largest particles when H is positive.

NUMERICAL SOLUTION OF IMADE

From the above analyses we conclude that spatial advection and turbulent diffusion, condensation and evaporation, emission and deposition, and nucleation affect the composition and size distribution of ambient urban aerosol particles. In this section we discuss the numerical methods employed for solving the IMADE as given in equation (20).

Most atmospheric aerosol data are given in terms of the logarithm of the size coordinate, D_p, so we would like the IMADE to predict size-resolved composition based on the logarithm of D_p instead of particle mass, m. Defining $\mu=\ln(D_p/D_{p0})$ as the new size coordinate, where D_{p0} is a reference particle diameter, we can convert the m-based composition, q_i, to a μ-based composition, p_i via $q_i \mathrm{d}m=p_i \mathrm{d}\mu$. The mass of species i in the particle mass range m to $m+\mathrm{d}m$ is $q_i \mathrm{d}m$, and is equal to the mass of species i in the log diameter size range μ to $\mu+\mathrm{d}\mu$, that is $p_i \mathrm{d}\mu$. Rearranging yields $q_i=p_i(\mathrm{d}\mu/\mathrm{d}m)$. If we assume the particles are spherical with density ρ_p and diameter D_p, then $m=(\pi/6)\rho_p D_p^3$, so we obtain

$$q_i=\frac{2p_i}{\pi\rho_p D_p^3}=\frac{p_i}{3m} \quad (25)$$

which when substituted into equation (20) yields

$$\begin{aligned}
&\frac{\partial p_i(\mu,\mathbf{x},t)}{\partial t} \quad \text{(local rate of change)}\\
&+\mathbf{V}(\mathbf{x},t)\cdot\nabla p_i(\mu,\mathbf{x},t) \quad \text{(spatial advection)}\\
&=H_i(\mu,\mathbf{x},t)p(\mu,\mathbf{x},t)-\frac{1}{3}\frac{\partial H p_i(\mu,\mathbf{x},t)}{\partial\mu} \quad \text{(cond./evap.)}\\
&+\nabla\cdot(\mathbf{K}(\mathbf{x},t)\nabla p_i(\mu,\mathbf{x},t)) \quad \text{(spatial diffusion)}\\
&+E_i(\mu,\mathbf{x},t) \quad \text{(emissions)}\\
&+N_i(\mu,\mathbf{x},t) \quad \text{(nucleation)} \qquad (26)
\end{aligned}$$

where $p=\Sigma_i^s p_i$. In this section we describe how each of the terms in equation (26) is solved in a three-dimensional airshed model.

OPERATOR SPLITTING

Equation (26) shares many features with equations that govern the transport and transformation of the gas-phase species. Advection and turbulent diffusion of aerosol compounds are identical to advection and turbulent diffusion of gas-phase species. Since the secondary aerosol species are formed by gas-phase processes, the solution to equation (26) must take place in conjunction with the solution to a similar equation that describes the dynamics of the gas-phase species, and therefore we solve equation (26) within a host gas-phase airshed model. Gas-phase reactions form condensible organic and inorganic compounds. When the concentration of these compounds exceeds their vapor pressure they are condensed on the existing aerosol particles, or possibly nucleate to form new aerosol particles.

In all current three-dimensional airshed models, operator splitting is used; that is, one or more physical or chemical processes are solved separately from the remaining processes (McRae *et al.*, 1982). Thus, where gas-phase and aerosol-phase processes are identical, such as with turbulent diffusion, the same operator can be used on both aerosol-phase and gas-phase components. To integrate the aerosol-specific processes into a pre-existing airshed model, additional operators are employed that solve the terms unique to the aerosol dynamics.

LARGE-SCALE TRANSPORT TERMS

The large-scale transport terms, advection and turbulent diffusion, have the same form for gas and aerosol transport. Thus it is logical to use the gas-phase operators to solve these terms in equation (26), but such a choice has implications for solving the other terms. If the transport operator in UAM diffuses aerosol composition between adjacent cells, the size coordinate, μ, must have the same discretization in all cells. This places a constraint on the numerical methods that can be employed to solve other terms in equation (26). For instance, the moving section methods that have been successfully employed to calculate the condensation and evaporation terms cannot be used if the size bins cannot change with time (unless renormalizations are employed at the end of each integration step) (Gelbard, 1990; Kim and Seinfeld, 1990). Since fixed-section numerical methods are available for solving the condensation/evaporation term, we have chosen to use a fixed discretization of μ and solve the large-scale aerosol transport terms in the gas-phase operators.

NUCLEATION

In the model, ambient SO_2(g) is oxidized by reaction with OH radical to H_2SO_4(g) (Calvert *et al.*, 1985). As discussed above, under certain atmospheric conditions such as those that occur near the coast in the SoCAB, specifically low aerosol loading, cooler temperatures, and higher relative humidities, this H_2SO_4(g) may nucleate with H_2O(g) to form new particles. These particles are estimated to grow to 0.01 μm in a few minutes under the conditions when nucleation is favored (Hamill, 1975). Since we are not explicitly modelling particles below about 0.01 μm, we approach nucleation in the following *ad hoc* manner. For a given atmospheric temperature and pressure, we first calculate the H_2SO_4(g) concentration that results in the formation of one nucleus per cm^3 per second at the given ambient temperature and relative humidity. To do this efficiently, we fit the nucleation rates calculated by Jaeckel-Voirol and Mirabel (1989) and obtain the empirical relation

$$C_{\text{crit.}H_2SO_4}=0.16\exp(0.1T-3.5\,r.h.-27.7) \qquad (27)$$

where the temperature, T, is in Kelvin, the relative humidity scale 0–1 is used, and $C_{\text{crit.}H_2SO_4}$ is the critical concentration in $\mu g\,m^{-3}$. If the ambient H_2SO_4(g) concentration exceeds this value, the amount of excess is removed from the gas phase and placed in the smallest aerosol size section. In effect, this algorithm specifies that nucleation will prohibit the H_2SO_4(g) concentration from exceeding the critical super-saturation concentration by forming new particles that rapidly grow to the size of the smallest particles represented by the model. The number of particles produced by this nucleation operator is somewhat arbitrary in that it depends on the smallest particle size handled by the model. Any error produced by this treatment is mitigated in the SoCAB because the vast majority of the aerosol loading is due to primary emission and condensation of secondary compounds. In locations where nucleation is more significant, this treatment may not be sufficiently accurate.

CONDENSATION AND EVAPORATION

Equation (26) contains two condensation and evaporation terms, each corresponding to two changes to

the size distribution that occur during these processes. The first term, $H_i p$, describes increases or decreases in aerosol mass, p_i, due to condensation or evaporation; as compounds condense p_i increases, and as compounds evaporate p_i decreases. The second term, $-(1/3)(\partial H p_i/\partial \mu)$, describes movement of the particle distribution in size space; as compounds condense each particle increases in size, moving the size distribution to higher values of μ, whereas as compounds evaporate each particle becomes smaller moving the size distribution toward smaller values of μ.

Of these two terms, the first is the easier to solve numerically. Both H_i and p may change during condensation or evaporation; H_i may change because for some compounds the surface equilibrium concentration, $C_{s,i}$, is dependent on the particle composition distribution. Thus care must be taken when integrating the first term that time steps are sufficiently small and that numerical errors are kept under control. This requirement is not difficult to meet because this term is an initial value problem.

The second term has the form of an advection or convection operator (e.g. Oran and Boris, 1987), but "moves" particles in the size coordinate. Chock (1985, 1991) and Chock and Dunker (1983) have reviewed numerous numerical algorithms for solving spatial advection and have identified the accurate space derivatives (ASD) method as both the most accurate and the most time consuming, and the Chapeau-function Taylor–Galerkin (CFTG) as being of lesser accuracy and faster (Gazdag, 1972; Donea *et al.*, 1987). Chock (1991) reports that the computer time consumed by the ASD method is about 3.5-times that consumed by the CFTG method. Chock used complex Fourier transforms to implement ASD, but we have been able to use a real-valued Fourier transform implementation that increases the speed of ASD by almost exactly a factor of two. In our implementation the ASD method uses about 1.8-times more computer time than CFTG.

In Chock's evaluations, like those of most others, the spatial advection algorithms are assessed under the assumption that the velocity field is divergence-free, a reasonable assumption for atmospheric wind fields. But the divergence-free assumption does not apply to condensation and evaporation since it implies that H_i is the same for all values of μ. The values of H_i may be unequal, and even of different sign, so divergence free tests and assumptions are not applicable to the aerosol condensation/evaporation problem. In the derivation of the CFTG algorithm, the divergence-free assumption is employed in evaluation of the third-order term in the Taylor expansion (Donea *et al.*, 1987, p. 472). In the derivation of the ASD method (Gazdag, 1972) no such assumptions are made. There is another advantage to the ASD method. Since Fourier transforms are used to determine the derivatives with respect to μ, information from all the available data is used to estimate each derivative, whereas with the CFTG method only adjacent node values are used. Still, even if the CFTG method does not have the accuracy of the ASD method, the time savings might be sufficient to warrant using CFTG anyway.

To decide between the two algorithms, another important difference between spatial advection and aerosol condensation/evaporation must be considered. In spatial advection the velocity fields are inputs to the model, no computer time (at least not within the air pollutant model) is expended in their calculation. This is in distinct contrast to aerosol condensation and evaporation calculations where a significant portion of the computer time is expended in the thermodynamics calculation that determines the particle surface concentrations, $C_{s,i}$ (Wexler and Seinfeld, 1991). As a result the additional computer time used by ASD is not significant compared to that used by CFTG, since they are both dominated by that used to predict the surface concentrations of the volatile species. Thus we have chosen the ASD method for solving the condensation and evaporation terms of equation (26). If a fast algorithm for the thermodynamic calculation is developed, a reassessment of the optimal numerical algorithm for this term should be undertaken.

The ASD method is based on a Taylor expansion of p_i about the current value of t. Each of the resulting temporal derivatives is converted to size derivatives using the condensation/evaporation equation terms in equation (26), and the size derivatives are calculated with Fourier transforms. In Chock's implementation of the ASD algorithm, only two Fourier transforms are required for each order in time of the method. For the third order expansion recommended by Gazdag, six Fourier transforms are required for each species, so for s species $6s$ Fourier transforms are performed for each time step. Fourier transforms only provide reasonable derivative estimates if $p_i(\mu)$ is periodic in μ. In the previous discussion of the μ-boundary conditions, it was determined that $p_i(\mu)$ should be zero outside the modelled range. Since $p_i(\mu)$ is zero both above and below the range of μ, it is periodic over μ.

The calculation of $H_i(\mu)$ is accomplished via equation (2). The only variable in its evaluation that is not a constant is $\Delta C_i = C_{\infty,i} - C_{s,i}$, which may change with composition. The integration time step will be chosen small enough that the H_i are, in essence, constant during the step. $C_{\infty,i}$ is obtained from the initial gas-phase concentrations. For non-volatile species, $C_{s,i} \equiv 0$. For the volatile species, $C_{s,i}$ is dependent on the temperature, composition, and phase state of the particle. Furthermore, if the particle contains multiple phases, $C_{s,i}$ is dependent on the distribution of species among these phases. The calculation of the phase state and particle surface concentrations is performed with AIM (Wexler and Seinfeld, 1991). AIM assumes that multiple aerosol phases are in equilibrium. If the aerosol contains water, its activity is equal to the ambient *r.h.* AIM uses a constrained minimization algorithm to find the minimum Gibbs free energy

phase state. Equilibrium constants are used to calculate the surface concentrations.

WATER CONTENT

Except for water, all of the aerosol compounds are either directly emitted in the aerosol phase, or their transport between the gas and aerosol phase is calculated. Water is assumed to be in equilibrium between the gas and aerosol phases. For a completely aqueous-phase aerosol, the water content of the aerosol can be calculated by solving equation (26) with equation (5). Effloresced particles contain no water, so water transport and water content are zero. The transition between purely aqueous and purely solid phases is not governed by equation (5) and thus is computationally challenging. A simple, accurate, and computationally expensive remedy to this problem is to periodically perform a Gibbs free energy minimization of the aerosol in order to discern its equilibrium-phase state; a separate solution of equation (26) is then developed to account for this water transport. Unfortunately, these minimizations consume an enormous amount of computer time in a large grid-based model and as a result another remedy is sought. At the beginning of a time step (typically 6 min) a Gibbs free energy minimization must be performed so that the surface concentrations are available for calculating the H_i. After this minimization, a readjustment of the water content is performed for any particles whose phase state had changed in the previous time step. This is strictly an *ad hoc* solution that maximizes computational efficiency at some expense in accuracy.

THE ALGORITHM

In this section we summarize the aerosol operator algorithm. The operator is designed to accurately and efficiently calculate the composition and size distribution of the aerosol. Figure 1 is a flow chart of the algorithm. The inputs to the operator are initial gas-phase composition, initial aerosol-phase composition and size distribution, and ambient temperature, relative humidity, and the rate of the relative humidity change, $dr.h./dt$.

To begin with, the change in single-solute concentration with relative humidity is calculated by interpolation of data available in Pilinis and Seinfeld (1987). Then the AIM code (Wexler and Seinfeld, 1991) is used to calculate the equilibrium surface concentrations. This is the most time consuming portion of the code. If a new phase has appeared or disappeared, the water content of the aerosol is adjusted accordingly.

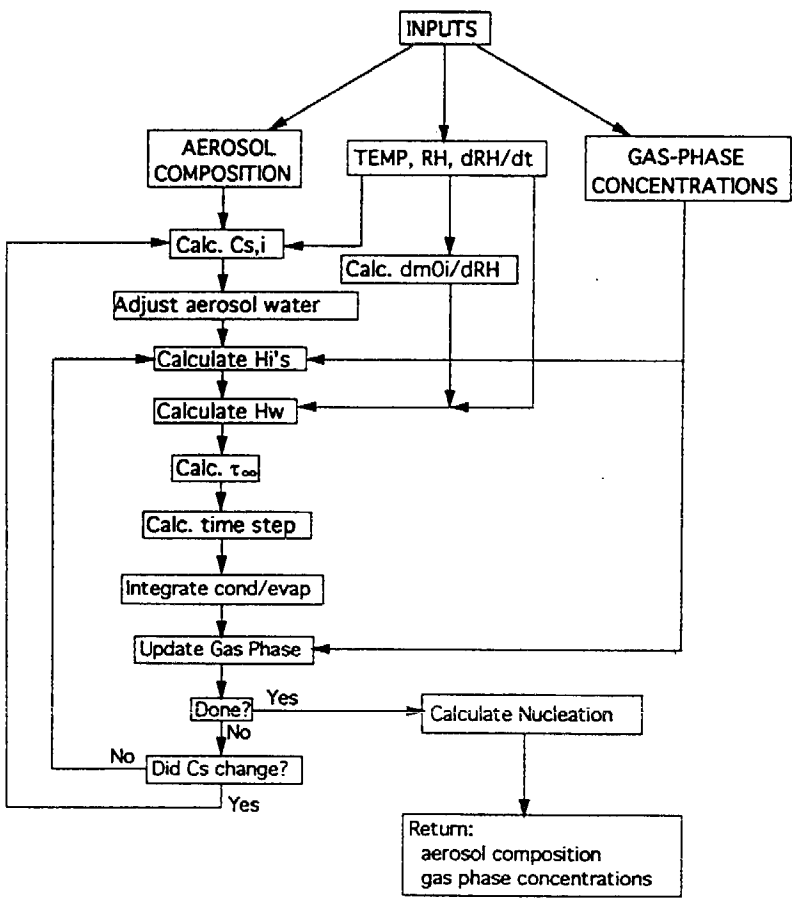

Fig. 1. Flowchart of aerosol operator.

Next the H_i and H_w values are calculated. These will be used in the solution of equation (26) in a number of ways. First, the H_i are the condensation/evaporation rates for the aerosol so are essential for the solution, but second, they are the inverse of the time constant for change in the mass of the particle due to condensation or evaporation of species i. If H_i^{-1} is large, the particle composition is not changing very fast, so new values of H_i may not have to be calculated very often.

The other time constant that may affect the size of the time step is $\tau_{\infty,i}$, the time constant for changes in the gas-phase species due to condensation or evaporation. $\tau_{\infty,i}$ is defined as

$$\tau_{\infty,i} \equiv \left| \frac{1}{C_{\infty,i}} \frac{\mathrm{d}C_{\infty,i}}{\mathrm{d}t} \right|^{-1} = \left| \frac{-1}{C_{\infty,i}} \int_0^\infty H_i q \mathrm{d}m \right|^{-1}. \quad (28)$$

Substituting equation (2) for H_i, using $q_i \mathrm{d}m = p_i \mathrm{d}\mu$ to convert from the m to the μ size coordinate, and using $D_p = D_{p0}\exp(\mu)$ to eliminate D_p in favor of μ gives

$$\tau_{\infty,i} = \left[\frac{1}{C_{\infty,i}} \int_0^\infty 2\pi D_p D_i q \frac{|\Delta C_i|}{\frac{2\lambda}{\alpha_i D_p} + 1} \right]^{-1} \mathrm{d}m = \left[\frac{1}{C_{\infty,i}} \int_{-\infty}^{+\infty} 2\pi D_{p0} \exp(\mu) D_i p \frac{|\Delta C_i|}{\frac{2\lambda}{\alpha_i D_{p0} \exp(\mu)} + 1} \right]^{-1} \mathrm{d}\mu \quad (29)$$

which in discretized form is

$$\tau_{\infty,i} = \left[\frac{2\pi D_i D_{p0}}{C_{\infty,i}} \sum_k \exp(\mu^k) p^k \Delta\mu \frac{|\Delta C_i^k|}{\frac{2\lambda}{\alpha_i D_{p0} \exp(\mu^k)} + 1} \right]^{-1} \quad (30)$$

where μ^k, p^k, and ΔC_i^k are the values of the size coordinate, aerosol concentration, and ambient-surface concentration difference for the kth size section, respectively, and $\Delta\mu$ is the size of these sections. When $\tau_{\infty,i}$ is large, the gas-phase concentrations do not change quickly and therefore do not constrain the integration time step. If $\tau_{\infty,i}$ is small the ambient concentrations change quickly due to condensation/evaporation, and short time steps must be taken to integrate the change in the gas-phase concentrations accurately.

Using the gas-phase and aerosol-phase time constants we are able to determine the time step used with the ASD method to solve the condensation/evaporation terms. The time step must be short enough that (1) the ambient concentration of volatile species remains constant, (2) the surface equilibrium concentration of volatile species remains constant, and (3) the Courant number $H_i \Delta t / \Delta\mu$ does not exceed 0.4 (Gazdag, 1972).

The ambient concentration remains constant if $\Delta t \ll \tau_\infty$ for all compounds. In the SoCAB, ammonium nitrate is the volatile compound of primary concern. When the aerosol contains solid ammonium nitrate, the surface concentrations of ammonia and nitric acid are fixed. The surface concentrations are also fixed if ammonium nitrate osmotically dominates the aerosol (Wexler and Seinfeld, 1990). This occurs when there is roughly 5-times as many moles of nitrate as sulfate, providing essentially all of the anions are neutralized by ammonium. Since the surface concentrations do not change when the aerosol contains solid NH_4NO_3, or when it is aqueous, but osmotically dominated by NH_4NO_3, the H_i^{-1} do not limit the time step. If neither of these cases hold, the surface concentrations will remain constant only if $\Delta t \ll H_i^{-1}$.

The ASD algorithm changes the aerosol-phase concentrations and distributions due to condensation and evaporation, but these processes simultaneously deplete or enrich the gas-phase concentrations. These alterations to the gas-phase concentrations are calculated using conservation of mass for each condensing compound.

If condensation during the time step does not substantially alter the aerosol composition in a section, or if the particles are solid or osmotically dominated by the condensing compound, the surface equilibrium concentrations need not be recalculated, and the algorithm can restart at the calculation of the H_i. If the surface equilibrium concentrations are substantially altered, the algorithm must restart by performing the time-consuming Gibbs free energy minimization.

After some number of passes through these loops, the 6 min time step for the operator is complete. If after all condensation/evaporation is complete, the H_2SO_4(g) concentration exceeds the critical value given by equation (27), the excess sulfuric acid is condensed onto particles that appear in the smallest size section. Finally the algorithm returns the updated gas and aerosol compositions.

CONCLUSION

Particles in urban and regional air pollution are transformed in number and size by a host of physical and chemical processes. We have shown in this work that the time scale for coagulation to take place is too long to significantly influence particle number or size distributions in the SoCAB. Coagulation will only be significant in locations with aerosol loading higher than the peak loadings in Los Angeles. We examined gravitational settling and demonstrated that, in comparison to deposition and turbulent diffusion, it too may be ignored for PM_{10}. Homogeneous H_2SO_4–H_2O nucleation was shown to be a significant generator of new particles where the aerosol loading is low and the gas concentration of SO_2 is high. In the SoCAB this occurs exclusively in Long Beach. In many locations outside the SoCAB, these conditions are more prevalent so nucleation is most likely a significant generator of sub-micron particles in cleaner urban and regional locations.

We deduce that the physical processes that dominate the size and composition of urban particles are

advection, turbulent diffusion, condensation and evaporation, emissions, and deposition. The advective and diffusive terms transport particles and gaseous pollutants indentically, and since the particle model must be solved in conjunction with a gas-phase model in order to properly simulate the condensation and evaporation processes, transport operators modify both the gaseous and particle phase together. Deposition is treated by a resistance model, as it is for the gas phase, but with modified coefficients. Condensation and evaporation modify both gaseous and particulate concentrations, and their size distribution. The condensation and evaporation terms have the same form as advection terms, so that numerical methods suitable for advection can be used to solve condensation and evaporation.

The result of these analyses is an equation that describes the temporal evolution of the size and composition distribution of an internally mixed aerosol subject to the chemical and physical processes that dominate in the urban and regional atmosphere. Numerical methods available from the literature are suitable for solving these terms. The next step in this work is evaluating the model on ambient data, and investigating the sensitivity of the predictions to the assumptions employed here. These results will be reported in a companion paper.

Acknowledgements—A.S.W. would like to thank David Chock for providing access to his ASD and CFTG codes. This work was supported by the South Coast Air Quality Management District.

REFERENCES

Allen A. G., Harrison R. M. and Erisman J. (1989) Field measurements of the dissociation of ammonium nitrate and ammonium chloride aerosols. *Atmospheric Environment* **23**, 1591–1599.

Atkinson R., Winer A. M. and Pitts J. N. Jr (1986) Estimation of nighttime N_2O_5 concentrations from ambient NO_2 and NO_3 radical concentrations and the role of N_2O_5 in nighttime chemistry. *Atmospheric Environment* **20**, 331–339.

Bassett M. E., Cassmassi J. C., Durkee K. R. and Hogo H. (1991) Final air quality management plan, 1991 revision. Final technical report V-E. Episodic PM-10 model development and application for the South Coast Air Basin. South Coast Air Quality Management District.

Calvert J. G., Lazrus A., Kok G. L., Heikes B. G., Walega J. G., Lind J. and Cantrell C. A. (1985) Chemical mechanisms of acid generation in the troposphere. *Nature* **317**, 27–35.

Carmichael G. R., Peters L. K. and Kitada T. (1986) A second generation model for regional-scale transport/chemistry/deposition. *Atmospheric Environment* **20**, 173–188.

Chock D. P. (1985) A comparison of numerical methods for solving the advection equation—II. *Atmospheric Environment* **19**, 571–586.

Chock D. P. (1991) A comparison of numerical methods for solving the advection equation—III. *Atmospheric Environment* **25A**, 853–871.

Chock D. P. and Dunker A. M. (1983) A comparison of numerical methods for solving the advection equation. *Atmospheric Environment* **17**, 11–24.

Covert D. S. and Heintzenberg J. (1984) Measurement of the degree of internal/external mixing of hygroscopic compounds and soot in atmospheric aerosols. *Sci. total Envir.* **36**, 347–352.

Donea J., Quartapelle L. and Selmin V. (1987) An analysis of time discretization in the finite element solution of hyperbolic problems. *J. comp. Phys.* **70**, 463–499.

Eldering A., Solomon P. A., Salmon L. G., Fall T. and Cass G. R. (1991) Hydrochloric acid: a regional perspective on concentrations and formation in the atmosphere of southern California. *Atmospheric Environment* **25A**, 2091–2102.

Gazdag J. (1972) Numerical convective schemes based on accurate computation of space derivatives. *J. Comp. Phys.* **13**, 100–113.

Gelbard F. (1990) Modeling multicomponent aerosol particle growth by vapor condensation. *Aerosol Sci. Technol.* **12**, 399–412.

Gery M. W., Whitten G. Z., Killus J. P. and Dodge M. C. (1989) User's guide for the urban airshed model. Volume I: User's manual for UAM(CB-IV). SYSAPP-90/018a, final report prepared for the South Coast Air Quality Management District for Contract Number 89112A.

Gill P. S., Graedel T. E. and Weschler C. J. (1983) Organic films on atmospheric aerosol particles, fog droplets, cloud droplets, raindrops, and snowflakes. *Rev. geophys. Space Phys.* **21**, 903–920.

Hamill P. (1975) The time dependent growth of H_2O–H_2SO_4 aerosols by heteromolecular condensation. *J. Aerosol Sci.* **6**, 475–482.

Hering S. (1990) SCAQS sampler data plots. Report to the California Air Resources Board, Contract No. A832–086.

Hildemann L. M., Cass G. R. and Markowski G. R. (1989) A dilution stack sampler to collection of organic aerosol emissions: design, characterization and field tests. *Aerosol Sci. Technol.* **10**, 193–204.

Hogo H., Seignur C. and Yocke M. A. (1985) Draft SCAQMD STAR project working paper No. 1: Technical description of a photochemical air quality model with extensions to calculate aerosol dynamics and visibility.

Jaecker-Voirol A. and Mirabel P. (1989) Heteromolecular nucleation in the sulfuric acid–water system. *Atmospheric Environment* **23**, 2053–2057.

John W., Wall S. M., Ondo J. L. and Winklmayr W. (1990) Modes in the size distribution of atmospheric inorganic aerosol. *Atmospheric Environment* **24A**, 2349–2359.

Kiang C. S., Cadle R. D., Hamill P., Mohnen V. A. and Yue G. K. (1975) Ternary nucleation applied to gas to particle conversion. *J. Aerosol Sci.* **6**, 465–474.

Kim Y. P. and Seinfeld J. H. (1990) Simulation of multicomponent aerosol condensation by the moving section method. *J. Colloid interf. Sci.* **135**, 185–199.

Li S.-M., Anlauf K. G. and Wiebe H. A. (1993) Heterogeneous nighttime production and deposition of particle nitrate at a rural site in North America during summer 1988. *J. geophys. Res.* **98**, 5139–5157.

Marlow W. H. (1981) Size effects in aerosol particle interactions: the van der Waals potential and collision rates. *Surface Sci.* **106**, 529–537.

McMurry P. H. and Stolzenberg M. R. (1989) On the sensitivity of particle size to relative humidity for Los Angeles aerosols. *Atmospheric Environment* **40**, 497–507.

McRae G. J., Goodin W. R. and Seinfeld J. H. (1982) Numerical solution of the atmospheric diffusion equation for chemically reacting flows. *J. Comp. Phys.* **45**, 1–42.

National Research Council (1991) *Rethinking the Ozone Problem in Urban and Regional Air Pollution.* National Academy Press, Washington, D.C.

Oran E. S. and Boris J. P. (1987) *Numerical Simulation of Reactive Flow.* Elsevier, New York.

Pandis S. N., Seinfeld J. H. and Pilinis C. (1992) Heterogeneous sulfate production in an urban fog. *Atmospheric Environment* **26A**, 2509–2522.

Pilinis C. (1990) Derivation and numerical solution of the

species mass distribution equations for multicomponent particulate systems. *Atmospheric Environment* **24A**, 1928–1940.

Pilinis C. and Seinfeld J. H. (1987) Continued development of a general equilibrium model for inorganic multicomponent atmospheric aerosols. *Atmospheric Environment* **21**, 2453–2466.

Pilinis C. and Seinfeld J. H. (1988) Development and evaluation of an Eulerian photochemical gas-aerosol model. *Atmospheric Environment* **22**, 1985–2001.

Pleim J., Venkatram A. and Yamartino R. J. (1984) The dry deposition model. Volume 4. ADOM/TADAP model development program. Ontario Ministry of the Environment, Rexdale, Ontario, Canada.

Rood M. J., Covert D. S. and Larson T. V. (1987) Hygroscopic properties of atmospheric aerosol in Riverside, California. *Tellus* **39B**, 383–397.

Rood M. J., Shaw M. A., Larson T. V. and Covert D. S. (1989) Ubiquitous nature of ambient metastable aerosol. *Nature* **337**, 537–539.

Russell A. G. and Cass G. R. (1986) Verification of a mathematical model for aerosol nitrate and nitric acid formation and its use for control measure evaluation. *Atmospheric Environment* **20**, 2011–2025.

Russell A. G., McRae G. J. and Cass G. R. (1985) The dynamics of nitric acid production and the fate of nitrogen oxides. *Atmospheric Environment* **19**, 893–903.

Sehmel G. A. (1980) Particle and gas dry deposition: a review. *Atmospheric Environment* **14**, 983–1011.

Seinfeld J. H. (1986) *Atmospheric Chemistry and Physics of Air Pollution.* Wiley, New York.

Slinn S. A. and Slinn W. G. N. (1980) Predictions for particle deposition on natural waters. *Atmospheric Environment* **14**, 1013–1016.

Shaw G. E. (1989) Production of condensation nucleii in clean air by nucleation of H_2SO_4. *Atmospheric Environment* **23**, 2841–2846.

Shaw M. A. and Rood M. J. (1990) Measurement of the crystallization humidities of ambient aerosol particles. *Atmospheric Environment* **24A**, 1837–1841.

Tanner R. L. (1982) An ambient experimental study of phase equilibrium in the atmospheric system: aerosol H^+, NH_4^+, SO_4^{2-}, NO_3^-–NH_3(g), HNO_3(g). *Atmospheric Environment* **16**, 2935–2942.

Tuazon E. C., Atkinson R., Plum C. N., Winer A. M. and Pitts J. N. Jr (1983) The reaction of gas phase N_2O_5 with water vapor. *Geophys. Res. Lett.* **10**, 953–956.

Turpin B. J. and Huntzicker J. J. (1991) Secondary formation of organic of aerosol in the Los Angeles basin: a descriptive analysis of organic and elemental carbon concentrations. *Atmospheric Environment* **25A**, 207–215.

Van Dingenen R. and Raes F. (1991) Determination of the condensation accommodation coefficient of sulfuric acid on water–sulfuric acid aerosol. *Aerosol Sci. Technol.* **15**, 93–106.

Van Doren J. M., Watson L. R., Davidovits P., Worsnop D. R., Zahniser M. S. and Kolb C. E. (1991) Uptake of N_2O_5 and HNO_3 by aqueous sulfuric acid droplets. *J. phys. Chem.* **95**, 1684–1689.

Wesley M. L. and Hicks B. B. (1977) Some factors that affect the deposition rates of sulfur dioxide and similar gases on vegetation. *J. Air Pollut. Control Ass.* **27**, 1110–1116.

Wexler A. S. and Seinfeld J. H. (1990) The distribution of ammonium salts among a size and composition dispersed aerosol. *Atmospheric Environment* **24A**, 1231–1246.

Wexler A. S. and Seinfeld J. H. (1991) Second generation inorganic aerosol model. *Atmospheric Environment* **25A**, 2731–2748.

Wexler A. S. and Seinfeld J. H. (1992) Analysis of aerosol ammonium nitrate: departures from equilibrium during SCAQS. *Atmospheric Environment* **26A**, 579–591.

Wexler A. S., Eldering A., Pandis S. N., Cass G. R., Seinfeld J. H., Moon K. C. and Hering S. V. (1992) Modeling aerosol processes and visibility based on the SCAQS data. California Air Resources Board publication A932-054 and EQL Report 36, California Institute of Technology.